

---

REVISTA  
**PESQUISA  
NAVAL**

---

NUMBER 28 - 2016

---



DIRECTORATE-GENERAL FOR NUCLEAR AND TECHNOLOGICAL  
DEVELOPMENT OF THE NAVY (DGDNTM)



---

REVISTA

# PESQUISA NAVAL

NUMBER 28 - 2016

---

REVISTA  
**PESQUISA  
NAVAL**

The mission of the *Revista Pesquisa Naval* is to provide a formal channel of communication and dissemination of national scientific and technical productions for the scientific community, by publishing original articles that are a result of scientific research and contribute to the advancement of knowledge in areas of interest for the Brazilian Navy. Articles published in the journal do not reflect the position or the doctrine of the Navy and are the sole responsibility of the authors.

#### SPONSORSHIP

Directorate-General for Nuclear and Technological Development of the Navy - DGDNTM

#### EDITOR-IN-CHIEF

**Admiral Bento Costa Lima Leite de Albuquerque Junior**

*Director General of Nuclear and Technological Development of the Navy*

#### ASSISTANT EDITORS

**RADM Alfredo Martins Muradas**

*Director of Naval Systems Analysis Center - CASNAV*

**RADM Marcos Lourenço de Almeida**

*Director of Admiral Paulo Moreira Marine Institute - IEAPM*

**RADM (NE) André Luis Ferreira Marques**

*Director of the Technological Center of the Navy in São Paulo*

**RADM (NE) Luiz Carlos Delgado**

*Director of Navy Research Institute - IPqM*

#### EDITORIAL BOARD

**CAPT Antônio Capistrano de Freitas Filho**

**CAPT José Fernando De Negri**

**CDR Benjamin Dante Rodrigues Duarte Lima**

**LCDR (NE) Elaine Rodino da Silva**

**2SG-RO Rogério Augusto dos Santos**

**3SG-ELEC Renato Ellyson Oliveira Cavalcante**

#### EDIÇÃO

Directorate-General for Nuclear and Technological Development of the Navy - DGDNTM

[www.marinha.mil.br/dgdntm/revista](http://www.marinha.mil.br/dgdntm/revista)

#### EDITORIAL PRODUCTION

Zeppelini Publishers / Instituto Filantropia

[www.zeppelini.com.br](http://www.zeppelini.com.br)

#### EDITORIAL COMMISSION

Adriano Joaquim de Oliveira Cruz - UFRJ - Rio de Janeiro/RJ/Brazil

Aldebaro Barreto da Rocha Klautau Júnio - UFPA - Belém/PA/Brazil

Aletéia Patrícia Favacho de Araújo - UNB - Brasília/DF/Brazil

André Andrade Longaray - FURG - Rio Grande/RS/Brazil

Andre Luiz Lins de Aquino - UFAL - Maceió/AL/Brazil

Cintia de Moraes Borba - FIOCRUZ - Rio de Janeiro/RJ/Brazil

Genaina Nunes Rodrigues - UNB - Brasília/DF/Brazil

Giovane Quadrelli - UCP - Petrópolis/RJ/Brazil

Gilson Brito Alves de Lima - UFF - Rio de Janeiro/RJ/Brazil

Jaci Maria Bilhalva Saraiva - CENSIPAM - Brasília/DF/Brazil

José Maria Parente de Oliveira - ITA - São José dos Campos /SP/Brazil

José Mario De Martino - FEEC/UNICAMP - Campinas/SP/Brazil

Jose Manoel Seixas - UFRJ - Rio de Janeiro/RJ/Brazil

Luciano Zogbi Dias - FURG - Rio Grande/RS/Brazil

Maria Eveline de Castro Pereira - FIOCRUZ - Rio de Janeiro/RJ/Brazil

Marcos Evandro Cintra - UFERSA - Mossoró/RN/Brazil

Marcelo Sperle Dias - UERJ - Rio de Janeiro/RJ/Brazil

Mirian Enriqueta Bracco - UERJ - Rio de Janeiro/RJ/Brazil

Natanael Nunes de Moura - UFRJ - Rio de Janeiro/RJ/Brazil

Newton Narciso Pereira - USP - São Paulo/SP/Brazil

Nivaldo Silveira Ferreira - UENF - Campos dos Goytacazes /RJ/Brazil

Paulo Sérgio Soares Guimarães - UFMG - Belo Horizonte /MG/Brazil

Raul Francé Monteiro - PUC-Goiás - Goiânia/GO/Brazil

Ricardo Coutinho - IEAPM - Rio de Janeiro/RJ/Brazil

Thiago Pontin Tancredi - UFSC - Florianópolis /SC/Brazil

Vivian Resende - UFMG - Belo Horizonte/MG/Brazil

Walter Roberto Hernández Vergara - UFGD - Dourados /MS/Brazil

THE REVISTA PESQUISA NAVAL IS SPONSORED BY

FUNDAÇÃO CONRADO WESSEL

**FCW**

Revista Pesquisa Naval / Diretoria-Geral de Desenvolvimento Nuclear e Tecnológico da Marinha  
v. 1, n. 1, 1988 - Brasília - DF - Brasil - Marinha do Brasil

Anual

Título abreviado: Pesq. Nav.

ISSN Impresso 1414-8595 /

ISSN Eletrônico 2179-0655

1. Marinha - Periódico - Pesquisa Científica. Diretoria-Geral de Desenvolvimento Nuclear e Tecnológico da Marinha.

CDU 001.891.623/.9  
CDD 623.807.2

**1 PRESENTATION**

*Bento Costa Lima Leite de Albuquerque Junior*

**OPERATING ENVIRONMENT**

**2 A RISK CLASSIFICATION MODEL FOR ORGANIC AIRCRAFT OPERATIONS: A MULTIPLE CRITERIA APPROACH**

Modelo de classificação de risco para operações com aeronaves embarcadas: uma abordagem multicritério

*Luiz Fernando do Nascimento, Mischel Carmen Neyra Belderrain*

**13 THE OPERATIONAL RISK MANAGEMENT APPLIED TO THE SCIENTIFIC DEVELOPMENT OF "THE BLUE AMAZON" - AMAZÔNIA AZUL**

O gerenciamento do risco operacional aplicado ao desenvolvimento científico da Amazônia Azul

*Guilherme Pires Black Pereira*

**NAVAL ARCHITECTURE AND PLATFORM**

**21 INVESTIGATION ON STRUCTURAL RESPONSE, INDUCED BY SLAMMING EFFECT IN A MONOHULL SEMIDISPLACEMENT SHIP BY MEANS OF SUBSTRUCTURED MODELING**

Investigação sobre a resposta estrutural, induzida pela batida de proa em embarcação monocasco de semiplano, por meio de modelagem por subestruturação

*fabio da Rocha Alonso, Waldir Terra Pinto*

**HUMAN PERFORMANCE AND HEALTH**

**34 ACCIDENTS WITH WATERWAY TRANSPORTS DUE TO EXTREME WEATHER CONDITIONS**

Acidentes com transportes hidroviários em ocasião de extremos meteorológicos

*Suanne Honorina Martins dos Santos, Maria Isabel Vitorino, Jefferson Inayan de Oliveira Souto, Edson José Paulino da Rocha*

**DECISION-MAKING PROCESS**

**45 LITHOLOGY DISCRIMINATION BY SEISMIC ELASTIC PATTERNS: A GENETIC FUZZY SYSTEMS APPROACH**

Discriminação litológica por atributos sísmicos elásticos: uma abordagem por sistemas fuzzy-genéticos

*Eric da Silva Praxedes, Adriano Soares Koshiyama, Marley Maria Bernardes Rebuzzzi Vellasco, Marco Aurélio Cavalcanti Pacheco, Ricardo Tanscheit*

**SENSORS, ELECTRONIC WARFARE AND ACOUSTIC WARFARE**

**57 COMPARISON BETWEEN THE THEORETICAL ESTIMATION AND THE MEASUREMENTS OF THE MAIN FIGURES OF MERIT OF QUANTUM WELL INFRARED PHOTODETECTORS**

Comparação entre a estimativa teórica e as medidas das principais figuras de mérito de fotodetectores infravermelhos a poços quânticos

*Ali Kamel Issmael Junior, Fábio Durante Pereira Alves, Ricardo Augusto Tavares Santos*

---

**71 BLIND AND ASSISTED SIGNAL DETECTION FOR UWB SYSTEMS  
BASED ON THE IEEE 802.15.4A STANDARD**

Detecção cega e assistida de sinais em sistemas UWB baseados no padrão IEEE 802.15.4A

*Aline de Oliveira Ferreira, Cesar Augusto Medina Sotomayor, Fabian David Backx,  
Raimundo Sampaio Neto*

**82 BRAZILIAN PASSIVE SONAR: ADVANCES AND TECHNOLOGY  
SHOWCASE**

Sonar passivo nacional: avanços e demonstração de tecnologia

*Fabricio de Abreu Bozzi, William Soares Filho, Fernando de Souza Pereira Monteiro,  
Carlos Alfredo Órfão Martins, Gustavo Augusto Mascarenhas Goltz,  
Orlando de Jesus Ribeiro Afonso, Cleide Vital da Silva Rodrigues,  
Fernando Luiz de Magalhães, Leonardo Martins Barreira*

**INFORMATION AND COMMUNICATIONS TECHNOLOGY**

**93 AN ARCHITECTURE TO MANAGE SOFTWARE ENGINEERING PROJECTS  
AIMED AT INTEGRATION WITHIN THE BRAZILIAN ARMED FORCES**

Uma arquitetura para a gestão dos projetos de engenharia de *software* visando à integração nas Forças Armadas

*Geraldo da Silva Souza, Rodrigo Abrunhosa Collazo, Jones de Oliveira Avelino,  
Carlos Eduardo Barbosa*

## PRESENTATION

The Navy, over time, has been a leader in the area of Science, Technology, and Innovation (ST&I), with results that go beyond the Navy Force, generating achievements and benefits for the country. The pioneering spirit of Admiral Álvaro Alberto da Mota e Silva, patron of the Navy's ST&I and a Brazilian scientist, stands out. He dreamed up and implemented the National Nuclear Energy Commission (CNEN) and the National Council for Scientific and Technological Development (CNPq) in the 1950s, and was its first president.

The Naval Force has always sought to improve itself. With its legacy achieved in the area of ST&I as its guide until today, it changed its organizational structure. It changed the name of the Secretary of Science, Technology and Innovation of the Navy, SecCTM, to the Board of Directors of Nuclear and Technological Development of the Navy (DGDNTM). It is the responsibility of the Board of Directors to plan, organize, direct, and control all of the Navy's ST&I activities, including the relevant Submarine Development Program (PROSUB) and the Navy's Nuclear Program (PNM).

These programs, which will allow Brazil to obtain its first nuclear powered submarine thorough design and construction, have shown that the benefits derived from the Naval Force's ST&I investments continue to go beyond the exclusive area of the Navy. Its beneficiaries include the areas of electric power generation and health, because, in partnership with the Nuclear Industries of Brazil (INB) and the Nuclear and Energy Research Institute (IPEN), we are working on achieving Brazilian autonomy in the production of nuclear fuel for the nuclear power plants in Angra dos Reis (RJ) and in the implementation of the the

Brazilian Multipurpose Reactor (RMB), which will produce radiopharmaceuticals.

The demand for new technologies has led the Navy to establish new Strategic Partnerships with the academic and business sectors, as well as with other governmental institutions, as it guides the concept of innovation known as the Triple Helix. Some legal documents of cooperation have already been signed and cooperation are being expanded with activities drawing on mutual knowledge, such as workshops and symposia with several institutions in different regions of Brazil.

In this context, the Naval Research Journal has, since its first edition in 1988, made a relevant contribution to the dissemination of the Navy's CT & I activities, and is therefore an important instrument for interaction with the academic and business sectors and with other governmental bodies. As I present a new collection of scientific articles, I take this opportunity to salute all those who, in some way, have collaborated to achieve this level of scientific and technological development. Bravo Zulu!

Pleasant reading!



**BENTO COSTA LIMA LEITE DE ALBUQUERQUE JUNIOR**  
Fleet Admiral  
Director General of Nuclear and Technological  
Development of the Navy

# A RISK CLASSIFICATION MODEL FOR ORGANIC AIRCRAFT OPERATIONS: A MULTIPLE CRITERIA APPROACH

Modelo de classificação de risco para operações com aeronaves embarcadas: uma abordagem multicritério

Luiz Fernando do Nascimento<sup>1</sup>, Mischel Carmen Neyra Belderrain<sup>2</sup>

**Abstract:** The use of organic aircraft by warships from the Brazilian Navy provides a substantial improvement in their operational capabilities. This study aims to present a predictive method for risk classification of organic aircraft operations. To this end, a multiple criteria decision aiding method, called ELECTRE TRI-C, is used, through which completely ordered risk categories are associated to the tasks to be performed. As a result, a framework that helps the decision-making process is obtained. By means of an objective method, it is possible to quantify the risk associated to air operations. Risk classification allows developing previously announced lines of action, such as the definition of the appropriate level to authorize the execution of operations, or to carry out specific procedures according to the corresponding level of risk. In addition, risk classification allows the modification of the operation's attributes before it is carried out, in order to make it acceptable.

**Keywords:** Aviation safety. Risk classification. Multicriteria decision aid. ELECTRE TRI-C.

**Resumo:** A utilização de aeronave orgânica pelos navios de guerra da Marinha do Brasil permite uma melhora substancial nas suas capacidades operacionais. Este trabalho visa apresentar um método preditivo para a classificação de risco em operações com aeronaves embarcadas. Para isso, foi utilizado o método multicritério de apoio à decisão ELECTRE TRI-C, no qual são utilizadas categorias de risco completamente ordenadas, às quais as operações são designadas. Como resultado, obtém-se uma metodologia que apoia o processo de tomada de decisão, possibilitando classificar o risco associado às operações aéreas. A classificação de risco permite o desenvolvimento de linhas de ação divulgadas *a priori*, como a definição do nível hierárquico apropriado para autorizar a realização da operação ou a condução de procedimentos de segurança específicos a serem realizados em função do nível de risco associado. Além disso, possibilita a modificação dos atributos da operação antes da sua realização, a fim de torná-la aceitável.

**Palavras-chave:** Segurança de aviação. Classificação de risco. Apoio multicritério à decisão. ELECTRE TRI-C.

## 1. INTRODUCTION

The use of helicopters by warships is an operational necessity.

The increase in combat capacity is significant because of the increased mobility, autonomy, and speed of the naval environment with the use of the aircraft. All attributes of the shipboard aircraft are transferred to the ship at sea. On the

other hand, the risks associated with the use of the aircraft are added to those already existing in ships.

Managing risks becomes important in this situation as the helicopter is expected to carry out a variety of operations, with a mobile landing pad full of fuel tanks, missiles, and ammunition, as well as the reduced space and the difficulty in getting external help.

<sup>1</sup> Analyst in the Operational Research Division of the Naval Systems Analysis Center – Rio de Janeiro, RJ – Brazil. Master of Science from Instituto Tecnológico de Aeronáutica – São José dos Campos, SP – Brazil. E-mail: luiz.fernando@casnav.mar.mil.br

<sup>2</sup> Associate Professor in Instituto Tecnológico de Aeronáutica – São José dos Campos, SP – Brazil. PhD in Aeronautical and Mechanical Engineering from Instituto Tecnológico de Aeronáutica – São José dos Campos, SP – Brazil. E-mail: carmen@ita.br

In aviation safety, operational risk is the assessment, in terms of expected probability and severity, of the consequences of a hazard, taking into account the worst predictable situation (ICAO, 2013). In other words, it is the probability of occurrence of an event, multiplied by the estimate of the intensity, or extent of the losses that may result from the exposure to a hazard. In the pursuit of an objective risk assessment, hazard identification and the conduction of risk management processes become appropriate, which, in addition to identification, include estimation, analysis, assessment, and reporting of hazards.

Risk management approaches, following the identification of hazards, conduct a risk ordering according to criteria that use the worst possible consequence that could result from those hazards and the likelihood of the occurrence of damage. In this way, all the components of the risk will be found, which will be subject to control measures established by the organization.

Many researchers have already dealt with risk and safety management in their research. Shyur (2008) developed an analytical method based on accidents and safety indicators to quantify aviation hazards caused by human error. Dagdeviren and Yuksel (2008) used the multiple criteria analytic hierarchy process (AHP) to perform safety assessments in the work system of a manufacturing organization. Johnson et al. (2008) present how organizations and institutions learn from large-scale accidents, and the constraints that may affect such learning. Lee (2006) developed a quantitative model for calculating risk factors in aviation safety as a means of increasing the effectiveness of the risk management system. Liou et al. (2007) used a multicriteria model to perform a quantitative measurement of air safety indexes. Liou et al. (2008) presented a method to build a risk management system for airlines. However, a model for risk classification in aircraft operations, as carried out in this study, was not found in the literature.

In this context, this study aimed to obtain a methodology to support the classification of risk in operations with shipboard aircraft, using the ELECTRE TRI-C multiple criteria method. This was chosen because it is non-compensatory, and because it defines a risk category by means of a single reference alternative, being the most representative of the class.

There is a problem of decision support, which consists in obtaining a risk classification for tasks with aircraft that are about to take off with a ship as a platform. Permission from a competent authority is required to carry out this flight.

However, the authority does not often have a clear picture of the risks associated with the operation that is about to take place. The present climatic conditions, aircraft maintenance conditions and pilot experience among others, are attributes of this task and influence the severity and likelihood of an undesired occurrence during the flight.

## 2. THEORETICAL CONSIDERATIONS

Hazard identification and risk management are the main processes and basic components of safety management.

According to the *International Civil Aviation Organization* (ICAO) (2013), a hazard is defined as a condition or an object with the potential to cause injury to personnel, damage to equipment or structures, loss of material or reduction in the capacity to perform a given function. On the other hand, risk can be defined as the assessment – expressed in terms of probability and severity prediction – of the consequences of a hazard, taking the worst predictable situation as a reference (ICAO, 2013).

Risk management is a generic term that encompasses risk assessment and mitigation of the consequences of hazards that threaten the capabilities of an organization. Its purpose is to provide the foundation for balanced resource allocation.

Operational risk management is a key component in an organization's operational safety management.

## 3. MODELING

### 3.1. ELECTRE TRI-C

The ELECTRE TRI-C multiple criteria method is a variation of the ELECTRE TRI method proposed by Yu (1992), later called ELECTRE TRI-B, in order to distinguish them. ELECTRE TRI-C was proposed by Dias et al. (2010), and its main characteristic is the use of a single reference alternative to define categories, as the most representative of the class. ELECTRE TRI-C is, therefore, a multiple criteria classification method, in which the alternatives are compared to reference alternatives. These references contain the characteristics that represent each category. Thus, the method presented here handles situations in which the objective is to help the decision-maker to assign each operation to a predefined risk category.

### 3.2. MODELING OF THE RISK ASSESSMENT CRITERIA

In this article, an aviation operation performed by a shipboard aircraft, denoted by  $a$ , was evaluated by a family of risk assessment criteria, denoted by  $F = \{g_1, g_2, \dots, g_j, \dots, g_{10}\}$ .

The criteria used in this work are those presented in the Brazilian Navy's aviation safety manual (BRASIL, 2013) and consist of contributing factors to accidents included in the databases of the Brazilian Navy (BN).

Thus,  $g_j(a)$  represents the risk associated with operation, and  $a$  as a function of criterion  $g_j, j=1, 2, \dots, 10$ . The selected criteria were created and modeled according to the requirements (Roy, 1999):

- criterion  $g_1$  – type of operation: defines the type of operation to be performed. On tactical flights, the emotional factor is more required of pilots than on learning flights. Due to this, the decision-maker defined four levels for this criterion. The type of operation with the lowest risk is the performance of a daytime training; the highest, a night tactical flight;
- criterion  $g_2$  – expected period and duration of the flight: It has been proven that activities carried out at night are the most affected with respect to human attention. Associated with this, the duration of the flight leads to a greater potential risk for the task to be performed owing to the fatigue. Six levels were defined, in which the lowest risk is a daytime flight with a duration of less than three hours, and the one with the highest risk is a night flight lasting more than six hours;
- criterion  $g_3$  – pilot experience: after flying for a certain number of hours, a pilot achieves a degree of experience that helps them in unforeseen situations and emergencies. In addition, the greater the number of hours flown in the same aircraft, the greater the pilot's cognitive and psychomotor proficiency of the aircraft;
- criterion  $g_4$  – type of task and meteorological conditions: meteorological conditions are important risk components. The instrument meteorological conditions (IMC) show an increase in the pilot's workload in relation to the visual meteorological conditions (VMC). Associated with the type of operation, this creates risk situations with several known precedents;
- criterion  $g_5$  – equipment degradation: flight equipment is essential for safe aircraft operations. Dependency increases

in night flights and under IMC. Reliable communications equipment is important for the control of the aircraft by the ship and in areas of intense air traffic;

- criterion  $g_6$  – bingo: Is the aircraft model's distance to the ground or surface ship with pickup capability. In case of malfunction, the further from a landing site, the greater the risk;
- criterion  $g_7$  – ceiling x visibility: visibility restrictions make navigation more complicated and increase the risk of collisions;
- criterion  $g_8$  – moonlight x overcast: the light reflected by the moon is an aid to nocturnal visual flights. Lack of brightness increases the possibility of collision with obstacles. The incidence of clouds is another factor that, combined with lack of luminosity, increases the risk of the mission;
- criterion  $g_9$  – state of the sea: most of the aeronautical occurrences with shipboard helicopters occur at landing or takeoff. As the ship is a moving landing platform, the state of the sea directly influences the mission's risk;
- criterion  $g_{10}$  – period of aerial activity: the period of aerial activity is the time spent by the aircraft operator engaged in activities related to work after completion of the appropriate rest. A period longer than 12 hours with less than 8 hours of rest will result in loss owing to fatigue and poor attention, perception, and judgment.

### 3.3. MODELING THE SET OF RISK CATEGORIES

Since the purpose of this application is to provide a risk classification to decision-makers, four risk categories are proposed in this section, with very clear meanings for the decision-making context. These categories are defined in Table 1.

The four categories were created to receive future operations which, in this work, are subject to decision or are alternatives. Thus, their associated risk levels will be assigned. These categories were also created and completely ordered, from the riskiest ( $C_1$ ) to the least risky ( $C_4$ ). Table 1 also shows a possible decision level required to authorize the operation after obtaining the final result.

Table 2 shows the reference alternatives in the form of the qualitative ordinances provided in each criterion. Each number represents an ordered risk level associated with the respective criterion. Subsequently, these performances will be

converted to numerical values, after the coding procedure is carried out. For more details, see Nascimento (2012).

For further understanding, category  $C_1$  (very high risk) is taken as an example. The fictitious reference alternative, that is, the most representative of the class, would be: a tactical night flight, lasting more than 6 hours; pilot with less than 500 hours of experience in the model and less than 500 hours of total experience; accomplishment of a task, except clarification; IMC, with loss of non-directional beacon (NDB); bingo of over 150 nautical miles; ceiling of 200 feet and maximum visibility of 0.5 nautical miles; waning moon and overcast (OVC); rough seas; period of aerial activity greater than 6 h and less than 12 h, and rest between periods of less than 8 h.

### 3.4. DEFINITION OF DISCRIMINATORY THRESHOLDS

The indifference threshold ( $q_j$ ) is the largest difference in performance in which the indifference situation is validated, in criterion  $g_j$ , between two alternatives  $a$  and  $a'$ , where  $q_j = g_j(a) - g_j(a')$ . Thus, comparisons are made on an equal basis between all levels of each criterion. If in any of them the indifference between levels is noticeable, the greater of them

will be the difference to be defined for  $q_j$ . In this study, the form of ordering the levels leads to a null  $q_j - q_j=0, j=1, 2, 3, \dots, 10$  —, because in the comparisons between the criteria levels, situations of indifference are not found.

As in  $q_j$ , the threshold of preference ( $p_j$ ) is the smallest difference in performance in which the situation of strict preference occurs, in criterion  $g_j$ , between two alternatives  $a$  and  $a'$ , where  $p_j = g_j(a) - g_j(a')$ .

Another definition to be clarified is the preference direction, which helps to inform the preferences of the decision-makers among all pairs of levels in the scale. You can have a direction of increasing or decreasing preference in a certain criterion. The first one portrays the situation in which preference grows when performance also increases, that is, the idea of the decision-maker is to maximize performance. The second one portrays the opposite situation, in which preference grows when performance decreases, that is, the decision-maker aims to minimize performance.

When dealing with risk, this study handles criteria with direction of decreasing preference. In other words, the decision-maker prefers to lower the performance, or, in this case, the risk, in order to maximize the preference. As for the scale,

**Table 1.** Definition of the risk categories.

	Categories			
	$C_1$	$C_2$	$C_3$	$C_4$
Risk level	Very high (not tolerable)	High (not tolerable)	Medium (tolerable)	Low (accepted)
Authorization required	Higher command	Ship's command	Person in charge of the shipboard detail	Commander of the aircraft

**Table 2.** Definition of reference alternatives.

$C_h$	Risk level	$b_h$	Criteria									
			$g_1$	$g_2$	$g_3$	$g_4$	$g_5$	$g_6$	$g_7$	$g_8$	$g_9$	$g_{10}$
$C_1$	Very high (not tolerable)	$b_1$	4	6	5	5	6	4	6	8	6	5
$C_2$	High (not tolerable)	$b_2$	3	4	4	4	5	3	4	6	4	4
$C_3$	Medium (tolerable)	$b_3$	2	2	2	2	3	2	3	4	3	3
$C_4$	Low (acceptable)	$b_4$	1	1	1	1	1	1	1	2	1	1

$C_h$ : risk categories;  $b_h$ : reference alternatives.

all criteria will be modeled according to a coding procedure. According to Martel and Roy (2006), the coding procedure allows obtaining an equivalent ordered range of preferences, in which the difference between two consecutive levels should maintain the meaning of the preference. Thus, all the criteria were modeled with a scale of 0 – lowest risk – to 100 – highest risk. Table 3 shows the definition of the thresholds.

### 3.5. DEFINITION OF CRITERIA WEIGHTS

In this study, the weight of the criteria was defined according to procedures observed in Figueira and Roy (2002). Table 4 shows the weights of the criteria obtained by the SRF software, an implementation of the aforementioned procedure and presented in Figueira and Roy (2002).

The names of the criteria are written in white cards, which are ordered from the most important criterion to the least important according to the perspective of decision-makers. It should be considered that some criteria might have the same importance. Then, the difference in importance of the successive

ordering levels obtained is expressed by the number of white cards introduced between the levels. It is understood that the number of white cards between two consecutive orderings is the difference of importance between criteria. If there are no white cards between the cards with the names of the criteria, it means that these criteria have the same importance. The  $z$ -value means how many times the last criterion is more important than the first.

Initially, it was defined with the decision-makers that there are three groups of *ex aequo* criteria. After ordering them, a white card unit was placed between them. This means that the same difference observed between the first and second ordering was observed between the second and third ordering. It was also defined that  $z=2$ , and thus, non-normalized and normalized weights were obtained.

### 3.6. DEFINITION OF VETO THRESHOLDS

Each operation performed by shipboard aircraft was considered as an alternative or subject to decision-making.

**Table 3.** Discriminatory thresholds.

Thresholds	Criteria									
	$g_1$	$g_2$	$g_3$	$g_4$	$g_5$	$g_6$	$g_7$	$g_8$	$g_9$	$g_{10}$
Indifference ( $q_i$ )	0	0	0	0	0	0	0	0	0	0
Preference ( $p_i$ )	20	15	15	15	15	20	15	12	15	15

**Table 4.** Definition of criteria weight ( $z=2$ ).

Criteria	Order	Number of white cards	Non-standard weights	Standard weights
$g_1$	1		1.00	0.06
$g_2$	1		1.00	0.06
$g_6$	1		1.00	0.06
		1		
$g_3$	2		1.50	0.10
$g_5$	2		1.50	0.10
$g_8$	2		1.50	0.10
		1		
$g_4$	3		2.00	0.13
$g_7$	3		2.00	0.13
$g_9$	3		2.00	0.13
$g_{10}$	3		2.00	0.13
Total		2	15.50	1.00

$z$ : how many times the criterion with higher value is more important than the criterion with lower value.

Each of these operations, denoted by  $a$ , were evaluated with the aforementioned multiple criteria method, and classified according to their associated risk.

In order to adjust and validate the multiple criteria model developed, 30 alternatives, that is, 30 operations, were defined along with the decision-makers in order to obtain the risk ratings for each one. The tasks with numbers 1–24 were obtained from the BN database. Those with numbers 25–30 are fictitious tasks created with the purpose of modeling the values of the veto thresholds.

In a compensatory risk classification, in which the risk calculated by a single criterion may influence the final risk classification, it is possible in some situations to have a low overall risk rating, despite the fact that the task was classified as very high risk in a given criterion analyzed in isolation. This is detrimental to the assessment, as this criterion may be decisive for the occurrence of an accident.

In order to resolve this discrepancy, veto thresholds were modeled for some criteria. Thus, if in a single criterion a particular alternative obtains a performance worthy of changing the risk classification of the whole operation, this criterion will exercise its veto power, aiding in the correct

classification of the task. Table 5 presents the restrictions imposed by the decision-makers.

### 3.7. CREDIBILITY LEVEL

The credibility level ( $\lambda$ ) is the minimum degree of credibility that is deemed necessary by decision-makers to validate the statement “ $a$  overcomes  $b$ ,” taking all criteria into account. Comparisons between the credibility index ( $\sigma$ ) obtained in the overcoming relationship and the  $\lambda$  chosen by the decision-maker are made successively. Since  $\sigma$  is the sum of the weights of the criteria in favor of the overcoming relationship, we can define  $\lambda$  as the sum of the weights of the minimum amount of criteria that the decision-maker intends to be in favor of the overcoming.

It is verified that the greater the  $\lambda$ , the more restrictive the model, because with a high  $\lambda$ , many criteria are needed in favor of the overcoming in order to consolidate it. For example, when choosing  $\lambda=0.70$ , at least 2 of the criteria with greater weight are needed in favor of overcoming, because if 3 of them are against – since the sum of their weights is  $\epsilon 0.39$  – the overcoming will not occur. Five possibilities with different levels of credibility were presented, and it was decided, then, that  $\lambda=0.65$  would be used.

**Table 5.** Description of the veto thresholds.

Criteria	Veto threshold	Veto description
$g_3$	80	Classifies the operation as having at least medium risk, if the difference between the evaluation of the operation and category $C_4$ is greater than or equal to 80
$g_4$	80	Classifies the operation as having at least medium risk, if the difference between the evaluation of the operation and category $C_4$ is greater than or equal to 80
$g_5$	70	Classifies the operation as having at least medium risk, if the difference between the evaluation of the operation and category $C_4$ is greater than or equal to 70
$g_7$	40	Classifies the operation as having at least high or medium risk, if the difference between the evaluation of the operation and category $C_3$ or $C_4$ is greater than or equal to 40, respectively
$g_9$	40	Classifies the operation as having at least high or medium risk, if the difference between the evaluation of the operation and the category $C_3$ or $C_4$ is greater than or equal to 40, respectively
$g_{10}$	40	Classifies the operation as having at least high or medium risk, if the difference between the evaluation of the operation and the category $C_3$ or $C_4$ is greater than or equal to 40, respectively

## 4. RESULTS AND DISCUSSION

The set of operations was evaluated in the light of the set of ten previously established criteria. The results of the evaluation are shown in Table 6. The credibility indexes of the overcoming relationships between the alternatives and the reference alternatives are shown in Table 7. These indexes were then compared with the  $\lambda$  chosen  $-0.65$  – in order to obtain the final results of the classification, which are presented in Table 8, in which they are confronted with the classifications given by the decision-makers.

It was observed in operations  $a_5$ ,  $a_6$ ,  $a_{11}$ , and  $a_{12}$  that the decision-makers minimized the risk classification. These alternatives obtained high performances in the criteria with greater veto power, that is, weights too high for the classification imposed by them. This made the model designate such alternatives at a risk level above that indicated by them. A risk perception problem in which the rationality of the model presents the solution and the explanation for the new classification.

In alternatives  $a_7$  and  $a_{23}$ , it was observed that the decision-makers were more rigorous than the risk classification model. These alternatives obtained low enough performances

**Table 6.** Performances of alternatives.

Alternative	Criteria									
	$g_1$	$g_2$	$g_3$	$g_4$	$g_5$	$g_6$	$g_7$	$g_8$	$g_9$	$g_{10}$
$a_1$	10	25	10	30	20	10	5	5	5	5
$a_2$	10	25	40	10	20	10	35	20	5	15
$a_3$	10	5	30	30	0	10	5	5	5	5
$a_4$	10	65	40	10	0	35	35	20	5	15
$a_5$	35	65	30	30	20	10	5	30	35	35
$a_6$	35	5	10	10	50	10	35	20	35	35
$a_7$	35	65	30	10	0	35	5	5	5	15
$a_8$	35	25	40	30	20	10	35	20	35	35
$a_9$	10	25	30	30	50	60	35	30	5	35
$a_{10}$	60	35	65	40	0	35	25	65	55	35
$a_{11}$	85	55	40	65	0	60	55	65	15	35
$a_{12}$	85	35	40	40	50	60	55	75	55	35
$a_{13}$	85	55	65	90	0	60	95	65	55	35
$a_{14}$	60	55	40	90	0	35	95	75	55	35
$a_{15}$	60	95	65	65	70	85	55	75	55	35
$a_{16}$	60	55	65	90	0	60	95	65	55	55
$a_{17}$	85	35	40	65	70	60	55	65	55	75
$a_{18}$	60	95	40	40	50	85	55	75	55	75
$a_{19}$	60	55	90	65	90	85	55	85	95	75
$a_{20}$	85	95	65	90	70	60	95	75	55	75
$a_{21}$	60	55	90	90	90	85	95	85	55	75
$a_{22}$	85	95	90	65	90	85	55	95	55	95
$a_{23}$	85	95	65	90	90	60	55	95	55	55
$a_{24}$	85	95	90	90	90	85	95	85	55	55
$a_{25}$	10	20	10	10	10	10	25	20	15	95
$a_{26}$	10	25	90	10	0	35	5	5	5	5
$a_{27}$	35	25	10	90	0	10	35	20	5	15
$a_{28}$	35	25	10	65	80	10	35	20	5	15
$a_{29}$	10	5	10	65	0	10	95	20	5	5
$a_{30}$	10	5	10	10	0	10	35	20	95	5

in the criteria with greater veto power to obtain a lower risk classification than that of the decision-makers.

Alternatives  $a_{25}$  to  $a_{30}$  were fictitious tasks designed to adjust the veto thresholds. Technically, there are situations in which the performance of an alternative in a single criterion can influence the entire risk classification of the task. For example, alternative  $a_{25}$ , despite presenting characteristics of a low risk task in the criteria  $g_1$  to  $g_9$ , obtained a very high-risk performance in criterion  $g_{10}$ . That is sufficient, according to technical criteria, for it to be classified as a high-risk task at a minimum. The model, using the veto thresholds, was able to reach the classification previously established by the decision-makers.

Table 9 presents a comparison between the categorization presented by the decision-makers and the classification delivered by the multiple criteria method. For the same  $\lambda = 0.65$  – a total of 73.3% of the tasks assigned to a single category (SC) were obtained, that is, 22 of the 30 alternatives. The set of reference alternatives fulfills the strict separability requirement, since  $\lambda^b=0.03$ .

The accuracy index I (ACR I) represents the proportion of designations in which ELECTRE TRI-C presented a single category as a response, with the same being chosen by the decision-maker, divided by the total number of alternatives ( $m=30$ ) or by the total number of tasks assigned to a single category ( $m=UC$ ). The type II accuracy

**Table 7.** Credibility indexes of the overcoming relationships after adjustments.

Alternative	$\sigma(a, b_h)$				$\sigma(b_h, a)$			
	$b_1$	$b_2$	$b_3$	$b_4$	$b_1$	$b_2$	$b_3$	$b_4$
$a_1$	1.00	1.00	1.00	0.74	0.00	0.00	0.02	0.81
$a_2$	1.00	1.00	0.93	0.64	0.00	0.00	0.16	1.00
$a_3$	1.00	1.00	1.00	0.77	0.00	0.00	0.02	0.75
$a_4$	1.00	0.96	0.87	0.65	0.00	0.00	0.18	0.93
$a_5$	1.00	0.96	0.94	0.13	0.00	0.00	0.63	1.00
$a_6$	1.00	1.00	0.93	0.24	0.00	0.00	0.55	1.00
$a_7$	1.00	0.96	0.94	0.72	0.00	0.00	0.07	0.83
$a_8$	1.00	1.00	0.93	0.04	0.00	0.00	0.74	1.00
$a_9$	1.00	1.00	0.87	0.07	0.00	0.00	0.73	1.00
$a_{10}$	1.00	1.00	0.48	0.00	0.00	0.00	0.81	0.93
$a_{11}$	1.00	0.94	0.39	0.00	0.00	0.00	0.77	0.93
$a_{12}$	1.00	0.86	0.21	0.00	0.00	0.58	1.00	1.00
$a_{13}$	1.00	0.00	0.00	0.00	0.00	0.00	0.90	0.93
$a_{14}$	1.00	0.00	0.00	0.00	0.00	0.00	0.90	0.93
$a_{15}$	1.00	0.80	0.06	0.00	0.00	0.87	1.00	1.00
$a_{16}$	1.00	0.00	0.00	0.00	0.00	0.00	0.90	0.93
$a_{17}$	1.00	0.81	0.00	0.00	0.00	0.84	1.00	1.00
$a_{18}$	1.00	0.67	0.00	0.00	0.00	0.67	1.00	1.00
$a_{19}$	1.00	0.00	0.00	0.00	0.00	1.00	1.00	1.00
$a_{20}$	1.00	0.00	0.00	0.00	0.00	1.00	1.00	1.00
$a_{21}$	1.00	0.00	0.00	0.00	0.00	1.00	1.00	1.00
$a_{22}$	0.79	0.00	0.00	0.00	0.00	1.00	1.00	1.00
$a_{23}$	0.92	0.55	0.00	0.00	0.00	1.00	1.00	1.00
$a_{24}$	0.93	0.00	0.00	0.00	0.00	1.00	1.00	1.00
$a_{25}$	0.87	0.00	0.00	0.00	0.00	0.00	0.20	1.00
$a_{26}$	1.00	0.90	0.90	0.00	0.00	0.00	0.02	0.75
$a_{27}$	1.00	0.87	0.87	0.00	0.00	0.00	0.22	0.93
$a_{28}$	1.00	0.93	0.77	0.00	0.00	0.00	0.37	1.00
$a_{29}$	1.00	0.00	0.00	0.00	0.00	0.00	0.06	0.85
$a_{30}$	1.00	0.00	0.00	0.00	0.00	0.00	0.10	0.85

$\sigma$ : credibility index;  $b_h$ : reference alternatives.

index (ACR II) represents the proportion of designations in which ELECTRE TRI-C presented a response equal to that of the decision-maker, divided by the total number of alternatives ( $m=30$ ).

The ACR I index, for  $m=30$ , was 53.3%, since 16 out of 30 alternatives presented a single category as response, the same one was chosen by the decision-maker. For  $m=SC$ , the ACR I index was 72.7%. The ACR II index was 80%, since 24 of the 30 alternatives were

designated in accordance with the one previously established by the decision-maker. These results were approved by the decision-makers, proving the capacity of the ELECTRE TRI-C method as an evaluation and operational risk analysis tool.

The results obtained with the multicriteria model and the classification determined by the decision makers were compared before using the methodology. The summary of designation results is summarized in Table 10.

**Table 8.** Results of designations after adjustments.

	Risk classification of the decision-makers	Risk classification of ELECTRE TRI-C		Risk classification of the decision-makers	Risk classification of ELECTRE TRI-C
$a_1$	Low	Low	$a_{16}$	High	High
$a_2$	Low	Low	$a_{17}$	High	High
$a_3$	Low	Low	$a_{18}$	High	High
$a_4$	Low	Low	$a_{19}$	Very high	Very high/high
$a_5$	Low	Medium	$a_{20}$	Very high	Very high/high
$a_6$	Low	Medium	$a_{21}$	Very high	Very high/high
$a_7$	Medium	Low	$a_{22}$	Very high	Very high/high
$a_8$	Medium	Medium	$a_{23}$	Very high	High
$a_9$	Medium	Medium	$a_{24}$	Very high	Very high/high
$a_{10}$	Medium	Medium	$a_{25}$	High	High/medium
$a_{11}$	Medium	High	$a_{26}$	Medium	Medium
$a_{12}$	Medium	High	$a_{27}$	Medium	Medium
$a_{13}$	High	High	$a_{28}$	Medium	Medium
$a_{14}$	High	High	$a_{29}$	High	High/medium
$a_{15}$	High	High	$a_{30}$	High	High/medium

**Table 9.** Results of the second designation of Electre Tri-C.

$\lambda$	$\lambda^b$	UC	ACR I		ACR II
			$m=30$	$m=UC$	$m=30$
0.65	0.03	22 (73.30%)	53.30%	72.70%	80.00%

ACR I: accuracy index I; ACR II: accuracy index II;  $\lambda$ : credibility level;  $\lambda^b$ : separability index; SC: single category; m: number of alternatives.

**Table 10.** Summary of the designation results.

$C_h$	Nature of the risk category	ELECTRE TRI-C ( $\lambda=0,65$ )	Decision-makers
$C_1$	Very high	0 (0.00%)	6 (20.00%)
$[C_1, C_2]$	Very high or high	5 (16.70%)	
$C_2$	High	9 (30.00%)	9 (30.00%)
$[C_2, C_3]$	High or Medium	3 (10.00%)	
$C_3$	Medium	8 (26.60%)	9 (30.00%)
$C_4$	Low	5 (16.67%)	6 (20.00%)
Total		30 (100.00%)	30 (100.00%)

$C_h$ : risk categories;  $\lambda$ : credibility level.

## 5. CONCLUSION

This study used a multiple criteria decision aiding method, aiming to improve the risk assessment process of a warship when operating with helicopters.

The risk assessment process is part of an even broader process, named the risk management process, in which, in addition to the evaluation, consisting of the identification, analysis and measurement of risks, we can list the establishment of a context, the monitoring and the review, communication and consultation and the treatment of risks as integral parts of the process as a whole.

In the BN, aviation safety management is focused on the risks that are inherent to the activities of the organization that relate to the aerial activity. The current focus is not only on the investigation of accidents or serious incidents, that is, on the consequences of deviations that cause accidents, but also on the organizational processes that create conditions for the occurrence of such deviations.

A multiple criteria method, called ELECTRE TRI-C, was chosen to be part of a risk assessment process of warship. This method became suitable for the accomplishment of this study mainly for two reasons: because it is a non-compensatory multiple criteria method and the risk categories are defined by a single reference alternative, which is the most representative of the class.

ELECTRE TRI-C was then used for the evaluation of operations that are normally carried out on board and

satisfactory results were obtained regarding the assessment of the overall risk present. The following are some of its strengths: the possibility of classifying the overall risk of the task as a function of high risk and the possibility of changing the attributes of the task classified as high risk before it is performed in order to work with acceptable risk levels.

Regarding its implementation, the method presented a total of 73.3% of the tasks assigned to a single category and an accuracy of 53.3%, so that the decision-makers agreed that some judgments as to the risk classification of tasks that were designated differently could be changed, and validated the new designation.

Thus, this article achieved its global objective, obtaining a methodology to support risk classification of operations with shipboard aircraft, using the ELECTRE TRI-C multiple criteria method.

After the previous steps, the data obtained are used to perform the classification of tasks provided by the decision-maker in order to validate the model. After adjustments made to find the preferences of the decision-maker, the model was considered valid, as it reached high accuracy, and the decision-maker was satisfied with the results obtained. It should be noted that each landing platform has its known precedent history. Thus, for each platform, a new modeling must be performed, taking into account the particularities of the platform and the preferences of the commanders.

## REFERENCES

BRASIL. Ministério da Defesa. Comando da Marinha. Diretoria Geral do Material da Marinha. DGMM-3010. *Manual de segurança de aviação*. 3. rev. Rio de Janeiro, 2011a.

DAGDEVIREN, M.; YÜKSEL, I. Developing a fuzzy Analytic Hierarchy Process (AHP) model for behavior-based safety management. *Information Sciences*. v. 178, p. 1717-1733, 2008.

DIAS, J.A.; FIGUEIRA, J.R.; ROY, B. ELECTRE TRI-C: a multiple criteria sorting method based on characteristic reference actions. *European Journal of Operational Research*, v. 204, p. 565-580, 2010.

FIGUEIRA, J.; ROY, B. Determining the weights of criteria in the ELECTRE type methods with a revised Simos' procedure. *European Journal of Operational Research*, v. 139, p. 317-326, 2002.

INTERNATIONAL CIVIL AVIATION ORGANIZATION. *DOC 9859-AN/474: safety management manual*. 3. ed. Montreal. 2013. 251 p.

JOHNSON, C. W.; KIRWAN, B.; LICU, A.; STASTNY, P. Recognition primed decision making and the organisational response to accidents: überlingen and the challenges of safety improvement in European air traffic management. *Safety Science*, v. 47, p. 853-872, 2009.

- LEE, W. K. Risk assessment modeling in aviation safety management. *Journal of Air Transport Management*, v. 12, p. 267-273, 2006.
- LIYOU, J. J. H.; TZENG, G. H.; CHANG, H. C. Airline safety measurement using a hybrid model. *Journal of Air Transport Management*, v. 13, p. 243-249, 2007.
- LIYOU, J. J. H.; YEN, L.; TZENG, G. H. Building an effective safety management system for airlines. *Journal of Air Transport Management*, v. 14, p. 20-26, 2008.
- MARTEL, J.; ROY, B. Analyse de la signification de diverses procédures d'agrégation multicritère. *INFOR*, v. 44, n. 3, p. 191-215, 2006.
- NASCIMENTO, L. F. *Modelo multicritério de apoio à decisão para classificação de risco em operações com aeronaves embarcadas*. 2012. 148 f. Dissertação (Mestrado em Engenharia Aeronáutica e Mecânica, área de Produção) - Instituto Tecnológico de Aeronáutica, São José dos Campos, SP. 2012.
- ROY, B. Decision aid today: What should we expect? In: GAL, T.; STEWART, T.; HANNE, T. *Multicriteria decision making: advances in MCDM models, algorithms, theory and applications*. Boston: Kluwer Academic, 1999. p. 1.1-1.35.
- SHYUR, H. L. A quantitative model for aviation safety risk assessment. *Computers & Industrial Engineering*, v. 54, p. 34-44, 2008.
- YU, W. *Aide multicritère à la décision dans la cadre de la problématique Du tri: concepts, méthodes et applications*. 1992. Thèse (Docteur en Informatique) - Université Paris-Dauphine, Paris.

# THE OPERATIONAL RISK MANAGEMENT APPLIED TO THE SCIENTIFIC DEVELOPMENT OF “THE BLUE AMAZON” – AMAZÔNIA AZUL

O gerenciamento do risco operacional aplicado ao desenvolvimento científico da Amazônia Azul

Guilherme Pires Black Pereira<sup>1</sup>

**Abstract:** Rather than anticipating risks and avoiding accidents, the operational risk management (ORM) tool, which can be easily used for consultation by any crew member, can be used as a source of information and operational knowledge, as it is crucial for the dissemination of know-how. This is very important to specific activities that require a high degree of technical knowledge. Owing to the continuous need for renewal of crew and the implementation of new technologies, it has become a necessity to add to the practical knowledge of innovation of technology, the expertise of the on board researchers to improve the process, thereby providing all interested parties with a functional tool which would have historic and statistic information. This tool also aims at increasing the maneuvering security, the ability to operate new equipments, and the development of new techniques. The application of this tool can, for instance, help in the information management related to the Amazônia Azul. This research was based on theoretical knowledge related to ORM and contextualized on the operational environment from DHN ships, based on experiences on board the Oceanographic Ship “Antares,” from 2011 to 2013. This article aims at demonstrating how risk management tools can be widely used in the research and naval activities of the Brazilian Navy, as they are already used by Navy Aviation, including on board aviation.

**Keywords:** Operational risk management. Knowledge management. Risks. Operational research. Security. Decision tool. Decision making process. Antares. Diretoria de Hidrografia e Navegação. Amazônia Azul.

**Resumo:** Mais do que antecipar riscos e prevenir acidentes, a ferramenta do Gerenciamento do Risco Operacional (GRO), de consulta simples e de fácil acesso a qualquer tripulante, pode ser utilizada como fonte de transmissão de informações e conhecimentos operacionais, contribuindo para a disseminação do *know-how* operativo, extremamente importante em atividades específicas, que requerem elevado grau de conhecimento técnico. Diante da necessidade da constante renovação de pessoal e da implementação de novas tecnologias, urge a importância de aproximar o conhecimento prático às inovações e evoluções tecnológicas, assimilando a *expertise* do pesquisador embarcado, que traz em sua bagagem acadêmica a vontade de inovar e melhorar os processos, provendo a todos os interessados uma ferramenta prática e de fácil registro histórico e estatístico. Essa ferramenta visa também ao incremento da segurança das manobras, à destreza de operação de novos equipamentos e ao desenvolvimento de técnicas inovadoras ou inéditas, em determinada atividade. A aplicação produtiva dessa ferramenta pode, por exemplo, auxiliar no gerenciamento do conhecimento sobre as atividades de pesquisa na Amazônia Azul. Tal pesquisa foi realizada com base nos conhecimentos teóricos relacionados ao GRO e contextualizados para o ambiente operacional dos Navios de Pesquisa da Diretoria de Hidrografia e Navegação (DHN), com base nas experiências vivenciadas a bordo do Navio Oceanográfico “Antares”, de 2011 a 2013. O objetivo deste artigo é demonstrar como as ferramentas de gerência de risco poderiam ser amplamente utilizadas nas atividades de pesquisa e de navios da Marinha do Brasil, da mesma forma como já são amplamente empregadas pela Aviação Naval, inclusive embarcada.

**Palavras-chave:** Gerenciamento do Risco Operacional. Gerência do conhecimento. Riscos. Pesquisa operacional. Segurança. Auxílio à decisão. Processo decisório. Antares. Diretoria de Hidrografia e Navegação. Amazônia Azul.

<sup>1</sup> Lieutenant, Brazilian Navy Officer graduated from Naval School in 2006 and specialized in Hydrography at the Directorate of Hydrography and Navigation in 2010. Responsible for Planning and Control Section of Operational Oceanography Division of the *Centro de Hidrografia da Marinha* - Rio de Janeiro, RJ-Brazil. E-mail: gblack.mb@gmail.com

## 1. INTRODUCTION

Operational risk management (ORM) is not only a process used to identify and control risks. According to its description in item 4.2 of the published standards *Aviation Safety Manual: DGMM-3010*, from the General Directorate of Material of the Navy (DGMM), “lack of resources limits our ability to neutralize the risks and also the level of losses that we are willing to accept. Managing operational risk is to conciliate these two limitations with the benefits to be obtained from an operation” (MARINHA DO BRASIL, 2011, p. 4-1).

The use of ORM in Brazilian Navy ships can provide to Commanders, Operations Heads, and Division Heads, a useful tool to reduce the risks inherent in operations. This process establishes a specific methodology for the anticipation of hazards and for the assessment of risks with greater precision, and includes the following steps: hazards identification; risk assessment; risk decision; the implementation of risk control measures; and supervision over the effectiveness of such measures.

Currently, the knowledge about ORM in the Brazilian Navy is disseminated by internal orders of the military organization, and by rules issued by the Force Commands, which are generally associated with aviation security. This can be found in a broad and normative format when consulting the chapter 4 of the DGMM-3010 publication (MARINHA DO BRASIL, 2011), which addresses the subject; however, it is inserted in the aviation security context. The wide use of this tool by the Naval Aviation aims at mitigating the risks inherent in air operations, which has greatly contributed to the safety of these operations, including the naval and surface means.

We want to demonstrate that this process can also be widely applied in light of knowledge management, promoting their effective application in other activities and military organizations. In this study, ORM applicability is specially exemplified in research activities conducted by the ships of the Directorate of Hydrography and Navigation (DHN) and, in general, by the ships of the Brazilian Navy.

When considered from the perspective of knowledge management, the implementation of ORM through the constant updating of its matrix, as well as for the prevention of accidents and mitigation of risk, enables the constant evolution and formal transferring of operational knowledge, improvement, and

the development of new techniques. In addition, it encourages the systematic search for improvement of procedures, with consequent reduced risks to personnel and equipment. Therefore, such an instrument contributes to the success of a military-naval operation or research commission, most commonly known under the Directorate of Hydrography of the Navy as Hydrographic Survey (HS).

The implementation on ships of all procedures included in the technical instructions (TIs) and in the internal rules in force – accompanied by the observation of precedents – provides the Hydrographer Official and corporals specialized in hydrography and navigation (HN) with technical support in the execution of research activities, and enables the execution of procedures with excellence and safety, with the identification, analysis, and quantification of the risks involved. This process subsidizes the creation of new methods and the enhancement of those already established, aiming at keeping up to date with the technological development of the equipment and its interoperability with other systems.

Therefore, protecting the integrity of the crew, researchers, and scientific equipment is prioritized, and the updating of internal rules and TIs in force on the DHN is subsidized. In addition, the risk management worksheet can be considered as an important tool to support decisions (SD) for the captains of vessels, when far from land and under poor availability of communication. This worksheet supports a safer decision as it enables the commander to concentrate on the most important factors or on those that might put at risk the safety of the crew that is on board and under his responsibility.

Similarly, ORM provides documentary support for the solution of conflicts of the binomial planning-execution, concerning the established, but not accomplished goals for data collection during research activities, especially those in the course of long operations at sea or of long duration commissions. In these situations, justifying the necessary adjustments to the initial planning during the execution of the work is imperative.

Under this approach, ORM is an important facilitator, as its regular and continuous adoption enables the historical record of the experiences on board ships, with a focus on operational knowledge management. Specifically in the case of research ships, in addition to the crew, students, teachers,

and doctors (researchers) of the scientific community are also important contributors, as their participation greatly contributes to the technical and operational development of the research activities of the Brazilian Navy.

## 2. THEORETICAL BACKGROUND

The Brazilian Navy is evolving every day and aims at a promising future for the institution and its members. In this context, the project for the creation of the Second Squad is an example. Its optimistic focus on overcoming challenges and perseverance to comply with the guidelines issued by the Federal Government, by means of the publication of the National Defense Strategy (NDE), promotes a relentless search for excellence in fulfilling its constitutional mission.

Other challenges to be overcome are related to physical factors of the area of operations, the northern coast. The marine environment of that area is strongly influenced by the discharge of significant amounts of fresh water and sediments coming from the Amazon River, which change the characteristics of the aquatic environment and affect the performance of the sonars. The fact that the area is located in the equatorial region imposes particular climatic conditions that provide a special feature to the environment, directly influencing the propagation of electromagnetic waves, and therefore interfering in the detection and communications disciplines. The region has peculiar bathymetric characteristics, presenting small depths up to quite significant distances from the shore. These and other characteristics will require study and experimentation to adapt the equipment, the means, techniques, tactics, men, that is, the Naval Force, to the new environment and new operating conditions. The experience accumulated over the several decades that the Brazilian Navy has been operating in the region through their District Forces will contribute to overcome this challenge. (BRASIL, 2010, p. 74)

As valuable as the technological updating is the learning from the experiences obtained during the operations, including those carried out in partnership with other navies, as they provide a significant improvement in the scientific and technological development of our country. The words of His Excellency, Rear Admiral José Renato de Oliveira, in his Order of the Day alluding to the Operations Day demonstrate the concern of the Brazilian Navy with “doing well”:

The date of August 19, which is chosen annually to celebrate operations day, invariably leads us to the beginnings of Evolution Squadron, and today, after 130 years since its creation, we can see how we evolved operationally. Throughout this journey, we operated a variety of naval means, from where we learned valuable lessons, and also learned a lot from the allied navies. These aspects have enabled us to try our own paths in the development of operational procedures, doctrines, and local technologies. (OLIVEIRA, 2014, p. 1)

Deeply investigating the Brazilian Continental Shelf, our Blue Amazon, is critical to the country’s development. Expanding knowledge about biodiversity and understanding the conditions under which it occurs, enables us to conduct further studies about the still unknown marine life, and to facilitate the mapping of biological communities, and living beings which inhabit in its vertical column or along their slopes, when these communities and their inhabitants are also favored by the constant kinematics of sediments clearly identified on the seabed slope.

Studying and identifying the environment where such biodiversity is possible and correlating it with the physicochemical parameters collected from seawater, which are processed and analyzed by research vessels, helps us to understand how these conditions contribute to life and to the concentration of primary and secondary organisms. This may practically represent, for example, facilitation and guidance of fishing activities on our coast based on scientific studies. This is the science in favor of the development of care for human needs.

Then, why do we need to collect data on the abyssal plains and on the mountain ranges that arise abruptly in

the ocean? The study on the impact of these formations in the displacement of ocean water in its different layers, and on its association to the masses of water moving over the globe, helps us to deepen the knowledge about the marine currents. Therefore, its effects along the Brazilian coasts are possible to be identified – on the transport of sediment and nutrients to shallower water. Consequently, understanding the phenomena related to coastal engineering and the creation or extinction of beaches is also possible. Such data could also be used in the prevention and analysis of natural phenomena originated in the ocean and with great potential for affecting the continent.

To understand the benefits of implementation of the ORM, it is also important to know the reasoning and the importance of the activities. The risks of the research activity, for example, are mostly derived from the use of the platform “ship,” and not from the activities themselves. This platform is already an environment that involves risks (with significant potential for accidents) intrinsic to the activities. Each class and each type of ships have peculiarities of operation which depends on its structural characteristics, the arrangement of propulsion and auxiliary machinery, the dimensions of the superstructure and side height, among others. The research vessels, in particular, usually have several dedicated support equipment, such as electromechanical winches, hydraulic winches fitted with steel cables, A-frames, transducers installed in the hull, portable transducers, profilers, and vertical and horizontal seawater samplers.

### 3. OPERATIONAL RISK MANAGEMENT IMPLEMENTATION IN RESEARCH ACTIVITIES

According to the Annex C of the standards issued by the Brazilian Navy (2011), *Aviation Safety Manual: DGMM-3010*, the implementation of the risk worksheet facilitates the measurement of the total risk identified in an operation. This measurement provides many benefits such as

- Preservation of the experience and knowledge accumulated by a certain organization with respect to risk factors for the performance of its tasks, in an objective and accessible manner;

- standardization of procedures for the risk assessment in a certain group;
- identification of the lowest risk course of action if a mission can be accomplished in different ways;
- the Commander can establish numerical ranges considered acceptable to the overall risk of an operation; therefore, even in his or her absence, the criteria for risk acceptance may be observed;
- the Commander can define the hierarchical level required to authorize a certain operation, depending on the level of risk involved;
- the modification of operation’s parameters, whose total risk is within the range defined as unacceptable, to lower the risk to an acceptable value;
- the definition of specific procedures for each risk range if sufficient information is not available in advance to estimate the risk of an operation.

Crews of the Brazilian Navy vessels usually have an intuitive perception of the risk of a certain activity, regardless of any mathematical process. However, the accuracy of this perception decreases as the circumstances related to the activities cease to be predominantly favorable or unfavorable – or if experimental or unprecedented activities are performed by a certain team, for example, the operation of a new equipment. The importance of conducting briefing and debriefing of events urges, which should be conducted by someone with more operational experience, not necessarily by the person on board with the best technical expertise. Safety and operating procedures to be adopted should be indicated carefully, in addition to identifying the most significant failures of implementation, comparing the expected results with the actual results in the debrief session.

In this context, it is worth remembering the phrase by Leonardo da Vinci (2014): “the experience never fails, just our opinions fail to expect from experience what it is not able to offer.”

If knowledge on certain activity is low or null, the difficulty of identifying risks is significant. This may compromise the safety of personnel and material involved. Therefore, the highest possible level of care, seriousness, and concentration of the team involved are required, both in planning and execution.

As Da Vinci (2014) also stated, “first comes the dedication, then the skills.”

The knowledge acquired by using manuals, photos, and videos, assists the development of know-how and can never be abandoned. This is often the only source of knowledge available, and is very important for the implementation of innovations and improvements in the techniques available. Inexperience cannot be considered a problem; it should be considered a challenge, not being a decisive factor to justify any kind of failure. Consequently, to carefully follow all recommendations and safety procedures of the equipment in the manufacturer's manual is important, avoiding, whenever possible, to concentrate just in the summary, which is named "tips" and is produced by another team of other organization (military or civilian).

Da Vinci (2014) also warns, "those who are enchanted with practice without science are like helmsmen entering the ship without rudder or compass, never being sure of their destiny."

Along with the supporting equipment, many other devices are installed and used, enabling the collection and analysis of environmental data, which serve as a source for various academic studies and the enhancement of scientific knowledge. This data feed the National Bank of Oceanographic Data (in Portuguese, *Banco Nacional de Dados Oceanográficos* – BNDO), under the management of the Hydrographic Center of the Navy (in Portuguese, *Centro de Hidrografia da Marinha* – CHM). Access to BNDO is granted to all stakeholders in the scientific community upon request. These studies support knowledge acquisition, and development of various studies in Brazil and around the world, and are of vital importance for the development of civil and military scientific research and for the society as a whole.

The analysis of data collected in the ocean enhances the knowledge about natural phenomena, contextualizing them in the evolution of society. This analysis is intended to improve the quality of life, when it is correlated with the new knowledge and other previous studies, and therefore enhances, demonstrates, expands, or even challenges old theories by encouraging the elaboration of new questions and inquiries. As a beneficial consequence, there is the emergence of new theories, which cyclically generate the need for new jobs and further studies, demonstrating the truth of the popular maxim "knowledge generates knowledge."

Then, how important it is to launch and constantly maintain meteoceanographic buoys along our coast? Studying the interactions between the ocean and the atmosphere is

relevant to understand certain phenomena, such as the climate change in certain regions of interest. Brazil, for example, has several sources for such studies. One of those sources is the network of meteoceanographic buoys of type "ATLAS," which collects and continuously disseminates, including via satellite, several meteorological and oceanographic data, and constantly shares updated and important local ocean data to various scientific studies. These studies are in general scarce and their use are inputs for numerical models of environmental forecasting, enabling its continuous improvement and making it more efficient and reliable for the members of aircraft crews.

In Brazil, the "PIRATA" Project (Network of Fixed Buoys in the Tropical Atlantic for Forecast and Research) is implemented by means of cooperation between scientific institutions in Brazil, France, and the United States of America. Currently, it is composed of 8 buoys of ATLAS type, of which 5 from the original design and 3 from its southwestern extension – have their maintenance under the responsibility of Brazil, and counts with representatives from DHN and the National Institute for Space Research (in Portuguese, *Instituto Nacional de Pesquisas Espaciais* – INPE). During "PIRATA" commission held regularly by a DHN ship, eight moored buoys of ATLAS type are collected, fixed, and launched. These buoys, which compose the current network under Brazilian responsibility, are intended to maintain the operation of the program in the country and to collect oceanographic and meteorological data in the region between Vitória (ES) and the parallel of 15° N and the meridian 030° W and 038° W.

Another example of commission of Brazilian Navy ships that carry out research activities is the National Buoy Program (in Portuguese, *Programa Nacional de Boias* – PNBOIA), which aims at collecting oceanographic and meteorological data in the Atlantic, by means of a network of meteoceanographic drifting and moored buoys. This project supports the meteorological and oceanographic activities in Brazil, favoring the sectors of Civil Defense, Agriculture, Coastal Zone, Living Resources, Satellite Data Validation, Petroleum and Environmental Industries, Offshore Facilities, Ports & Coastal Structures, Maritime Transport, Navigation Safety and Safeguarding Human Life at Sea.

By means of PNBOIA commissions, various means of DHN are employed with the purpose of contributing to

the Brazilian scientific community, obtaining and providing meteorological and oceanographic data in ocean areas of interest for Brazil, launching meteoceanographic moored buoys. The examples mentioned earlier clarify the importance of carrying out research activities in the Blue Amazon, because the area includes interests of study for the scientific and strategic-military communities of the Brazilian Navy, in addition to the need to comply with various international cooperation agreements to which Brazil is a signatory, with quality and responsibility. Especially in these days, in which topics such as “Blue Amazon,” “Nuclear Technology Transfer,” and “Pre-Salt Exploration” have great visibility and strategic importance, the Brazilian Navy gained prominent role in the Armed Forces and proved to be essential for the development of the country.

In many activities carried out on ships, provided that there is an appropriate technical-operative knowledge, it would be relatively easy to illustrate a practical application of the ORM as a source of knowledge and risk and safety management methods. However simple the activity may be, if the potential impact of this risk is significant or catastrophic, it cannot be disregarded, especially because the ship platform represent itself a recognized risk.

### 3.1. EXAMPLE: IDENTIFICATION OF RISKFACTORS IN OCEANOGRAPHIC ACTIVITIES

Following the description in Chapter 4 of the *Aviation Safety Manual: DGMM-3010* (MARINHA DO BRASIL, 2011), the ORM matrix is a table whose entries are pre-defined levels of severity and probability, from which a standardized classification of the risk, or the risk assessment code (RAC), is obtained.

The application of the level “Adequate ORM” is suggested in the following example, owing to the clarity of the match to the description of such level, as stated in item 4.6.2 of this publication:

Consists of the complete application of the steps of ORM process, the planning of an operation, or the evaluation of a procedure. For the hazard identification and analysis of possible control measures, deliberate ORM is based on individual experience and on “brainstorm” techniques, which is why it

benefits from the teamwork. It is used in planning future operations, review of standard operating procedures, training or maintenance, and development of damage control plans or emergency responses. (MARINHA DO BRASIL, 2011, p. 7-8)

As a result of observation experiences aboard the oceanographic ship “Antares” in the period from 2011 to 2013, two distinct moments of ocean data collection activity were identified, in which it was possible to identify some limiting factors, and therefore of potential risk, whose correct observation greatly contributed to the operation safety and for efficient data collection. Among all relevant aspects observed, the following aspects stand out:

#### Releases and gatherings in water at CTD-Rosette:

- in bad weather conditions and rough seas;
- wrong positioning of the vessel relative to the drift (maneuver);
- inexperience of the service staff;
- failure of the winch;
- failure of the A-Frame;
- shocks in the ship’s side owing to rolling and pitching movements;
- momentary fuel suppression in hydraulic;
- improper handling and operation of the winch;
- rupture of steel or electromechanical cable.

#### While in the oceanographic station (with the equipment near the surface, remaining totally submerged):

- abrupt change in environmental conditions;
- inexperience of the service staff;
- failure in the winch;
- improper handling and operation of the winch;
- need to reposition the ship owing to the large variation of the angle between the bow and the direction of the ship’s drift (maneuver);
- need to reposition the ship owing to the approach of “curious vessels” and fishing vessels (maneuver);
- performing stations in large slope regions (shock against mountain range);
- steel cable or electromechanical wound around the propeller of the ship;

- friction of steel or electromechanical cable on the side or sharp parts of the ship (for example, rollers);
- rupture of steel or electromechanical cable.

#### 4. EXPECTED RESULTS

The identification of key risk factors is essential in risk management. The list of such risk factors should be continuously updated, based on personal and team's experience. The parameters related to the severity and the probability of occurrence of these factors must be kept update, preferably during or shortly after the debriefing, thus enabling to further describe the occurrence of such events. Similarly to the Hazards Reports (widely known in Aviation), these parameters also enable the identification of the need to promote possible improvements in the implementation or planning activities, because in addition to serving as historical data, it also facilitates statistical monitoring of the occurrences of the same kind or related to the same activity.

Based on Chapter 2 of the *Aviation Safety Manual: DGMM-3010* (MARINHA DO BRAZIL, 2011), it is observed that the implementation of ORM process requires organization and allocation of responsibilities. Some basic guidelines, already adapted to the research activities carried out by those responsible for ships, could be followed to guide the implementation of the ORM. They are the following:

- knowledge certification to all the crew about the Commander criteria for the acceptance of the operational risk;
- identification and exposure, during the briefing session, of all identified or known hazards, proposing control measures to mitigate them to the Commander;
- ongoing advice to the decision of the Commander with respect to the full or partial compliance with the information extracted from the ORM Matrix, informing the Immediately Superior Commander (IMSUPCOM) on the conditions observed in the field (in the sea) and the need for adjustments to the initial planning, owing to eventual restrictions or observation of significant risks, aiming at the success of the commission as a whole;
- debriefing and proposition of new procedures, internal rules and TIs, based on historical and statistical records of the ORM matrix spreadsheets, concisely and justifiably;
- maintenance of checklists of updated procedures and operating manuals;
- compliance with the Planned Maintenance System (PMS) of research and operating equipment;
- performing statistical control of use of ORM spreadsheets that could be consolidated in Hydrographic Surveys reports (HSR) or End of Commission Reports (ECR), in order to identify trends that may contribute to future accidents;
- planning and implementation of educational and motivational activities to leverage a organizational culture focused at preventing accidents and encouraging the intellectual production and the proper recording of experiences and knowledge acquired during the commissions.

ORM process, from the perspective of knowledge management and applied to research activities and ships of the Brazilian Navy, directly meets several objectives, guidelines, and strategic actions of the scientific and technological development, as well as of the 2014 publication *Standards for Scientific and Technological Development Plan and Innovation of the Brazilian Navy* (PDCTM): SecCTM-611, from the Secretariat of Science, Technology, and Innovation of the Navy (SecCTM) (MARINHA DO BRASIL, 2014).

#### 5. CONCLUSION

The elaboration of this study can be considered a contribution that meets specifically the subparagraphs b and c cited below concerning actions for strategic objective No. 5 of the PDCTM: SecCTM-611:

- produce and publish scientific papers;
- communicate the activities of Science, Technology, and Innovation (ST&I) that the Brazilian Navy develops, in academia and institutions in general, associating them with the socioeconomic development and the defense of the country.

Similarly, it can be said that the suggestion of implementation of the ORM in research activities and ships of the Brazilian Navy, already widely used by the Research and Prevention of Aeronautical Accidents (in Portuguese, *Serviço de Investigação*

e *Prevenção de Acidentes Aeronáuticos – SIPAAerM*), subordinate to the Directorate of Navy Aeronautics (DAerM), has been providing significant progress and success in preventing accidents and supporting Naval Aviation Safety, which also contributes to meeting the strategic guidelines disseminated by SecCTM in PDCTM as described in Chapter 1, item 1.3 of the PDCTM: SecCTM-611. Among all the guidelines, the following should be highlighted:

- dissemination of opportunities of implementation of core technologies and key technologies of areas of interest, with emphasis on some specific fields (such as operating environment, human performance and health, and decision-making);
- search for technical consultancy and partnerships in basic and applied research in the academic sector for staff qualification, with emphasis on some areas of interest (such as operating environment, human performance and decision-making);

- identification and implementation of mechanisms for knowledge management aimed at preserving the intellectual capital of ST&I;
- implementation of strategic management model, keeping track of the lessons learned for the benefit of institutional learning;
- systematic use of assessment measures by means of performance indicators of research and scientific and technological development activities in the SCTMB;
- implementation of a Knowledge Management System.

The higher and more amplifying is the exchange of experiences and knowledge, the greater the promotion of a safety culture, and the smaller the chances of errors or failures. Therefore, it will be easier to identify potential risks and there will be better incentive to historical and statistical recording of ORM's capability to manage useful knowledge in naval operations.

## REFERENCES

BRASIL, Capitão-de-Mar-e-Guerra Flávio Macedo. *A descentralização da Área-Rio e a criação da segunda esquadra: perspectivas e desafios a serem vencidos*. Rio de Janeiro: Escola de Guerra Naval, 2010. Disponível em: <<http://www.egn.mar.mil.br/arquivos/biblioteca/monografias/cpem/2010/017%20CMG%20BRASIL.pdf>>. Acesso em: 18 ago. 2014.

DA VINCI, Leonardo. *Frases de Leonardo da Vinci*. Disponível em: <[http://pensador.uol.com.br/frases\\_de\\_leonardo\\_da\\_vinci/](http://pensador.uol.com.br/frases_de_leonardo_da_vinci/)>. Acesso em: 27 ago. 2014.

MARINHA DO BRASIL. *Manual de Segurança da Aviação: DGMM-3010*. 3.ª rev. Rio de Janeiro: Diretoria-Geral do Material da Marinha, 2011.

MARINHA DO BRASIL. *Normas para o Plano de Desenvolvimento Científico-Tecnológico e de Inovação da Marinha (PDCTM): SecCTM-611*. Brasília: Secretaria de Ciência, Tecnologia e Inovação da Marinha, 2014.

OLIVEIRA, Contra-Almirante José Renato de. Ordem do Dia n.º 2/2104 do Comando da Força de Superfície, alusiva ao Dia das Operações. *Boletim de Ordens e Notícias Especial*, Niterói, n. 578, 2014.

# INVESTIGATION ON STRUCTURAL RESPONSE, INDUCED BY SLAMMING EFFECT IN A MONOHULL SEMIDISPLACEMENT SHIP BY MEANS OF SUBSTRUCTURED MODELING

Investigação sobre a resposta estrutural, induzida pela batida de proa em embarcação monocasco de semiplaneio, por meio de modelagem por subestruturação

Fabio da Rocha Alonso<sup>1</sup>, Waldir Terra Pinto<sup>2</sup>

**Abstract:** This study aims at investigating the local structural response of a monohull, semidisplacement vessel which has been subject to an increase in maximum speed from 18 to 27 knots. First, the entire hull's secondary structure is modelled by space frame finite elements and the structural response is simulated for different constraints conditions. The aim of this analysis is to identify a combination of constraints that lead to critical internal forces. Second, the hull's tertiary structure is modelled, at the impact region, by shell finite elements. This local substructure is then merged with the frame element model of the vessel, which represents the remaining structures of the vessel. Simulations are carried out with this model for critical boundary conditions. The assessment of the parametric analysis is based on DNV recommendations, which adopt Von Mises as failure criteria and suggest expressions for slamming pressure and contact area estimations. Simulations are carried out by commercial finite element software ABAQUS. The results suggest the efficiency of the computational model adopted and indicate that the hull under study presents structural elements with plastic deformations in areas adjacent to impact and stern regions, when submitted to bow thruster induced efforts.

**Keywords:** Substructures. Slamming effect. Monohull semi displacement vessel. Structural

**Resumo:** O presente trabalho busca realizar uma análise estrutural do casco de uma embarcação submetida a uma carga estática majorada da pressão de *slamming*, por meio de um estudo de caso em que uma embarcação monocasco, em regime de semiplaneio, tem sua velocidade máxima aumentada de 18 para 27 nós. A análise estrutural é realizada por meio da modelagem computacional do casco em elementos de pórtico 3D, simulando a estrutura secundária, conectada a subestruturas que simulam a estrutura terciária na região de impacto e anteparas, por meio de modelagem com elementos finitos de casca. Uma carga de *slamming* é, então, aplicada na região de impacto, sendo que os parâmetros de avaliação das análises, bem como a definição da pressão de *slamming*, basearam-se nos critérios de validação estabelecidos pela Sociedade Classificadora DNV, que define o critério de Von Mises como critério de falha. O comportamento estrutural estático dos modelos foi obtido utilizando o Método de Elementos Finitos, auxiliado pelo *software* comercial ABAQUS. Os resultados apontam para a eficiência do modelo computacional adotado e indicam que o casco em estudo apresenta elementos estruturais com deformações plásticas em zonas adjacentes às regiões de impacto e de popa, quando submetido aos esforços induzidos pela batida de proa.

**Palavras-chave:** Subestruturação. Efeito de *slamming*. Embarcações monocasco de semiplaneio. Análise estrutural. Von Mises.

**1.** Mechanical Engineer. Master in Ocean Engineering. Military Technology Engineer, Naval Station of Rio Grande - Rio Grande, RS - Brazil. E-mail: fabio.alonso@marinha.mil.br

**2.** PhD in Ocean Engineering. Associate Professor at *Universidade Federal do Rio Grande* - Rio Grande, RS - Brazil. E-mail: waldir.pinto@gmail.com

## 1. INTRODUCTION

The search for the modernization of the propulsion system of high-speed vessels by replacing its motorization normally entails new speeds higher than the values defined in the original designs. Therefore, new values of hydrodynamic stress over the hull of the vessel will appear, which depend on the type of hull geometry and the vessel's hydrodynamic regime. According to Bertran (2000), slamming-induced stresses are usually much higher than the pressure field variation owing to the passage of the wave along the hull of the vessel, and they have the potential to cause vessel structure failure as a result of the high magnitude of the local loads and the vibrations induced by the impact of the hull, which can lead to material fatigue.

According to Santos (2011), slamming-induced stresses are the impact forces caused by the sea waves hitting the hull, and the impact forces owing to the reentry of the bow in the sea, being a frequent effect in small, very rigid boats, which reach high speeds. According to Lewis (1998) and Mansour and Liu (2008), slamming-induced stresses can cause structural damage in the lower region of the vessel, where the greatest pressure impact occurs. This may include the creation of bulging and folding of the vessel's internal plates and structures — from its deformations —, and material failure may occur.

Therefore, verifying if high-speed vessels will support hydrodynamic loading conditions after a modernization project that will result in new speed limits is very important to prevent any structural damage to the hull and guarantee the safety of navigation.

Aiming at enhancing the knowledge about the effect of slamming on monohull vessels with a semidisplacement type, as well as its consequences on the structure of the hull of vessels to be modernized, we opted for a case study of the modernization of the propulsion system of the Navy Patrol and Policing (LPPN) boat Miraguaia, which belongs to the Brazilian Navy. This is a high-speed craft of the PCF (Patrol Craft Fast) Mark II class, whose hull has semidisplacement characteristics. It has a V-shape in the bow, being twisted to a fairly flat U-shaped stern (Figure 1), and straight lines represent the back of the vessel associated with a wide, vertical transom (Figure 2). All plating from the hull, deck, bulkheads, and other

structural elements of the vessel are made of 5086 H 321 aluminum alloy.

Table 1 shows some of the main characteristics of the LPPN Miraguaia's design.

The vessel will serve as a model for carrying out a computational analysis aiming at obtaining the structural response of the vessel's hull in relation to the stresses imposed by slamming on structural elements of the hull, due to the replacement of

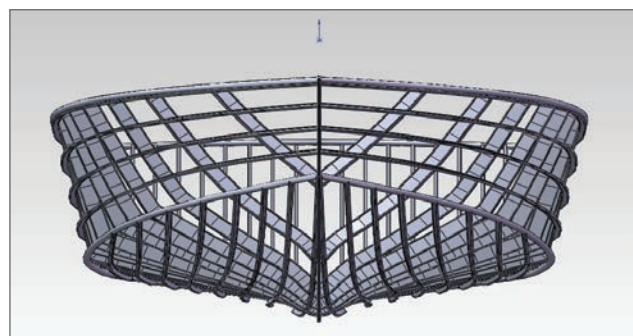


**Figure 1.** Navy Patrol and Policing (LPPN) boat Miraguaia - cage profile.



**Figure 2.** Navy Patrol and Policing (LPPN) boat Miraguaia - “transom”-type stern and straight lines at the rear.

**Table 1.** Main design features of the Miraguaia Navy Patrol and Policing.

Length (L)	15.24 m
Length of waterline (Ls)	13.8 m
Entrance (B)	4 m
Draft loaded AV (front)	0.73 m
Draft loaded AR (rear)	1.3 m
Displacement loaded	16 t
Pontal (D)	1.5837 m
Maximum Design Speed	18 knots
Hull Fabrication Material and Structure	Al 5086 H321
Propulsion	2 GM 8V-71 engines, 315 HP

the two GM 8 V 71, 315 HP engines for two Volvo Penta D9, 575 HP engines, after which it is estimated that the maximum design speed of 18 knots will be raised to a maximum speed of 27 knots.

This study aimed at developing a computational analysis method to verify the structural response of a mono-hull vessel operating in the semidisplacement mode, when subjected to the stresses generated by the impact of slamming, by means of a computational modeling process analysis, using the substructuring technique. In this model, the impact regions and bulkheads are modeled at the tertiary level by means of finite hull elements, and the remainder of the vessel is modeled at the secondary level by means of finite spatial portico elements.

The main concern of the structural analysis is to evaluate possible damages to the structure caused by the impact of the re-entry of the hull's bow on the water surface, where the loads are estimated based on the recommendation of the classification society Det Norske Veritas (DNV), and the structural analysis is carried out by the substructuring technique.

## 2. CRITERIA ANALYSIS

The development of the structural analysis consisted in the elaboration of computational models, through the Finite Element Method — and supported by commercial software ABAQUS.

The resistance limits imposed on the ABAQUS software, in order for it to develop the analysis processing, are defined according to the acceptance criteria cited in the DNV rules and standards – Structures, Equipment\_Hull Structural Design, Aluminium Alloy, July 2012 –, which states that the equivalent tension for vessels constructed of aluminum alloy can be defined as shown in Equation 1:

$$\sigma_e = 180f_1(\text{N/mm}^2) \quad (1)$$

With factor  $f_1$ , being defined according to Equation 2:

$$f_1 = \frac{\sigma_f}{240} \quad (2)$$

Where:

$\sigma_f$  is the limit of aluminum's elasticity, and is equal to 206.842 MPa.

Therefore,

$$f_1 = 0,861$$

$$\sigma_e = 153,13 \text{ Mpa}$$

According to Neves (2004), slamming occurs in the region of the hull located between 20 and 25% of the length of the vessel's front. Therefore, the application of the slamming loading to the hull under study is defined as the region surrounding the transverse frame 4, thus becoming 21% of the length of the vessel's front, as shown in Figure 3.

As an analysis criterion, the hypothesis that the slamming pressure will be decomposed into a force that will act on the points interconnecting the longitudinal frame with transverse frame 4 was considered.

### 2.1. DETERMINING SLAMMING FORCE AND PRESSURE

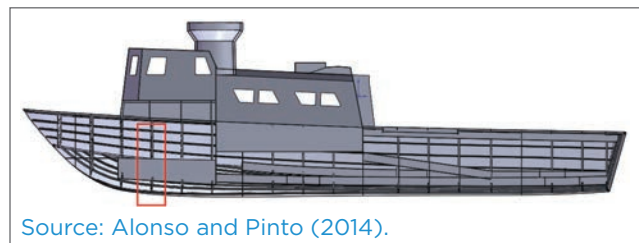
According to DNV (DNV, 2012), the project's slamming pressure value is obtained through Equations 3 to 5. These equations are defined as bottom slamming pressure ( $P_{sl}$ ), lateral slamming pressure ( $P'_{sl}$ ) and sea pressure ( $p$ ), for loading below the waterline, respectively.

For:

$$\left( \frac{U_0}{\sqrt{L}} \right) \geq 3$$

The pressure is given by the formula:

$$P_{sl} = 1,3k_t \left( \frac{\Delta}{nA} \right)^{0,3} T_0^{0,7} \frac{50 - \beta_x}{50 - \beta_{cg}} a_{cg} \quad (3)$$



Source: Alonso and Pinto (2014).

**Figure 3.** Location of transverse frame 4.

$$P'_{sl} = \frac{0,7C_L C_H}{A^{0,3}} \left( 0,6 + \frac{0,4U}{\sqrt{L}} \sin \gamma \sin \alpha + \right) \quad (4)$$

$$\frac{2,1a_0}{C_B} \sqrt{\frac{0,4U}{\sqrt{L}} \left( 0,6 \cos \alpha \left( \frac{x}{L} - 0,4 \right) \right)^2}$$

$$p = a_i \left[ 10b_o + \left( k_s - 1,5 \frac{b_o}{T} \right) C_w \right] \quad (5)$$

Where:

$n$  = number of hulls;

$A$  = project's loading area in  $m^2$ ;

$a_0$  = acceleration parameter;

$a_c$  = load distribution factor;

$x$  = distance, in m, from the stern to the position considered;

$T_0$  = draft in  $L/2$ , in m, in the normal operation condition in normal operating condition at service speed;

$C_H$  = correction factor for loading point above the water line;

$\Delta$  = displacement, in tonnes, of salt water through the project's draft;

$\beta_\xi$  = deadrise angle (in degrees) in the transversal section considered;

$K_l$  = longitudinal distribution factor;

$C_B$  = block coefficient;

$C_w$  = wave coefficient;

$\beta_{\chi_{BG}}$  = deadrise angle in the longitudinal center of gravity (LCG);

$h_0$  = vertical distance (in meters) from the water line to the loading point;

$\alpha$  = angle of water line entry of the loading region (transverse plane of transverse frame 4);

$K_s$  = sea load distribution factor;

$C_L$  = correction factor for boat length.

Table 2 summarizes the values obtained from the pressures acting on the vessel's hull; it is possible to observe that the sea

**Table 2.** Values of the pressures acting on the hull.

Pressure acting	kN/m <sup>2</sup>
$P_{sl}$	31.80
$P'_{sl}$	13.98
$p$	41.67

pressure value corresponds to the highest pressure value acting on the hull, which is the value assigned for the loading of the slamming.

To determine the force resulting from the slamming pressure applied on the impact region, some hypotheses were adopted:

- The slamming pressure applied is considered an increased static load, determined according to rules established by the classification society DNV;
- The area of application of the slamming pressure at each edge of the vessel is distributed in the polygon formed by two adjacent transverse frames, keel, and knuckle in the region of transverse frame 4 (AUGUSTO, 2007), as shown in Figure 4, where PS and QR represent, respectively, the distance between keel and cantilever, and PQ/2 and SR/2 represent the distance between transverse frames.

Once the mentioned hypotheses were defined, the slamming force ( $F_{sl}$ ) was calculated with the following data:

Slamming pressure ( $p$ ) = 41670 N/m<sup>2</sup>

Total area of the load distribution polygon ( $A_{DC}$ ) = 1.216 m<sup>2</sup>

$F_{sl}$  = 50,670.72 N

### 3. CONSTRUCTION OF COMPUTATIONAL MODELS FOR NUMERICAL ANALYSIS

The so-called “substructured” model is modeled based on the model constructed with 3D portico elements, defined by

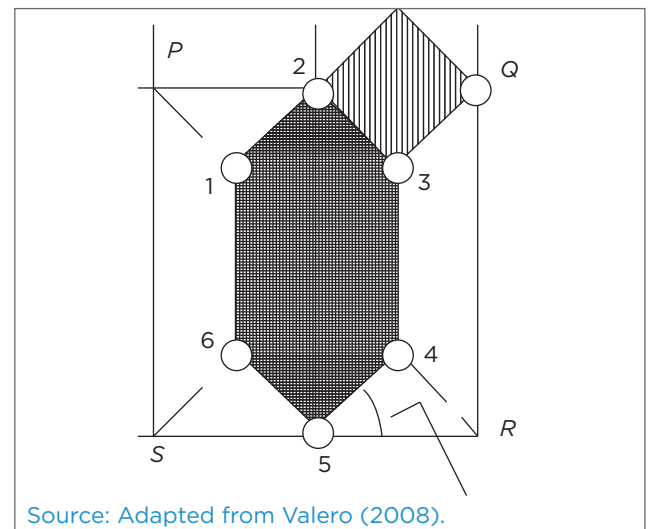


**Figure 4.** Distribution of loads in the structure.

the coordinates of the interconnection points between transverse frames, longitudinal frames, and bulkheads; a spatial sketch is created with these interconnection points joined by wire elements (Figure 5).

According to Orozco (2009) and Augusto (2007), and in compliance with DNV (2012) rules and standards, reinforced panels can be analyzed with the application of the simple beam theory, when the concept of cooperating plate is used for the flange of the profiles of the secondary structure, next to the hull plate.

The calculation for determining the final values of the effective width for the flange of the cooperating plate was performed as determined by DNV.

The effective width of the flange is determined by Equation 6:

$$b_e = C \times b_f \quad (m) \quad (6)$$

Where:

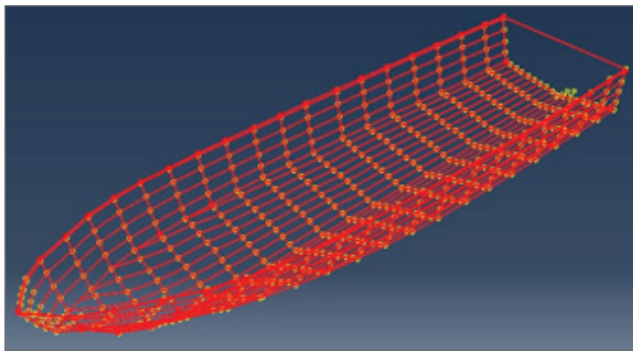


Figure 5. Plan of 3D lines - Space model in wires.

$b_e$  = effective width of the profile flange for the cooperating plate;

$b_f$  = Width of the load range. According to DNV, for common beam systems,  $b = 0.5$ ;

$(l_1 + l_2)$ , in which  $l_1$  and  $l_2$  are the gaps between beam supports within the frame;

$C$  = a constant defined by DNV.

Thus, the type I profiles, which determine the cross sections of the transverse frames and longitudinal frames, have their respective lower flanges dimensioned according to the cooperating plate principle, depending on the effective width (Figure 6). However, according to DNV, the effective width of the cooperating plate flange must not be less than the width of the free flange. Therefore, we have the value of the cooperating plate of the profile I of the transverse frames, which is equal to the value of the profile flap.

As substructures, two independent parts, named “sub\_hull\_bow” and “sub\_bulkheads”, were created, which simulate the impact regions and the watertight bulkheads of the vessel, respectively.

The substructure part sub\_hull\_bow refers to the modeling of the vessel’s hull region. The region is limited by transverse frame 3 on the front and by transverse frame 6 on the rear. For the modeling of the substructure sub\_hull\_bow, the reference points used were those of the delimited region, to be later interconnected by wires, limiting the hull regions between the structural elements existing in the modeled region. After the construction of the base structure of the

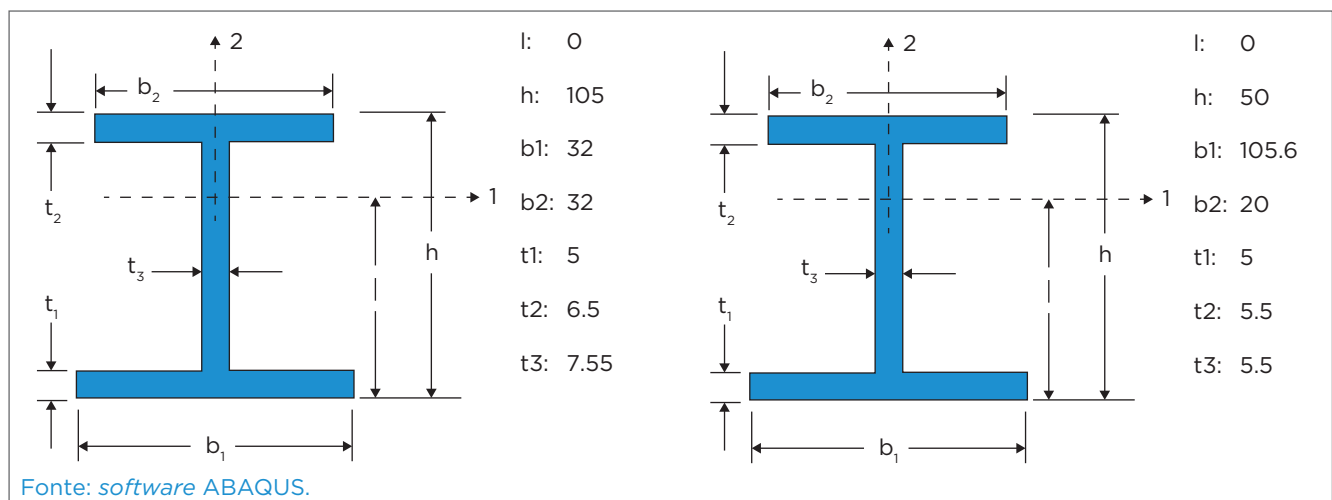


Figure 6. Contributing plate. Left view: I profile of the transverse frames. Right view: profile I of the longitudinal frames. Source: ABAQUS software.

hull region, the shell for this region is modeled (Figure 7), with 5086 H321 aluminum alloy and 5 mm thick.

The modeling of the substructure sub\_bulkheads used the same modeling principle as substructure sub\_hull\_bow, based on the coordinates of the interconnecting points between transverse frames and spacers, which delimit bulkheads 1, 2, 3, 4, and stern (Figure 8). The material properties of the bulkheads are the same as those assigned to the hull shell.

### 3.1. VALIDATION OF THE MESH FOR THE MODELS

The size of the mesh element of the base model was defined as determined by the classification society DNV in the DNV\_High Speed\_Design Principles\_Design Loads rulebook, which specifies that the size of the element can be assigned to the equal size of the measure between reinforcements. Therefore, since the measurement between reinforcements for the transverse frames is equal to the measurement of spacing between consecutive longitudinal frames – that

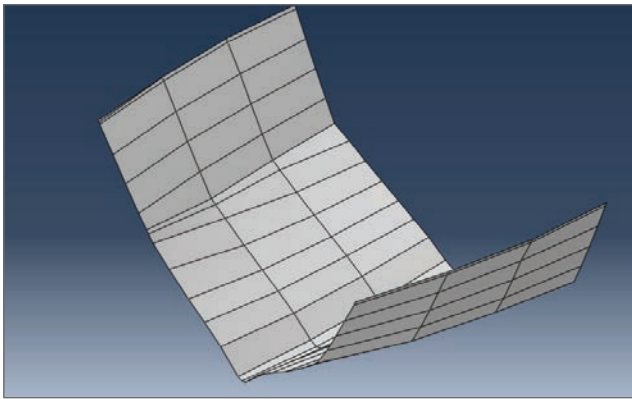


Figure 7. Substructure sub\_hull\_bow.

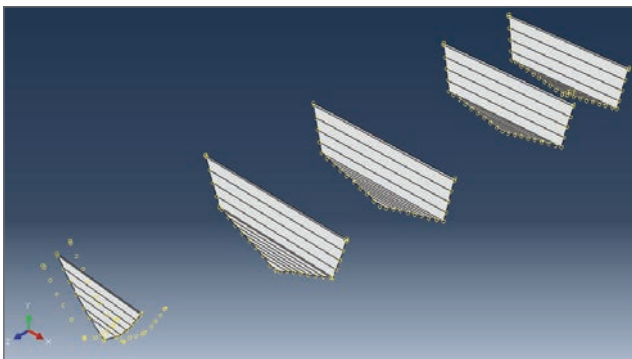


Figure 8. Substructure bulkheads.

is, 200 mm –, then this value was determined as the size of the beam element.

The element defined for the model was a Timoshenko (flexible shear), three-dimensional, linear 2-node beam element.

The meshes of the sub\_hull\_bow and sub\_bulkheads substructure models, assigned in the ABAQUS software with plate elements, were validated in comparison to an analytical calculation method, so that they could guarantee the reliability of the presented results. To this end, it was determined that the validation of the numerical method would be conducted by comparison to the maximum deflection criteria of a fully set rectangular plate, as established by Timoshenko and Woinowsky-Krieger (1959).

For this analysis, we verified the maximum deflection displacement in the geometric center of a plate with dimensions 800x200x0.005 mm, set in its four edges, thus representing a plate, which refers to the tertiary structure of the Miraguaia speedboat, and is located between two transverse frames and two longitudinal frames, both geometrically consecutive.

#### 3.1.1. Analytical calculation for fully set plate deflection

For the analytical calculation of the deflection in fully set plates, a 200 mm wide, 5086 H321 aluminum alloy (a), 800 mm long (b) and 5 mm high (h) plate was used as the model, over which a load of 1,000 N/m<sup>2</sup> is evenly distributed over the surface of the plate, which is set at all four edges.

For the plate under study, the b/a ratio equals 4. According to Timoshenko and Woinowsky-Krieger (1959), we have the maximum deflection at the geometric center of the plate (where  $x=y=0$ ), for this case, as shown Equation 7:

$$w_{x=y=0} = 0,0026 \cdot \frac{q \cdot a^4}{D} \quad (7)$$

Therefore, for the plate under study, we have:

$$w_{x=y=0} = 5.0122 \times 10^{-6} \text{ m}$$

#### 3.1.2. Numerical calculation for the fully set plate, using ABAQUS.

Considering that the computational model of the hull structure and its substructures were modeled directly in the ABAQUS software, the modeling of the plate was done using the same generation resources of the other models, such as reference points, wires, and plate.

The ABAQUS library element suggested for processing was the three-dimensional quadrilateral 4-node plate, tension/displacement, with six-degree-freedom-per-node, and reduced integration, named S4R (Figure 9).

For the analyzes performed in the ABAQUS processing module, a 5086 H321 aluminum alloy plate was considered, with characteristics and dimensions similar to that used to perform the analytical calculation. The loading and contour conditions applied to the plate are 1,000 N/m<sup>2</sup> and set at the four edges, respectively.

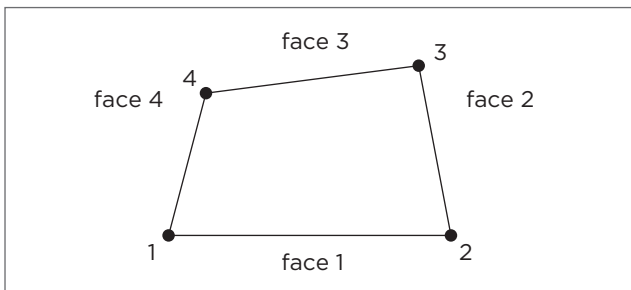


**Figure 9.** Shell element, 4 knots (S4R) – Source: ABAQUS’ Manual.

**Table 3.** Mesh test - Shell element.

Element Size	Maximum deflection (mm) ABAQUS	Maximum deflection (mm) - Analytical calculation	% Errors
50	0.03898	0.05012	22.23
40	0.03941		21.37
30	0.04486		10.49
<b>20</b>	<b>0.04883</b>		<b>2.59</b>
15	0.04904		2.15
10	0.0503		-0.36

Table 3 shows the results obtained for six different sizes for the plate elements used, as well as the percentage error of the numerical result in relation to the analytical result.

It is observed in Table 3 that the size-10 plate element is the one that presents the best result when compared to the analytical method. However, the elements with sizes 15 and 20 present error values in relation to the analytical results equal to 2.15 and 2.59%, respectively, which are acceptable values to validate the mesh, as a function of the gain in the decrease of the computational work, when the validated mesh migrate to the more complex model. Then, taking into account the computational gain, it was defined that the validated mesh is element size 20.

### 3.2. DEFINING THE MESH OF THE UNSTRUCTURED MODEL

Table 4 shows the meshes and element types assigned to each part of the model, and Figures 10 to 12 illustrate the final meshes assigned to the parts of the substructured model.

The connection of the substructures models to the base model occurs through the interaction of these, through the connectivity of the coincident nodes at the interconnecting points between the stringer and transverse frames 3 to 6 of the STRUCTURE model with the matching nodes at the same points of the sub\_hull\_bow model. With the substructure sub\_bulkheads, connectivity is applied to the matching nodes at the interconnection points between the longitudinal frames, bulkheads 1 to 4, and stern.

This connectivity between the parts of the model occurs through welding-type connectors, which enables the connection between two nodes in the space, providing a total connection between these nodes, aligning their directions on the three local axes; and the connectors suggested by the

**Table 4.** Final mesh of the substructured model.

Model	Elements			Final mesh		
	Type	Size	No. nodes	Denomination	Quantity of elements	Quantity of nodes
Structure	Beam	200	2	B31	2.570	2.061
Sub_hull_bow	Hull	20	4	S4R	30.021	30.399
Sub_bulkheads	Hull	20	4	S4R	51.670	53.227

ABAQUS software, used in the modeling, are CONN 3D 2 type, as shown in Figure 13.

Figure 14 shows the interaction of the substructures with the base model through the solder-type connectors.

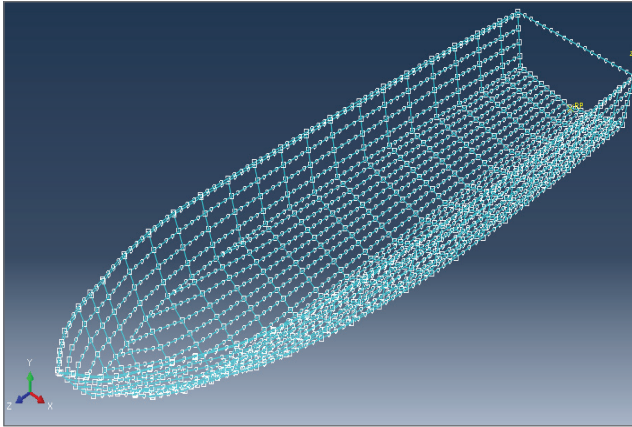


**Figure 10.** Mesh of the substructured model. Structure part.

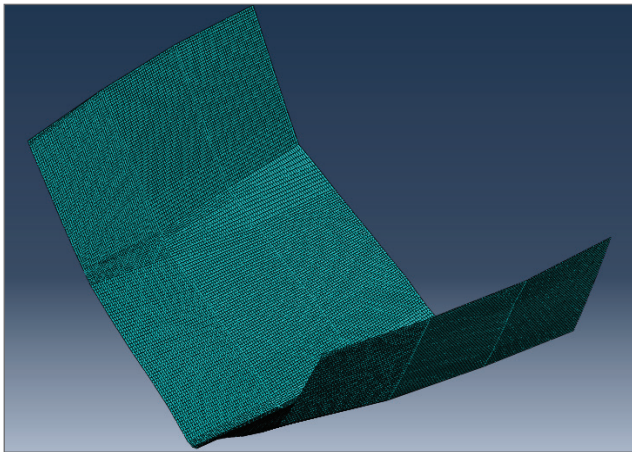


**Figure 11.** Mesh of the substructured model. Sub\_casco\_proa part.

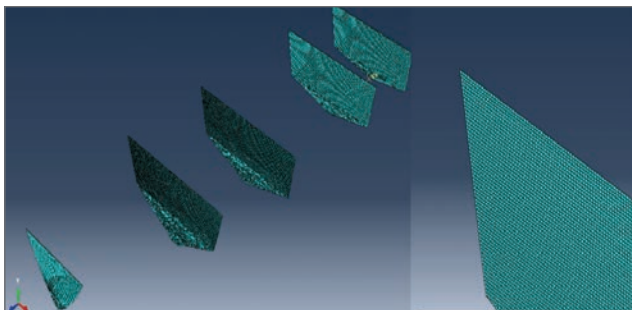


**Figure 12.** Mesh of the substructured model. Left view: mesh of the sub\_bulkheads part. Right view: detail of the mesh on bulkhead 3.

### 3.3. LOADING CONDITION FOR THE UNSTRUCTURED MODEL

In order to simulate the loading imposed by the slamming pressure in the impact region, the hypothesis adopted was that the slamming pressure of  $p = 41.673 \text{ kPa}$  is decomposed into slamming force, being applied simultaneously on the interconnection points between the bottom and transverse frame 4 and on the knots of the meshes created, referring to these points. Therefore, the slamming force ( $F_{sl}$ ) will be applied in a concentrated manner to the 15 knots contemplating the connections between the bottom longitudinals and transverse frames 4, with a force value of  $3,378,048 \text{ N}$  per node.

### 3.4. BINDING CONDITION FOR THE UNSTRUCTURED MODEL

The binding conditions imposed on the substructured model were defined based on the results obtained from the structural response analysis of the stucture\_hull model. Three hypotheses were then attributed to boundary conditions that attempt to simulate a biding occurrence when slamming at the surface of the sea

- Condition 1: all interlocking nodes between the longitudinal frames and the stern transverse frame will be labeled, allowing

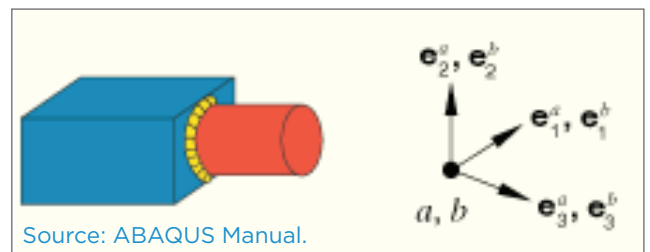


**Figure 13.** Solder-type connector.a

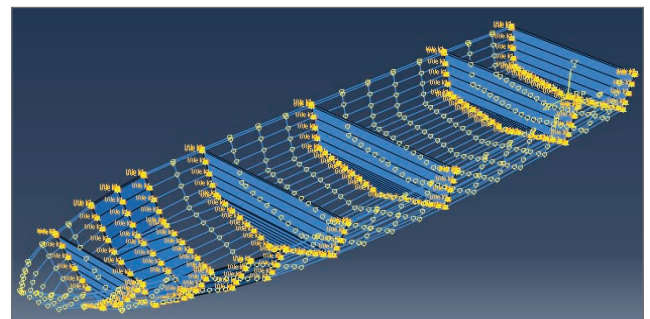


**Figure 14.** Substructured model. Solder-type connectors.

the rotational movement of the structural relative to the stern, simulating the reaction response to the bow thrust.

- Condition 2: all interlocking nodes between the longitudinal frames and the stern transverse frame will be set, not allowing rotational movement of the structure relative to the stern.
- Condition 3: is based on the labeling of interlocking nodes between longitudinal frames and the stern transverse frame, associated to another set labeled points of interconnection

between transverse frame and longitudinal frames, and this set is variable in each analysis, with the bonding condition of the stern transverse frame remaining, as well as the loading condition in the transverse frame 4.

After the loading conditions, the bonding and the mesh of the structure\_hull were defined, the analyses were processed, varying the binding conditions, as previously described. Table 5 shows the results obtained in the simulations and, as can be

**Table 5.** Results of the analysis of the structure model.

Contour condition	Stress Von Mises (MPa)		Deformation	
	Value	Element	Value	Element
Condition 1				
stern_labeled	446.3000	2211	0.002847	1285
Condition 2				
stern_set	360.4000	2614	0.004481	2626
Condition 3				
stern/cav15	293.9000	202	0.003392	1292
stern/cav14	257.9000	22	0.002766	1289
stern/ant4	277.9000	67	0.002405	1293
stern/cav13	261.6000	71	0.002327	1297
stern/cav12	229.1000	74	0.002248	1307
stern/cav11	218.9000	78	0.002202	1508
stern/cav10	196.8000	82	0.002034	1512
stern/ant3	181.1000	86	0.001961	1516
stern/cav9	158.3000	90	0.001927	1520
stern/cav8	135.1000	94	0.001881	1524
stern/cav7	114.8000	635	0.001547	1628
stern/ant2	124.0000	103	0.001152	645
stern/cav6	111.8000	2584	0.001025	1333
stern/cav5	74.5600	2580	0.000634	645
stern/cav3	51.2800	2559	0.000560	645
stern/cav2	54.5100	2559	0.000588	645
stern/ant1	54.0300	2559	0.000596	645
stern/cav1	53.8800	2559	0.000590	645
stern/bow	154.2000	2021	0.001040	2124

observed in condition 3, the variation of the position of the second labeled bond does not add any more requirements to the bonds imposed in conditions 1 and 2, in which the nodes of the longitudinal frames and stern transverse frame are labeled and set, respectively.

Figure 15 shows a comparative graph between the Von Mises tension values obtained in the analyses carried out in the ABAQUS software and the tension limit value of 153.13 MPa, as specified by the DNV, represented by the blue line in the graph, in which it is possible to verify that the bonding condition of the interconnection points between sills and stern transverse frames is the most requested condition, and therefore it is adopted as a condition of bonding for the substructured model.

#### 4. RESULTS OBTAINED IN THE STATIC ANALYSIS OF THE SUBSTRUCTURED MODEL

Figure 16 shows the distribution of tensions along the structure using a graphical model in which structural elements with tension values close or equal to the threshold tension of 153.13 MPa are

presented as elements with reddish tones. Structural elements with tension values higher than the threshold tension are represented by the white color. This graphic model aims at facilitating the identification of the location of the elements with requests with tension limit values equal to or greater than the threshold tension of 153.13 MPa along the structure.

When observing Figure 16, it can be noticed that the maximum tension is located at the upper edge, next to the bonding point, with a value equal to 716.41 MPa. Considering that the bonding condition is hypothetical, and that the element requested by the maximum stress is the profile of the edge of the hull, we chose to discard such a request.

Other tension regions with higher tension than the limit stress and which is established in accordance with DNV are easily identified, and some of these requested elements are located at the edge of the vessel, that is, in non-watertight areas of the hull, and therefore will be neglected.

However, the graphical model shows the existence of structural elements with a tension above the limit level, located in the knuckle timber next to the stern transverse frame, in the lateral longitudinal frames between transverse frames 14 and 13, and between transverse frames 6 and 7, as shown in Figures 17 and 18.

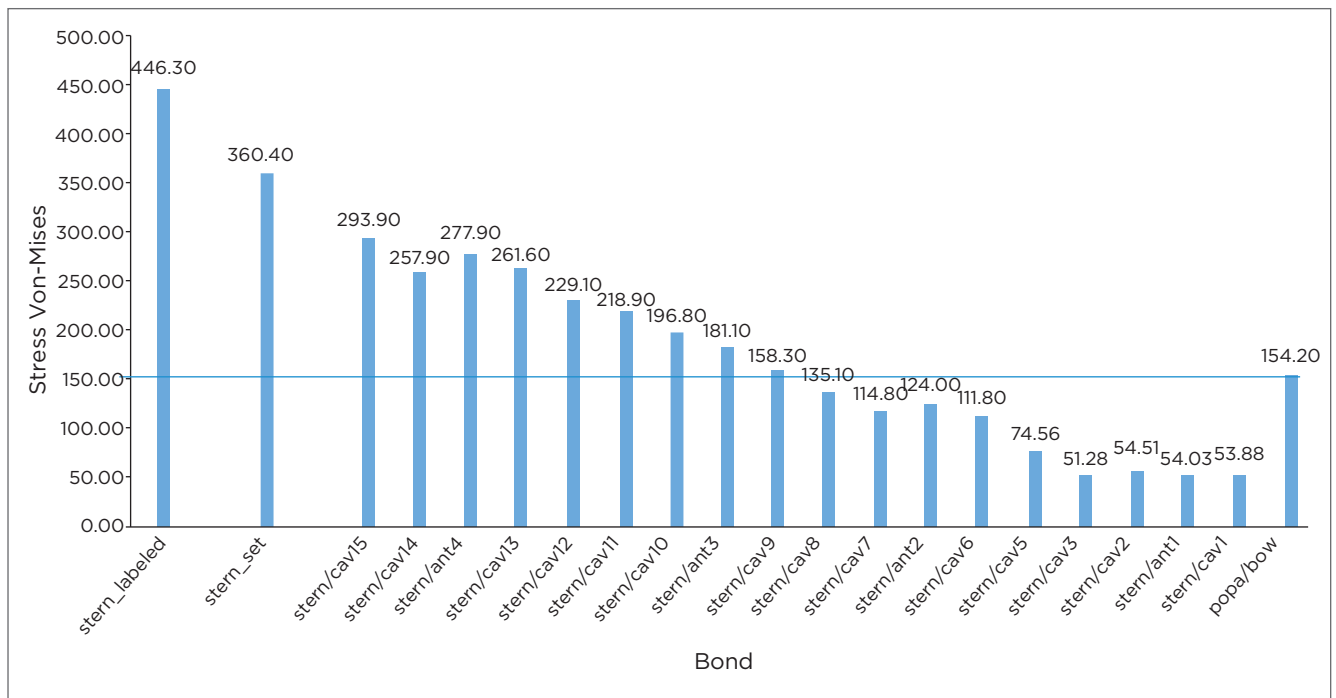


Figure 15. Von Misses stress x bonds.

Table 6 shows the values of the tensions that exceed the preset limit value of 153.13 MPa in the stern and impact regions, as shown in Figures 17 and 18.

#### 4.1. DISCUSSION AND SYNTHESIS OF RESULTS

Table 7 shows the deviation in the tension values of the other elements requested with critical tension values above the limit of 153.13 MPa, and in relation to the value of the material flow limit, which, in the case is 206.82 MPa.

## 5. CONCLUSIONS

The modeling process using the substructuring of impact regions and bulkheads — with finite shell elements, with finite shell elements, simulating the plating units connected to the vessel's hull modeled in finite elements of space porticos — is of great value for the structural analysis of small high-speed vessels, as it enables the verification of the local effects in the impact region, as well as the visualization of the distribution of the load along the structure of the vessel's hull, through the transmission of tensions along its structural

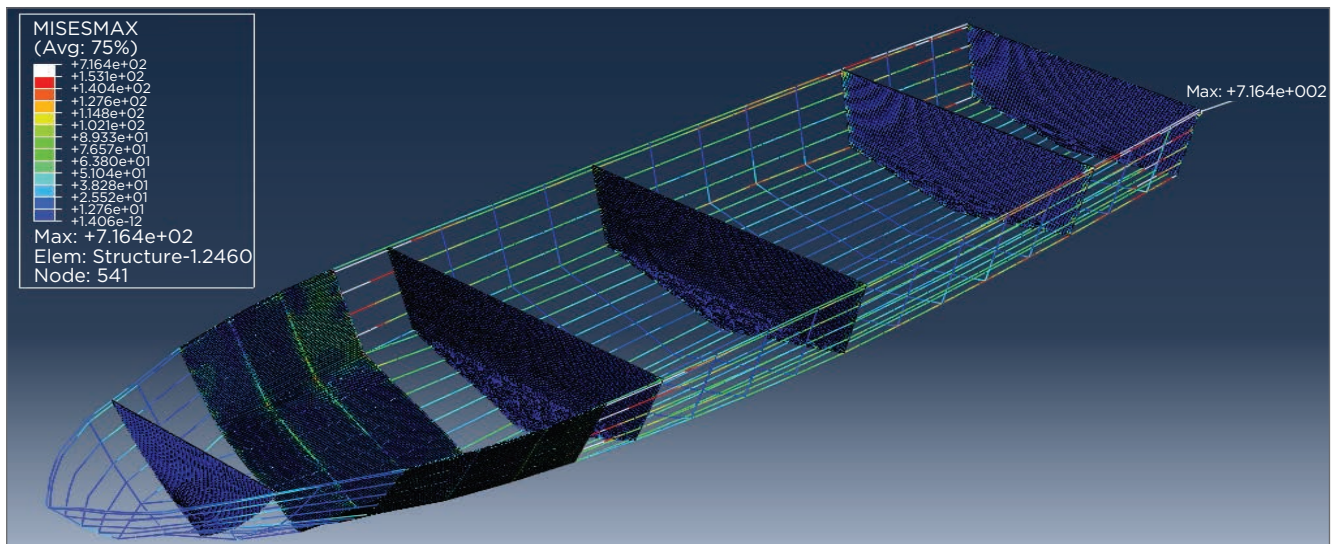


Figure 16. Tension distribution on the structure.

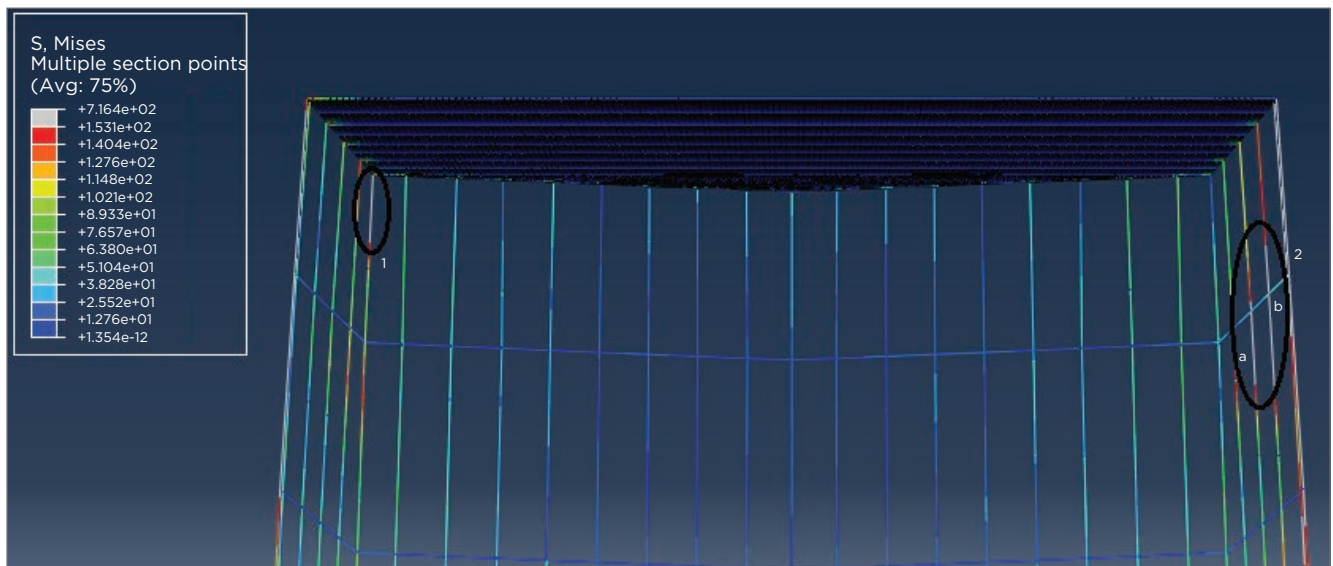


Figure 17. Details of critical tensions acting on the stern region.

elements; this is due to the connectivity of the substructure to the base structure.

In other binding systems applied in local impact analysis, such as the impact region (ALONSO AND PINTO, 2014; SANTOS, 2011), it is not possible to obtain this global tension distribution response, being limited only to the delimited region between the sets. However, with the applied method, it is possible to observe the existence of mesh elements located outside the impact region in the tension distribution along the substructured model, with tension values close to or higher

**Table 6.** Critical tensions on stern and impact regions.

Hull region	Longitudinal frame requested	Tension value (MPa)	Element type
Stern	1	215.35	B31
	2 a	211.29	B31
	2 b	246.85	B31
Impact	1	182.81	B31
	2	197.79	B31

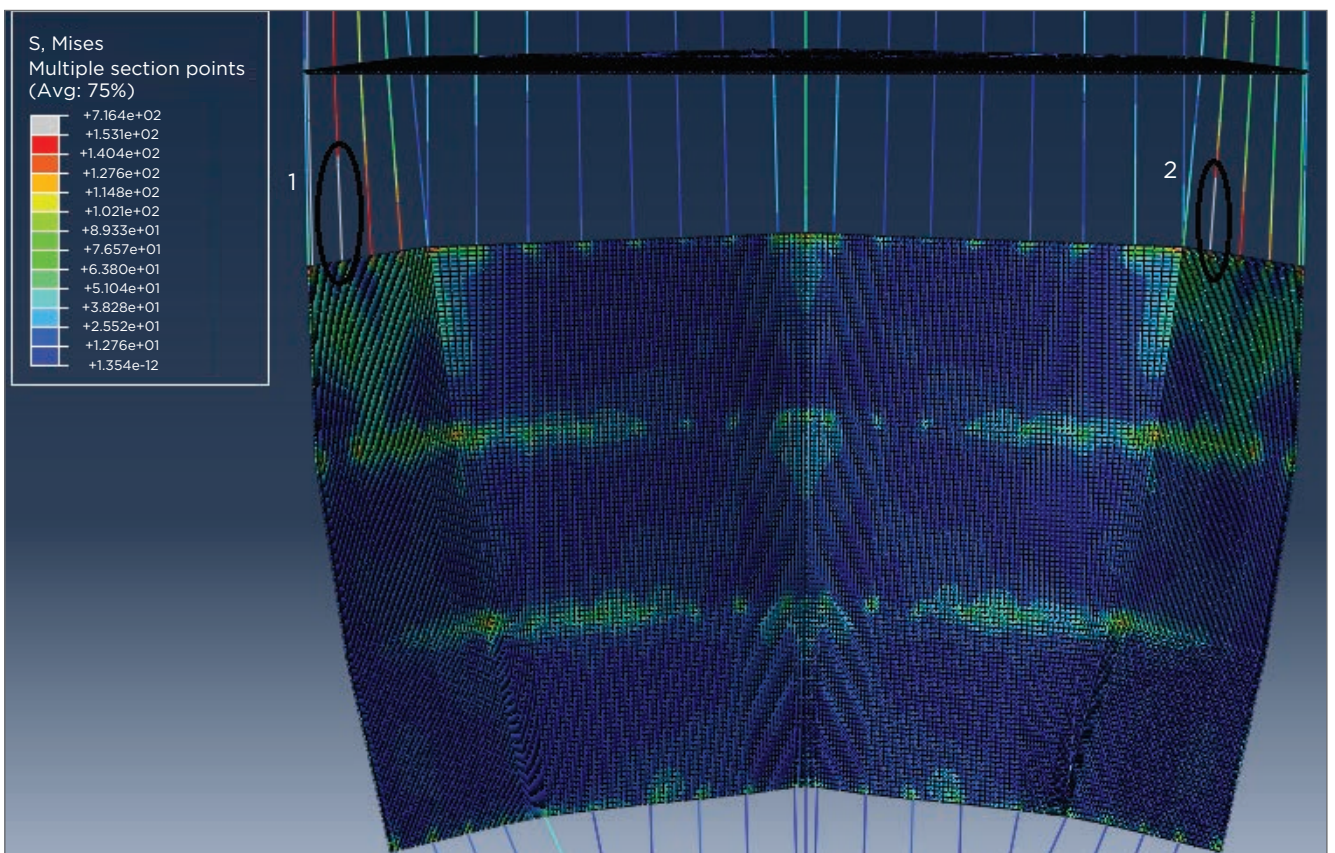


**Figure 18.** Details of critical tensions acting on the impact region.

**Table 7.** Deviation values regarding the limiting tension and the drain tension.

Hull region	Longitudinal frame requested	Tension value (MPa)	% of deviation to the limit tension DNV (153.13 MPa)	% of deviation to the draining limit (206.82 MPa)
Stern	1	215.35	40.63	4.12
	2 a	211.29	37.98	2.16
	2 b	246.85	61.20	19.35
Impact	1	182.81	19.38	-11.61
	2	197.79	29.16	-4.36

than the pre-established tension limit, thus indicating the need for more detailed analysis in those regions.

In the case study applied to the modernization of the LPPN Miraguaia boat, it can be concluded that the structure of the vessel's hull will undergo plastic deformation in areas adjacent to the impact and stern regions, when requested by the slamming, as shown in item 4. Therefore, it is necessary to carry out further analyses, in which the local structures in the deformed regions must be more geometrically detailed.

However, it can be concluded that the use of substructured models is of great value to the process of analysis of the structural strength of high speed vessels, as it facilitates a local analysis of the structure of the hull in the substructured region, as well as the identification of the overall tension distribution along the base model, using a less complex geometry, in relation to the actual structure of the vessel, thus providing less computational work, obtaining the structural response of the model studied.

## REFERENCES

ABAQUS CAE, version 6.13. Dessault Systems Corp. SIMULIA, 2013.

ALONSO, F.R.; PINTO, W.T. Uma investigação sobre o comportamento estrutural de uma embarcação de semiplano frente ao carregamento estático induzido pela batida de proa. 25º Congresso Nacional de Transporte Aquaviário, Construção Naval e Offshore- SOBENA, Rio de Janeiro, 15p., nov.2014

AUGUSTO, O.B. Análise Estrutural de Navios. Escola Politécnica da Universidade de Pernambuco, Departamento de Engenharia Naval e Oceânica, Recife, 146 p., 2007.

BERTRAN, V. Practical Ship Hydrodynamics. Butterworth-Heinemann Linacre House, Jordan Hill, Oxford, 2000. 280 p.

DNV. Det Norske Verita. Hight Speed Ligth Craft and Naval Surface Craft\_Structures, Equipaments\_Design Principles, Design Loads, 2012.

LEWIS, E.V. The Principles of Naval Architecture\_Stability and Strength\_Volume I. Second edition. Jersey City-NJ, USA: The Society of Naval Architects and Marines Engineers. 1998. 310 p.

MANSOUR, A.; LIU, D. The Principles of Naval Architecture Series\_Strength of Ships and Ocean Structures. First edition. Jersey City-NJ,

USA: The Society of Naval Architects and Marines Engineers. 2008.

NEVES, M.S. Dinâmica do Navio. Programa de Engenharia Oceânica, Departamento de Engenharia Naval e Oceânica. UFRJ. 2004.

OROZCO, J.C.G. Contribuição ao estudo de painéis reforçados: Comparação entre o método chapa ortotrópica e o método dos elementos finitos. São Paulo, 2009, 194 p. Dissertação (Mestrado em Engenharia Naval e Oceânica, Escola Politécnica da Universidade de São Paulo).

SANTOS, M.A.S. Análise do Comportamento Estrutural de uma lancha Salva-vidas. Lisboa, 2011. 121 p. Dissertação (Mestrado em Engenharia Mecânica), Universidade de Lisboa.

TIMOSHENKO, S.; WOINOWSKY-KRIEGER, S. Theory of Plates and Shells. Second Editon. New York, USA: McGraw-Hill Book Company,1959. 580 p.

VALERO, C.A.M. Efeito da superestrutura sobre a resistência longitudinal de embarcações de pequeno porte: aplicação e análise estrutural para um navio militar da Marinha Colombiana. São Paulo, 2008. 178 p. Dissertação (Mestrado em Engenharia Naval e Oceânica), Universidade de São Paulo.

# ACCIDENTS WITH WATERWAY TRANSPORTS DUE TO EXTREME WEATHER CONDITIONS

Acidentes com transportes hidroviários em ocasião de extremos meteorológicos

Suane Honorina Martins dos Santos<sup>1</sup>, Maria Isabel Vitorino<sup>2</sup>, Jefferson Inayan de Oliveira Souto<sup>3</sup>, Edson José Paulino da Rocha<sup>4</sup>

**Abstract:** This study correlates the occurrence of accidents with waterway transports, as a consequence of extreme meteorological events which occurred in northeastern Amazonia from 2008 to 2013. The data used were obtained from the National Institute of Meteorology (INMET). For the wind reanalysis of zonal and meridional components, the data were obtained at the National Centers for Environmental Prediction (NCEP)/National Center for Atmospheric Research (NCAR). The main results indicated that in the rainy season (December to May), rainfall is the biggest factor for accidents which occur during this period, due to the strong influence of precipitation systems, such as the inter-tropical convergence zone (ITCZ), mesoscale convective systems (MCS), instability lines (ILs), and Upper-tropospheric Cyclonic Vortices (UTCV), just as in the season with least rainfall (June to December) the wind is considered the main variable that causes accidents in this mode of transportation. In this context, the support from the weather forecast is essential, and can be an asset for the reduction of accidents in the rivers of Pará, especially in the northeastern Amazon, favoring the safety of the users of these means of transportation.

**Keywords:** Waterway transport. Extreme weather. Safety of users.

**Resumo:** Este estudo correlaciona a ocorrência de acidentes com transportes hidroviários em consequência de eventos extremos meteorológicos ocorridos no nordeste da Amazônia no período de 2008 a 2013. Os dados utilizados foram captados do Instituto Nacional de Meteorologia (INMET). Para reanálise de vento das componentes zonal e meridional, os dados foram captados no *National Centers for Environmental Prediction (NCEP)/National Center for Atmospheric Research (NCAR)*. Como principais resultados, constatou-se que no período chuvoso (dezembro a maio) a precipitação é a maior responsável pelos acidentes ocorridos, em virtude da forte influência de sistemas precipitantes, como, por exemplo, zona de convergência intertropical (ZCIT), sistema convectivo de mesoescala (SCM), linhas de instabilidade (LIs) e vórtice ciclônico de alto nível (VCAN). Já no período menos chuvoso (junho a dezembro) o vento é tido como a principal variável que ocasiona acidentes nesse modal de transporte. Nesse sentido, é primordial o auxílio da previsão de tempo, podendo ser uma ferramenta redutora de acidentes nos rios do Pará, especialmente no nordeste da Amazônia, favorecendo a segurança dos usuários desse meio de transporte.

**Palavras-chave:** Transportes hidroviários. Extremos meteorológicos. Segurança dos usuários.

1. Civil Engineer. Master in Environmental Sciences, *Universidade Federal do Pará* - Belém, PA - Brazil. E-mail: suanemartins@oi.com.br

2. Meteorologist. PhD in Meteorology. Professor, *Universidade Federal do Pará* - Belém, PA - Brazil. E-mail: vitorino@ufpa.br

3. Meteorologist, *Universidade Federal do Pará* - Belém, PA - Brazil. E-mail: inayan@outlook.com

4. Meteorologist. PhD in Meteorology. Professor at the Graduate Program in Environmental Sciences, *Universidade Federal do Pará* - Belém, PA - Brazil. E-mail: eprocha@ufpa.br

## INTRODUCTION

The extreme weather conditions observed in the northeastern region of the State of Pará poses risks for navigation. This article discusses how elements such as heavy rains, gusty winds, low visibility, and rough waves are potential conditions for accidents of vessels navigating the waterways.

In the face of weather extremes, the most precarious vessels do not have electronic equipment to aid navigation or salvage equipment, such as life jackets and boats, in sufficient numbers to contribute to the success of navigation, and hence making rescue impossible in extreme cases. Even with the commitment of the Eastern Amazon Port Authority (CPAOR) and the National Waterway Transportation Agency (ANTAQ) demonstrating a tendency to substitute vessels that are unsafe, this substitution is still a distant reality, since extreme weather conditions generate vulnerability and cause serious damage to their structure and to human life. It is common for residents of riverside communities and inland waterway operators to use boats as a basic means of transporting passengers and cargo, as boats are quite common in the region. This activity generates a direct relationship between the social and economic life of these individuals and the rivers of the Amazon.

Even during the less rainy period, precipitation in the Amazon does not cease, but only decreases. During this period, precipitation tends to be more localized and usually originates from differential heating between surfaces. The effects of the breeze circulations are more prominent during the less rainy period in the region (KOUSKY, 1980; COHEN, 1995).

Amazonia stands out in South America as one of the regions with the most intense convective activity, and because a large part of its population uses the waterways as its mode of transport for people as well as for cargo, the number of accidents due to extreme weather conditions is expressive. Therefore, the atmospheric conditions could be considered as determining factors for accidents with boats. In this context, the monitoring and prediction of weather and climate are of fundamental importance for the success of navigation on the waterways, thus being a conditioning factor for the safety of navigation. It is necessary to emphasize the importance of investigating the accidents with cargo and passenger waterway transportation, relating them to extreme weather

conditions in the northeastern region of the State of Pará, and pointing out the socioeconomic consequences for users of the Amazonian rivers.

The rivers of the state of Pará are important for the transportation and economy of the region, which comprise 60% of the national waterway network, with an average of 14.5 million passengers who traveled through the Amazon basin in 2011 and 2012, according to the executive report by ANTAQ (2013). In this context, water-related accidents are increasingly frequent, either because of lack of safety or because of human action (malpractice, recklessness, lack of maintenance, mechanical and structural problems, excess passengers, and cargo) and/or nature (extreme weather conditions), generating socioeconomic losses, and even causing the death of the people who occupy these vessels.

Therefore, this research is essential due to the wide seasonal and spatial understanding of waterway accidents due to meteorological extremes of precipitation and wind, addressed through its quantitative and qualitative aspects. However, it is expected that this study of accidents with waterway vessels in the northeastern of the Amazon due to weather extremes collaborates for the prevention and reduction of the accident risks with both passengers and cargo. Thus, two case studies will be characterized: one for the rainy season and the other for the less rainy season, evidencing the atmospherical behavior during the occurrence of the accident.

## 1. THE IMPORTANCE OF WATERWAY TRANSPORTATION

In the history of mankind, it is notable that humans have used small maritime and fluvial vessels for traveling, the commercialization of their products, the search for independence and the discovery of new lands. Maritime and/or fluvial waterway transportation is one of the most important modalities for industry and logistics in Brazil (BASTOS, 2006).

Cecatto (2002) indicates that the waterway model is fundamental to promote and integrate the country internally and externally. After all, there are 8 basins with 48,000 km of navigable rivers, bringing together at least 16 waterways and 20 river ports. Between 1998 and 2000, 69 million tons were moved. Modernized and adapted to the demands of a

globalized world, maritime transports can reduce domestic distances and be decisive in consolidating the Southern Common Market (MERCOSUR), as well as increasing trade relations with other continents.

Carmo Filho *et al.* (2006) corroborate that the Pará river transportation has different particularities from the rest of the Brazilian territory. It is no wonder: during the flood season, it is possible to count on a hydrographic network of up to 80,000 km of waterways (PINTO *et al.*, 2011), a safety margin for the passage of larger vessels, freight transports and mixed and passenger navigation, as is the case of the huge ocean liners that travel through the great rivers of the Amazon.

Novaes (2004) states that water transportation refers to all types of transport carried out on water. In this scope are the fluvial, lacustrine, and maritime transport. Keedi and Mendonça (2000) state that, when compared to road transport, waterways have lower costs, lower fuel consumption, greater transport capacity, better safety conditions, lower rates of damage, and lower environmental impact. This modal is indicated by its advantageous features such as those already mentioned. Even so, they are vulnerable when under the influence of climatic variables.

As waterway vessels are a common means of transportation in the Amazon Region, users are susceptible to accidents while navigating Amazonian rivers.

Chopra and Meind (2011) indicate that the main advantage of water transport is the low operating costs. As ships have relatively large capacity, fixed costs can be absorbed by large volumes. Thus, the ease of low-cost transportation with this mode is an advantage over other modes of transport.

Patrício (2007, p. 02) states that:

In addition to stimulating industrial, commercial and tourist activities, fluvial transport incorporates new social and environmental aspects, as it plays an important role for the sustainable development of the region, preserving the cultural identity and strengthening the socialization network of communities and their peoples.

The process of intensification of the Amazon Region was originated by the layout of the hydrographic network, in which the natural path is the river, the main means of subsistence

of the local population. This population is a minority, but not irrelevant to the state, and therefore contributes to the economy by generating income through the commercialization of its products, as well as the purchase of freely marketed goods in the region.

## 2. ACCIDENTS IN WATERWAY TRANSPORTATION AND THE CLIMATE OF THE AMAZON REGION

Considering the importance of the waterway transport modalities, developing studies that analyze the accidents due to extreme weather is very important, since the Amazonian atmosphere has very large water availability, as well as precipitating systems that influence the rainy and less rainy periods in the region.

According to Ferreira (2000), the waterway is subject to a relatively large range of accident types, and the frequency of these events depends on another range, not smaller, of factors. For accidents occurring in the Amazon Basin, there are great difficulties in obtaining reliable information and statistical data on accidents, as there is a divergence between some of the information. The regulations of the Navy contemplate several definitions for accidents involving waterway transport, but the accidents with definitions that are more interesting to this article are those caused mainly by extreme weather conditions. The accidents covered were acquired through consultation to CPAOR surveys for the period of 2008–2013.

The vessels involved in accidents are of all sizes, types, and shapes. The results show that all vessels are subject to the most diverse types of accidents caused by meteorological extremes.

The climate of the Amazon Region is formed by the combination of several factors combined. Cloudiness controls the energy distribution associated with spatial and temporal patterns of rainfall in the region, relating rains to solar radiation, to temperature and to atmospheric humidity with the annual precipitation cycle. Thus, in the rainy season there is a reduction in air temperature and radiation and an increase in air humidity, unlike in the less rainy season.

Being located in the equatorial region, the climate of Amazon is hot and humid. Fisch *et al.* (1998, p. 102) show that,

although this behavior has not been a constant during the last 15,000 years. Changes in the Earth-Sun relationship caused significant changes in the amount of solar energy received by planet Earth, changing the composition of the predominant atmospheric systems and, consequently, the climate.

These changes in climate, mainly due to the thermal contrast between sea and land, contribute to the increase and/or decrease in precipitation, thus altering the level of rivers, which interferes with the navigation conditions. On the coast of Pará and Amapá, the average rainfall is about 2,300 mm. year<sup>-1</sup> and the annual total reaches 3,500 mm. Precipitation is also high and the region does not have a defined dry season. The instability lines (ILs) that are formed along the coastline during the afternoon, forced by sea breezes, are responsible for this characterization (NOBRE, 1990). The rainy period or strong convective activity in the central region of the Amazon (near 5° S) may be associated with the penetration of frontal systems of the southern region, interacting with the local convection and organizing such a convection, between November and March. The period without large convective activity occurs from May to September, and the months from April to October and December to February characterize the transition period between one regime and another, when the region presents high precipitation (>900 mm) in the Western and Central parts of the Amazon, within the geographic position of Bolivia. In the months of June, July, and August, the precipitation maximum moves north over Central America in the central part of the Hadley cell domain, characterizing the dry season. This behavior is completely in line with the annual cycle of convective activity in the region (HOREL, 1989).

The El Niño is characterized by the occurrence of sea surface temperature (SST). The El Niño - Southern Oscillation (ENSO) phenomenon has two phases: one positive, La Niña, and one negative, El Niño, characterized by a warmer period. The phenomena caused by ENSO are attenuating changes in the precipitation regime and, according to the intensity of the event, may result in severe droughts (MOLION, 2000). According to Alves *et al.* (1998), in the majority of the years with El Niño, below-average rainfall was observed in the northeastern sector of Eastern Amazonia, and in the La Niña years above the average there

were marked water warming and behavioral changes in the Walker cell, causing increased precipitation in the region of the state of Pará.

The wind, characterized by the movement of air in relation to the terrestrial surface in the vertical and horizontal directions, is one of the great causes of accidents with waterway vessels (AYODE, 2003). Wind is generated through different atmospheric pressure gradients, moving from high-pressure areas to low-pressure areas. The trade winds are winds that come from the subtropical regions of high pressure for the equatorial strip, characterized by being a hot and low-pressure area (SADOURNY, 1994).

Precipitating meteorological systems are presented as those that produce precipitation in the Amazon in both the rainy and the less rainy periods. Among the mesoscale precipitating systems, the intertropical convergence zone (ITCZ), the upper-tropospheric cyclonic vortices (UTCVs), the South Atlantic convergence zone (SACZ), the frontal systems (FSs), the easterly wave disturbances (EWDs), the ILs, and the circular mesoscale convective systems (FERREIRA, 2008; ROCHA; GANDU, 1996; SODRÉ, 2013) offer intense precipitation in the study area, located northeast of the state of Pará.

Camponogara (2012) states that the Pará precipitation regime is modulated by the sea breeze, the ILs, the EWDs, the ITCZ, the Alta de Bolivia (AB), and the UTCVs.

Melo (2009) states that the ITCZ consists of a linear band of deep cloudiness in the equatorial strip of the Atlantic Ocean, which connects convection regions in South and Central America (West) and Africa (East). In order to understand the influence and the performance of this band of nebulosity in the place of study, one needs to know that this system of great horizontal portion occurs near the Equator, embracing this equatorial strip of the globe. Their interaction, according to Ferreira (1996), depends on the interaction of the characteristics of the atmosphere and of the ocean, not necessarily occurring all at once. As precipitation is linked to local convection, it becomes one of the most important variables in the tropics, and is essential to the understanding of the ITCZ's mechanisms.

The ITCZ is formed by the convergence of trade winds in the southern hemisphere, low pressure, high sea surface temperatures, intense convective activity and precipitation, determining the intensity of the rains in the north and northeastern

regions. Souza (2005) and Adler (2009) assert that SST anomalies in the Pacific and Atlantic oceans affect the latitudinal position of the ITCZ longitudinally. In the Atlantic Ocean, the ITCZ moves, on average, 14° N in the months of August and September and 2° S in the months of March and April. This movement is associated to the strengthening or weakening of the trade winds coming from the southeast and northeast.

The UTCV is characterized by a low-pressure center with a duration of a few days that originates in tropical and extratropical latitudes (RAMIREZ, 1996). In Brazil, tropical UTCVs operate more frequently from December to February, lasting for 4–11 days. When they originate in the continent, they influence the precipitation in the north and northeast of Brazil.

It is important to account for the interaction of the UTCV with other systems, such as the AB and SACZ. In the summer, the AB contributes to the rains, mainly in the Brazilian North and part of the northeast and central-west (FERREIRA *et al.*, 2009).

The ZCAS is a typical summer system in South America. According to Rocha and Gandu (1996), it is a band of cloudiness and precipitation that extends from the northwest to southeast over South America and shows interaction between tropical and extratropical systems, with hot and humid air masses from the Amazon and the South Atlantic. The cloudiness of the ZCAS is characterized from northwest to southeast and ends up extending from the south of the Amazon region to the center of the South Atlantic (KOUSKY, 1988). In summer and autumn, the ZCAS is one of the main precipitating systems in Southern Amazonia (ROCHA; GANDU, 1996).

The EWDs are a consequence of the barotropic and baroclinic instability of flushes, corresponding to horizontal and vertical wind shear (MACHADO *et al.*, 2009). The EWDs further intensify meteorological systems such as MCSs, associating with tropical storms or even hurricanes in the northern equatorial Atlantic (BARBOSA, 2005). The EWD is little known in the South American continent, because its activity is not significant compared to what happens in Africa, but it has a fundamental action in the modulation of the convection of events of mesoscale and synoptic scale that come from the ocean, thus interfering in precipitating systems such as ITCZ, IL, and mesoscale convective complexes (MCCs).

The ILs are convective systems that contribute to the formation of rains near the coast of Pará and Amapá and to the precipitation that occurs in Central Amazonia. Cohen (1989) classified these systems as instability line with propagation (ILP), which spreads inland; and coastal instability line (CIL). The first one is subdivided into two types: ILPs type 1, which go inland, and ILPs type 2, which dissipate in a short space. The CILs have the coast as their apex, where they form and dissipate. According to Cohen (1989), the stability lines are one of the atmospheric systems operating in the Pará area that collaborate with 45% of the rains during the rainy season.

ILs contribute to the formation of cumulonimbus clouds and are formed by the circulation of sea breeze. The rains in the Amazon are linked to the ILs coming from the coast, driven by sea breezes (GARSTANG *et al.*, 1994). These Amazonian ILs go through six stages in their life cycle: genesis, intensification, maturity, weakening, re-sensitization, and dissipation. At these stages, these lines lose and gain strength. They form in the late afternoon, losing strength as they propagate on the continent, dissipating and later gaining strength once again. If this movement happens at night, the convective activity will be smaller (MOLION; KOUSKY, 1985).

Sodré (2013) *apud* Machado and Rossow (1993) states that the convective system, when mature, forms large amounts of stratus and cirrus clouds. MCSs are often associated with intense precipitation, strong gusts of wind and even tornadoes. Sodré (2013) shows that the frequency of MCS is considerable throughout the territory of the State of Pará. In his division of the study area, there are regions that present greater quantitative, mainly around the Bay of Marajó, where there is a dependence of abundant availability of humidity both from the rivers and the ocean.

In his division, Sodré (2013) corroborates information on convective systems that attract extreme weather events in the region where the accidents concentrate, in which the Marajó Bay is located.

### 3. RESULTS AND DISCUSSION

Two case studies of accidents with waterway transport due to meteorological extremes will be shown: one in the rainy season and another in the less rainy season. These cases are

related to the determining causes of extreme precipitation (case 1) and wind (case 2).

The accident occurred with a fishing boat on February 18, 2011, at 7:40 pm, on Costa do Taparí, near Ponta da Romana, in the municipality of Curuçá, Pará. According to the CPAOR survey, the cause of the shipwreck was determined as “great atmospheric instability”, causing the death of a 19-year-old male victim.

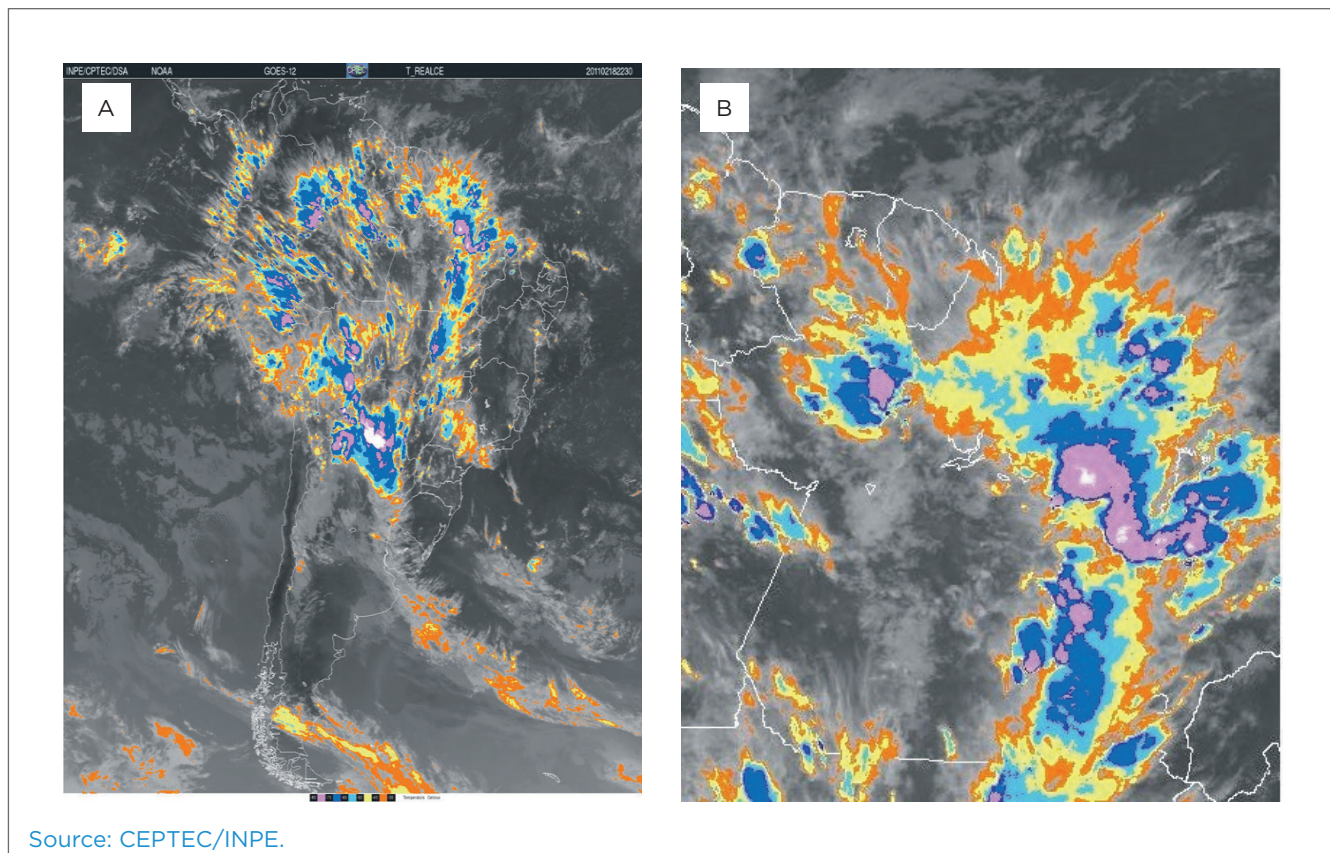
The infrared satellite images shown in Figure 1 for the local time of 7:30 pm show intense convective activity in much of Brazil, specifically in the eastern portion of the State of Pará, covering the entire region of study. It is important to note that February 2011 was influenced by the cold phase of ENOS (La Niña), with a Southern Oscillation Index (SOI) of -1.2°C — *National Centers for Environmental Prediction (NCEP)/National Center for Atmospheric Research (NCAR)*, which favors increased precipitation. The atmospheric instability observed in Brazil is related to the presence of two baroclinic systems on the south and southeast, better known

as cold fronts, which, when connected to the Amazonian atmosphere, produce large amounts of cloudiness and, consequently, intense precipitation. These atmospheric characteristics are common during the rainy period of La Niña years in the region (SOUZA *et al.*, 2000).

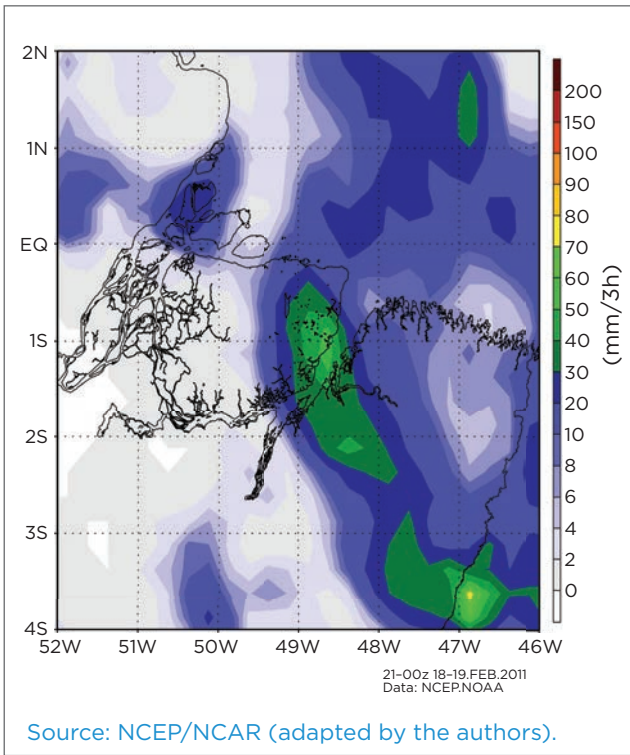
The accumulated precipitation associated with the cloudiness pattern (Figure 1B) can be verified in Figure 2, with rainfall around 70 mm/3h and 115 mm/day at the National Institute of Meteorology (INMET) station in Belém, a unit used as basis for data extraction.

Figure 3 shows that, for case 1, the wind of the surface was weak in a northeast direction in the region of the accident (subarea 1). It may be noted that the continent’s winds are of lesser intensity than those on the Atlantic Ocean. This may be related to the large amount of deep cloudiness in the lower atmosphere.

The accident, as already stated, was of the shipwreck type, according to the Brazilian Maritime Authority Regulations for Administrative Inquiries about Accidents and Facts of



**Figure 1.** Infrared images from satellite GOES-12, highlighted for February 18, 2011 at 10:30 p.m. (7:30 p.m. local time): (A) South America cutout image and (B) Pará State cutout image.



**Figure 2.** Hourly rainfall (mm/3h); accumulated from three hours for the period from 6:00 p.m. to 9:00 p.m. (local time) for February 18, 2011.

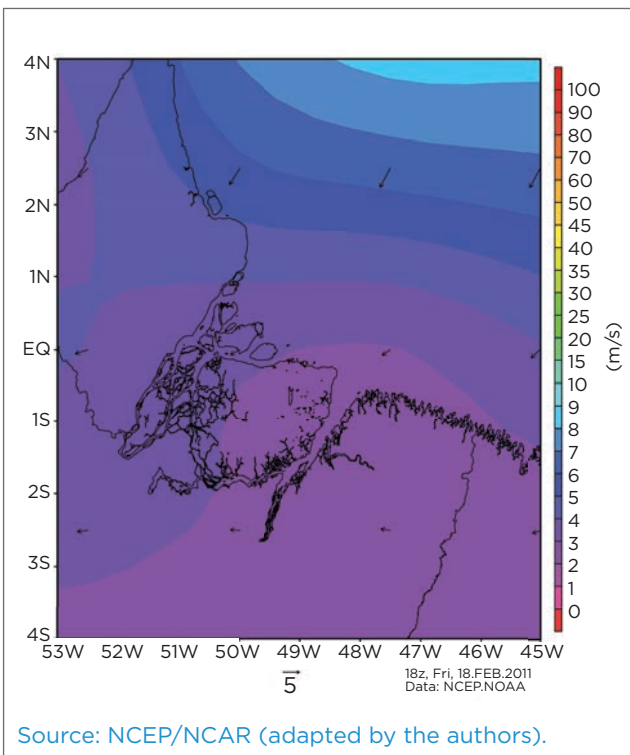


**Figure 3.** Horizontal surface wind (direction and speed) on February 18, 2011.

Navigation (NORMAM-09/DPC), caused by total or partial sinking of the vessel due to loss of buoyancy from water boarding in its internal spaces, due to its heeling, overhanging, or flooding. The vessel was classified simply as a small vessel because it was a fishing boat.

On the day of the precipitation extreme in subarea 1, the tide was low, with 0.1 m at 5:26 p.m., according to the tide table of the Brazilian Hydrography and Navigation Board (DHN), but there was an evolution to high tide at 11:00 p.m., with a height of 3.6 m. In theory, the conditions for the accident may have been provided by the sandbars, among other means of friction that are closer to the bottom of the boat, causing the embankment or flood.

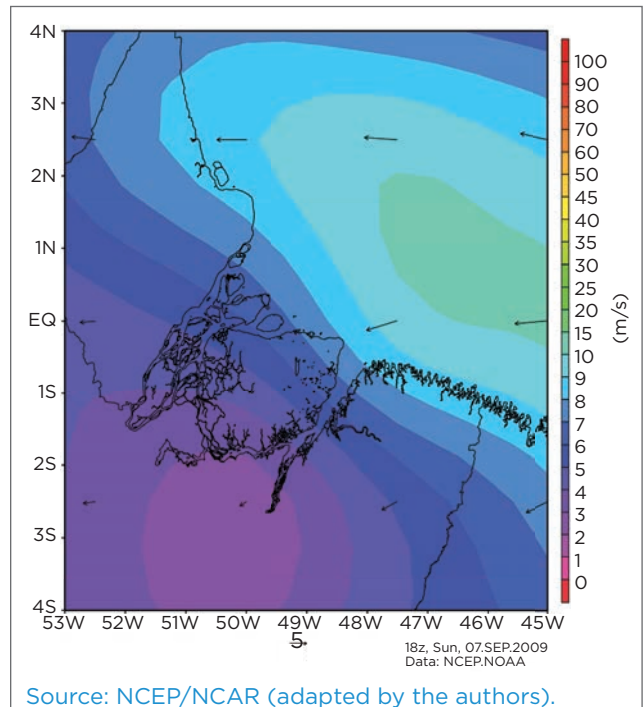
The accident in case 2 occurred with a motor boat on September 7, 2009, at 3:00 p.m., local time, in Guajará Bay, near the SOTAVE terminal in Icoaraci, in the city of Belém, Pará (subarea 1). According to the Port Authority's inquiry, the cause of the shipwreck-type accident was "the large volume of water entering the vessel due to strong waves", resulting in the death of a 21-year-old man.

According to NCEP/NCAR, the SOI of September 2009 was 0.8°C, that is, not relevant to influence the atmosphere under study, mainly because the season is less rainy, without the performance of large-scale precipitating meteorological systems. This can be confirmed by the satellite images (Figure 4), in which there is no precipitating cloudiness in most of Brazil, including subarea 1, but the performance of two frontal systems in the southeast of Brazil. In addition, the images show that there was no rain at the time of the accident — the cause confirmed by CPAOR was "agitated waves". In addition, one can observe the presence of high clouds, high stratus, and cirrus type that do not provoke rain.

The flow on the dominant surface is from the east, whose intensity is much higher than the winds of case 1. It can be noted in Figure 5 that the intensity of the surface winds in the proximities of the ocean with the Tocantins River is quite pronounced, even on a large scale. In addition, the INMET automatic station presented 10.4 m/s winds at the Belém station. This information agrees with the determining cause of the accident by CPAOR. According to Kousky (1980), the sea breeze can be observed from 12 a.m. to 4:00 p.m., a period that comprises the accident episode, which may have intensified larger waves by sea breeze winds.

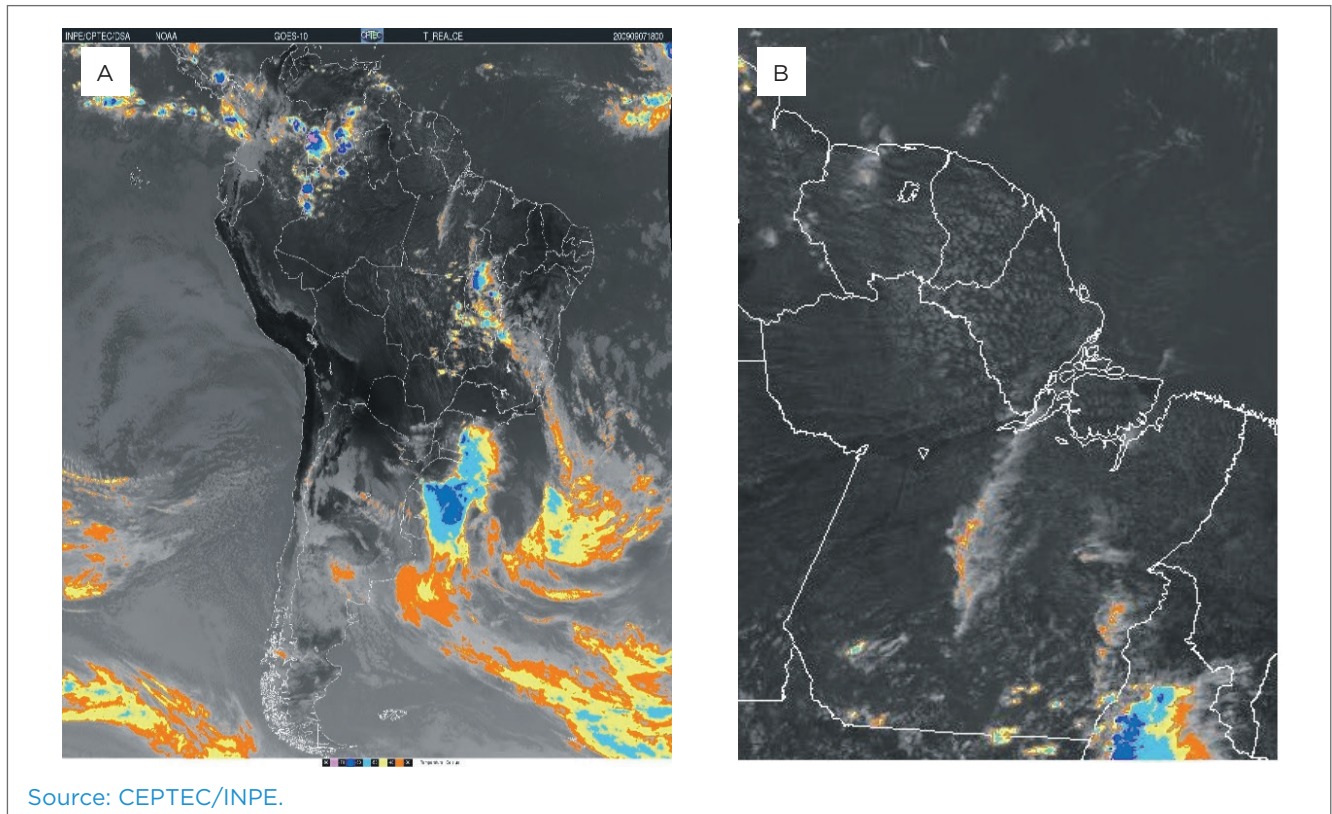
Some authors, such as Ferreira (2006), comment that the wind is one of the most important phenomena in our atmosphere. In the case of the water environment, it is the precursor of agitated waves, having a dangerous strength that creates situations of risk and vulnerability to the small boats that sail under the strong action of the winds. Franco (1993) assures that the wind blows on the surface of the sea forming small undulations, called capillary waves, with a height of a few millimeters, which can increase as the wind continues to act, thus forming waves of gravity that do not cease with the end of the wind. According to the Center for Sea Studies (2005), the wind speed influences the size of the waves. Therefore, intense winds form bigger waves. For wave formation above 1 m, a wind speed of 10 m/s is required.

Wave dynamics associated with tidal variation are important for understanding what happens at the moment of agitation. Figure 6 shows the tide and wind variation on the surface of subarea 1. It can be seen that the high tide schedule matches the time of the most intense winds in the region,



Source: NCEP/NCAR (adapted by the authors).

**Figure 5.** Horizontal surface wind (direction and speed) at 3pm (local time) on September 2, 2009.



Source: CEPTEC/INPE.

**Figure 4.** Infrared images from satellite GOES-12, highlighted for September 7, 2009, at 6:00 p.m. (local time): (A) South America cutout image and (B) Pará State cutout image.

favoring the formation of giant waves, consequently causing the accident.

In general, boats that navigate Amazonian rivers carry loads and passengers. When these loads are not fixed, they contribute to the instability, especially in the case of intense precipitation, as was with case 1, and of agitated waves, as with the case 2. These forces become dynamic in the same proportion of the leveling of the vessel over the water, causing the vessel to overhang.

#### 4. THE ECONOMIC ASPECTS OF ACCIDENTS WITH WATERWAY TRANSPORTATION

In the Amazon, boats are the most common means of transportation, economically viable and time-efficient. They are the main means of transportation in the region, providing mobility to its inhabitants, and used in practically all locomotion needs outside the communities, since they are the means that best adapt to the conditions of loads and passengers and the operation of the rivers. River transport is an environmentally friendly, cost-efficient transport medium, and its similarity to other modes is that they also have to deal with climatic events that affect navigability (SCHWEIGHOFER, 2007).

The biggest difficulty for the movement of passengers in the Amazon, according to ANTAQ (2013), is regular transportation. Most vessels do not have systems with adequate technologies (CEVNI, 2009). Thus, in case of reduced visibility due to fog, rain, or other reasons, boats are invited to sail by radar.

Padovezi (2003) states that accidents with water transport may prove to be uneconomical if they are not integrated into efficiency or safety. The risks of accidents are imminent, mainly due to the precariousness of the vessels and their structure in holding people and cargo. In addition, there is no concern for safety in this type of transport, and overcrowding, one of the most common causes in boat transport, is frequent. The reality of navigation in the Amazon is marked by the negligence of its navigators regarding the revision and renovation of parts and equipment. Thus, vessels travel in a vulnerable way, due to not being covered by insurance, which often masked by low budget reforms, making them difficult for monitor by responsible entities (ANTAQ, 2013). When extreme events occur, accidents become quite common. The adaptation of vessels to inland waterways is very expensive to the detriment of safety, which makes economic activity unfeasible. If this were to happen, ticket costs would rise and people who depend on this mode would be jeopardized, since boat transport still has low cost (ANTAQ, 2013).

Sousa *et al.* (2008, p. 03) explain:

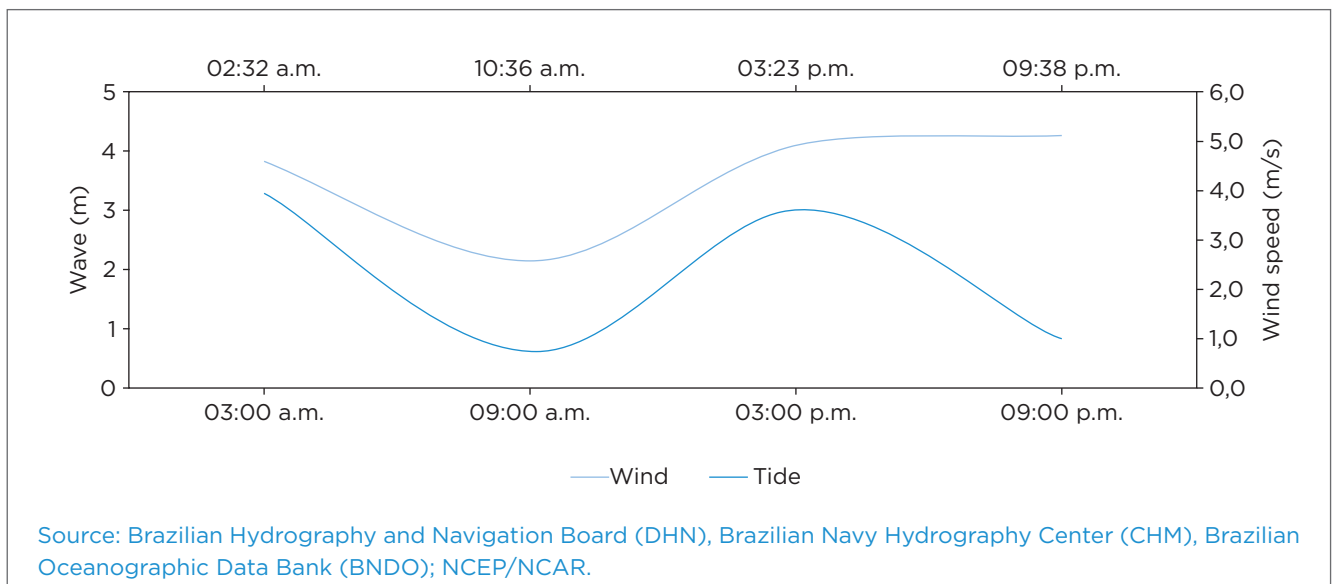


Figure 6. Joint evolution of tide level and wind speed for case 2.

Therefore, what we witness are mixtures of passengers and luggage scattered in the seats, which can be fatal in cases of accidents, where people fight for survival and can be surprised by luggage or cargo in general.

The poor disposition of the loads and of the passengers can cause serious stability problems in the boat, due to *marolas* (small sea waves), strong wind and maneuvers. In case of extreme events, such disorganization can even cause shipwrecks and, consequently, human casualties.

Waterway transportation offers options for entrepreneurs who want to save on the transport of large volumes, since, among the three most common types of transport (road, rail, and water), considering the final result, it is the cheapest.

## 5. CONCLUSIONS

This study aimed to show the fundamental importance of the knowledge and the use of atmospheric and morphological characteristics of the surface for the safety of

waterway transport in the northeast of the Eastern Amazon. Thus, the use of meteorological products by weather pilots and weather and climate forecasting may, to a certain extent, reduce accidents in waterways caused by weather extremes.

The most frequent determining cause of meteorological extremes observed was atmospheric instability, which consequently causes intense precipitation. This may be related to the performance of global, synoptic and meso-scale precipitating meteorological systems such as ITCZs, UTCVs, ILLs, and circular mesoscale convective systems.

For case study 2, the occurrence of the accident is associated with the intensification of the winds, especially the northeast trade winds, inherent to the time of the year in which the event occurred.

The use of tools that help predicting the weather in river navigation may contribute to the reduction of the occurrence of accidents with fatal victims. Therefore, it is accepted that, with reduction of accidents, socioeconomic impacts will also decrease, since waterway vessels are the most common means of transport in the state of Pará and the Amazon as a whole.

## REFERENCES

- ADLER, R.F.; HUFFMAN, G.J.; CHANG, A.; FERRARO, R.; XIE, P.-P.; JANOWIAK, J.; RUDOLF, B.; SCHNEIDER, U.; CURTIS, S.; BOLVIN, D.; GRUBER, A.; SUSSKIND, J.; ARKIN, P.; NELKIN, E. The Version 2 Global Precipitation Climatology Project (GPCP) Monthly Precipitation Analysis (1979-Present). *Journal of Hydrometeorology*, v. 4, p. 1147-1167, 2003.
- AGÊNCIA NACIONAL DE TRANSPORTES AQUAVIÁRIOS. *Caracterização da oferta e da demanda do transporte fluvial de passageiros da região amazônica*. Agência Nacional de Transportes Aquaviários - Brasília: ANTAQ, 2013. 108p. : il.
- ALVES, J.M.B.; CAMPOS, J.N.B.; SOUZA, E.B.; REPELLI, C.A. Produção agrícola de subsistência no Estado do Ceará com ênfase aos anos de ocorrência de El Niño e La Niña. *Revista Brasileira de Agrometeorologia*, v. 6, n. 2, p. 249-56, 1998.
- AYODE, J.O. *Introdução à climatologia para os trópicos*. Rio de Janeiro: Bertrand Brasil, 2003.
- BARBOSA, R.L. *Interação das perturbações convectivas iniciadas na costa norte do Brasil com distúrbios ondulatórios de leste*. 2005. Dissertação (Mestrado em Meteorologia) - Instituto Nacional de Pesquisas Espaciais - INPE, São José dos Campos, SP, 2005.
- BASTOS, M.M.R.D. *Geografia dos transportes: trajetos e conflitos nos percursos fluviais da Amazônia paraense: um estudo sobre acidentes em embarcações*. Dissertação (Mestrado) - Universidade de Uberlândia, Uberlândia, MG, 2006.
- CAMPONOGARA, G. *Extremos de precipitação diária em Belém Pará e estrutura vertical da atmosfera*. Dissertação (Mestrado) - Instituto de Astronomia, Geofísica e Ciências Atmosféricas, Universidade de São Paulo, São Paulo, SP, 2012.
- CARMO FILHO, M.M.; ROCHA, A.C.B.; SOARES FILHO, A. Qualidade da infraestrutura de transporte fluvial de carga e sua importância para os pólos de desenvolvimento. In: FREITAS A.; PORTUGAL, L.S. (Orgs.). *Estudos de transporte e logística na Amazônia*. Manaus: Novo Tempo, 2006. v.1. p. 145-166.
- CAVALCANTI, I.F.A.; FERREIRA, N.J.; DIAS, M.A.F.S.; SILVA, M.G.A.J. *Tempo e clima no Brasil*. São Paulo: Oficina de textos, 2009.
- CECATTO, C.A. Importância do transporte marítimo no Brasil. Inbound/Outbound da Qualilog. *Revista EngWhere*, n. 23, 2002. Disponível em: <[http://www.ecivilnet.com/artigos/pdf/importancia\\_do\\_transporte\\_maritimo\\_no\\_brasil.pdf](http://www.ecivilnet.com/artigos/pdf/importancia_do_transporte_maritimo_no_brasil.pdf)>. Acesso em: 05 mar. 2014.
- CENTRO DE ESTUDOS DO MAR. Universidade Federal do Paraná, 2005. <[http://www.cem.ufpr.br/praiapagina/pagina.php?menu=ondas\\_formacao](http://www.cem.ufpr.br/praiapagina/pagina.php?menu=ondas_formacao)>. Acesso em: 20 out. 2014.

- CHOPRA, S.; MEINDL, P. *Gestão da cadeia de suprimentos: estratégia, planejamento e operações*. 4. ed. São Paulo: Pearson, 2011.
- COHEN, J.C.P.; SILVA DIAS, M.A.F.; NOBRE, C.A. Aspectos climatológicos das linhas de instabilidade na Amazônia. *Climanálise – Boletim de Monitoramento e Análise Climática*, 1989.
- FERREIRA, A.N. *Estudo de acidentes na hidrovía Tietê-Paraná: aspectos preventivos*. Dissertação (Mestrado) – Escola Politécnica da Universidade de São Paulo, Departamento de Engenharia Naval e Oceânica, Universidade de São Paulo, São Paulo, SP, 2000. 168 p.
- FERREIRA, D. *Eventos extremos da zona de convergência intertropical sobre o atlântico durante o período chuvoso da Amazônia*. Dissertação (Mestrado em Ciências Ambientais) – Programa de Pós-graduação, Universidade Federal do Pará, Belém, PA, 2008.
- FISCH, G.; MARENGO, J.M.; NOBRE, C.A. Uma revisão geral sobre o clima da Amazônia. *Acta Amazônica*, v. 28, n. 2, p. 101-126, 1998.
- KEEDI, S.; MENDONÇA, P.C.C. *Transporte e seguros no comércio exterior*. 2. ed. São Paulo: Aduaneiras, 2000.
- KOUSKY, V.E.; CAVALCANTI, I.F.A. Precipitation and atmospheric circulation anomaly patterns in the South American sector. *Revista Brasileira de Meteorologia*, v. 3, p. 199-206, 1988.
- MACHADO, L.A.T.; ROSSOW, W.B. Structural characteristics and radiative properties of tropical cloud clusters. *Monthly Weather Review*, v. 121, p. 3234-3259, 1993.
- MADDOX, R.A. Mesoscale convective complexes. *Bulletin of the American Meteorological Society*, v. 61, p. 1374-1387, 1980.
- MARENGO, J.; NOBRE, C.A.; CULF, A.D. Climatic impacts of “Friagens” in forested and deforested areas of the Amazon Basin. *Journal of Applied Meteorology and Climatology*, v. 36, p. 1553-1566, 1997.
- MELO, A.B.C.; CAVALCANTI, I.F.A.; SOUZA, P.P. Zona de convergência intertropical do Atlântico. In: CAVALCANTI, I.F.A.; FERREIRA, N.J.; SILVA, M.G.A.J.; SILVA DIAS, M.A.F. *Tempo e clima no Brasil*. São Paulo: Oficina de Textos, 2009. p. 27-31.
- MOLION, L.C.B.; BERNARDO, S.O. Dinâmica das chuvas no nordeste brasileiro. In: CONGRESSO BRASILEIRO DE METEOROLOGIA, 2000, Rio de Janeiro, RJ. *Anais...*, 2000, p. 1334-1342. Disponível em: <<http://www.cbmet.com/cbm-files/12-7ea5f627d14a9f9a88cc694cf707236f.pdf>>. Acesso em: 24 abr. 2015.
- NOVAES, A.G. *Logística e gerenciamento da cadeia de distribuição*. Rio de Janeiro: Elsevier, 2004.
- OLIVEIRA, A.S.; NOBRE, C.A. *Meridional penetration of frontal system in South America and its relation to organized convection in the Amazon*. São José dos Campos. Instituto Nacional de Pesquisas Espaciais - INPE 3407-PRE/674. 1986.
- PADOVEZI, C.D. *Conceito de embarcações adaptadas à via aplicado à navegação fluvial no Brasil*. Tese (Doutorado) – Escola Politécnica da Universidade de São Paulo, Departamento de Engenharia Naval e Oceânica, Universidade de São Paulo, São Paulo, SP, 2003.
- PATRÍCIO, J.C.S.O. *Transporte fluvial misto na Amazônia: aspectos socioeconômicos do trecho Belém-Acará*. Dissertação (Mestrado em Economia) – Universidade da Amazônia, Belém, PA, 2007.
- PINTO, L.A.F.; LEE, J.M.; JONQUA, J.P.C.B. A importância do transporte fluvial para a unidade operacional da Amazônia. In: ENCONTRO NACIONAL DE ACESSIBILIDADE INTRA-REGIONAL: modos de vida, tradição e modernidade no transporte fluvial na Região do Baixo Amazonas-PA, 31., 2011.
- RAMIREZ, M.C.V. *Padrões climáticos dos vórtices ciclônicos em altos níveis no Nordeste do Brasil*. Dissertação (Mestrado) – INPE-6408-TDI/618, São José dos Campos, SP, 1996.
- RICOEUR, P. *O conflito das interpretações: ensaios de hermenêutica*. Rio de Janeiro: Imago, 1978.
- ROCHA, A.G.; GANDU, A.W. South Atlantic Convergence Zone. In: *Climanálise – edição especial*. CPTEC/INPE, p. 140-142, 1996.
- SADOURNY, R. *O clima da terra*. Lisboa: Instituto Piaget, 1994.
- SCHWEIGHOFER, J. The impact of extreme weather and climate change on inland waterway transport. *Journal of Natural Hazards*, v. 72, p. 23, 2014.
- SODRÉ, G.R.C. *Estudo da convecção de mesoescala em diferentes superfícies na Amazônia Oriental*. Dissertação (Mestrado) – Programa de Pós-graduação em Ciências Ambientais, Universidade Federal do Pará, Belém, PA, 2013.
- SOUSA, J.R.A.; ALMEIDA, R.M.B.; ROLIM, P.A.M. Influência do dipolo do Atlântico nas precipitações do leste da Amazônia/Litoral Norte Brasileiro (Macapá-AP, Belém-PA e São Luís-MA). In: CONGRESSO BRASILEIRO DE METEOROLOGIA, 8., Belo Horizonte/MG, 1994.
- SOUSA, A.C.; SILVA NETO, M.C.; MORAES, H.B. Análise da Segurança das Embarcações da Amazônia. 22º Congresso Nacional de Transportes Aquaviários, Construção Naval e Offshore- SOBENA-Sociedade Brasileira de Engenharia Naval. Rio de Janeiro, RJ. 2008.
- SOUZA, E.; KAYANO, M.; TOTA, J.; PEZZI, L.; FISCH, G.; NOBRE, C. On the influences of the El Niño, La Niña and Atlantic dipole pattern on the Amazonian rainfall during 1960-1998. *Acta Amazônica*, v. 30, n. 2, p. 305-318, 2000.

# LITHOLOGY DISCRIMINATION BY SEISMIC ELASTIC PATTERNS: A GENETIC FUZZY SYSTEMS APPROACH

Discriminação litológica por atributos sísmicos  
elásticos: uma abordagem por sistemas fuzzy-genéticos

Eric da Silva Praxedes<sup>1</sup>, Adriano Soares Koshiyama<sup>2</sup>, Marley Maria Bernardes  
Rebuzzi Vellasco<sup>3</sup>, Marco Aurélio Cavalcanti Pacheco<sup>4</sup>, Ricardo Tanscheit<sup>5</sup>

**Abstract:** This work proposed a new methodology for lithological discrimination – using the Genetic Programming for Fuzzy Inference Systems model (GPFIS) – a genetic fuzzy system based on Multi-Gene Genetic Programming. The main advantage of our approach is the possibility to identify, through seismic patterns, the rock types in new regions without requiring opening wells. Thus, we wanted a reliable model that provides two flexibilities for the experts: to evaluate the membership degree of a seismic pattern to the several rock types and the chance to analyze the model output at a linguistic level. Therefore, the final tool must lead to more knowledge and support to the decision maker. In addition, we evaluated other seven classification models (from statistics and computational intelligence), using a database from a well located in the Brazilian coast.

**Keywords:** Classification. Lithology. Oil & Gas. Genetic Fuzzy Systems.

**Resumo:** Este trabalho propôs uma metodologia para discriminação litológica de novas jazidas de petróleo por meio do uso de Sistemas Fuzzy-Genéticos — em destaque o modelo *Genetic Programming Fuzzy Inference System* (GPFIS). A vantagem da modelagem sugerida é possibilitar identificar, mediante padrões sísmicos, o tipo de rocha de uma determinada região sem a necessidade de abrir novos poços. Assim, busca-se um modelo com boa acurácia, aprendizado automático e que proporcione duas características desejáveis aos especialistas: avaliar o grau de pertinência de um determinado padrão sísmico aos diferentes tipos de rocha e a oportunidade de analisar em nível linguístico a resposta do modelo. Portanto, a ferramenta final elaborada oferece apoio à decisão, assim como a extração e descoberta de conhecimento. Além do modelo GPFIS, foram avaliadas sete outras metodologias para classificação, por intermédio de dados de um poço da costa brasileira.

**Palavras-chave:** Classificação. Litologia. Óleo & Gás. Sistemas Fuzzy-Genéticos.

**1.** Master's student in Electrical Engineering at *Pontifícia Universidade Católica do Rio de Janeiro* – Rio de Janeiro, RJ – Brazil. E-mail: praxedes@ele.puc-rio.br

**2.** Research Assistant, Master's degree in Electrical Engineering at *Pontifícia Universidade Católica do Rio de Janeiro* – Rio de Janeiro, RJ – Brazil. E-mail: adriano@ele.puc-rio.br

**3.** PhD in Computer Science at the University College London (UCL). Professor at the Department of Electrical Engineering, *Pontifícia Universidade Católica do Rio de Janeiro* – Rio de Janeiro, RJ – Brazil. E-mail: marley@ele.puc-rio.br

**4.** PhD in Computer Science at the University College London (UCL). Professor at the Department of Electrical Engineering, *Pontifícia Universidade Católica do Rio de Janeiro* – Rio de Janeiro, RJ – Brazil. E-mail: marco@ele.puc-rio.br

**5.** PhD in Computer Science at the University of London (UL). Professor at the Department of Electrical Engineering, *Pontifícia Universidade Católica do Rio de Janeiro* – Rio de Janeiro, RJ – Brazil. E-mail: ricardo@ele.puc-rio.br

## 1. INTRODUCTION

One of the most important tasks in the industry of oil exploration and production is lithological identification. Lithology corresponds to the description of the macroscopic and physical characteristics of a rock, such as color, texture, grain size, and mineral content (SCHLUMBERGER, 2014; U.S. GEOLOGICAL SURVEY, 2014). On the basis of that description, and knowing the location of each type of rock in the well, it is possible to infer the location of formations generating hydrocarbon content, and, especially, the reservoir required for the occurrence of an oil field system.

There are several sources of information for this task, but one of the main ones to subsidize lithological identification is logging. This method consists of physical measurements taken by tools that are introduced gradually along the well. Because logging tools measure the properties of the rocks underground, their records are mainly geological (DOVETON, 2002). Traditionally, statistics techniques are used to provide lithological identification by studying profiles. One of the most used techniques is the discriminating analysis (BUSCH et al., 1987). Besides this practice, computational intelligence techniques have been used with some level of success, especially the use of neural networks, support vector systems, and Fuzzy inference systems (SANTOS et al., 2003; MINGJUN et al., 2011; LEITE, 2012; BOSCH et al., 2013; ZHENG; MO., 2014).

However, in most papers, the profiles used in lithological identification are those available in the wells, such as those of gamma rays, neutron porosity and resistivity. This information is only known after the wells are opened. In the previous stage, that is, outside the well, the only records of the surface available are the attributes deriving from seismic surveys.

In order for the identification models to be applied outside the wells, it is necessary to use characteristics that are present both inside and outside the wells. In the wells, where lithology is known through conventional profiles and other data, the models are trained and, afterwards, tested to check for accuracy. Outside the wells, with the same characteristics, the models are applied so that the quality of their result is assessed by a geologist or a geophysician.

For that to happen, such model should be improved both in terms of accuracy of the standard approach (linear

discriminant analysis) and of providing experts with interpretations of the obtained results. A viable alternative are the Genetic Fuzzy Systems (CÓRDON et al., 2001; HERRERA, 2008), which provide their users with relative accuracy and good linguistic comprehension of the classifications made by the model. Based on the *Genetic Programming Fuzzy Inference System* (GPFIS) (KOSHIYAMA et al., 2014), this study aims at assessing the quality of this approach in terms of techniques of classification of computational and statistical intelligence.

This study was organized as follows: the next section describes notions about the physics of rocks, and presents a deep approach of the problem faced. Section 3 disposes the GPFIS model, adequate for the aforementioned classification problem. Section 4 reports the other models of classification used, metrics of evaluation, the experimental procedure, as well as the results and discussions. And, finally, Section 5 presents the final considerations and further studies.

## 2. RESEARCH METHODOLOGY

This section shows some notions about the physics of rocks and analyzes the problem approached. It also presents the GPFIS model (KOSHIYAMA et al., 2014), especially designed to solve classification problems. Since the model is based on multigene genetic programming (SEARSON et al., 2007; HINCHLIFFE et al., 1996), the first part shows this variation of classic genetic programming; the GPFIS model was formulated right after.

### 2.1. NOTIONS ABOUT ROCK PHYSICS AND APPROACHED PROBLEM

The rock physics theory is the field of geophysics that provides the relationships between seismic elastic attributes, measured from the surface of the Earth, from inside the wells or in laboratories, and the petrophysical properties of rocks (AVSETH et al., 2005). It provides the understanding and the theoretical tools to improve the characterization based on elastic data. The sensitivity of seismic signatures to the parameters of the reservoirs has been known for years. With the huge increment in seismic acquisition and processing, and with the need to interpret the amplitudes for the detection of hydrocarbons and the characterization and monitoring of reservoirs, came the practical need to quantify

the relationship between seismic data and rock properties. Empirical equations have been published by several authors to relate, in terms of quantity, the petrophysical properties, and the elastic attributes. Some of them are Han's equations (1986), which relate the compressional and shear velocities to the volume of clay and porosity.

Among the existing seismic elastic attributes, one of the most used ones is acoustic impedance, both compressional (IP) and shear (IS). It defines itself as the product between density and velocity of the compressional and shear wave propagation in a medium (HAN, 1986; TELFORD et al., 1990). Impedances can be calculated both inside and outside the well. In the well, one of the ways to calculate them is the product between the density profile and the profile measuring compressional and shear transit times. Outside the well, it is possible to produce volume with impedance values through the process called seismic inversion, which uses the equation by Aki and Richards and the angle gathers to obtain such volumes (AVSETH et al., 2005). With compressional and shear impedances, it is possible to create a model with well data to classify the lithology and to extrapolate them to seismic data.

This study used data from a well in the Brazilian coast. The well selected for this study is located in a region with a mixed system for the formation of sedimentary rocks. The lithology found in this well was interpreted by an expert geologist who used the conventional profiles of gamma ray wells, density, photoelectric and compressional sonic factor, besides the petrographic description of lateral samples and facies of the image profiles (resistive and acoustic). This lithological interpretation showed seven different types of rocks: arenite, grainstone, calcarenite, mudstone, packstone, sandy mudstone, and shales. These types were grouped into four different classes, because the characteristics that discriminate the rocks in the same class are not detected in the seismic scale. Table 1 shows the combination to create the four classes, from the lithology of the first column to the groups in classes of the second column. The other columns indicate the volume of data each class has after being grouped.

Classification required not only the direct values of the impedances (IP and IS), plus two attributes calculated based on them. The first was the difference between IP and IS (IP - IS), whereas the second calculation was Poisson's

ratio (PR):  $RP = \frac{(IP^2 - 2IS^2)}{2(IP^2 - IS^2)}$ . The choice of these other

attributes was based on the study of rock physics, which points them as good lithological discriminants (AVSETH et al., 2005; CASTAGNA et al., 1993). Figure 1 shows the graphic between IP and IS, with the data of the well used. The four classes are identified by the following colors: *yellow = arenite, red = mix, blue = carbonate, and green = background*. When both impedances are used together, it is possible to observe that all data, according to the studies (AVSETH et al., 2005; CASTAGNA et al., 1993), are located along a narrow, positively oriented region (see Figure 1, for example).

With the attributes IP, IS, IP-IS, and PR, a model was searched in order to infer, based on these seismic derivatives and transformations, the type of rock: arenite, mix, carbonate, or background. The advantage of GPFIS is the possibility to offer this interpretation at a linguistic level, besides the fact that the expert can decide the type of rock through the level of pertinence of a seismic sample to the different classes.

## 2.2. MULTIGENE GENETIC PROGRAMMING

Genetic programming (GP) (POLI et al., 2008) is a technique of evolutionary computing inspired by the concepts of natural selection and genetic recombination. Multigene genetic programming (MGGP) (SEARSON et al., 2007; HINCHILIFFE et al., 1996) can be seen as a generalization of traditional GP, since it indicates an individual is a complex tree structure (functions) which, as it occurs in GP, receives a set of  $X_j$  terminals (attributes of pattern recognition, time series lag etc.), in order to predict the  $Y$  outlet. The representation of MGGP is similar to that of GP concerning the tree structure;

**Table 1.** Types of lithology and groups used in the analyzed well.

Lithology	Class	Padrões	Patterns
Arenite	Arenite	1,991	33.21%
Grainstone	Mixed	1,803	30.08%
Calcarenite	Carbonate	1,480	24.69%
Mudstone			
Packstone	Background	721	12.03%
Sandy mudstone			
Shales			

however, for MGGP, an individual is a complex tree structure (Figure 2).

Each tree in this structure is a partial solution for the problem. It is easy to see that, when  $D = 1$ , MGGP is reduced to the solution obtained by a classic GP ( $d=1, \dots, D$ ). The process of evaluation and selection are similar to those in GP. Regarding the recombination operators, the operation of MGGP mutation is similar to that executed in classic GP. In the case of crossing operation, it is necessary to distinguish it in the level in which the operation is conducted, being possible to apply the crossing in low and high levels. The low level is the space in which it is possible to manipulate the structures (mathematical terminals and operations) of the equations present in an individual. Both the mutation and the crossing, in the low level of MGGP, are similar to those conducted in GP.

An example of high-level crossing is presented in Figure 3. The high level is the space in which the equations present in the individual are manipulated in a macro universe. So, it is

possible to observe that, based on two random points, equations of one individual to another are exchanged.

In general, the evolutionary procedure of MGGP is different from GP due to the addition of two parameters: maximum number of trees per individual and high level crossing rate. In the case of the maximum number of trees per individual, there is always a high value so that there are no obstacles in the process of synthesizing the solution. Regarding the high-level crossing rate, this parameter should be previously defined. Its value must always be presented in the table of algorithm configurations.

### 2.3. GPFIS MODEL

This section approaches the GPFIS model for classification (KOSHIYAMA et al., 2014). Therefore, this paper describes its construction stages, since the mapping of precise values in levels of pertinence to fuzzy sets, and the inference procedure, which is subdivided in formulation, partitioning, and aggregation. After the inference process, decision and evaluation are conducted.

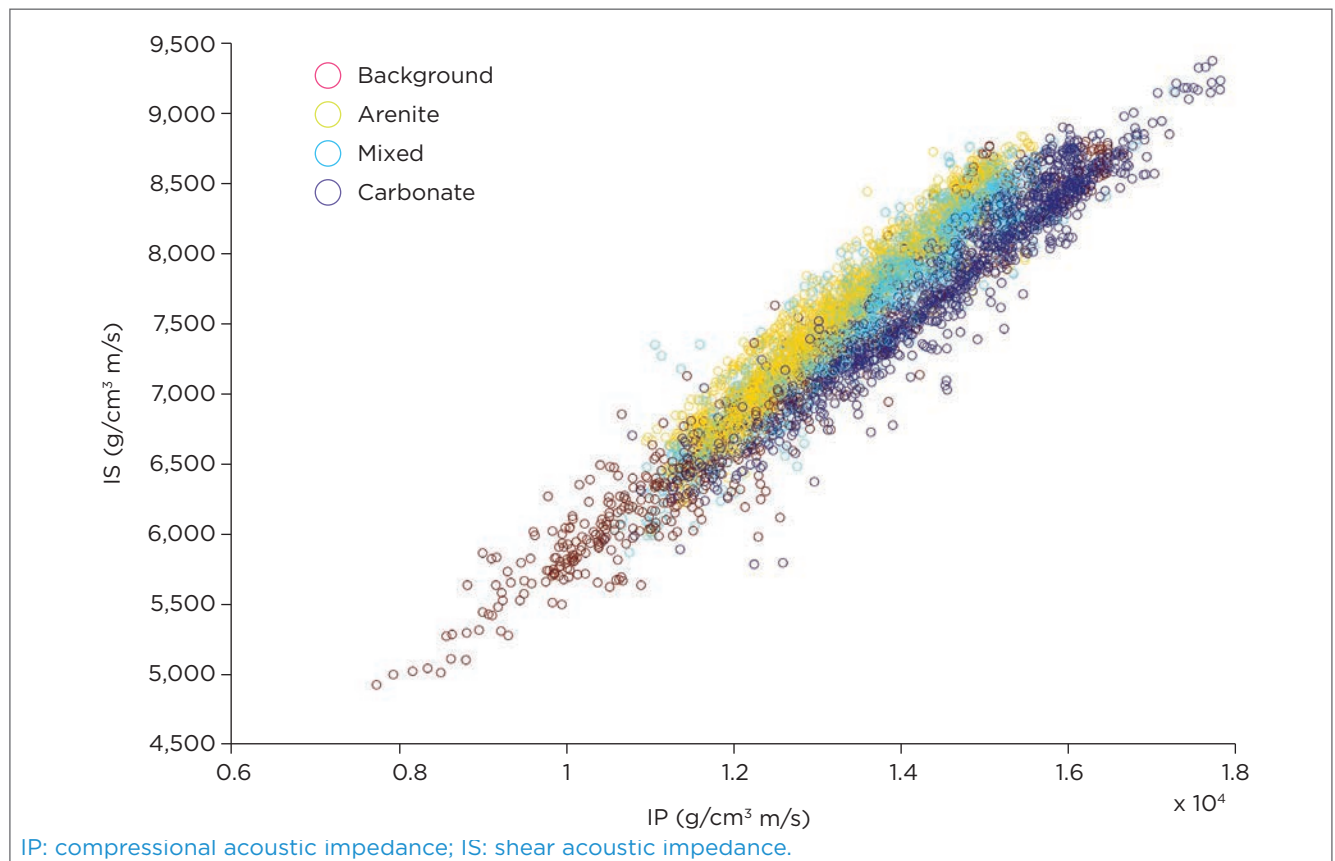


**Figure 1.** Relation between IP and IS and the types of rocks.

### 2.3.1. Fuzzification

In classification, the main information available is the  $n$  patterns  $x^p = [x^p_1, x^p_2, \dots, x^p_K]$  of the  $KX_k$  attributes present in the database ( $p=1, \dots, n$  e  $k=1, \dots, K$ ). The information of the  $n$  patterns is used to distinguish to which  $b$ -th class a new  $x^*p$  pattern belongs ( $b=1, \dots, H$ ). The fuzzification stage establishes the  $A_{jk}$  fuzzy sets associated with each  $k$ -th attribute. In the analyzed case, the attributes are:  $X_1 = IP, X_2 = IS, X_3 = IP-IS,$  and  $X_4 = RP$ .

The fuzzification stage considers three factors: functional form, definition of the support of each pertinence function  $\mu_{A_{jk}}(x_{pk})$ , and appropriate linguistic label, qualifying the subspace comprehended by the pertinence function with an adjective corresponding to the context. After a discussion with experts on the subject, the disposition of pertinence functions for each  $X_k$  is given by Figure 4.

With the fuzzification of each pattern, the inference stage uses the information contained in each  $A_{jk}$  to better predict the class of  $x^*p$ .

### 2.3.2. Inference

The following sections present the subdivision of the inference process in the GPFIS model. In this sense, the first

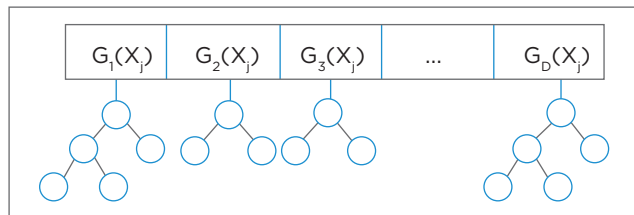


Figure 2. Example of a multigene individual.

stage consists of formulation, that is, when the premises are elaborated by the use of MGGP. The second stage is partitioning, in which, in a set of premises, a single consequent term must be associated to each of them. Then, a base of rules is established, in which each rule of the same consequent is weighed, and its activation is aggregated (aggregation stage).

#### 2.3.2.1. Formulation

To sum up, the GPFIS model searches a set of functions in accordance with the following representation (Equation 1 e 2):

$$\mu_{c_p \in 1}(x_p) = g \left[ f_{d \in s_1} \left( \mu_{A_{j1}}(x_{p1}), \dots, \mu_{A_{jk}}(x_{pk}) \right), \dots, \right. \\ \left. f_{d \in s_2} \left( \mu_{A_{j1}}(x_{p1}), \dots, \mu_{A_{jk}}(x_{pk}) \right) \right] + \\ \mathcal{E}_{p1} \Rightarrow \mu_{c_p \in 1}(x_p) = \hat{\mu}_{c_p \in 1}(x_p) + \mathcal{E}_{p1} \quad (1)$$

...

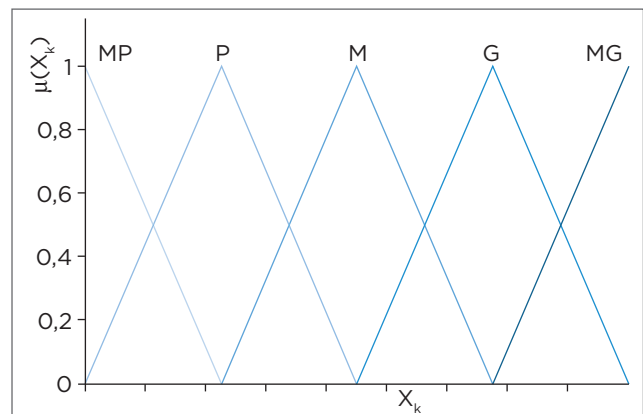


Figure 4. Pertinence functions for  $X_k$  variables.

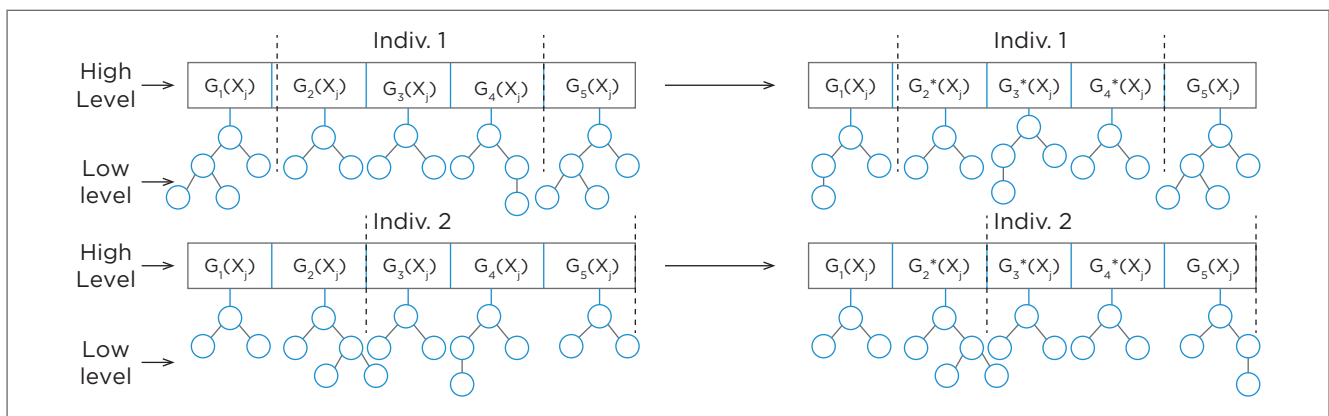


Figure 3. High-level crossing operation.

$$\begin{aligned} \mu_{c_p \in H}(x_p) &= g \left[ f_{d \in s_H} \left( \mu_{A_{j_1}}(x_{p1}), \dots, \mu_{A_{j_K}}(x_{pK}) \right), \dots, \right. \\ & \left. f_{d \in s_H} \left( \mu_{A_{j_1}}(x_{p1}), \dots, \mu_{A_{j_K}}(x_{pK}) \right) \right] + \\ \varepsilon_{p1} &\Rightarrow \mu_{c_p \in 1}(x_p) = \hat{\mu}_{c_p \in H}(x_p) + \varepsilon_{pH} \end{aligned} \quad (2)$$

The elements belonging to each expression are described as follows:

- $f_{d \in s_b} \left( \mu_{A_{j_1}}(x_{p1}), \dots, \mu_{A_{j_K}}(x_{pK}) \right)$ : the function  $f_{d \in s_b} : [0,1]^K \rightarrow [0,1]$ ,  $d=1, \dots, D$  describes the form of relationship of the pertinence functions of each  $k$ -th attribute regarding the  $b$ -th class, each  $f_{d \in s_b} \left( \mu_{A_{j_1}}(x_{p1}), \dots, \mu_{A_{j_K}}(x_{pK}) \right)$  describes a fuzzy rule, based on t-norm, t-conorm operators, negation etc., with the purpose of representing logical connectives (*and*, *or* and *no*) and linguistic modifiers (*much* and *little*, for example). The  $d \in s_b$  index is better described in the section “partitioning,” but, generally, it indicates the  $d$ -th functions (rule premise) that are related with the  $b$ -th class;
- $g \left[ f_{d \in s_b} \left( \mu_{A_{j_1}}(x_{p1}), \dots, \mu_{A_{j_K}}(x_{pK}) \right), \dots, f_{d \in s_b} \left( \mu_{A_{j_1}}(x_{p1}), \dots, \mu_{A_{j_K}}(x_{pK}) \right) \right]$ : the function  $g: [0,1]^{\text{card}(s_b)} \rightarrow [0,1]$  is an aggregation operator whose role is to gather the levels of action regarding a set of rules associated to each  $b$ -th class in a final value;
- $\mu_{c_p \in H}(x_p)$  measures the level of pertinence of  $x_p$  to the  $h$ -th class. It is always  $\{0,1\}$ , that is, the  $p$ -th pattern belongs to the  $h$  class or not;
- $\hat{\mu}_{c_p \in H}(x_p)$  measures the estimated level of pertinence of  $x_p$  to the  $h$ -th class, assuming values between  $[0,1]$ ;
- $\varepsilon_{pb}$ : deviation between the observed and the estimated.

The objective of the GPFIS model is to search the  $f_d \left( \mu_{A_{j_1}}(x_{p1}), \dots, \mu_{A_{j_K}}(x_{pK}) \right)$  in order to produce an estimation  $\hat{\mu}_{c_p \in H}(x_p)$  that minimizes  $\sum_{p=1}^n (\varepsilon_{pb})^2$ . For that, the GPFIS model uses elements of MGPP, in order to synthesize the set of rule premises  $f_d \left( \mu_{A_{j_1}}(x_{p1}), \dots, \mu_{A_{j_K}}(x_{pK}) \right)$ . By the availability of a set of premises  $f_d \left( \mu_{A_{j_1}}(x_{p1}), \dots, \mu_{A_{j_K}}(x_{pK}) \right)$ , it is necessary to define a consequent class (that is, to transform  $f_d \left( \mu_{A_{j_1}}(x_{p1}), \dots, \mu_{A_{j_K}}(x_{pK}) \right)$  into  $f_{d \in s_b} \left( \mu_{A_{j_1}}(x_{p1}), \dots, \mu_{A_{j_K}}(x_{pK}) \right)$ . The partitioning techniques, subject of the next topic, are the mechanisms that can be

used to choose a class that is better associated with each  $f_d \left( \mu_{A_{j_1}}(x_{p1}), \dots, \mu_{A_{j_K}}(x_{pK}) \right)$ .

### 2.3.2.2. Partitioning

Be  $d=1, \dots, D$  the set of indexes of the functions  $f_d \left( \mu_{A_{j_1}}(x_{p1}), \dots, \mu_{A_{j_K}}(x_{pK}) \right)$  and  $S=\{s_0, s_1, s_2, \dots, s_H\}$  the set of  $d$  parts, in which  $s_b$  are the indexes of the destined to the  $h$ -th class,  $s_0$  is the set of the  $f_d \left( \mu_{A_{j_1}}(x_{p1}), \dots, \mu_{A_{j_K}}(x_{pK}) \right)$  addressed to no specific class (that is, the discarded antecedents). The method of the certainty or confidence level evaluates the level of compatibility of the antecedent part  $f_d \left( \mu_{A_{j_1}}(x_{p1}), \dots, \mu_{A_{j_K}}(x_{pK}) \right)$ , regarding all H classes (CÓRDON et al., 2001; KOSHIYAMA et al., 2014). That is, the wish is to define the rule consequently, that is more reliable to this given premise. Therefore, for each one of the H classes, a confidence level is computed to the  $b$  class  $b (CD_b)$ , given by Equação 3:

$$CD_b = \frac{\sum_{p \in b} f_d \left( \mu_{A_{j_1}}(x_{p1}), \dots, \mu_{A_{j_K}}(x_{pK}) \right)}{\sum_{p \in b} \sum_{p \in b} f_d \left( \mu_{A_{j_1}}(x_{p1}), \dots, \mu_{A_{j_K}}(x_{pK}) \right)} \quad (3)$$

The  $CD_b$  can be assessed as the identification of the antecedent part to the patterns of the  $b$  class, regarding the total compatibility of the antecedent part to the  $b$  class and the others. So,  $0 \leq CD_b \leq 1$ , in which  $CD_b = 1$  means total compatibility, and  $CD_b = 0$ , therefore, the opposite. The definition of the  $C$  class of the  $f_d \left( \mu_{A_{j_1}}(x_{p1}), \dots, \mu_{A_{j_K}}(x_{pK}) \right)$  is given by steps, for every  $d=1, \dots, D$ , rule premise:

- $CD_b$  is calculated for all H classes;
- The  $b$ -th class is defined for  $f_d \left( \mu_{A_{j_1}}(x_{p1}), \dots, \mu_{A_{j_K}}(x_{pK}) \right)$  to maximize  $CD_b$ ;
- The index of  $f_d \left( \mu_{A_{j_1}}(x_{p1}), \dots, \mu_{A_{j_K}}(x_{pK}) \right)$  in the respective  $s_b$ ;
- In case  $f_d \left( \mu_{A_{j_1}}(x_{p1}), \dots, \mu_{A_{j_K}}(x_{pK}) \right)$  has  $CD_b = 0$  for every  $b$ , its index is inserted in  $s_0$ .

So, not every  $f_d \left( \mu_{A_{j_1}}(x_{p1}), \dots, \mu_{A_{j_K}}(x_{pK}) \right)$  will be associated with a specific consequent, and there may be some inactive consequents. After the definition of  $f_{d \in s_b} \left( \mu_{A_{j_1}}(x_{p1}), \dots, \mu_{A_{j_K}}(x_{pK}) \right)$ , that is, the base of fuzzy rules, it is possible to assess to which class  $x_p = [x_{p1}, x_{p2}, \dots, x_{pK}]$  is more pertinent. Since the same class can have different associated rules, it is necessary to aggregate the activations

coming from the compatibility of  $x_p$  for each rule, in order to generate the final estimation  $\hat{\mu}_{c_p \in H}(x_p)$ .

### 2.3.2.3. Aggregation

In the Genetic-Fuzzy System field, it is common to use the maximum aggregation operator. Even though this approach has some advantages in certain situations, at the same time it handles all the rules with the same level of influence or weight. In some situations, such as the analyzed application, an approach weighing the rules could bring better results, as mentioned in other studies – see a compilation with results in Koshiyama et al.(2014). The convex combination aggregation operator, used in this study, proposes to aggregate the rules referring to the consequent term, according to the Equation 4:

$$\begin{aligned}
 &g \left[ f_{d \in s_b} \left( \mu_{A_{j1}}(x_{p1}), \dots, \mu_{A_{jk}}(x_{pK}) \right), \dots, \right. \\
 &f_{d \in s_b} \left( \mu_{A_{j1}}(x_{p1}), \dots, \mu_{A_{jk}}(x_{pK}) \right) \left. \right] = \\
 &\sum_{d \in s_b} \tau_{d \in s_b} f_{d \in s_b} \left( \mu_{A_{j1}}(x_{p1}), \dots, \mu_{A_{jk}}(x_{pK}) \right), \\
 &\text{com} \sum_{d \in s_b} \tau_{d \in s_b} = 1, \text{ e } \tau_{d \in s_b} \geq 0 \tag{4}
 \end{aligned}$$

This operator generalizes the arithmetic mean, in which the weights  $\tau_{d \in s_b}$  can be any values between [0,1], with the restriction that they add up to 1. Likewise, the interpretation changes, so that  $\tau_{d \in s_b}$  indicates the level of influence of this rule in the final result. After the aggregation stage, each  $\hat{\mu}_{c_p \in 1}(x_p), \dots, \hat{\mu}_{c_p \in H}(x_p)$  is obtained, however, it is necessary to define the class associated to the  $p$ -th pattern.

### 2.3.3. Decision

For the explored formulation, the decision for the belonging of the  $p$ -th pattern  $x_p$  to the class  $b=1, \dots, H$  is given by:

$$\begin{aligned}
 &\hat{C}_p(x_p) = \\
 &\arg_b \max \left( \hat{\mu}_{c_p \in 1}(x_p), \dots, \hat{\mu}_{c_p \in b}(x_p), \dots, \hat{\mu}_{c_p \in H}(x_p) \right) \tag{5}
 \end{aligned}$$

In the Equation 5  $\hat{C}_p(x_p)$  is the estimated class, a result of the  $b$ -th argument that has the maximum value in the expression (5). The idea is to show that  $x_p$  belongs to the class with which it is more compatible, according to the available

rules. When there is a tie, decision heuristics can be applied (the class with the highest proportion), or no specific class is attributed with  $x_p$ .

### 2.3.4. Evaluation

To sum up, the evaluation of the GPFIS model is defined by a primary objective, minimization of error, and by a secondary one, reduction of the individual's complexity. The primary objective dominates the form of positioning individuals in the population, whereas the second manifests itself as a tiebreaker.

The function of the evaluation for classification problems, is given by the mean classification error (MCE - Equation 6):

$$EMC = \frac{\sum_{p=1}^n |C_{p \in b}(x_p) - \hat{C}_{p \in b}(x_p)|}{n} \tag{6}$$

In which, for a given pattern  $x_p$ ,  $|C_{p \in b}(x_p) - \hat{C}_{p \in b}(x_p)| = 0$ , se  $C_{p \in b}(x_p) = \hat{C}_{p \in b}(x_p)$  and 1, when  $C_{p \in b}(x_p) \neq \hat{C}_{p \in b}(x_p)$ . The individual that minimizes MCE is considered the best in the population.

The second objective is the reduction of complexity, based on the method of lexicographic parsimony pressure (LUKE; PANAIT, 2002). The idea behind the method is: for two individuals with identical performance, the best among them is the one that has fewer nodes in the tree. This indicates the rules with fewer antecedents, less operators of concentration/dilation, negation, and individuals with less  $f_d(\mu_{A_{j1}}(x_{p1}), \dots, \mu_{A_{jk}}(x_{pK}))$ ; therefore, with a smaller base of fuzzy rules. With the evaluation, each individual can be selected and recombined to generate a new population. This process goes on until a stop criterion is hit. In this moment, the last population returns.

## 3. RESULTS AND DISCUSSIONS

### 3.1. DESCRIPTION OF THE EXPERIMENTS

Besides the GPFIS model, other classification models were also used. Table 2 presents each one of them, with the parameters composing them. It is worth mentioning that the choice of value for each parameter is owed to preliminary tests, aiming at selecting the best configuration. For the Pitt-GFS, the same number of pertinence functions and

profile used in GPFIS were considered (Figure 4) for each attribute, in order to turn the approaches as close as possible.

The well analyzed has 5,995 patterns, in total. The way to assess the accuracy of each method was the 10-fold cross-validation, accounting for the total of 5,394 training patterns and 601 test patterns, in each folder. The results reported are a result of the mean of three executions in each folder of the 10-fold cross-validation, for each method. The metrics calculated were total accuracy, which does not discriminate the unbalancing between classes and mean accuracy. The advantage of mean accuracy for application comprehends the fact that it considers the imbalance between classes (arenite has more patterns than the background, for instance); therefore, it penalizes classifiers that privilege the dominant class to the detriment of the others.

Table 3 has the parameters used in the GPFIS model. The product operator was used for conjunction, as well as

**Table 2. Classifiers and parameters used.**

Model	Parameter
GPFIS	Table 3
SFGBR, <i>Pittsburgh</i> type (Pitt-GFS) (BASTIAN et al., 2000)	Table 3
Naive Bayes (NB) (MITCHEL, 2000)	-
KNN (MITCHEL, 2000)	3-nearest-neighbour, Euclidean distance
Classification tree (CART) (MITCHEL, 2000)	-
Linear discriminant analysis (DISC) (JOHNSON and WICHERN, 2002)	-
MGGP	Table 3
Multiple-layer perceptron (MLP) (MITCHEL, 2000)	One hidden layer, logistic activation function (hidden and outlet) and 10 neurons

GPFIS: *Genetic Programming Fuzzy Inference System*; SFGBR: *Genetic-fuzzy system for the base of rules*; Pitt-GFS: *Pittsburgh-type Genetic Fuzzy System*; KNN: *k-nearest-neighbors*.

negation, in order to increase the possible combinations of linguistic terms to formulate the premises. Even though negation made the rules less understandable in terms of linguistics, its use led to the bases of more compact rules.

In the case of MGGP, the process used was similar to that of Kishore et al. (2000), concerning the treatment of a multiple-class problem, such as that of binary classes. For that, MGGP was executed four times, dividing the number of feasible evaluations equally (5,000 for each execution), so that each execution leads to the elaboration of a discriminant function for a specific class. In the end of the four executions, the discriminant functions were gathered, and the patterns separated for the test phase were classified. For the evolutionary approaches, the evaluation function was the mean classification error. GPFIS was implemented in MATLABR2014b – for other computational details, see Koshiyama et al. (2014).

### 3.2. RESULT DESCRIPTION

Table 4 shows the results referring to the accuracy of the analyzed classifiers. It is possible to observe that, in general, the GPFIS model was more accurate, in average 4% more accurate than the multilayer perceptron (MLP). In comparison, Pitt-GFS had worse results than GPFIS and Naive Bayes (NB). The standard approach – the linear discriminant analysis (DISC) – led to results with worse performance than

**Table 3. Main configurations of the models based on genetic programming.**

Parameter	Value
Size of the population	100
Number of generations	200
Maximum height of the tree	5
Size of the tournament	2
High-level cross-rate	50%
Low-level cross-rate	85%
Mutation rate	10%
Elitism rate	1%
Lexicographic pressure	Yes
Input fuzzy sets	Figure 4
Fuzzy operators	Product and negation

that of GPFIS. Table 5 presents the accuracy of each model. Also, the GPFIS model obtained the best results, providing on an average 6.98% more classification accuracy than NB, the second best in this matter. It was also shown that the GPFIS model has mean posts (numerical scale of 1 to 8, so that the best model per fold has a post equal to 1, the second to 2, and so on), inferior to the other models – approximately half of the second best model per criterion.

Generally, the results of GPFIS are superior to those of the approach of the expert (DISC) in two items: better results, when assessed by the volume of properly classified patterns (accuracy), and balance of efforts to reach the maximum number of patterns of different classes (precision). It is worth mentioning that the NB approach, which requires little computational effort, also brought good results and is useful in situations that require continuous learning and short-term decisions.

The results suggest that the GPFIS model behaves relatively well in situations with low intensity of imbalance between classes, when compared to the other classifiers. An explanation for that comes from the analysis of the fuzzy rules (Table 6), in conjunction with Figure 5. For this example, the background lithology is considered. It is observed that the first rule, R1, established that if IS is small (P),

than the seismic pattern belongs to the background type. Also, R2 and R3, when assessed together, describe if IP is small, and IS is also small, so IP–IS is not medium or large. Then, the seismic pattern belongs to the background type of rock. To sum up, we observed that R1 and R2 delimit the region in which the patterns of the background class are located: small values of IP and IS (Figure 5); R3 cooperates with R2 in order to focus more on the patterns located in this region, relatively close to the mean IP and IS. By this construction of the discriminant region, the GPFIS model can provide good classification for the classes with fewer patterns for training.

Figure 5 illustrates the discriminant region of the GPFIS model with the base of rules according to Table 6. It is observed that the patterns of background lithology are located in the range of low and mean values of IP and IS. When a seismic pattern has high IP and IS values, according to the GPFIS model, it is classified as carbonate. Finally, consider a seismic pattern with IP around 14,000 g/cm<sup>3</sup> m/s and IS of 8,200 g/cm<sup>3</sup> m/s. After computing IP–IS and PR, it is possible to assess that the level of pertinence of this pattern for each lithology is: background=0.00, carbonate=0.02, arenite=0.60, and mixed=0.398. An expert can interpret this result in two ways:

**Table 4.** Mean accuracy in the test phase of the three executions per cross validation fold.

Fold	MLP	Pitt-GFS	GPFIS	MGGP	DISC	NB	CART	KNN
I	69.11%	57.22%	69.17%	47.17%	61.00%	<b>69.50%</b>	46.83%	48.33%
II	66.33%	57.15%	<b>68.73%</b>	57.48%	57.26%	57.76%	52.25%	53.92%
III	55.87%	54.09%	55.98%	44.69%	44.07%	<b>60.43%</b>	44.74%	45.74%
IV	60.60%	59.04%	63.44%	53.20%	46.74%	<b>69.95%</b>	45.58%	41.90%
V	51.53%	54.42%	<b>68.78%</b>	54.65%	50.25%	68.61%	56.09%	53.26%
VI	<b>62.99%</b>	55.04%	61.83%	56.82%	61.10%	51.92%	44.91%	46.91%
VII	46.52%	34.17%	<b>65.55%</b>	50.81%	40.57%	35.06%	43.57%	45.58%
VIII	51.78%	<b>52.06%</b>	49.83%	47.56%	46.67%	46.50%	41.17%	47.00%
IX	54.44%	54.22%	<b>58.50%</b>	58.22%	45.67%	51.33%	41.67%	45.67%
X	<b>57.79%</b>	49.81%	55.57%	52.63%	39.43%	46.26%	44.43%	48.25%
Mean	57.70%	52.72%	<b>61.74%</b>	52.32%	49.28%	55.73%	46.12%	47.66%
Post	2.8	4.6	<b>1.7</b>	4.2	6.05	3.9	6.8	5.95

MLP: Multi-layer *perceptron*; Pitt-GFS: Pittsburgh-type Genetic Fuzzy System; GPFIS: Genetic Programming Fuzzy Inference System; PGMG: multigene genetic programming; DISC: linear discriminant analysis; NB: Naive Bayes; CART: Classification tree; KNN: *k-nearest-neighbors*.

1. Define it as an arenite rock, based on the decision criterion of the most compatible class;
2. Establish that this pattern has around 60.0% of arenite, 39.8% of mix and traces of carbonate (maybe by noise measurement). This last interpretation occurs due to the

lack of homogeneity in the seismic pattern (for instance, large samples, or with areas of different topologies). Both types of interpretation can be useful to experts and are viable based on a fuzzy system for classification, such as the GPFIS.

**Table 5.** Mean precision in the test phase of the three executions per cross-validation fold.

Fold	MLP	Pitt-GFS	GPFIS	MGGP	DISC	NB	CART	KNN
I	60.16%	47.95%	<b>64.10%</b>	44.66%	61.30%	61.38%	41.35%	44.23%
II	60.05%	54.64%	<b>66.66%</b>	49.73%	60.84%	53.63%	47.00%	49.62%
III	56.95%	53.65%	60.05%	38.49%	51.95%	<b>61.47%</b>	46.57%	47.90%
IV	58.20%	58.39%	65.39%	46.33%	54.11%	<b>70.26%</b>	45.97%	44.07%
V	43.67%	56.44%	<b>69.66%</b>	50.23%	55.69%	67.89%	57.84%	56.08%
VI	58.22%	51.65%	61.64%	50.08%	<b>63.16%</b>	51.00%	42.31%	45.85%
VII	43.47%	34.39%	<b>64.47%</b>	42.79%	46.62%	36.11%	40.45%	41.95%
VIII	49.23%	52.99%	52.21%	43.10%	<b>52.50%</b>	46.70%	38.71%	46.11%
IX	48.43%	49.69%	<b>54.49%</b>	50.16%	44.82%	47.49%	38.37%	41.22%
X	<b>50.43%</b>	44.19%	48.87%	46.94%	36.66%	41.73%	39.20%	43.41%
Mean	52.88%	50.40%	<b>60.75%</b>	46.25%	52.77%	53.77%	43.78%	46.04%
Post	3.7	4	<b>1.6</b>	5.5	4	3.9	7	6.3

MLP: Multi-layer *perceptron*; Pitt-GFS: Pittsburgh-type Genetic Fuzzy System; GPFIS: Genetic Programming Fuzzy Inference System; PGMG: multigene genetic programming; DISC: linear discriminant analysis; NB: Naive Bayes; CART: Classification tree; KNN: *k*-nearest-neighbors.

**Table 6.** Base of Fuzzy rules of the best individual in the Genetic Programming Fuzzy Inference System (GPFIS) model.

Rule	Antecedent	Consequent	Weight
R1	If IP is not P or M and IP-IS is G and PR is G	Arenite	0.40
R2	If PR is not G	Arenite	0.19
R3	If IP-IS is MG	Arenite	0.41
R4	If IP is M and PR is G and IP-IS is not P nor M	Mixed	0.20
R5	If IS is G and IP-IS is M or G or MG	Mixed	0.80
R6	If IS is MG and IP-IS is M	Carbonate	0.50
R7	If IP is G and PR is M	Carbonate	0.23
R8	If IS is G and PR is M	Carbonate	0.52
R9	If IP-IS is not M and PR is not G	Carbonate	0.18
R10	If IS is P	Background	0.25
R11	If IP is P and IP-IS is not M	Background	0.49
R12	If IP is not MG and IS is P and IP-IS is not MG	Background	0.26

IP: compressional acoustic impedance; P: small; M: medium; IP-IS: compressional acoustic impedance-shear acoustic impedance; G: large; PR: Poisson's ratio; MG: very large; IS: shear acoustic impedance.

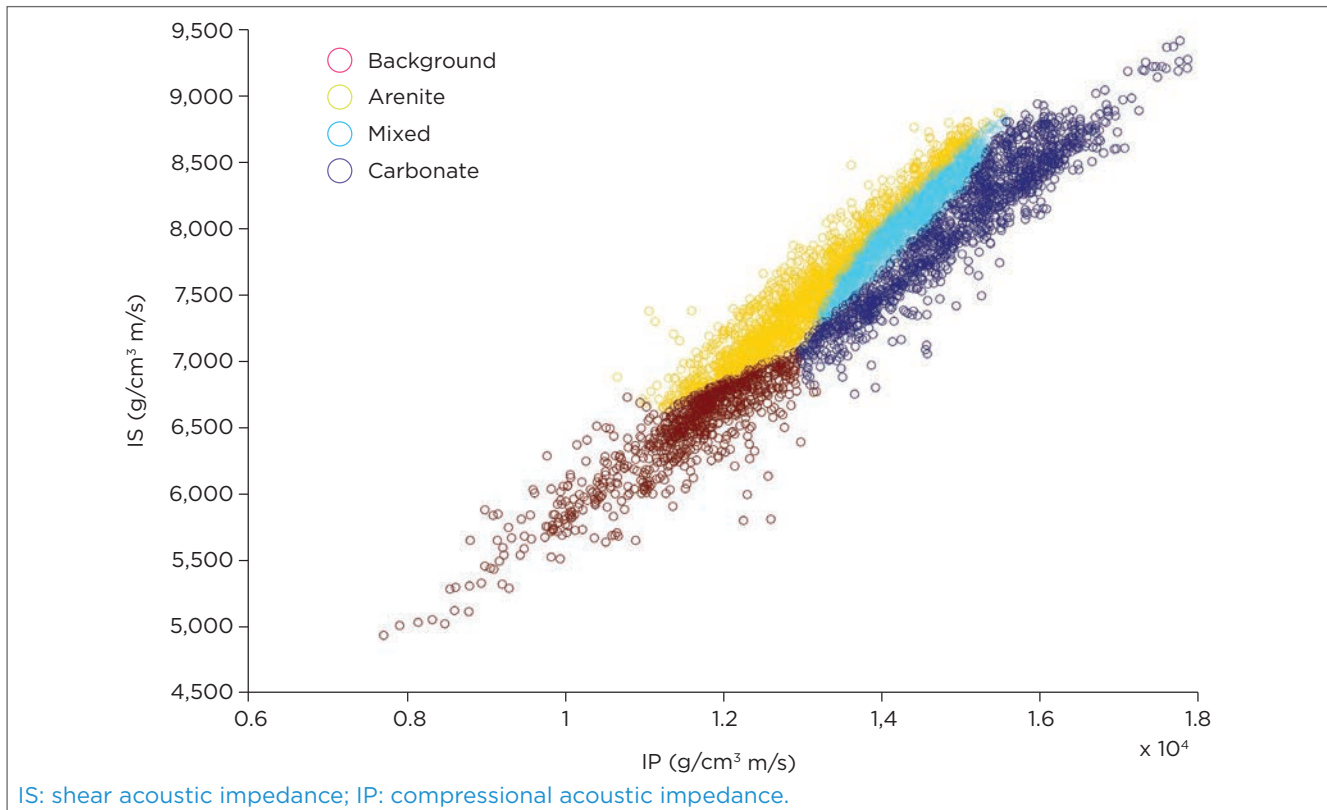


**Figure 5.** Classes predicted by the *Genetic Programming Fuzzy Inference System (GPFIS)* model.

## 4. CONCLUSIONS

This study reported the investigation about lithological discrimination based on seismic patterns. Several statistical classifiers were used (Naïve Bayes, discriminant analysis etc.), and intelligent computing (neural network, fuzzy-genetic classifier etc.). The GPFIS model provided the best results, in average, in comparison to the other models.

Because of the presence of imbalance of classes, there was an explanation as to why GPFIS had good results, through the analysis of the fuzzy rules. Finally, two different interpretations of the fuzzy rules were exposed.

Further studies should explore pre-processing techniques, for example, oversampling methods, to reduce the unbalancing effect of class patterns. Other approaches, such as the use of classifying committees, may help to develop the task of classification, or, still, assess the methodology for the other exploratory fields.

## REFERENCES

AVSETH, P.; MUKERJI, T.; MAVKO, G. *Quantitative seismic interpretation: applying rock physics tools to reduce interpretation risk*. Cambridge: Cambridge University Press, 2005.

BOSCH, D.; LEDO, J.; QUERALT, P. Fuzzy logic determination of lithologies from well log data: application to the KTB Project Data set (Germany). *Surveys in Geophysics*, v. 34, n. 4, p. 413-439, 2013.

BUSCH, J.M.; FORTNEY, W.G.; BERRY, L.N. Determination of lithology from well logs by statistical analysis. *Society of Petroleum Engineers Formation Evaluation*, v. 2, p. 412-418, 1987.

CASTAGNA, J.P.; BATZLE, M.L.; KAN, T.K. Rock physics: the link between rock properties and AVO response. *Investigations in Geophysics*, v. 8, p. 135-171, 1993.

- CÓRDON, O.; HERRERA, F.; HOFFMANN, F.; MAGDALENA, L. *Genetic Fuzzy Systems: evolutionary tuning and learning of fuzzy knowledge bases*. World Scientific, 2001.
- DOVETON, J.H. The geological application of wireline logs: a keynote perspective. *AAPG Methods in Exploration*, v. 13, p. 115-122, 2002.
- HAN, D. *Effects of porosity and clay content on acoustic properties of sandstone and unconsolidated sediments*. Unpublished Ph.D dissertation, Stanford University, 1986.
- HERRERA, F. Genetic Fuzzy Systems: taxonomy, current research trends and prospects. *Evolutionary Intelligence*, v. 1, n. 1, p. 27-46, 2008.
- HINCHLIFFE, M.; HIDDEN, H.; MCKAY, B.; WILLIS, M.; THAM, M.; BARTON, G. Modelling chemical process systems using a multi-gene. *Late Breaking Papers at the Genetic Programming*, p. 56-65, 1996.
- JOHNSON, R.A.; WICHERN, D.W. *Applied multivariate statistical analysis*. 5. ed. Nova Jersey: Prentice-Hall, 2002.
- KISHORE, J.K.; PATNAIK, L.M.; MANI, V.; AGRAWAL, V.K. Application of genetic programming for multicategory pattern classification. *IEEE Transactions on Evolutionary Computation*, v. 4, n. 3, p. 242-258, 2000.
- KOSHIYAMA, A.S.; VELLASCO, M.M.B.R.; TANSCHUIT, R. GPFIS: *Um sistema fuzzy-genético baseado em programação genética*. Dissertação de Mestrado. Departamento de Engenharia Elétrica. Rio de Janeiro: Pontifícia Universidade Católica do Rio de Janeiro, 2014, 222 p.
- LEITE, V.R.C. *Uma análise da classificação de litologias utilizando SVM, MLP e métodos Ensemble*. Dissertação de Mestrado. Departamento de Informática. Rio de Janeiro: Pontifícia Universidade Católica do Rio de Janeiro, 2012.
- LUKE, S.; PANAIT, L. Lexicographic parsimony pressure. In: LANGDON, W.B.L. et al., editor, *GECCO 2002: Proceedings of the Genetic and Evolutionary Computation Conference*, p. 829-836, Nova York: Morgan Kaufmann Publishers.
- MINGJUN, L.; HENGTANG, L.; ZAIBING, J. Application of genetic-BP neural network model in lithology identification by logging data in Binchang mining area. *Coal Geology & Exploration*, v. 39, n. 4, p. 8-12, 2011.
- MITCHELL, T.M. *Machine learning*. Burr Ridge: McGraw Hill, 1997.
- POLI, R.; LANGDON, W.B.; MCPHEE, N.F.; KOZA, J.R. *A field guide to genetic programming*. Rayleigh: Lulu, 2008.
- SANTOS, R.O.V.; VELLASCO, M.M.B.R.; ARTOLA, F.A.V.; DA FONTOURA, S.A.B. Neural net ensembles for lithology recognition. In: WINDEATT, T.; ROLI, F. (eds.), *Multiple classifier systems*, volume 2709, Lecture Notes in Computer Science, p. 246-255. Springer: Heidelberg, 2003.
- SCHLUMBERGER, Schlumberger Oilfield Glossary, (<http://www.glossary.oilfield.slb.com/Display.cfm?Term=lithology>). Visualizado em Março de 2014.
- SEARSON, D.; WILLIS, M.; MONTAGUE, G. Coevolution of nonlinear PLS model components. *Journal of Chemometrics*, v. 21, n. 12, p. 592-603, 2007.
- TELFORD, W.M.; GELDART, L.P.; SHERIFF, R.E. *Applied geophysics*. Cambridge: Cambridge University Press, 1990.
- U.S. GEOLOGICAL SURVEY, Earthquake Glossary, (<http://earthquake.usgs.gov/learn/glossary/?term=lithology>). Visualizado em Março de 2014.
- ZHENG, W.; MO, X. Complex lithology automatic identification technology based on fuzzy clustering and neural networks. *FSKD 2014: 11th International Conference on Fuzzy Systems and Knowledge Discovery*, pp.227-231, Berlim: Springer-Verlag.

# COMPARISON BETWEEN THE THEORETICAL ESTIMATION AND THE MEASUREMENTS OF THE MAIN FIGURES OF MERIT OF QUANTUM WELL INFRARED PHOTODETECTORS

Comparaç o entre a estimac o te rica e as medidas das principais figuras de m rito de fotodetectores infravermelhos a poos qu nticos

Ali Kamel Issmael Junior<sup>1</sup>, F bio Durante Pereira Alves<sup>2</sup>,  
Ricardo Augusto Tavares Santos<sup>3</sup>

**Abstract:** This paper presents a comparison between the theoretical estimation and the measures of the main figures of merit of quantum well infrared photodetectors (QWIP). Mathematical models of the main figures of merit such as absorption coefficient, dark current, and responsivity, available in the specialized literature, are analyzed, compared, and implemented in MatLab<sup>®</sup>. The results of numerical simulations are compared with experimental data published in other studies and show that the models which are properly adapted have great potential for use in projects of real devices.

**Keywords:** Photodetectors. Quantum Wells. Characterization. Military Applications.

**Resumo:** Este artigo traz uma discuss o da comparaç o entre estimac o te rica e medidas das principais figuras de m rito de fotodetectores infravermelhos a poos qu nticos (QWIP). Modelos matem ticos do coeficiente de absorc o, da corrente de escuro e da responsividade, dispon veis na literatura especializada, s o analisados, comparados e implementados utilizando a ferramenta computacional MatLab<sup>®</sup>. Os resultados das simulaç es s o comparados com dados experimentais publicados em outros estudos e indicam que os modelos, convenientemente adaptados, apresentam grande potencial para serem utilizados em projetos de dispositivos reais.

**Palavras-chaves:** Fotodetectores. Poos Qu nticos. Caracterizaç o. Aplicaç es Militares.

## 1. INTRODUCTION

Photodetection is now a technological reality that has increased the possibilities in several fields of knowledge. One of them is Defense, since the characterization of

objects or scenes by photodetectors with high sensitivity and selectivity in a wide infrared spectral range enables systems – such as missile guidance ones – to obtain more accuracy in the selection and hitting of a target.

**1.** Bachelor's degree in Electrical Engineering, with emphasis on Electronic Systems (1999), at "Universidade do Estado do Rio de Janeiro" (UERJ), Brazilian Navy Engineer Officer (since 2000) and expert in Electromagnetic Environment's Analysis (2007), at "Instituto Tecnol gico de Aeron utica" (ITA). He is currently an Assistant for the Management of the S-BR Combat System Development, in the "Coordenadoria-Geral do Programa de Desenvolvimento do Submarino com Propuls o Nuclear" (COGESN), Rio de Janeiro, RJ - Brazil. E-mail: ali.kamel@marinha.mil.br and alikamel@ig.com.br

**2.** Bachelor's degree in Aeronautical Sciences (1986) at "Academia da Fora A rea" (AFA). Graduated in Electrical Engineering (1997) at "Instituto Tecnol gico de Aeron utica" (ITA). Master's degree in Electrical Engineering and Computer Science (1998) at "Instituto Tecnol gico de Aeron utica" (ITA). Master's degree in Electrical Engineering at the Naval Postgraduate School (NPS) - USA (2006), Electrical Engineering degree at the Naval Postgraduate School - USA (2007). PhD in Physics (2008) at "Instituto Tecnol gico de Aeron utica" (ITA) and Postdoctoral researcher in the field of Terahertz detector arrays at the Naval Postgraduate School (NPS) - USA (2011). He is currently the Air Force Reserve Colonel in the "Fora A rea Brasileira" (FAB), Associated researcher at the Physics Department of the Naval Postgraduate School (NPS) and Collaborating Professor (volunteer) at the Electronic Engineering Division at "Instituto Tecnol gico de Aeron utica" (ITA) - S o Jos  dos Campos, SP - Brazil. E-mail: durante@ita.br

**3.** Graduated in Aeronautical Sciences and Military Pilot at the Academia da Fora A rea (AFA) in 1993. In 2001, he specialized in Electromagnetic Environment's Analysis and obtained a Master's degree in Electrical Engineering and Computer Science (2004) at "Instituto Tecnol gico de Aeron utica" (ITA). In 2009, he concluded the doctoral program also at "Instituto Tecnol gico de Aeron utica" (ITA). He is currently the Deputy Director of Operational Evaluation and Research and Development of the "N cleo do Instituto de Aplicaç es Operacionais" (NuIAOp) of the "Comando-Geral de Operaç es A reas" (COMGAR), in S o Jos  dos Campos, SP - Brazil E-mail: tavares.ricardoaugusto@gmail.com

Infrared radiation comes from the molecular agitation caused by the high temperatures of bodies and objects. More precisely, all bodies above the absolute zero emit radiation. Figure 1 (NASA, 2007) shows the location of infrared radiation inside the electromagnetic spectrum.

The infrared region of the electromagnetic spectrum, depending on the reference used, can be subdivided into four bands: near infrared (NIR), between 0.7 and 3.0  $\mu\text{m}$ ; mid-wavelength infrared (MIR), between 3.0 and 6.0  $\mu\text{m}$ ; long-wavelength infrared (LWIR), between 6.0 and 15.0  $\mu\text{m}$ ;

and very long-wavelength infrared (VLWIR), whose wavelength was higher than 15.0  $\mu\text{m}$  (ALVES, 2005). These subdivisions can be visualized in Table 1.

The atmosphere, where radiation is propagated, is composed of gas and suspended particles distributed through different temperatures and pressure, defined by altitude and geographic position. The gas and the particles can be placed in six different layers distributed according to the altitude variation. The lowest one – usually the scenario used in military applications – is the troposphere, which extends from

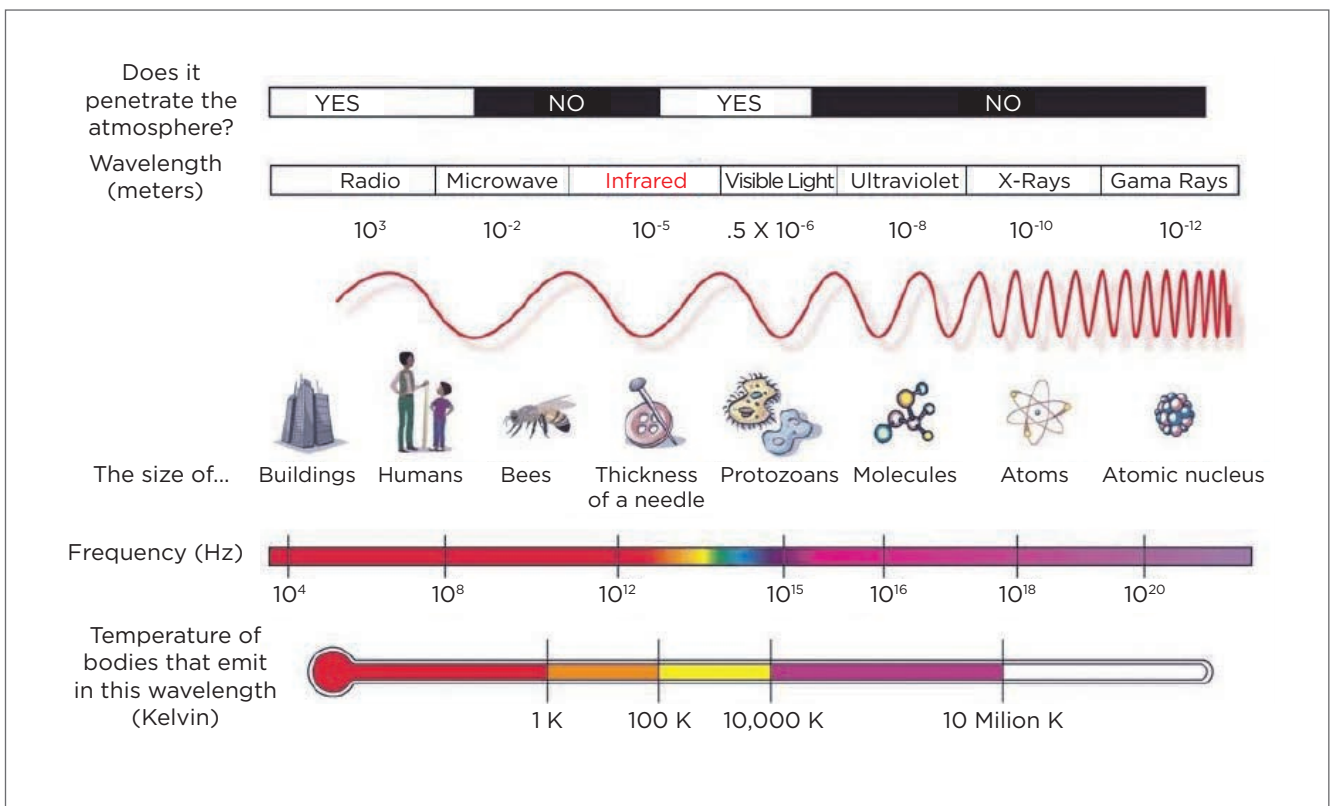


Figure 1. The electromagnetic spectrum and the location of infrared radiation (NASA, 2007).

Table 1. Subdivisions of infrared radiation band (ALVES, 2005).

Name	Abbreviation	Limits ( $\mu\text{m}$ )
Near infrared	NIR	0.75 to 3
Mid-wavelength infrared	MIR	3 to 6
Long-wavelength infrared	LWIR	6 to 15
Very long-wavelength infrared	VLWIR	15 a 1000

sea level to approximately 11 km (SANTOS, 2004), depending on the season and the latitude. In this layer, temperature falls whereas altitude rises, in a 6.5 K/km ratio; however, this ratio may change, and that can cause scattering effects (SANTOS, 2004). Infrared radiation attenuation mostly occurs in this layer, and its main components are water, carbon dioxide, clouds, and smoke. The other layers are stratosphere, mesosphere, ionosphere, thermosphere, and exosphere. When infrared is transmitted through the atmosphere, the gases make a selective absorption, and scattering is provoked by the suspended particles. Sometimes, there is some modulation caused by quick changes in temperature and/or pressure.

Water steam is a major attenuation factor for optical radiation, and it is prevalent in altitudes lower than 10 km. Attenuation above this level is despicable. Carbon dioxide is present until 5 km, approximately, and it only attenuates infrared radiation. Considering the attenuation effects of

the atmosphere, infrared detectors are designed to respond to frequency bands in which infrared radiation transmittance is maximum. Figure 2 shows that atmospheric transmittance limits the possibility of detection in three well-defined regions: 0.7–2.5  $\mu\text{m}$ , 3.0–5.0  $\mu\text{m}$ , and 8.0–15.0  $\mu\text{m}$ , therefore corresponding to bands NIR, MIR, and LWIR, respectively (BOSCHETTI, 2015).

In this context, quantum well infrared photodetectors (QWIP) have become a good choice for modern photodetection systems. In the case of military applications, there is a demand for detectors with special features to be used in the battlefield, in missions that might involve target recognition, environment imaging, or fields of interest – besides missile guidance. QWIP cameras are very attractive for this application because of its high selectivity and multispectral detection characteristics, enabling the detection and identification through high-resolution images (GUNAPALA et al., 2007; GUNAPALA, 2007; DYER; TIDROW, 1998).

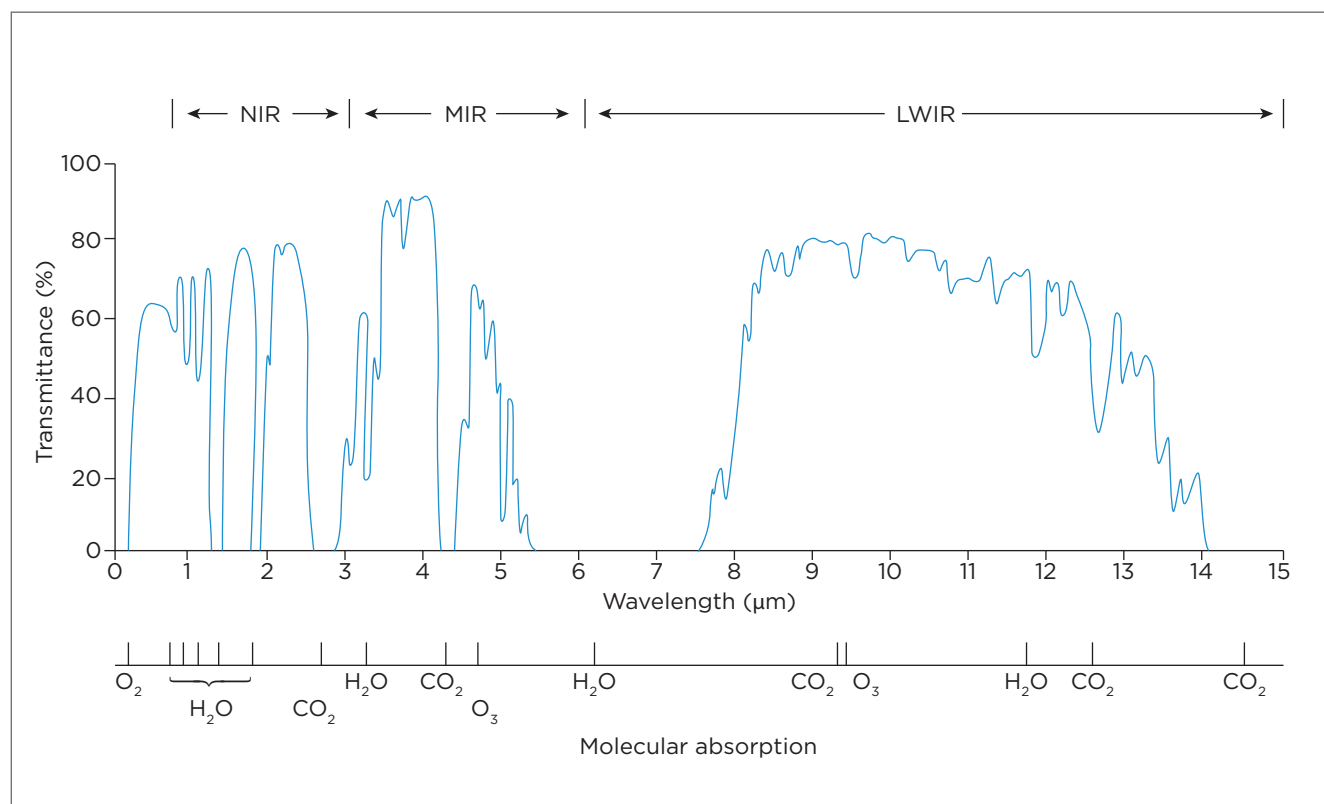


**Figure 2.** Atmospheric transmission spectrum, in the near, mid- and long-wavelength infrared bands. The spectrum corresponds to a layer of 1830 m of air at sea level, with 40% of relative humidity at 25°C. The bottom of the figure shows the lines of absorption of some components in the atmosphere, responsible for the transmission curve (BOSCHETTI, 2015).

Since they generate wide infrared spectral range images – 6–20  $\mu\text{m}$  – (GUNAPALA, 2007), with high discriminatory power – 640  $\times$  512 lines – (GUNAPALA, 2007) in more than one band simultaneously and at a significantly low cost (GUNAPALA, 2007) – these systems are a good option for use in infrared-guided weapons (DYER; TIDROW 1998). With the significant and increasing lethal power of these war systems, such technology becomes a factor that generates asymmetry for the Armed Forces employing it. Figure 3 presents some products in the market that already use this technology.

The knowledge about the characteristics of construction of the QWIP and its performance evaluation factors technically subsidizes future acquisitions of devices, and increases the chances of carrying out the project, its development and manufacture in Brazil. Besides, the study of figures of merit and the development of mathematical tools that simulate it speed up the process of development, with reduced costs. This fact contributes with the technological independence in defense systems.

The results presented in this paper are part of a line of analysis research and development of quantum well photodetectors with capacity of simultaneous detection in three infrared bands: NIR, MWIR, and LWIR. This study has been performed with “Laboratório de Guerra Eletrônica”

(LabGE), “Instituto de Tecnologia de Aeronáutica” (ITA), the Sensor Research Laboratory (SRL), at the Naval Postgraduate School (NPS), in USA, and the National Research Council (NRC), in Canada. The results, published by Alves (2005), Hanson (2006), Alves et al. (2006), Issmael Jr. et al. (2007), Issmael Jr. (2007), and Alves et al. (2008), show the great potential of these devices for military applications. The production of quantum well photodetectors requires:

- Modeling the structures of semiconductor materials;
- Simulating and adjusting the figures of merit within the project requirements;
- Increasing the crystalline structure, characterizing it and repeating the process, after adjusting it to the models and the techniques of simulation;
- Fabricating detectors/cameras; and
- Analyzing the performance.

This cycle can be repeated several times, until the techniques of the project and the models are refined enough to be repetitive, according to some characteristics. In this context, being limited to quantum wells sensitive to LWIR, this paper shows the analysis of some models available in the literature for the main figures of merit, absorption coefficient, dark current, and responsivity. It shows the results obtained by the simulations performed with MatLab® – version

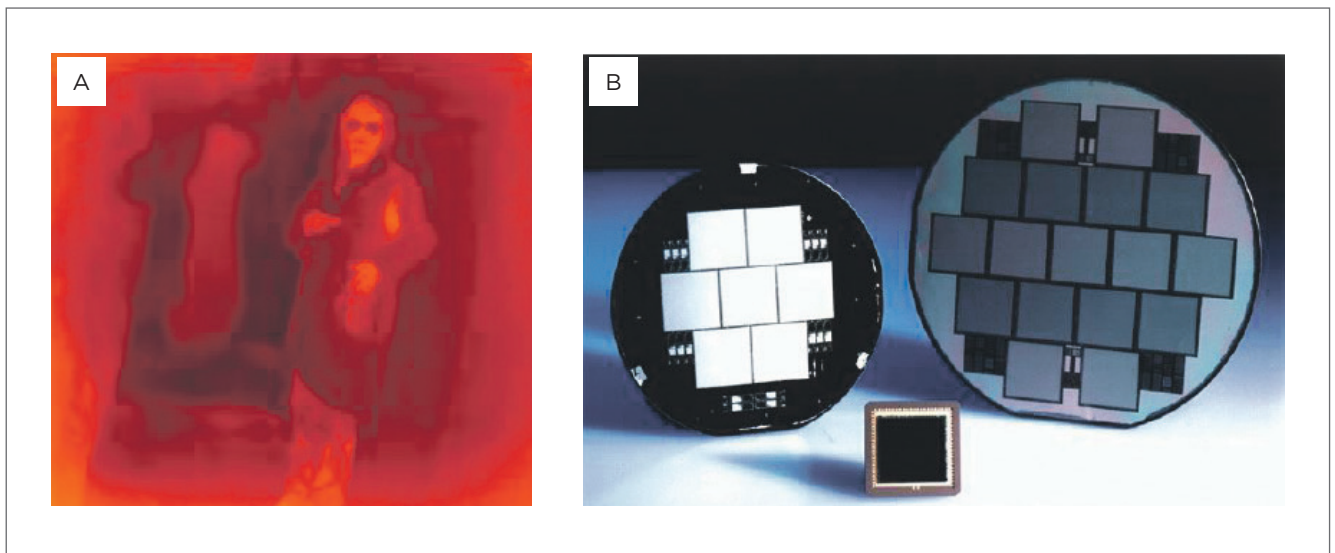


**Figure 3.** (A) Infrared image generated by a camera with quantum well infrared photodetectors (INOVAÇÃO TECNOLÓGICA, 2006); and (B) matrix of quantum well infrared photodetectors used for ballistic missile defense sensors (MISSILE DEFENSE AGENCE, 2007).

R2006b – from these models, and compares the results aiming at improving the models and their use. The importance of using MatLab® – besides its excellent performance, approved in studies of Engineering simulation – is owed to the fact that previous studies in this project were also conducted with it, so, there is no justification for the adaptation of other tools. This simplified the evolution of simulation routines in previous studies to obtain the results presented in this article.

## 2. METHODOLOGY

The denomination quantum well comes from potential well, which can be obtained when a semiconductor material is “grown” between two other semiconductors

– “sandwiched” –, with a larger energy gap, thus causing the formation of quantum energy levels, confining carriers in two dimensions. In this sense, infrared radiation can be absorbed, leading to excited carriers, so they go from a ground state to a higher state. When transition occurs between quantum levels inside the same band, it is called intersubband, and when it takes place between quantum levels, between the valence and conduction bands, is called interband. Figure 4 shows a diagram of bands in a quantum well-like structure. As observed in this figure, in intersubband transitions the energy transition is lower, enabling detection in the LWIR band – focus of this paper.

By selecting the material and controlling its composition and dimensions, the absorption spectrum, as well as

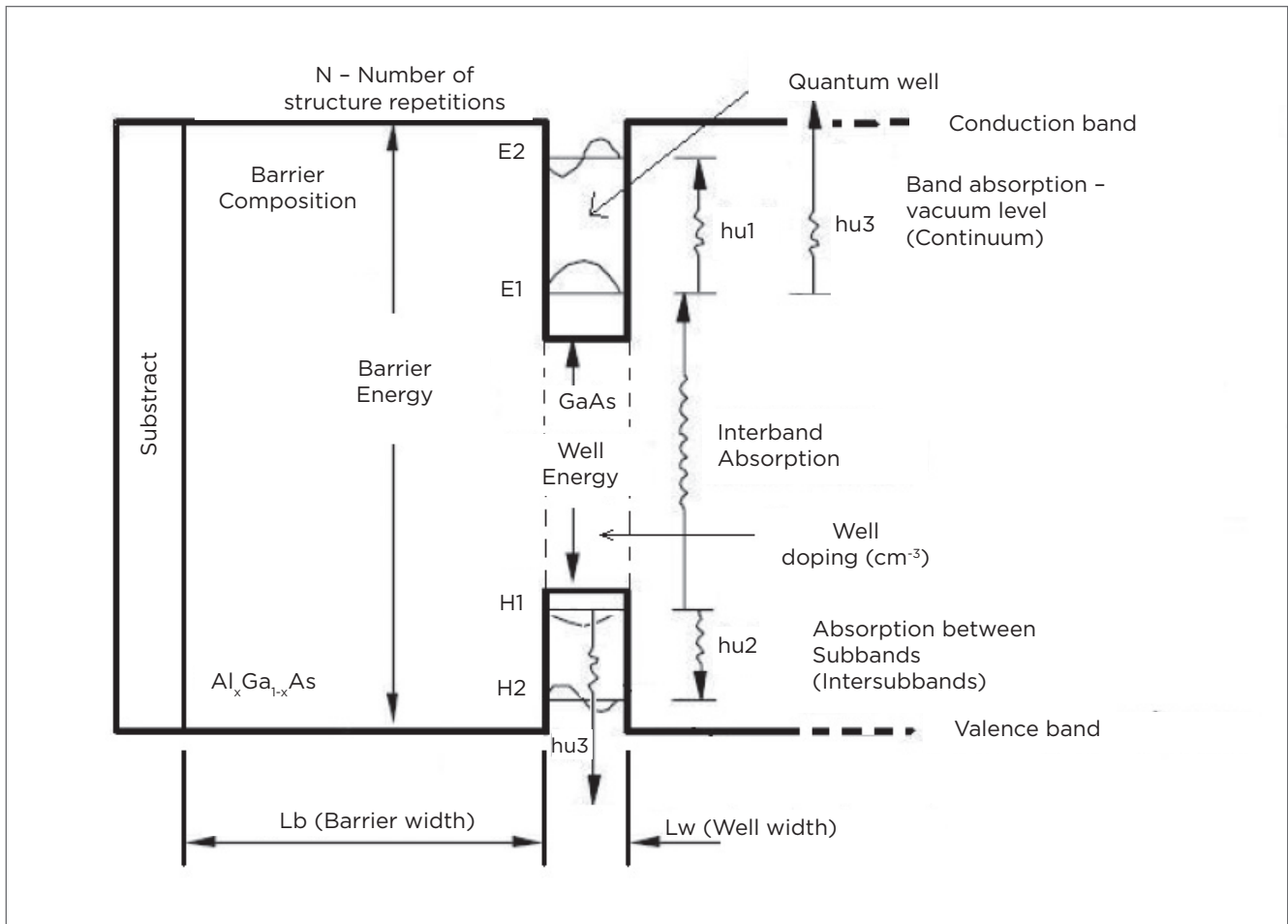


**Figure 4.** Band diagram, transitions between energy levels and the main building variables of a symmetric quantum well (ISSMAEL JUNIOR, 2007).

the other figures of merit, can be estimated. Therefore, we selected models available in the literature that could adequately describe the quantum phenomena of structures such as the one demonstrated in Figure 4, allowing the calculation of quantum energy levels, as well as the other parameters required to characterize the detectors. Structures reported in the literature were simulated in order to allow the validation of the models that were used to predict the features measured in a laboratory.

Table 2 presents the data from the samples used in simulations, all with wells composed of GaAs.

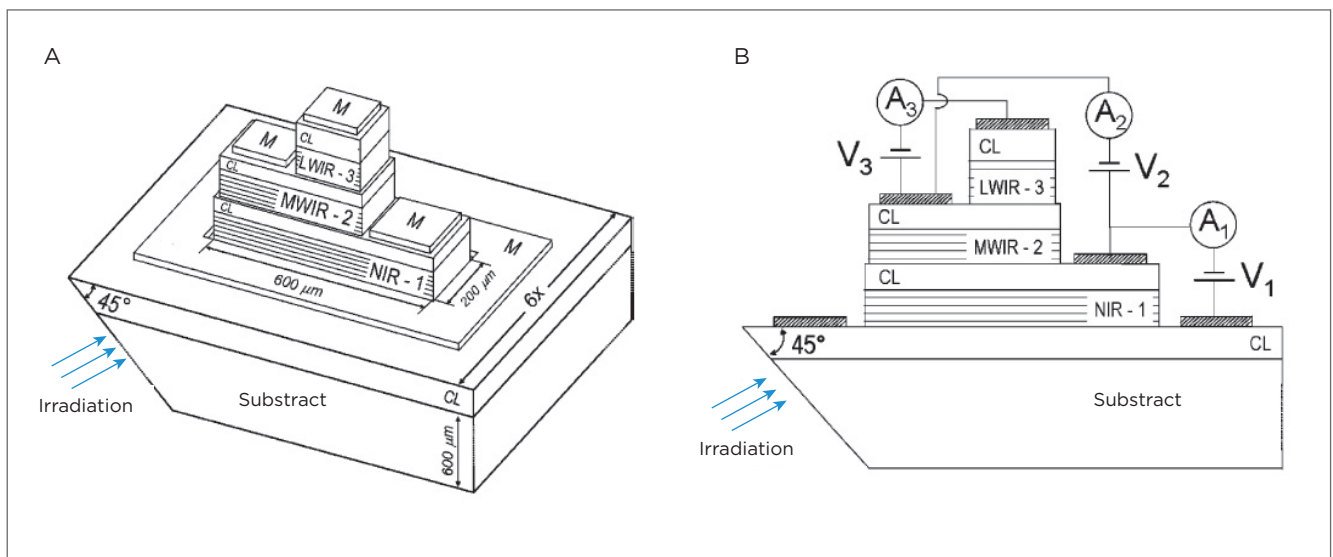
Figure 5 shows the multilayer photodetector and its polarization, which was built (ALVES, 2005) and is the base of the analysis of sample A.

Figure 6 (ALVES, 2005) presents the diagram of energy bands in sample A.

Figure 7 (ALVES, 2005) shows the image of the photodetector in sample A.

**Table 2.** Samples used in the simulations.

Sample	Reference	Barrier width (Lb) (ångström)	Well width (Lp) (ångström)	Barrier composition	Number of repetitions	Well doping (cm <sup>-3</sup> )
A	(ALVES, 2005) Page. 62	300	52	Al <sub>0,26</sub> Ga <sub>0,74</sub> As	20	0.5.10 <sup>18</sup>
B	(LEVINE, 1993) Page. R22 and R29 and (GUNAPALA e BANDARA, 1999) Pages. 23 and 34	500	40	Al <sub>0,26</sub> Ga <sub>0,74</sub> As	50	1.10 <sup>18</sup>
C	(LEVINE, 1993) Pages. R22 and R29	500	50	Al <sub>0,26</sub> Ga <sub>0,74</sub> As	25	0.42.10 <sup>18</sup>
D	(LEVINE, 1993) Page R18	305	40	Al <sub>0,29</sub> Ga <sub>0,71</sub> As	50	1.4.10 <sup>18</sup>



**Figure 5.** (A) Tridimensional Diagram of the multilayer detection device and (B) vertical cut of the device, emphasizing the independent building configuration of each layer associated with an infrared spectrum detection band (ALVES, 2005).

Figure 8 has the diagram of bands in the samples listed in Table 2.

First, we calculate the potential profile of the structures, considering that the dimensions in the growth axis  $z$  are several orders of magnitude lower than in plan  $x$ - $y$ , restricting the unidimensional confinement of the carriers – electrons in the conduction band and holes in the valence band. The potential is basically determined by the band offset in the interface, by the external electric field applied on the structure and by the distribution of charges. The first is obtained from parameters reported in the literature and empirical adjustments obtained in the laboratory. The second is known and controlled by the device user. The third requires knowledge of the confined energy levels, as well as their respective wave functions; in this case, the Schrodinger–Poisson equations must be solved in a self-consistent manner (ALVES, 2005). In order to solve differential equations and obtain eigenvalues and

eigenfunctions, Alves (2005) used the Shooting method (HARRISON, 2005) due to its versatility to calculate

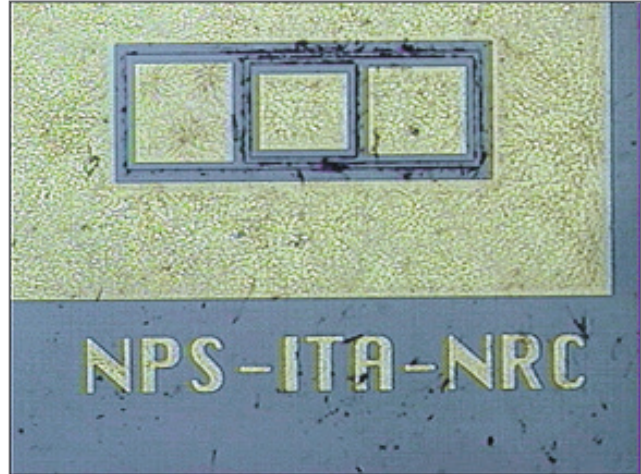


Figure 7. Image of the photodetector in sample A (ALVES, 2005).

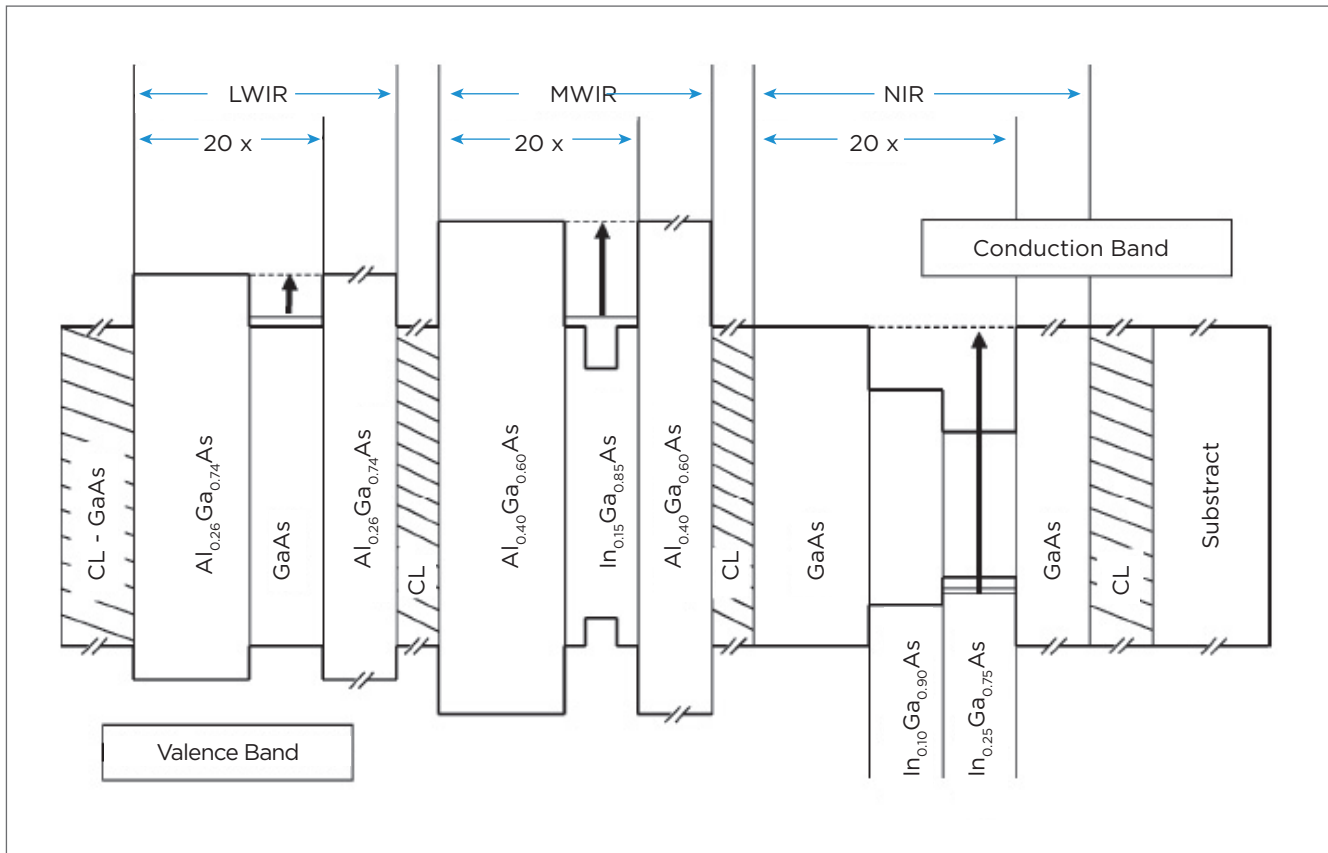


Figure 6. Diagram of the energy bands of 3-band quantum well infrared photodetectors. The width of each layer was not drawn in scale (ALVES, 2005).

complex structures. Next, equations that shape figures of merit are solved and detailed in the next section.

Experimental data to be compared with the simulations of A were obtained from measurements described in the study by Alves (2005), whereas the other samples were extracted directly from the graphs available in previously mentioned references – using the graph tool GraphData 1.0<sup>®</sup> – and the analyses – using the *software* Origin<sup>®</sup>.

### 3. RESULTS

#### 3.1. ABSORPTION SPECTRUM

The absorption spectrum represents the main characteristic of the crystalline structure sample, allowing its evaluation before the detector itself is manufactured. It indicates the band of operation of the detector and the type of quantum transition resulting from the interaction between photon and electron. The theoretical estimation of this spectrum can be obtained by Equations 1 and 2 (ALVES, 2005):

$$\alpha_{CbCb}(\hbar\omega) = \frac{q^2 d}{(m_e^*)^2 \epsilon_0 n_r c(\hbar\omega)} \left| \Psi_{\beta}(z) \right| \left| \frac{\partial}{\partial z} \Psi(z) \right|^2 X \cos^2 \varnothing \frac{\Gamma}{(E_{\beta} - E - \hbar\omega)^2 + (\Gamma/2)^2} \quad (1)$$

In which  $\alpha_{CbCb}$  is the absorption coefficient, considering transitions between the confined levels in the conduction band (bound-to-bound);  $d$  is the doping density;  $E_i$  and  $E_f$  represent the initial and final energy levels, respectively;  $q$  is the electron charge;  $c$  is the speed of light in the vacuum;  $\epsilon_0$  is the vacuum electric permittivity;  $\Gamma$  is the broadening parameter;  $\omega$  is the incident photon energy;  $m_e^*$  is the effective electron mass; and  $\varnothing$  is the angle between the incident flow and the growth axis.

$$\alpha_{CbC}(\hbar\omega) = \frac{q^2 d}{(m_e^*)^2 \epsilon_0 n_r c(\hbar\omega)} \frac{L_{fp}}{\pi} \sqrt{\frac{m_{e,b}^*}{2(E_f - V_o)}} X \left| \Psi_{\beta}(z) \right| \left| \frac{\partial}{\partial z} \Psi(z) \right|^2 X \cos^2(\varnothing) \quad (2)$$

In which  $\alpha_{CbC}$  is the absorption coefficient, considering transitions between one confined level and continuum levels in the conduction band;  $L_{fp}$  is the ratio between  $p$  and the wave vector  $k_{Lfp}$ ; and  $V_o$  is the barrier energy.

The characteristics of the sample are listed in Table 2. The parameters required to solve (1) and (2) are extracted from Vurgaftman and Meyer (2001). Therefore, the absorption spectrums of samples A and B were estimated for the temperature of 300 K. Amplitude absolute values presented differences in magnitude orders. This fact is owed to the

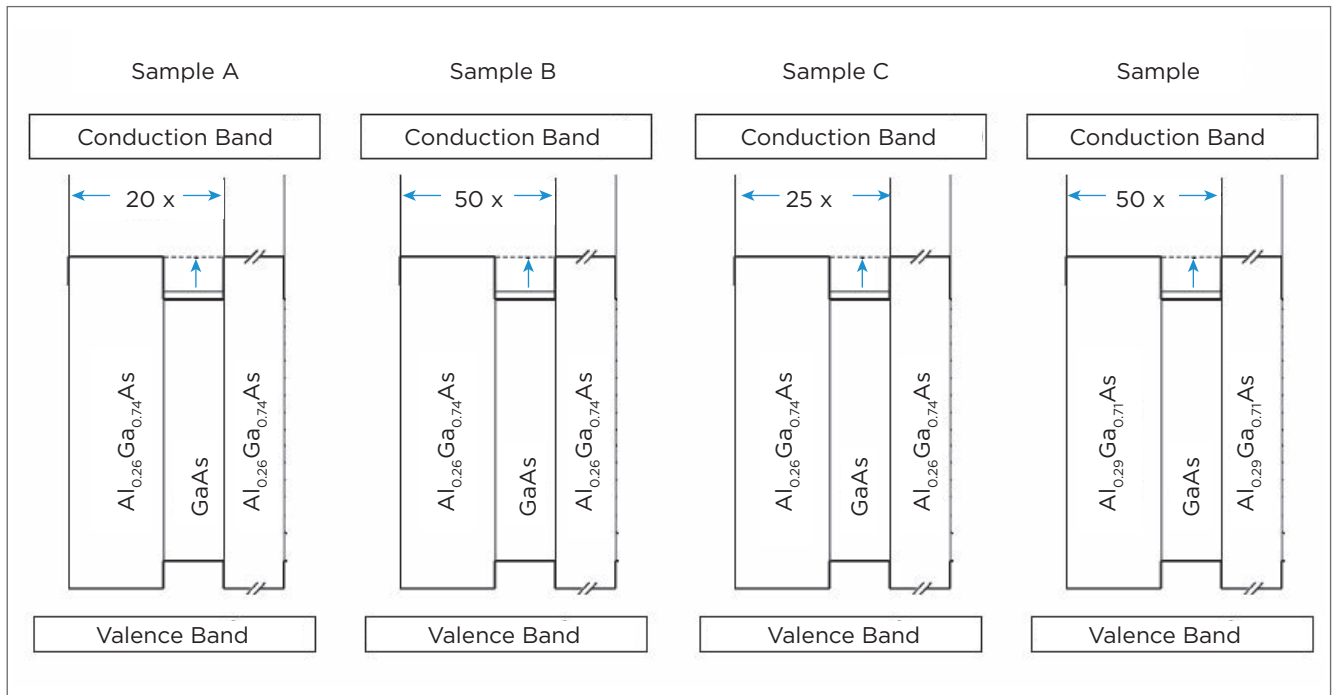


**Figure 8.** Diagram of the energy bands of photodetectors used in the simulations. The width of each layer was not draw in scale.

large number of uncertainties in the parameters of semiconductor materials composing the structure of the samples (VURGAFTMAN; MEYER, 2001). So, at the time of simulations, the priority was to determine the wavelength at the peak, without considering the broadening coefficient because of the aforementioned inaccuracy. When the absorption coefficient is normalized (Figure 9), good estimation is obtained, with errors lower than 6.03% for the wavelength at the peak. This shows that the calculation of confined levels using the shooting method is very reasonable.

### 3.2. DARK CURRENT

The dark current is the figure of merit that represents how much current is generated in the photodetector without the influence of incident radiation (that is, in the dark). Three mechanisms of dark current generation can be identified in quantum well devices: sequential resonant tunneling, temperature-assisted tunneling and thermionic effect. The calculation of the dark current is a complex procedure that depends on several magnitudes. The first magnitude to be calculated is the effective weighted mass of the electron in the detector, from the proportion of barriers and wells in the detector. The procedure is carried out by determining the effective masses of the electron in the barrier (FU; WILLANDER, 1998) – formed by the ternary composition AlGaAs from the binary compositions GaAs and AlAs – and in the well – formed only by the binary composition GaAs. The second magnitude is the weighted carrier mobility, which

is also obtained from the mobility in the barrier and in the well. The third magnitude is the velocity weighted saturation in the detector. These parameters were obtained considering the models from the Institute of Microelectronics's Site (2014). More details in Issmael Junior (2007).

One of the ways of presenting the dark current in QWIP is given by Equation 3 (LEVINE, 1993):

$$I_D(F) = \frac{e \cdot v_{drift} \cdot A \cdot m_w^*}{\pi \hbar^2 L} \int_{E_i}^{\infty} f^{FD}(E) \cdot T(E, F) dE \quad (3)$$

In which the term outside the integral is the density of states divided by the period of the multiple quantum wells ( $L$ ), and the term  $f^{FD}(E)$  represents the Fermi-Dirac distribution, given by Equation 4 (ALVES, 2005):

$$f^{FD}(E) = \frac{1}{1 + e^{\frac{E - E_F}{k_B T}}} \quad (4)$$

In which  $E_F$  represents the level of bidimensional Fermi,  $k_B$  is the Boltzmann constant, and  $T$  is temperature. The tunneling coefficient –  $T(E, F)$  – depends on the polarization voltage and, for a simple barrier, it can be represented by the Equations 5, 6 and 7 (ANDREWS; MILLER, 1991):

$$T(E, F) = \exp \left[ -\frac{4L_b}{3qV} \left( \frac{2m^*}{\hbar} \right)^{1/2} \left[ (V_o - E)^{3/2} - (V_o - E - qV)^{3/2} \right] \right] \quad (5)$$

for  $E_o < E < V_o - qV$ ;

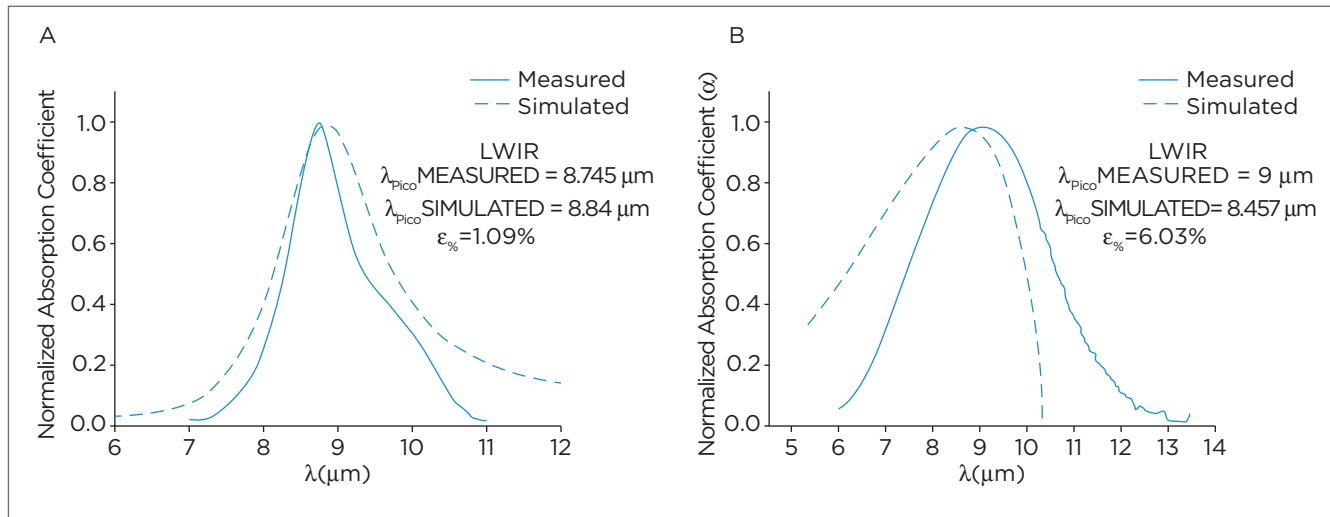


**Figure 9.** Comparison between estimated and measured values of the normalized absorption coefficient (A) in sample A (ALVES, 2005) and (B) in sample B (GUNAPALA; BANDARA, 1999).

$$T(E, F) = \exp \left( - \frac{4L_b \left( \frac{2m^*}{\hbar} \right)^{\frac{1}{2}} \left[ (V_o - E)^{3/2} \right]}{3qV} \right) \quad (6)$$

for  $V_o - qV < E < V_o$ ; e

$$T(E, F) = 1 \quad (7)$$

for  $E > V_o$ .  
 $V$  represents the voltage applied per period of well structure. In the case of electrons, the drift velocity ( $v_{drift}$ ) in function of the  $F$  field is given by Equation 8 (ALVES, 2005):

$$v_{drift} = \frac{\mu F}{\sqrt{1 + \left( \frac{\mu F}{v_{sat}} \right)^2}} \quad (8)$$

Using the mobility values ( $m$ ) equal to  $0.1 \text{ m}^2/\text{Vs}$  and the saturation velocity ( $v_{sat}$ ) equals to constant  $5.10^4 \text{ m/s}$ , the dark current was estimated for sample D (Table 1). The theoretical values presented a systematic error of 9% for all

temperatures. With this correction, we reach the result in Figure 10. Temperatures lower than 50 K are poorly represented by this model and were not included in the figure.

The models give a good representation of the phenomena, being a little bit further for values of polarization voltage lower than 1.0 V.

Then, the results in sample A (Table 1) were compared for temperatures 100, 90, 80, 77, 70, 60, 50, and 40 K. The correction factor was not applied for this structure, and the absolute values are presented in Figure 11.

The theory represents well the behavior of the real device for temperatures above 60 K and polarization voltage greater than 1.0 V, for the simplified criteria we considered. The discrepancies observed can be caused by several reasons, such as the fact that the configuration of the detector is part of a multilayer device, in which the NIR and MWIR layers can interfere in the measurements, and the increasing chances of tunneling induced by the external electrical field. Further studies should be conducted to obtain a single and generic

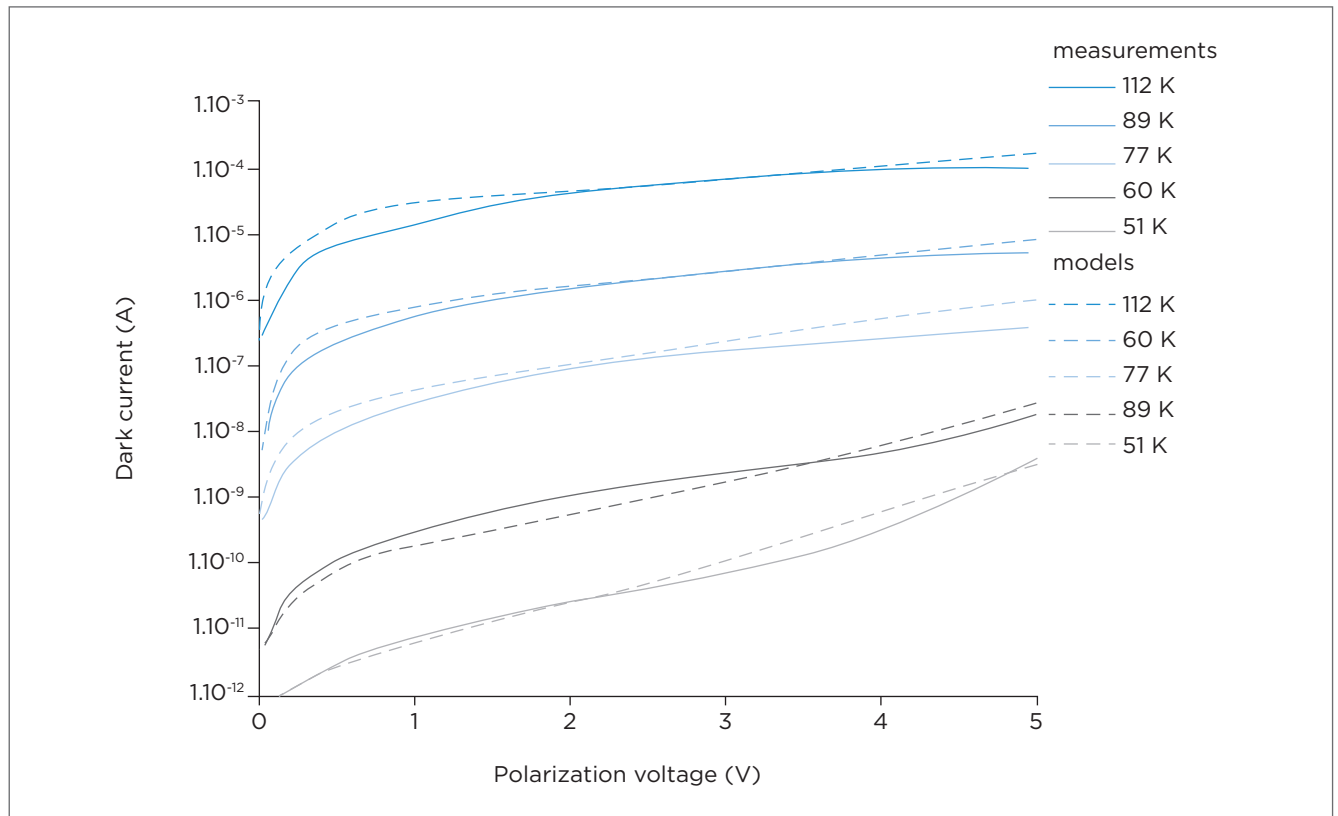


**Figure 10.** Comparison between the curves  $I \times V$  in the dark for sample D in Table with, with constant mobility and velocity saturation (ISSMAEL JUNIOR, 2007).

model. Since we did not have the detector of sample A at the time of simulations, it was not possible to take measurements with negative and positive polarization, which would allow a more accurate comparison and analysis with the result obtained.

### 3.3. RESPONSIVITY

Responsivity quantifies the photocurrent ratio generated by the photon radiation power incident in the detector. Mathematically is given by Equation 9 (ALVES, 2005):

$$R(F) = \frac{I_p(F)}{\Phi_o} \tag{9}$$

In which,  $I_p(F)$  is the photocurrent and  $F_o$  is the incident optical power.

The photocurrent can be expressed by Equation 10 (ALVES, 2005):

$$I_p(F) \approx \frac{2q\Phi_o}{\hbar\omega} \alpha L_w \sum_{n=1}^N e^{\frac{nL}{v_{drift}(F)\tau}} \tag{10}$$

In which  $\alpha$  is the absorption coefficient,  $\Phi_o$  is the incident optical power,  $\hbar\omega$  is the photon energy,  $q$  is the electron charge,  $L$  is the repetition period well/barrier,  $L_w$  is the width of the well,  $v(F)$  is the drift velocity of electrons influenced by the electrical field  $F$ ,  $e$   $\tau$  lifespan of the carrier extracted from the well. By combining these two expressions, we obtain the following Equation 11:

$$R_p(F) \approx \frac{2q}{\hbar\omega} \alpha L_w \sum_{n=1}^N e^{\frac{nL}{v_{drift}(F)\tau}} \tag{11}$$

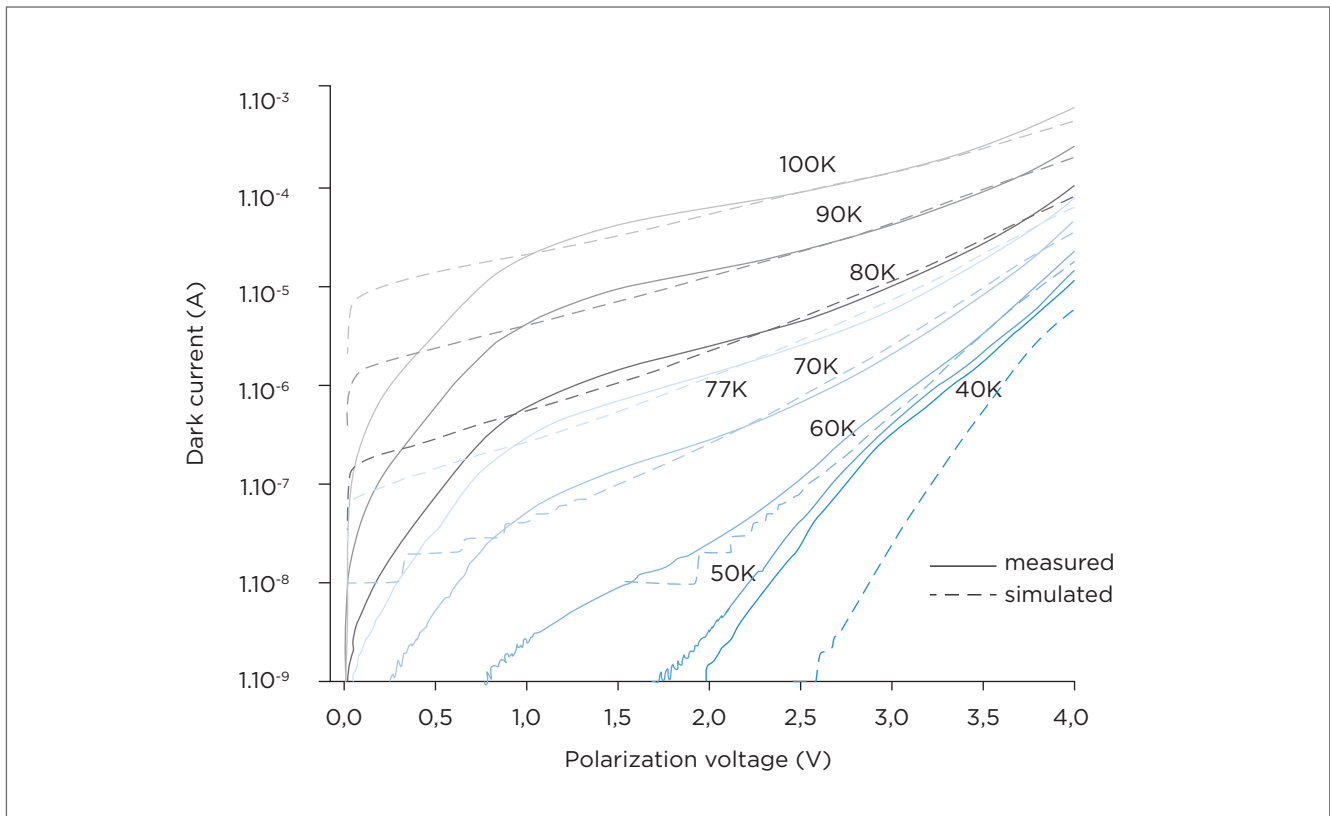


**Figure 11.** Comparison between the curves  $I \times V$  in the dark for sample A in Table 2, for temperatures of 40-100 K (ISSMAEL JUNIOR, 2007).

Simulations were carried out for the normalized responsivity of the photodetector by Alves (2005) – sample A in Table 1 – for voltages of 0.5, 1.0, and 1.5 V, temperature of 10 K. These curves were compared to the measurements taken by Hanson (2006). The error between the simulated and the measured wavelength at the peak was 2.53%, for the polarization voltage of 0.5 V – Figure 12; 1.68% for the polarization voltage of 1.0 V – Figure 13; and 1.17% for the polarization voltage of 1.5 V – Figure 14.

There is consistency between theoretical values and the measurements, with errors lower than 3%, decreasing while the polarization voltage increases. However, it is necessary to improve the model of the absorption coefficient, so that the simulations of responsivity get closer to reality, without using normalization.

#### 4. DISCUSSION AND FINAL OBSERVATIONS

With the objective of investigating the capacity of models in the literature to represent the main figures of

merit of QWIP, many comparisons were made. The difficulty to shape the phenomena at temperatures below 50 K was observed, besides the fact that, due to the high number of factors influencing the figures of merit – such as precision in growth, precision in bandoffset values, effective mass, bandgap, dopant ionization, among others – the absolute values of the amplitude have little significance in theoretical calculations. On the other hand, the methodology used to calculate the confined energy levels and their respective wave functions proved to be efficient (ALVES, 2005). Attempts to adapt the models have been made and require other cycles of manufacture in order to test its effectiveness. These results will be published in other studies.

Finally, the considerations made during the development of this paper cooperate with the effort of the Air Force to improve its technical knowledge in the field of infrared photodetection, aiming at leading our country toward independence and autochthonous development of this strategic field of knowledge.

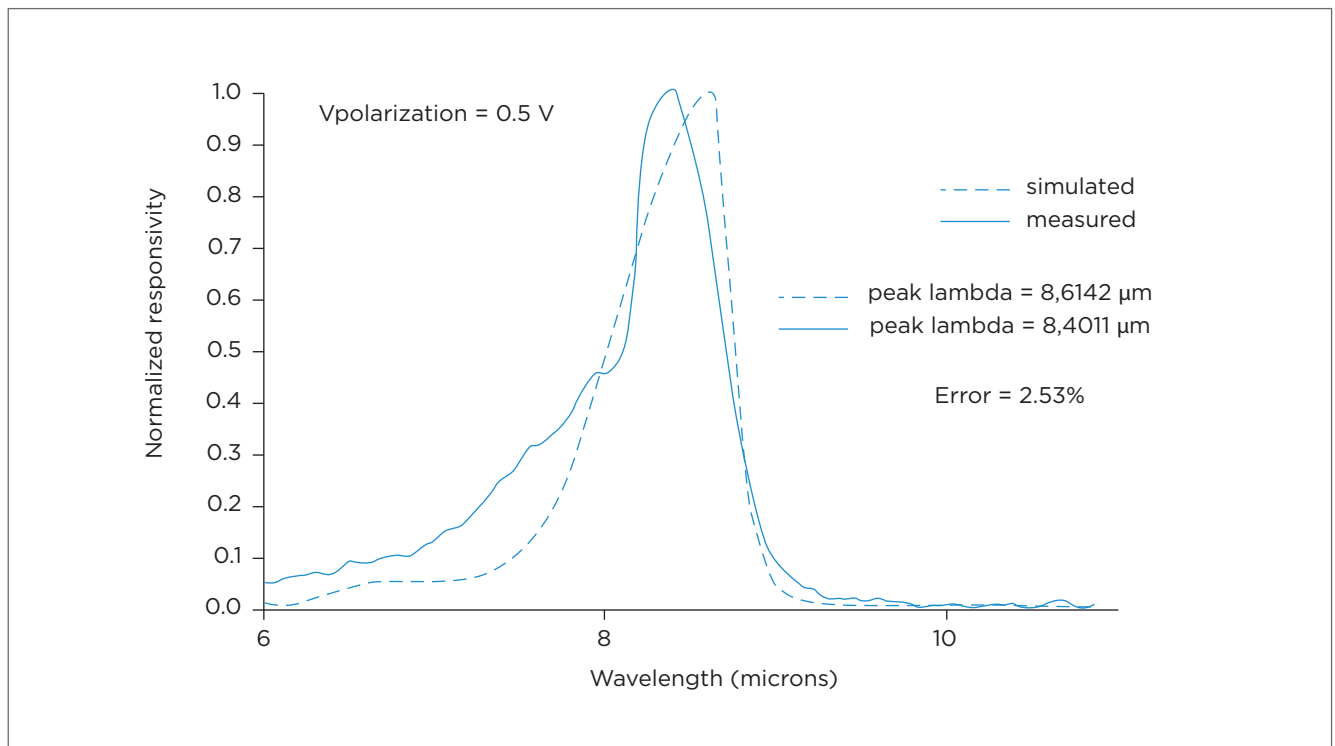


**Figure 12.** Normalized results of simulated and measured responsivity in function of the wavelength for polarization voltage of 0.5 V (ISSMAEL JUNIOR, 2007).

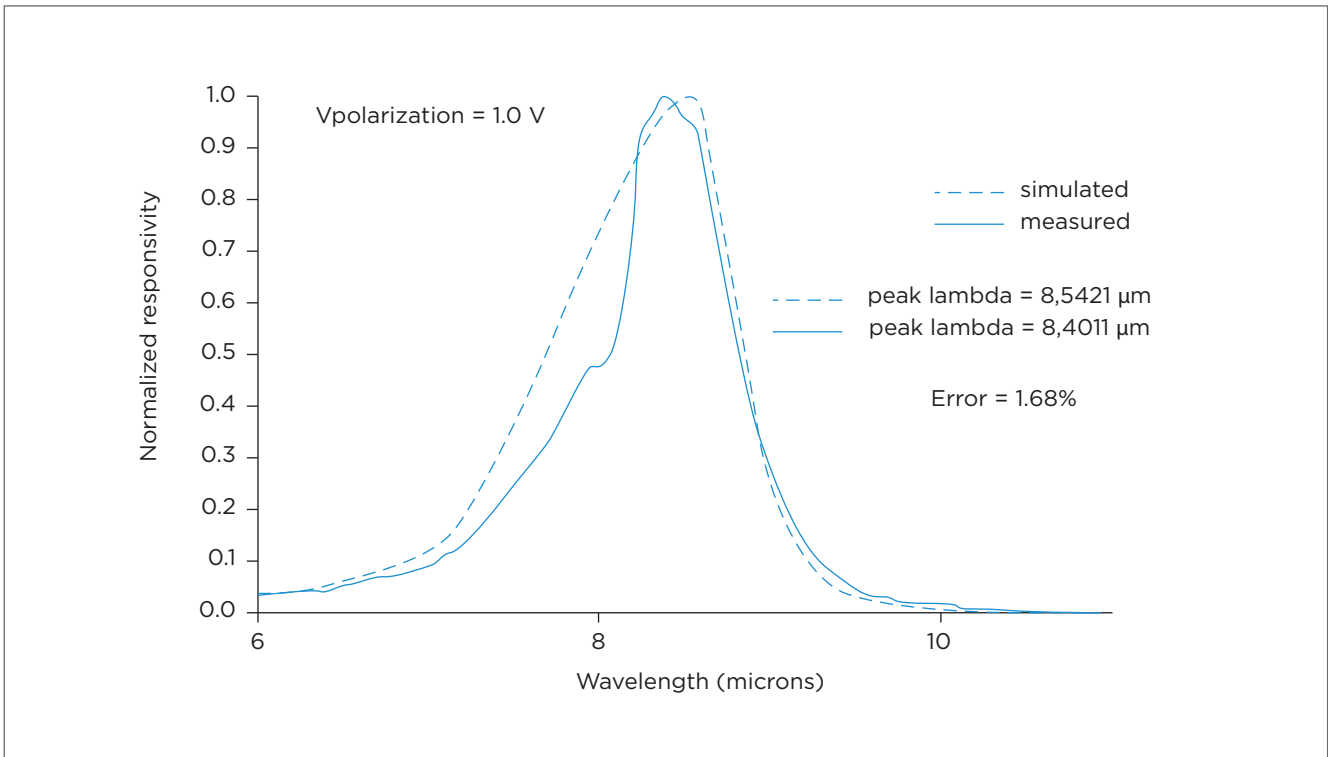


**Figure 13.** Normalized results of simulated and measured responsivity in function of the wavelength for polarization voltage of 1.0 V (ISSMAEL JUNIOR, 2007).

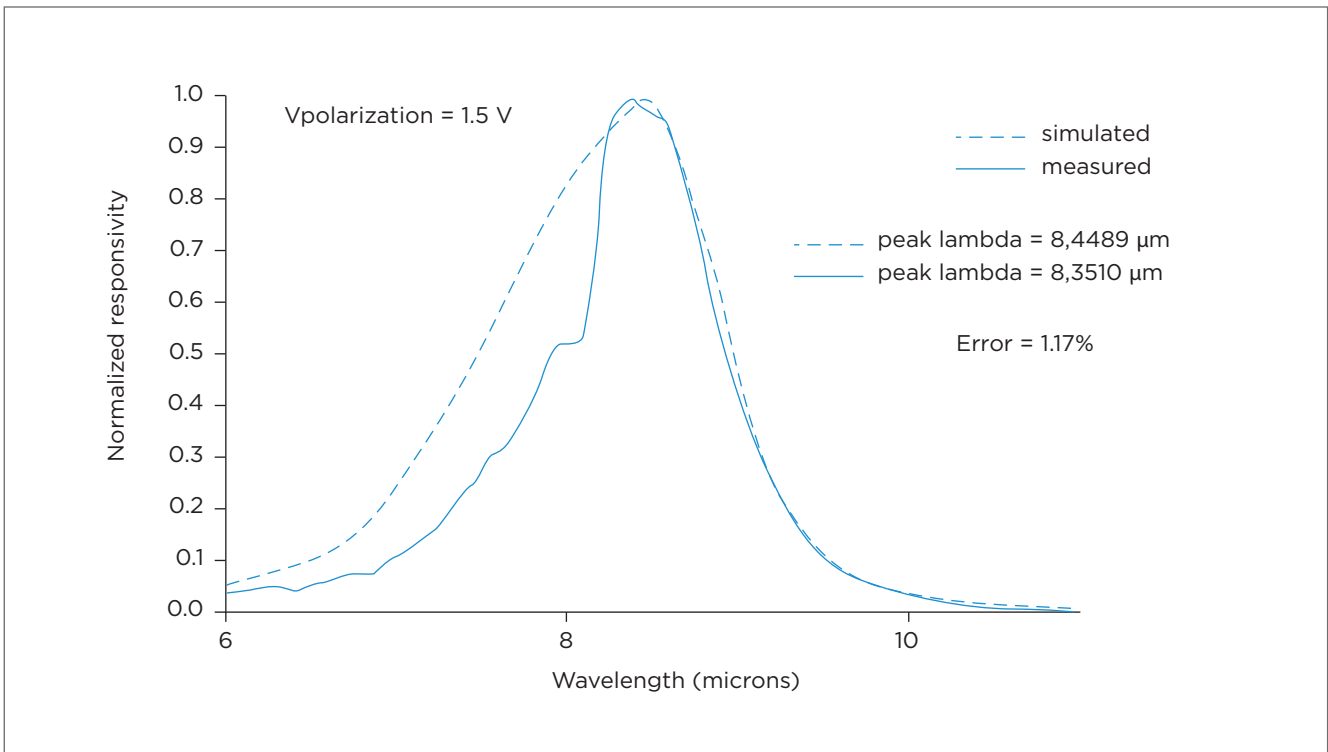


**Figure 14.** Normalized results of simulated and measured responsivity in function of the wavelength for polarization voltage of 1.5 V (ISSMAEL JUNIOR, 2007).

## REFERENCES

- ALVES, F.D.P. *Design and Analysis of a Multicolor Quantum Well Infrared Photodetector*. United States Naval Postgraduate School Master's Thesis, september 2005.
- ALVES, F.D.P.; TAVARES SANTOS, R.A.; AMORIM, J.; ISSMAEL JR., A.K.; KARUMASIRI, G. Widely Separate Spectral Sensitivity Quantum Well Infrared Photodetector Using Interband and Intersubband Transitions. *IEEE Sensors Journal*, v. 8, p. 842-848, 2008.
- ALVES, F.D.P.; KURUNASIRI, G.; HANSON, N.; BYLOOS, M.; LIU, H.C.; BEZINGER, A.; et al. NIR, MWIR and LWIR quantum well infrared photodetector using interband and intersubband transitions. *Infrared Physics & Technology*. Elsevier, v. 50, p. 182-186, 2007.
- ANDREWS, S.R.; MILLER, B.A. Experimental and theoretical studies of the performance of quantum well infrared detectors. *Journal of Applied Physics*, v. 2, n. 70, 1991.
- BOSCHETTI, C. *O espectro infravermelho*. Disponível em: <<http://www.las.inpe.br/-cesar/Infrared/espectro.htm>>. Acesso em: 15 abr. 2015.
- Dyer, W.R; Tidrow, M.Z. QWIP technology applications to ballistic missile defense. *Proceedings of SPIE*, v. 3553, p. 231-238, 1998.
- FU, Y.; WILLANDER, M. Optical coupling in quantum well infrared photodetector by diffraction grating. *Journal of Applied Physics*, v. 84, n. 10, 1998.
- GUNAPALA, S.D. *What is QWIP Technology?*
- GUNAPALA, S.D.; BANDARA, S.V. Quantum Well Infrared Photodetector (QWIP) Focal Plane Arrays. *Semiconductors and Semimetals*, v. 62, 1999.
- GUNAPALA, S.D.; BANDARA, S.V.; LIU, J.K.; SIR RAFOL; SHOTT, C.A.; JONES, R.; et al. 640x512 pixel four-band, broad-band, and narrow-band quantum well infrared photodetector focal plane arrays. Disponível em: <[https://www.researchgate.net/publication/233980001\\_640x512\\_pixel\\_four-band\\_broad-band\\_and\\_narrow-band\\_quantum\\_well\\_infrared\\_photodetector\\_focal\\_plane\\_arrays](https://www.researchgate.net/publication/233980001_640x512_pixel_four-band_broad-band_and_narrow-band_quantum_well_infrared_photodetector_focal_plane_arrays)>. Acesso em: 09 mar. 2007.
- HANSON, N.A. *Characterization and analysis of a multicolor quantum well infrared photodetector*. United States Naval Postgraduate School Master's Thesis, Monterey, California, June 2006.
- HARRISON, P. *Quantum wells, wires and dots: theoretical and computational physics*. 2 ed. Wiley, Chichester, UK, 2005.
- INOVAÇÃO TECNOLÓGICA. Sensor de infravermelho agora é capaz de ver em cores. *Site Inovação tecnológica*, 2006. Disponível em: <<http://inovacaotecnologica.com.br/noticias/noticia.php?artigo=010110060526>>. Acesso em: 15 abr. 2015.
- Institute of Microelectronic's site. *Low Field Mobility*. Disponível em: <<http://www.iue.tuwien.ac.at/phd/quay/node34.html>>. Acesso em: 30 nov. 2014.
- Institute of Microelectronic's site. *Semiconductor Alloys*. Disponível em: <<http://www.iue.tuwien.ac.at/phd/quay/node35.html>>. Acesso em: 30 nov. 2014.
- Institute of Microelectronic's site. *Velocity Saturation*. Disponível em: <<http://www.iue.tuwien.ac.at/phd/palankovski/node48.html>>. Acesso em: 30 nov. 2014.
- Issmael Junior, A.K. *Estudo, modelamento e simulação das principais figuras de mérito de fotodetectores infravermelhos à poços quânticos*. 106 f. Monografia – Instituto Tecnológico de Aeronáutica, São José dos Campos, 2007.
- ISSMAEL JR, A.K.; ALVES, F.D.P.; TAVARES SANTOS, R.A. *Estudo, modelamento e simulação das principais figuras de mérito de fotodetectores infravermelhos à poços quânticos*. IX Simpósio de Guerra Eletrônica, 2007. Disponível em: <[http://www.sige.ita.br/anais/IXSIGE/Artigos/GE\\_01.pdf](http://www.sige.ita.br/anais/IXSIGE/Artigos/GE_01.pdf)>. Acesso em: 15 abr. 2015.
- Levine, B.F. Quantum well infrared photodetectors. *Journal of Applied Physics*, v. 8, n. 74, 1993.
- MISSILE DEFENSE AGENCE. *Site da MDA*.
- NATIONAL AERONAUTICS AND SPACE ADMINISTRATION (NASA). *My NASA Data site*. Disponível em: <<http://mynasadata.larc.nasa.gov/ElectroMag.html>>. Acesso em: 24 mar. 2007.
- SANTOS, R.A.T. *Proposta de Metodologia para Estimação do Envelope Infravermelho de Aeronaves*. Tese (Mestrado) – Instituto Tecnológico de Aeronáutica, São José dos Campos, 2004.
- VURGAFTMAN, I.; MEYER, J.R.; RAM-MOHAN, L.R. Band parameters for III-V compound semiconductors and their alloys. *Journal of Applied Physics Review*, v. 89, n. 11, p. 5815-5875, 2001.

# BLIND AND ASSISTED SIGNAL DETECTION FOR UWB SYSTEMS BASED ON THE IEEE 802.15.4A STANDARD

Detecção cega e assistida de sinais em  
sistemas UWB baseados no padrão ieee 802.15.4a

Aline de Oliveira Ferreira<sup>1</sup>, Cesar Augusto Medina Sotomayor<sup>2</sup>,  
Fabian David Backx<sup>3</sup>, Raimundo Sampaio Neto<sup>4</sup>

**Abstract:** This paper explores the efficient detection of ultra wideband multiuser communication system's signal based on the IEEE std 802.15.4a. At first, the optimum receiver structure is considered, and then, after a few modifications, a modified receiver is presented. The optimality conditions of this new receiver are established. The modified receiver uses a filter matched to the effective code of the user of interest as the detection filter. Two distinct methods of effective code estimation are proposed: an assisted and a blind method. Adoption of the blind method is encouraged, because of its low computational complexity when compared to the most usual joint blind detection and interference suppression schemes, which require inversion of high dimension matrix. Simulation results show the performance of the modified receiver equipped with the proposed estimation methods for this communication system. Considering the specificities of the IEEE std 802.15.4a, the proposed receiver presents good performance results also in multiuser environment with multiple access interference.

**Keywords:** IEEE 802.15.4a. Blind estimation. Assisted estimation.

**Resumo:** Este artigo trata da detecção eficiente de sinais em sistemas de comunicação multiusuário de banda ultralarga baseados no padrão IEEE 802.15.4a. Considera-se inicialmente a estrutura do receptor ótimo para sistema monousuário e, a partir de alterações nesse receptor, apresenta-se um receptor modificado, cujas condições de otimidade são examinadas. Esse receptor utiliza como filtro de detecção um filtro casado ao código efetivo do usuário de interesse. Dois métodos distintos para estimar o código efetivo são propostos: um assistido e outro às cegas. Desses dois métodos, destaca-se o método às cegas, pois tem baixa complexidade computacional, se comparado à maioria dos métodos de detecção às cegas com supressão de interferência, que requerem a inversão de matrizes com dimensão elevada. Resultados de simulação computacional ilustram o desempenho do receptor modificado equipado com os métodos de estimação propostos para esse sistema de comunicação. Considerando-se as especificidades do padrão IEEE 802.15.4a, conclui-se que o receptor proposto também apresenta bom desempenho em cenários multiusuário com interferência de múltiplo acesso.

**Palavras-chave:** IEEE 802.15.4a. Estimação cega. Estimação assistida.

**1.** Master in Electrical Engineering from the *Pontifícia Universidade Católica do Rio de Janeiro* - Rio de Janeiro, RJ - Brazil. Technologist at the *Instituto de Pesquisas da Marinha* - Rio de Janeiro, RJ - Brazil. E-mail: aline@ipqm.mar.mil.br

**2.** PhD in Electrical Engineering from the *Pontifícia Universidade Católica do Rio de Janeiro* - Rio de Janeiro, RJ - Brazil. Researcher at the Center of Telecommunication Studies of the *Pontifícia Universidade Católica do Rio de Janeiro* - Rio de Janeiro, RJ - Brazil. E-mail: csmedina@cetuc.puc-rio.br

**3.** PhD in Electrical Engineering from the *Pontifícia Universidade Católica do Rio de Janeiro* - Rio de Janeiro, RJ - Brazil. Researcher at *Instituto de Pesquisas da Marinha* - Rio de Janeiro, RJ - Brazil. E-mail: fabian@marinha.mil.br

**4.** PhD in Electrical Engineering from the University of Southern California - Los Angeles, CA - United States of America. Professor at the Center of Telecommunication Studies of the *Pontifícia Universidade Católica do Rio de Janeiro* - Rio de Janeiro, RJ - Brazil. E-mail: raimundo@cetuc.puc-rio.br

## 1. INTRODUCTION

Ultra wideband (UWB) communications is a technology used to transmit data using low power pulses ( $\approx 0,5$  mW) in a bandwidth greater than 500 MHz (KSHETRIMAYUM, 2009). The UWB systems have been quite effective allowing transmission of pulses at rates up to 1.3 gigapulses per second, supporting data transmission with error-correcting codes of up to 675 Mbit/s.

Owing to the very large bandwidth, UWB systems can achieve high data rates even in noisy environments and operate at maximum noise level allowed for other communications systems, which facilitates secure communication. Since UWB transmitters send out short pulses periodically, the use of hardware, costs, and power consumption can be minimized, ensuring longer UWB devices lifetime (SCHOLTZ, 1993; 1998; 2000). Those many advantages motivate the development of new applications in addition to the usual applications in communication, such as home networks, wireless military communications (even in hostile electromagnetic environments), automotive radar, through-the-wall radar imaging, and accurate position of people or objects, even inside buildings.

This article considers the standard for WPANs (Wireless Personal Area Networks) IEEE std 802.15.4a (I. T. GROUP, 2007) for UWB physical layer. This standard has a hybrid scheme that combines BPSK modulation (Binary Phase-Shift Keying) and BPM (Binary Position Modulation), and also uses direct sequence spread spectrum (DSSS) and time hopping. Taking as a starting point the optimum receiver for UWB single-user system, a modified receiver, using a filter matched to the effective code of the user was proposed (OLIVEIRA, 2010; OLIVEIRA, SAMPAIO-NETO & MEDINA, 2011). In this article we add the multiuser signal model and an analysis on the applicability of the proposed receiver in environments with interference between users. This paper shows that the composition of effective codes of the users with minimal time displacement, guaranteed by the standard applied, results in *quasi*-orthogonal effective codes. This fact makes the proposed receiver suitable for use in multiuser systems.

The details of the transmission model, such as modulation and coding, are identified and explained in Section 2.1. Section 2.2 considers the optimal reception of the UWB

system with only one active user. On the basis of the modifications in the optimum receiver, Section 3 shows a modified receiver (OLIVEIRA, 2010; OLIVEIRA, SAMPAIO-NETO & MEDINA, 2011), whose optimality conditions are examined in Section 3.1. The receiver uses a detection filter matched to the effective code of the users, whose definition is shown throughout the section, and therefore requires the estimation of the effective code. Section 3.2 details two ways to estimate the effective code: an assisted and a blind method. Section 4 describes the transmission and reception model for UWB multiple access systems. In this section, arguments are provided to justify the use of the matched filter and estimation methods proposed for the effective code also in an environment in which, in addition to noise, multiple access interference (MAI) is present. This is particularly important in the case of blind detection. Indeed, the proposed method becomes very advantageous, because it does not require the inversion of matrices as occurs in most blind detection methods with suppression of interference (TSATSANIS & XU 1998; XU & TSATSANIS, 2001; XU & LIU, 2002; Xu *et al.* 2003; MEDINA, VINHOZA & SAMPAIO-NETO, 2008; MEDINA & SAMPAIO-NETO, 2010; LAMARE & SAMPAIO-NETO, 2005). Simulation results are presented in Section 5, whereas Section 6 gathers comments and conclusions.

## 2. SYSTEM MODEL

### 2.1. TRANSMITTED SIGNAL

The UWB modulation scheme employed by the IEEE std 802.15.4a is the combination of two different modulation techniques into a hybrid technique: BPM-BPSK, in which each symbol carries two bits of information. As shown in Figure 1, a symbol is transmitted in a duration  $T_{\text{symp}}$ , which is divided into two time intervals,  $T_{\text{BPM}} = T_{\text{symp}}/2$ . Similarly to the pulse position modulation (PPM), the first bit of information is responsible for determining whether the transmission will be executed in the first or second half of the symbol transmission frame. The second bit of information is responsible for determining the polarity of the transmitted pulses.

Each  $T_{\text{BPM}}$  interval is divided into two segments of equal duration. The first segment is composed of  $N_b$  slots of duration

$T_b \left( \frac{T_{BPM}}{2} = N_b T_b \right)$ . Similarly to the time hopping technique, each user is randomly assigned one of these slots, in which a burst of ultranarrow pulses  $N_c$  chips, with duration  $T_c$  is transmitted, where  $T_b = N_c T_c$ . The second segment with duration  $T_G = \frac{T_{BPM}}{2}$  is a guard interval characterized by the

absence of transmission, which serves to limit the intersymbol interference introduced by the transmission channel.

Assuming, without loss of generality, the transmission of the first symbol of a given user,  $0 \leq t \leq T_{\text{symbol}}$  the transmitted signal  $x(t)$  can be expressed as:

$$x(t) = [1 - 2b_1] \sum_{n=0}^{N_c-1} s_n c(t - b_0 T_{BPM} - b T_b - n T_c) \quad (1)$$

where:

$b_0, b_1 \in \{0,1\}$  are the transmitted bits,

$s_n \in \left\{ -\frac{1}{\sqrt{N_c}}, \frac{1}{\sqrt{N_c}} \right\}$  is the spreading code,

the values of  $b \in \{0,1, \dots, N_b - 1\}$  are determined by the time hopping code and

$c(t)$  is the chip pulse shaping filter.

Owing to the specific frame format for this standard, the signal transmitted in (1) can be rewritten as follows:

$$x(t) = d_0 f_0(t) + d_1 f_1(t), \quad (2)$$

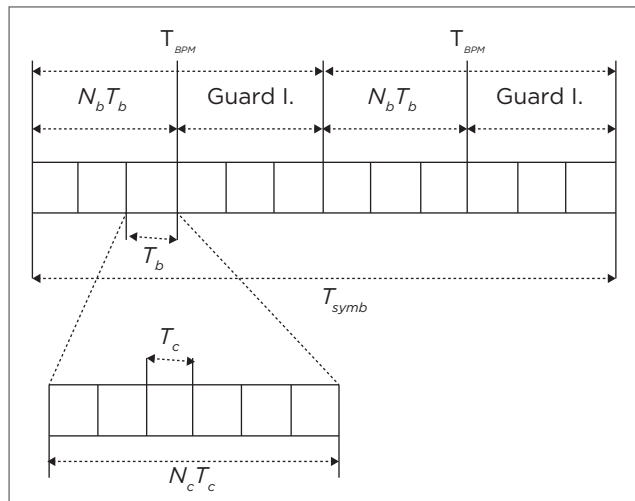


Figure 1. UWB symbol structure.

where:

$$d_0 = (1 - 2b_1)(1 - b_0),$$

$$d_1 = (1 - 2b_1)b_0 \text{ and}$$

$f_0(t)$  e  $f_1(t)$  are given by

$$f_0(t) = \sum_{n=0}^{N_c-1} s_n c(t - b T_b - n T_c)$$

$$f_1(t) = \sum_{n=0}^{N_c-1} s_n c(t - b T_b - n T_c - T_{BPM}). \quad (3)$$

Note that since the supports of  $f_0(t)$  and  $f_1(t)$  are disjoint, owing to the temporal displacement of  $T_{BPM}$  between  $f_0(t)$  and  $f_1(t)$ , these two functions form an orthogonal basis in the interval  $T_{\text{symbol}}$ . Thus, the modulation scheme employed by the IEEE std 802.15.4a may be viewed as a quaternary biorthogonal modulation, in which the basis functions move at each symbol interval. The constellation of associated signals is shown in Figure 2.

## 2.2. OPTIMUM RECEIVER

Initially considering the case of a single user, the signal received at baseband can be expressed as follows:

$$r(t) = b(t) * x(t) + n(t) = d_0 g_0(t) + d_1 g_1(t) + n(t) \quad (4)$$

where:

$b(t)$  is the complex impulse response of the equivalent baseband transmission channel (MOLISCH, 2007; 2009),

$n(t)$  is an additive complex circular white Gaussian noise and  $g_0(t)$  and  $g_1(t)$  are given by

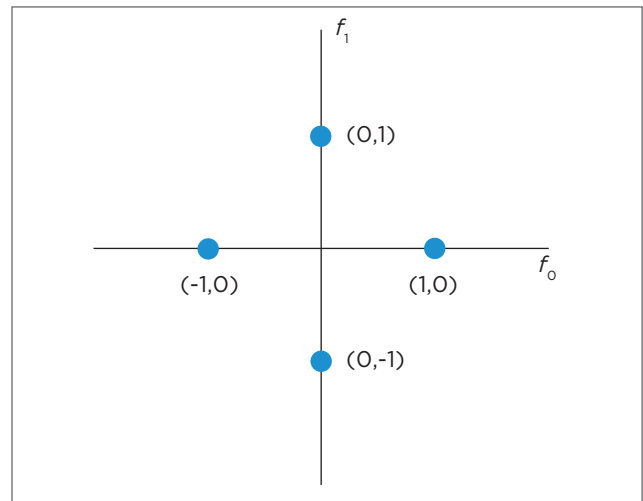


Figure 2. IEEE std 802.15.4a signal constellation.

$$\begin{aligned} g_0(t) &= b(t) * f_0(t) \\ g_1(t) &= b(t) * f_1(t). \end{aligned} \quad (5)$$

The length of the guard interval,  $T_G$  is such that supports of  $g_0(t)$  and  $g_1(t)$  are disjoint, and therefore  $g_0(t)$  and  $g_1(t)$  compose an orthogonal basis in the symbol interval. In this situation, taking (4) into account, the maximum likelihood (ML) receiver is composed of two filters matched to functions, which are generally complex,  $g_0(t)$  and  $g_1(t)$  whose outputs are sampled at the symbol rate and forwarded to a minimum distance detector, operating in the constellation of symbols shown in Figure 2.

The optimum receiver described earlier may be implemented as shown in Figure 3 (OLIVEIRA, 2010), where  $c_0^*(-t)$  is the impulse response of a filter matched to the chip pulse at the output of the channel, with  $c_0(t) = c(t) * b(t)$  and  $\mathbf{s} = [s_0, s_1, \dots, s_{N_c-1}]$  being the vectors containing the spreading code. Also in Figure 3,  $\odot$  denotes scalar product, and  $z_j = \mathbf{s}^H \mathbf{y}_j, j = 0, 1, \Re\{x\}$  extracts the real part of the complex  $x$ , and  $(\cdot)^H$  is the Hermitian operator.

### 3. PROPOSED RECEIVER

The optimum receiver shown in Figure 3 requires the explicit knowledge of the channel impulse response,  $b(t)$  to analogically implement the matched filter  $c_0^*(-t)$  which makes it complex to be executed.

This section describes (OLIVEIRA, 2010; Oliveira, Sampaio-Neto & MEDINA, 2011) a receiver structure that uses a filter matched to the chip pulse in the transmission, as illustrated in Figure 4. The filter output in each receiver branch is sampled at the chip rate. The samples of each branch are

stacked to form the vectors  $\mathbf{r}_0$  and  $\mathbf{r}_1$  of size  $M = N_c + \left\lceil \frac{T_G}{T_C} \right\rceil$ ,

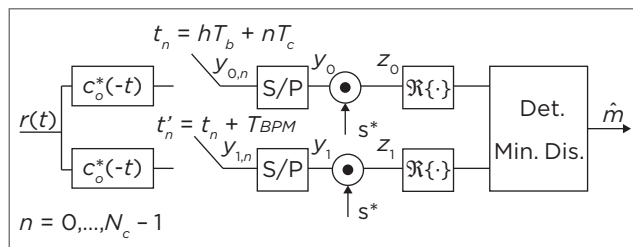


Figure 3. Implementation of the optimum receiver.

where  $\lceil x \rceil$  represents the smallest integer greater than or equal to  $x$ . These vectors have the following form:

$$\mathbf{r}_i = d_i \mathbf{s}_{ef} + \mathbf{n}_0^i, i = 0, 1 \quad (6)$$

where:

$$\mathbf{s}_{ef}[m] = \sum_{n=0}^{N_c-1} s_n b_{eq}[m-n] \quad m = 0, \dots, M-1 \quad (7)$$

is named the effective code, and is the result of the discrete convolution between the user spreading code,  $\mathbf{s}$ , and the impulse response of the equivalent discrete low-pass of the system:

$$b_{eq}[m] = b_{eq}(mT_c), m = 0, 1, \dots, \left\lceil \frac{T_G}{T_C} \right\rceil, \quad (8)$$

where:

$$b_{eq}(t) = c(t) * b(t) * c^*(-t). \quad (9)$$

Also in (6),  $\mathbf{n}_0^i, i = 0, 1$  is the vector containing the  $M$  input noise samples filtered by the filter matched to the chip pulse. As shown in Figure 4, implementation of this receiver requires knowledge of  $\mathbf{s}_{ef}$ . However, this effective code can be directly estimated without the explicit knowledge of the channel, as will be shown in the following sections.

#### 3.1. OPTIMALITY CONDITIONS OF THE PROPOSED RECEIVER

The aim of this section is to compare the inputs to the minimum distance detector of the receiver shown in Figure 3, which is optimal, to the inputs of the modified receiver shown in Figure 4. Comparing the two expressions, we seek conditions for  $\hat{z}_i = z_i$ , i.e. the conditions under which the modified receiver is also optimal according to the ML criterion.

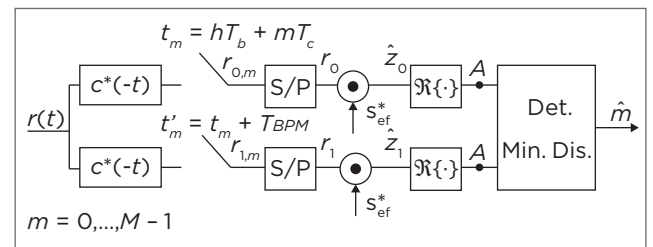


Figure 4. Implementation of the proposed receiver.

The output of the matched filter of the receiver depicted in Figure 3 is given by

$$\begin{aligned} y_i(t) &= r(t) * c_0^*(-t) = r(t) * c^*(-t) * h^*(-t) \\ &= p(t) * h^*(-t), \end{aligned} \quad (10)$$

where  $p(t)$  is given by:

$$p(t) = r(t) * c^*(-t). \quad (11)$$

It is then possible to observe that  $z_i, i \in \{0,1\}$  may be expressed as:

$$z_i = \sum_{n=0}^{N_c-1} s_n \int_{-\infty}^{\infty} p(\tau) h^*(\tau - t) d\tau \Big|_{t=nT_c+kT_b+iT_{BPM}}. \quad (12)$$

Approximating the integral in (12) using a Riemann sum with points spaced by  $T_c$ , replacing the sampling instant  $t = nT_c + kT_b + iT_{BPM}$  in (12), where  $n, k, i \in \mathbb{Z}$ , and also taking into account that both  $T_b$  and  $T_{BPM}$  are multiples of  $T_c$ , after some manipulations, the following is obtained:

$$z_i \cong T_c \sum_{n=0}^{N_c-1} s_n \sum_{m=0}^{M-1} p([m + N_i]T_c) h^*([m - n]T_c), \quad (13)$$

where  $N_i, i \in \{0,1\}$  is given by

$$N_i = \frac{kT_b + iT_{BPM}}{T_c}. \quad (14)$$

Taking (7) into account, for the receiver in Figure 4,  $\hat{z}_i, i \in \{0,1\}$  is

$$\begin{aligned} \hat{z}_i &= \sum_{m=0}^{M-1} s_{ef}^* [m] p(t) \Big|_{t=mT_c+kT_b+iT_{BPM}} \\ &= \sum_{n=0}^{N_c-1} s_n \sum_{m=0}^{M-1} h_{eq}^* [m - n] p(t) \Big|_{t=mT_c+kT_b+iT_{BPM}} \\ &= \sum_{n=0}^{N_c-1} s_n \sum_{m=0}^{M-1} p([m + N_i]T_c) h_{eq}^* [m - n]. \end{aligned} \quad (15)$$

Comparing  $z_i$  in (13) and  $\hat{z}_i$  in (15), we can conclude that for both receptors to be equivalent, that is, for  $z_i = \alpha \hat{z}_i$ , where  $\alpha$  is a positive constant, the following conditions must be met:

1. The approximation performed to replace the integral in (12) by a Riemann sum must be precise.
2. It is necessary that  $h(nT_c) = h_{eq}[n]$ .

A sufficient condition for condition 1 to hold, i.e.

$$\int_{-\infty}^{\infty} p(\tau) h^*(\tau - t) d\tau = T_c \sum_{j=-\infty}^{\infty} p(jT_c) h^*(jT_c - t) \quad (16)$$

is that chip pulse shaping filter,  $c(t)$ , has maximum frequency

given by  $f_{max} = \frac{1}{2T_c}$ . Thus, it is guaranteed equality between

the integral and the Riemann sum with partitions spaced by  $T_c$ . This condition is achieved, for example, when using a pulse shaping filter whose spectrum has square-root raised cosine

form with bandwidth  $B = \frac{1}{2T_c}$  and zero roll-off.

A sufficient, but not necessary condition to satisfy condition 2, i.e.,  $h(nT_c) = h_{eq}[n]$  is that the spectra of  $h(t)$  and  $h_{eq}(t)$  given by (9) are equal in frequency interval  $|f| \leq B$ , where  $B$  is the bandwidth of  $c(t)$ . In other words,  $H(f) = H_{eq}(f) = |C(f)|^2 H(f)$ ,  $|f| \leq B$  where  $H(f)$  is the Fourier transform of  $h(t)$  and  $C(f)$  is the Fourier transform of  $c(t)$  (OLIVEIRA, 2010).

Therefore, the conditions for the modified receiver to be optimal are directly related to the chip pulse shaping filter type chosen, first because it is the relationship between the chip pulse shaping filter bandwidth and the duration of the chip,  $T_c$ , which shows how accurate is the approximation of the integral by the Riemann sum in (13). Second, it is the spectrum of the pulse shaping filter that modifies the spectrum of the overall communication channel, causing possible differences between  $h(t)$  and  $h_{eq}(t)$ . The use of a square-root raised cosine filter with zero roll-off factor as chip pulse shaping filter guarantees equality between the modified receiver and the original receiver, since in this case the expressed equality conditions are met. However, since using zero roll-off factor is not feasible, the performance of the modified receiver is slightly degraded, being more similar to the optimal, the lower the roll-off used.

### 3.2. ESTIMATION OF THE EFFECTIVE CODE

As indicated in the previous section, the optimum filter in the receiver is considered the filter matched to the effective code. In this study, two types of estimators, an assisted and a blind, are presented (OLIVEIRA, 2010; OLIVEIRA, SAMPAIO-NETO & MEDINA, 2011).

### 3.2.1. Assisted estimation

If the optimality conditions are met, the observation noise,  $\mathbf{n}_o^i$  in (6), is white Gaussian, with covariance matrix  $\sigma_n^2 \mathbf{I}$ . In addition, the noise vectors  $\mathbf{n}_o^0$  and  $\mathbf{n}_o^1$  are statistically independent. Under these conditions, the ML estimate of  $\mathbf{s}_{ef}$  based on  $W$  observations of the pair  $(\mathbf{r}_0, \mathbf{r}_1)$  is given by:

$$\hat{\mathbf{s}}_{ef} = \frac{1}{W} \sum_{w=1}^W \left( d_0^{(w)} \mathbf{r}_0^{(w)} + d_1^{(w)} \mathbf{r}_1^{(w)} \right) \quad (17)$$

where:

$\mathbf{r}_i^{(w)}$ ,  $d_i^{(w)}$ ,  $i = 0, 1$ , are, respectively, the  $w$ -th vector received and pilot symbol transmitted, and  $W$  is the length of the training sequence.

### 3.2.2. Blind estimation

The second estimator for the normalized effective code,  $\mathbf{s}_{ef}$ , is a blind estimator obtained by

$$\hat{\mathbf{s}}_{ef} = \arg \max_{\omega} \omega^H \mathbf{R}_{01} \omega$$

subject to  $\|\omega\| = 1$  (18)

where:

$$\mathbf{R}_{01} = \mathbb{E}[\mathbf{r}_0 \mathbf{r}_0^H] + \mathbb{E}[\mathbf{r}_1 \mathbf{r}_1^H].$$

The solution to (18) is the eigenvector corresponding to the largest eigenvalue of  $\mathbf{R}_{01}$ , which coincides with the effective code of the user, since

$$\begin{aligned} \omega^H \mathbf{R}_{01} \omega &= \omega^H \left( \sigma_s^2 \mathbf{s}_{ef} \mathbf{s}_{ef}^H + 2\sigma_n^2 \mathbf{I} \right) \omega, \\ &= \sigma_s^2 \omega^H \mathbf{s}_{ef} \mathbf{s}_{ef}^H \omega + \|\omega\|^2 2\sigma_n^2 \\ &= \sigma_s^2 \left\| \omega^H \mathbf{s}_{ef} \right\|^2 + 2\sigma_n^2, \end{aligned} \quad (19)$$

and (19) is maximum if  $\omega = \alpha \mathbf{s}_{ef}$  where  $\alpha$  is a complex scalar of unit modulus.

In practice, the autocorrelation matrix  $\mathbf{R}_{01}$  can be estimated using a recursive process or a set of samples, such as

$$\hat{\mathbf{R}}_{01}(l) = \frac{1}{l} \sum_{w=1}^l \mathbf{r}_0^{(w)} \mathbf{r}_0^{(w)H} + \mathbf{r}_1^{(w)} \mathbf{r}_1^{(w)H}, \quad (20)$$

and the eigenvector corresponding to the largest eigenvalue of  $\mathbf{R}_{01}$  can be efficiently calculated by the power method (MEYER, 2001) as:

$$\begin{aligned} g(l) &= \hat{\mathbf{R}}_{01} \hat{\mathbf{s}}_{ef}^{(l-1)} \\ \hat{\mathbf{s}}_{ef}^{(l)} &= \frac{g(l)}{\|g(l)\|} \end{aligned} \quad (21)$$

for  $l = 1, 2, \dots$

## 4. MULTIPLE ACCESS SYSTEM MODEL

The transmitted signal  $x(t)$  with multiple users is the sum of the signals of the  $N_u$  users during the same symbol interval:

$$x(t) = \sum_{u=0}^{N_u-1} d_0^u f_0^u(t) + d_1^u f_1^u(t), 0 \leq t \leq T_{\text{ymb}} \quad (22)$$

where:

$(d_0^u, d_1^u)$  is the symbols pair transmitted from the  $u$ -th user.

The basis functions  $f_0^u(t)$  and  $f_1^u(t)$  are similar to those presented in (3), with the spreading codes,  $s_u$ , which are different for each user and time hopping codes,  $b_u \in \{0, 1, \dots, N_b - 1\}$ . The signal received at the  $i$ -th ( $i \in \{0, 1\}$ ) branch of the receiver of the  $u$ -th user,  $\mathbf{r}_i^u$ , is represented vectorially by

$$\mathbf{r}_i^u = \Gamma_u^T \left( \sum_{j=0}^{N_u-1} d_i^j \Gamma_j \mathbf{s}_{ef}^j \right) + \mathbf{n}, \quad (23)$$

where:

$\mathbf{n}$  is the noise present at reception,

$\mathbf{s}_{ef}^j$  is the effective code of  $j$ -th user, and

matrix  $\Gamma_u$  is given by

$$\Gamma_u = \begin{pmatrix} \mathbf{0}_{(N_{hop,u} \times M)} \\ \mathbf{I}_{(M \times M)} \\ \mathbf{0}_{(N_{end} - M - N_{hop,u} \times M)} \end{pmatrix} \quad (24)$$

where  $N_{hop,u} = \frac{b_u T_b}{T_c}$  and  $N_{end} = \frac{T_{\text{ymb}}}{T_c}$ .

The multiple access technology proposed by IEEE std 802.15.4a is the composition of time and code division. There are two alternatives to compose the symbol with multiple users. One alternative uses orthogonal time hopping for time division. In this mode, each user has an exclusive slot, that is,  $h_u$  is different for each user at each symbol interval. The significant advantage of this mode is the guarantee of a minimum displacement between the effective codes of the users. This displacement is essential to ensure that the effective code of a given user is almost orthogonal to the vector corresponding to the multiple access interference (MAI) during the observation interval, although the UWB channel causes a long time spreading. The main disadvantage of this mode is to limit the number of users who can transmit concurrently, as the transmission is limited to the maximum number of existing codes  $N_b$ . Owing to the symbol structure, for a spreading code length equal to 128 (usual number of chips per burst in IEEE std 802.15.4a), it is possible to have a maximum  $N_b = 8$ , that is, only 8 users could transmit during the same symbol interval. The other time division multiple access mode is the non-orthogonal time hopping, in which more than one user can transmit in the same slot. A characteristic of this mode that stands out is the higher capacity

on the number of users transmitting during the same symbol interval. However, this increased capacity is achieved at the cost of the overlapping of non-orthogonal spreading codes at the reception, deteriorating the performance of the system.

Figure 5 illustrates the cross-correlation properties of eight effective signatures for a given sample function of the channel using spreading codes of length 128, according to the IEEE std 802.15.4a. In the case of orthogonal time hopping, we can see that for displacements larger or equal to 128, the signatures result *quasi* orthogonal, having correlation coefficients lower than 0.01. In the case of non-orthogonal (zero displacement) time hopping, the correlation index does not exceed 0.25.

This fact motivates the use of the receiver with filter matched to the effective code also for environment with multiple users and non-orthogonal time hopping. As previously mentioned, this is particularly important in the case of blind detection, since the proposed method does not entail matrix inversion, unlike most blind detection methods with interference suppression. The same two methods of estimation of the effective code demonstrated in the case of a single user are applied. In the case of assisted estimation, similar to the case of a single user, the following holds:

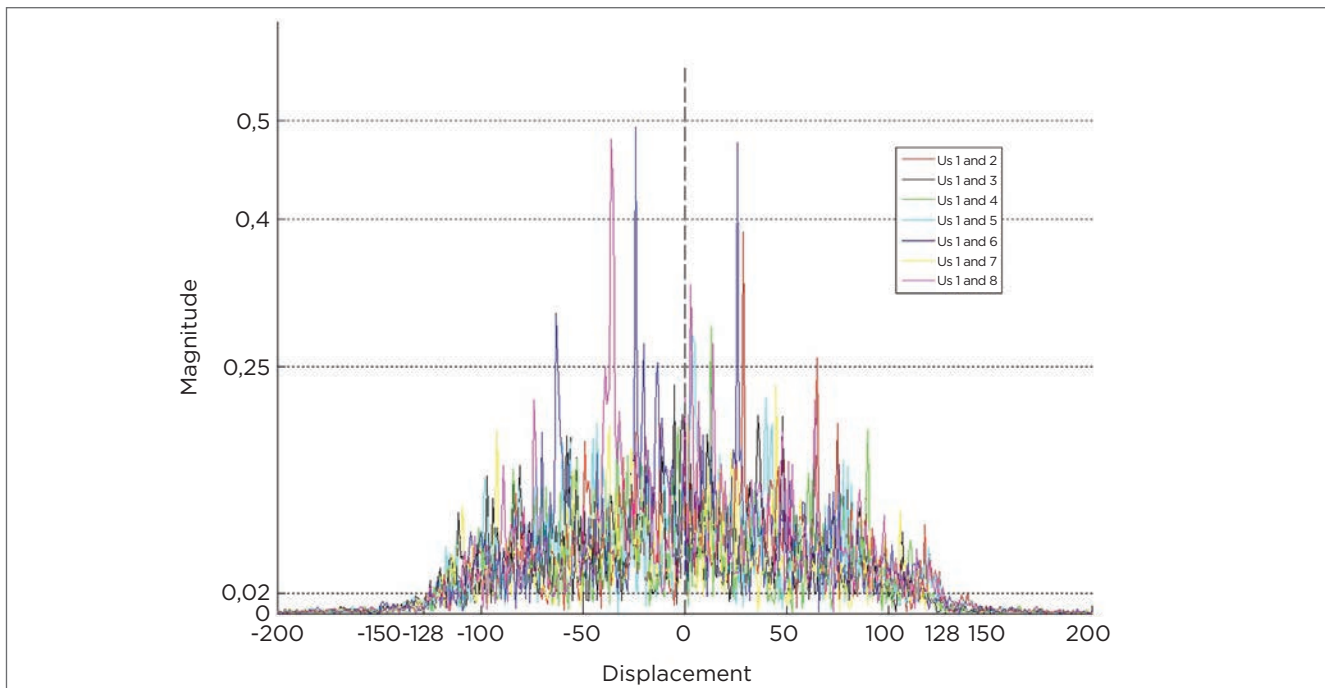


**Figure 5.** Graph of the correlation coefficients between the effective code of user 1 and other users for a given sampling function of the channel.

$$E [d_0^u r_0^u + d_1^u r_1^u] = s_{gf}^u \quad (25)$$

where:

$r_0^u$  and  $r_1^u$  are the vectors received in branches 0 and 1, respectively, of the proposed receiver of the  $u$ -th user, and  $d_0^u$  and  $d_1^u$  are transmitted pilots.

Thus, the effective code can be estimated similarly to the single-user case, by means of (17). On the other hand, the blind estimation method proposed for single-user environment results in the following for the case of multiple users:

$$\omega^H R_{01}^u \omega = \omega^H s_{gf}^u s_{gf}^{uH} \omega + \omega^H R_I \omega + 2\sigma_n^2, \quad (26)$$

where:

the autocorrelation matrix  $R_I$  is given by

$$R_I = E[\mathbf{i}\mathbf{i}^H] = E[\mathbf{i}_0\mathbf{i}_0^H] + E[\mathbf{i}_1\mathbf{i}_1^H] \quad (27)$$

where:

$\mathbf{i} = \mathbf{i}_0 + \mathbf{i}_1$  and  $\mathbf{i}_0$  and  $\mathbf{i}_1$  are vectors of MAI given by

$$\mathbf{i}_k = \Gamma_u^T \sum_{j=0, j \neq u}^{N_u-1} d_k^u \Gamma_j^T s_{gf}^j, k \in \{0, 1\}. \quad (28)$$

An upper limit for the expression (26) is given by

$$\max_{\omega, \|\omega\|=1} \omega^H R_{01}^u \omega \leq \sigma_s^2 \max_{\omega, \|\omega\|=1} \{\omega^H s_{gf}^u s_{gf}^{uH} \omega\} + \max_{\omega, \|\omega\|=1} \{\omega^H R_I \omega\} + 2\sigma_n^2$$

and therefore

$$\max_{\omega, \|\omega\|=1} \omega^H R_{01}^u \omega \leq \sigma_s^2 + \lambda_{\max} + 2\sigma_n^2 \quad (29)$$

where:

$\lambda_{\max}$  is the largest eigenvalue associated with  $R_I$ , which corresponds to the energy of the interference vector,  $\mathbf{i}$ , in the direction of maximum energy.

Considering (29), it can be concluded that the maximization of  $\omega^H R_{01}^u \omega$  should result in a vector similar to the desired,  $s_{gf}^u$ , when the ratio  $\sigma_s^2/\lambda_{\max}$  is high, whereas for lower values of this ratio, the solution is close to the normalized eigenvector  $\mathbf{e}_{\max}$  associated with  $\lambda_{\max}$ . In fact, when  $s_{gf}^u$  and the

interference vector are orthogonal,  $E[\mathbf{i} s_{gf}^{uH}] = 0$ , then  $s_{gf}^u$  is

eigenvector of  $R_{01}^u$ , with associated eigenvalue  $\sigma_s^2$ , leading to

$$\omega = \begin{cases} s_{gf}^u; & \text{para } \frac{\sigma_s^2}{\lambda_{\max}} > 1 \\ \mathbf{e}_{\max}; & \text{caso contrário} \end{cases}. \quad (30)$$

For the system considered, in general,  $\frac{\sigma_s^2}{\lambda_{\max}} \gg 1$ , yielding

a solution  $\omega$  really similar to  $s_{gf}^u$ . This is due to the fact that interference  $\mathbf{i}$  presents a peculiarity: because of time hopping and binary position modulation, BPM, the interference in each symbol, if present, always appears in a different place within the frame of the user of interest. This behavior prevents the interference vector  $\mathbf{i}$  from having a pronounced

preferential direction, and therefore its energy,  $\sigma_i^2 = \sum_{i=1}^N \lambda_i$ ,

is spread over the eigenvalues  $\lambda_i$  ( $i = 1, \dots, N$ ), of  $R_I$  and consequently  $\lambda_{\max} \ll \sigma_i^2$ . Thus, even for moderately low values of

signal-interference ratio  $\frac{\sigma_s^2}{\sigma_i^2}$  a ratio  $\frac{\sigma_s^2}{\lambda_{\max}} > 1$  is obtained.

## 5. RESULTS

The simulations consider the downlink of a system using the proposed receiver and a symbol structure in accordance to the IEEE std 802.15.4a. The pulse shaping filter employed is a square-root raised cosine pulse with roll-off factor  $a = 0,2$  with duration  $T_c = 2$  ns, which is mandatory in this standard. It is assumed that the receiver is perfectly synchronized with the transmitter. The number of slots for time hopping is  $N_B = 8$ , and the number of chips per burst is  $N_c = 128$ , producing one frame of 4,096 chip intervals per symbol. Thus, a system using orthogonal time hopping code supports a maximum of eight users. In all experiments, 200 transmissions of 2,000 bits each are simulated. The bits are transmitted uncoded. The spreading sequence for each user is obtained in each transmission according to the IEEE std 802.15.4a, and is maintained over the 2,000 bits transmitted. The UWB

channel used is in accordance with the model described in (MOLISCH, 2007; 2009). For each transmission, a new sampling function of the channel is generated. In the experiments, three estimates of the effective code of the user of interest are compared: the first estimate is obtained using the assisted method in (19) (Assisted), the second estimate is obtained using the blind method in (23) (Blind), and the third estimate is the perfect estimate of the effective code of the user (Perfect).

In the first experiment, a channel without large-scale fading corresponding to type 3 in (MOLISCH, 2007) (office with line of sight) is used. The results are shown in Figure 6 in terms of a signal-to-interference-plus-noise ratio (SINR),

which was obtained at the point A indicated on Figure 4. The first column (graphs I, II, and III) corresponds to values of  $E_b/N_0 = 10$  dB and the second column (graphs IV, V, and VI) corresponds to values of  $E_b/N_0 = 25$  dB. The graphs of the first row (I and IV) are for orthogonal time hopping with 8 users, the second row (II and V) is for non-orthogonal time hopping with 8 users, and the third row (III and VI) is for non-orthogonal time hopping with 18 users. The receiver with filter matched to the effective code of the user has a very good performance for the system with orthogonal time hopping and even for the system with non-orthogonal time hopping for low  $E_b/N_0$  ratios, where the white noise is predominant over the MAI (graphs I, II, and III). In fact, the SINR

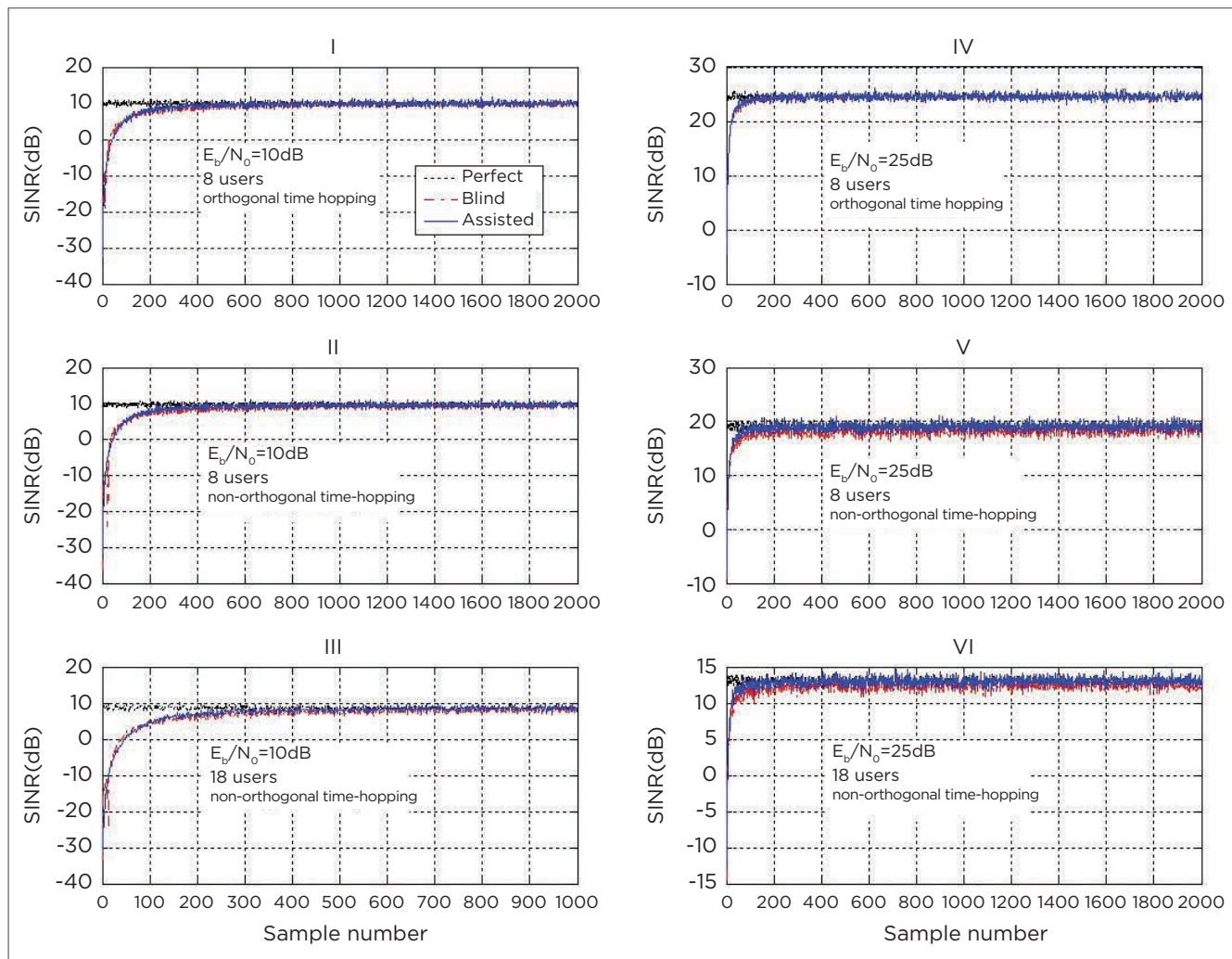


**Figure 6.** Comparison between the curves of SINR, channel without fading, for orthogonal and non-orthogonal time hopping,  $\frac{E_b}{N_0} = 10$  dB and  $\frac{E_b}{N_0} = 25$  dB and system loaded with 8 and 18 users.

achieved assuming perfect estimation is almost the same as the theoretical maximum SNR that a system operating with a single user (SU) could reach (10 dB for the first column and 25 dB for the second column). For the cases in which the time hopping codes are non-orthogonal and MAI is predominant over white noise (graphs V and VI), despite *quasi* orthogonality between the actual code  $s_{gf}^u$  and interference  $i$  from other users, the SINR achieved by the receiver with matched filter does not reach the maximum SNR of a SU system (which is by definition MAI-free). In these cases, there is a cost-benefit trade off that should be considered in order to adequately choose the type of receiver. Depending on the application, simplicity of the implementation of matched filter may be more important than the loss of performance in these scenarios. The estimators analyzed showed good performance, achieving similar results to those obtained with the matched filter, with the blind estimator presenting performance very similar to the assisted estimator even in cases in which the MAI is the main source of nuisance.

In the second experiment an ensemble of channels without large-scale fading corresponding to the type 3 in (MOLISCH, 2007) (office with line of sight) is also used. The results are shown in Figure 7 in terms of SINR obtained in point A of Figure 4, for a user of interest in a system with non-orthogonal time hopping, which starts with only one active user and receives a sudden additional load of seven active users after 1,000 symbols transmitted with  $E_b/N_0 = 10$  dB. In this experiment, it is possible to verify that the proposed estimation methods are quite robust with respect to convergence. In fact, even loading the system suddenly with a large number of users, once a good estimate for the effective code of the user of interest,  $s_{gf}^u$ , is achieved, the estimator is not deteriorated by interference between users.

In the third experiment, channels with large-scale fading corresponding to the type 6 in (MOLISCH, 2007) (outdoor without line of sight) are considered. Figure 8 shows the bit error rate (BER) for systems with eight users and non-orthogonal time hopping. For comparison purposes, Figure 8 shows the lower limit of bit error rate, represented by the case of a SU system, with a single user (therefore without MAI) and perfect estimate of the actual code. The bit error rate begins to be measured after 1,000 transmitted bits. It can be concluded from Figure 8 that the assisted and blind estimation methods have a good result

also for fading channels, showing a loss of tenths of dB when compared to the case of perfect estimation. On the other hand, this case presents a substantially coincident performance compared with the SU case, again confirming the *quasi* orthogonality between the effective code  $s_{gf}^u$  and interference from other users,  $i$ .

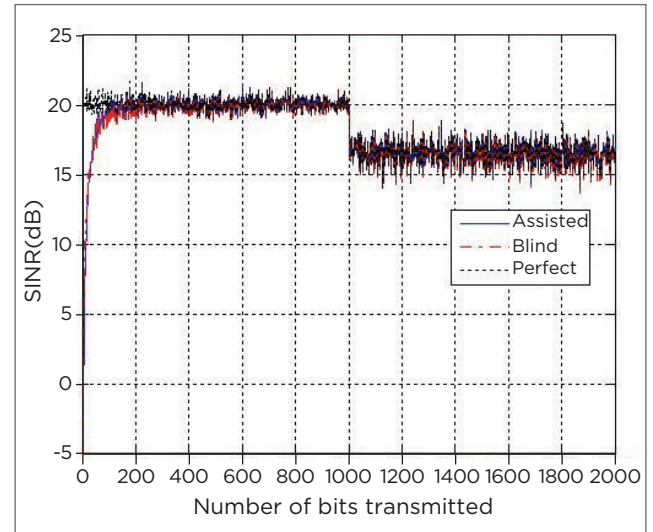


**Figure 7.** Comparison between SINR curves of the estimation methods for a system initially loaded with one active user and a sudden additional load of seven active users during the second half of the transmission, channel without fading,  $\frac{E_b}{N_0} = 20$  dB.

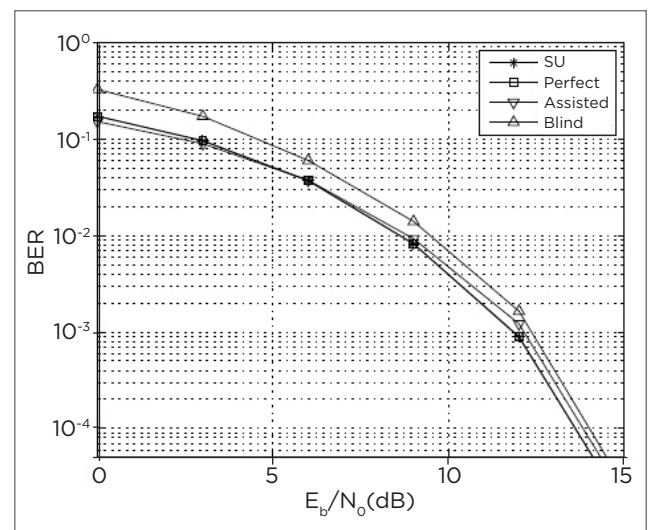


**Figure 8.** Comparison of the BER curves for the estimation methods, for a system with 8 users, fading channel.

## 6. CONCLUSION

This work addressed the reception of signals in a UWB transmission system, implemented according to the IEEE std 802.15.4a, with orthogonal and non-orthogonal time hopping. A modified receiver and the conditions under which this receiver is optimum according to the ML criterion were introduced to this system. This modified receiver uses as the detection filter, a filter matched to the effective code. Two different methods to estimate the effective code were proposed: one assisted and one blind.

It is important to mention that for the cases of a system with orthogonal time hopping in an environment with

multiple access interference and a system with non-orthogonal time hopping in an environment where the white noise predominates over MAI, these same receivers and estimators have shown good performance. This is of particular interest in the case of the receiver with the blind estimator, because the proposed method has a low computational complexity, compared with most blind detection methods with interference suppression that would require the inversion of high dimension matrices. For the case of a system with non-orthogonal time hopping in an environment in which the MAI predominates, the proposed estimators also show good performance, being more susceptible to degradation owing to the non-optimality of the matched filter.

## REFERENCES

- I.T. GROUP. Part 15.4: Wireless medium access control (MAC) and physical layer (PHY) specifications for low-rate wireless personal area networks. amendment 1: Alternate PHYs – IEEE802.15.4a-2007. Tech. Rep., IEEE Computer Society, 2007.
- KSHETRIMAYUM, R.S. An introduction to UWB communication systems. *IEEE Potentials*, v. 2009, p. 9-13, 2009.
- LAMARE, R.C. de; SAMPAIO-NETO, R. Blind adaptive code-constrained constant modulus algorithms for CDMA interference suppression in multipath channels. *IEEE Communications Letters*, v. 9, n. 4, p. 334-336, 2005.
- MEDINA, C.A.; SAMPAIO-NETO, R. A constrained IQRD-RLS blind detection algorithm for CDMA transmission systems in multipath channels. *The Seventh International Symposium on Wireless Communication Systems*, York, United Kingdom, 2010.
- MEDINA, C.A.; VINHOZA, T.T.V.; SAMPAIO-NETO, R. Reduced complexity blind channel estimation for adaptive constrained minimum variance receivers in MC-CDMA systems. *9th IEEE Workshop on Signal Processing Advances in Wireless Communications (SPAWC-2008)*. Recife, 2008.
- MEYER, C.D. *Matrix Analysis and Applied Linear Algebra*. SIAM: Society for Industrial and Applied Mathematics, 2001.
- MOLISCH, A.F. Ultra-wide-band propagation channels. *Proceedings of the IEEE*, v. 97, n. 2, p. 353-371, 2009.
- MOLISCH, A.F.; CASSIOLI, D.; CHONG, C-C.; EMAMI, S.; FORT, A.; KANNAN, B.; KÅREDAL, J.; KUNISCH, J.; SCHANTZ, H.G.; SIWIAK, K.; WIN, M.Z. A comprehensive standardized model for ultrawideband propagation channels. *IEEE Transactions on Antennas and Propagation*, v. 54, n. 11, p. 3151-3166, 2007.
- OLIVEIRA, A. de *Detecção em sistema de comunicação de banda ultralarga*. Dissertação de Mestrado, Rio de Janeiro, PUC, 2010.
- OLIVEIRA, A. de; SAMPAIO-NETO, R.; MEDINA, C.A. Detecção de sinais em sistemas UWB baseados no padrão IEEE 802.15.4. In: SIMPÓSIO BRASILEIRO DE TELECOMUNICAÇÕES (SBrT2011), XXIX. *Anais...* Curitiba, 2011.
- SCHOLTZ, R.A. Multiple access with time-hopping impulse modulation. *IEEE Military Commun. Conf. (MILCOM)*, Boston, MA, v. 2, p. 447-445, 1993.
- TSATSANIS, M.K.; XU, Z. Performance analysis of minimum variance CDMA receivers. *IEEE Transactions on Communications*, v. 46, n. 11, p. 3014-3022, 1998.
- WIN, M.Z.; SCHOLTZ, R.A. Impulse radio: How it works. *IEEE Communications Letters*, v. 2, p. 36-38, 1998.
- WIN, M.Z.; SCHOLTZ, R.A. Ultra-wide bandwidth time-hopping spread-spectrum impulse radio for wireless multiple-access communications. *IEEE Transactions on Communications*, v. 48, p. 679-691, 2000.
- XU, Z.; LIU, P. Code-constrained blind detection of CDMA signals in multipath channels. *Signal Processing Letters*, v. 9, n. 12, p. 389-392, 2002.
- XU, Z.; LIU, P.; TANG, E.J. Blind multiuser detection for impulse radio UWB systems. *2003 IEEE Tropical Conference on Wireless Communication Technology*, p. 453-454, mar. 2003.
- XU, Z.; TSATSANIS, M.K. Blind adaptive algorithms for minimum variance CDMA receivers. *IEEE Transactions on Communications*, v. 49, n. 1, p. 180-194, 2001.

# BRAZILIAN PASSIVE SONAR: ADVANCES AND TECHNOLOGY SHOWCASE

Sonar passivo nacional: avanços e demonstração de tecnologia

Fabricio de Abreu Bozzi<sup>1</sup>, William Soares Filho<sup>2</sup>, Fernando de Souza Pereira Monteiro<sup>3</sup>,  
Carlos Alfredo Órfão Martins<sup>4</sup>, Gustavo Augusto Mascarenhas Goltz<sup>5</sup>,  
Orlando de Jesus Ribeiro Afonso<sup>6</sup>, Cleide Vital da Silva Rodrigues<sup>7</sup>,  
Fernando Luiz de Magalhães<sup>8</sup>, Leonardo Martins Barreira<sup>9</sup>

**Abstract:** This paper summarizes the development of a technology showcase for a passive sonar system, covering the areas of signal acquisition and array processing. Using a hydrophone array with cylindrical geometry as the “wet” part of the sonar system, a signal acquisition system was assembled to read, preprocess, and send these signals over an Ethernet network. The Detection, Tracking and Classification System (SDAC) was used as the receiver of this signal, performing the processing and the display of the information obtained, being the graphic interface for the sonar operator (“dry” part of the sonar). In this development, a beamformer was implemented using the delay-and-sum method, chosen because of its fast processing, that was adequate for real-time processing requirement.

**Keywords:** Sonar. Cylindrical Array of Hydrophones, Underwater Acoustics Signal Processing. Beamforming.

**Resumo:** O presente trabalho sintetiza o desenvolvimento de um demonstrador de tecnologia de um sonar passivo, abrangendo as áreas de aquisição e processamento de sinais para arranjo de sensores. A partir da construção de um arranjo de hidrofones com geometria cilíndrica, que corresponde à parte “molhada” do sistema sonar, um sistema de aquisição de sinais foi montado para ler, pré-processar e enviar esses sinais em uma rede Ethernet. O Sistema de Detecção, Acompanhamento e Classificação de Contatos (SDAC) foi utilizado como o receptor dos sinais, realizando o tratamento e a exibição das informações, sendo ele a interface do demonstrador (parte “seca” do sonar). Nesse desenvolvimento foi realizada a implementação da formação de feixes, o que possibilitou a capacidade de discriminação direcional do sonar. O formador de feixes atraso-e-soma, escolhido devido à sua rapidez de processamento, se mostrou adequado para a exigência de processamento em tempo real.

**Palavras-chave:** Sonar. Arranjo Cilíndrico de Hidrofones. Processamento de Sinais Acústicos Submarinos. Conformação de Feixe.

**1.** Captain-Lieutenant. Master's degree in Electrical Engineering at Instituto Alberto Luiz Coimbra of Post-graduation and Research in Engineering at Universidade Federal do Rio de Janeiro - Rio de Janeiro, RJ - Brazil. Assistant at the Division of Hydroacoustic Equipment in the Underwater Acoustic Systems Group at Instituto de Pesquisas da Marinha - Rio de Janeiro, RJ - Brazil. E-mail: bozzi@ipqm.mar.mil.br

**2.** PhD in Electrical Engineering at Instituto Alberto Luiz Coimbra of Post-graduation and Research in Engineering at Universidade Federal do Rio de Janeiro - Rio de Janeiro, RJ - Brazil. Coordinator in the Signal Processing area of the Underwater Acoustic Systems Group at Instituto de Pesquisas da Marinha - Rio de Janeiro, RJ - Brazil. E-mail: william@ipqm.mar.mil.br

**3.** Master's Degree in Biomedical Engineering at Instituto Alberto Luiz Coimbra of Post-graduation and Research in Engineering at Universidade Federal do Rio de Janeiro - Rio de Janeiro, RJ - Brazil. Electronics Engineer at Amazul, collaborator of the Division of Hydroacoustic Equipment in the Underwater Acoustic Systems Group at Instituto de Pesquisas da Marinha - Rio de Janeiro, RJ - Brazil. E-mail: nandospm@gmail.com

**4.** Corvette captain, Master's degree in Oceanic engineering at Instituto Alberto Luiz Coimbra of Post-graduation and Research in Engineering at Universidade Federal do Rio de Janeiro - Rio de Janeiro, RJ - Brazil. Professor at the Center of Instruction Almirante Wanderkolk - Rio de Janeiro, RJ - Brazil. E-mail: carlos.martins@ipqm.mar.mil.br

**5.** Captain-lieutenant. Master's degree in Applied Computer Science at Instituto Nacional de Pesquisas Espaciais - São José dos Campos, SP - Brazil. In charge of the Division of Sign Processing and Acoustic Propagation of the Underwater Acoustic Systems Group at Instituto de Pesquisas da Marinha - Rio de Janeiro, RJ - Brazil. E-mail: goltz@ipqm.mar.mil.br

**6.** Master's degree in Oceanic Engineering at Instituto Alberto Luiz Coimbra of Post-graduation and Research in Engineering at Universidade Federal do Rio de Janeiro - Rio de Janeiro, RJ - Brazil. In charge of the Division of Hydroacoustic Equipment in the Underwater Acoustic Systems Group at Instituto de Pesquisas da Marinha - Rio de Janeiro, RJ - Brazil. E-mail: orlando@ipqm.mar.mil.br

**7.** PhD in Production Engineering at Instituto Alberto Luiz Coimbra of Post-graduation and Research in Engineering at Universidade Federal do Rio de Janeiro - Rio de Janeiro, RJ - Brazil. Assistant at the Division of Sign Processing and Acoustic Propagation in the Underwater Acoustic Systems Group at Instituto de Pesquisas da Marinha - Rio de Janeiro, RJ - Brazil. E-mail: cleide@ipqm.mar.mil.br

**8.** PhD in Mechanical Engineering at Instituto Alberto Luiz Coimbra of Post-graduation and Research in Engineering at Universidade Federal do Rio de Janeiro - Rio de Janeiro, RJ - Brazil, Assistant at the Division of Hydroacoustic Equipment in the Underwater Acoustic Systems Group at Instituto de Pesquisas da Marinha - Rio de Janeiro, - Brazil. E-mail: fernando.magalhaes@ipqm.mar.mil.br

**9.** Commander, PhD in Oceanic Engineering at Instituto Alberto Luiz Coimbra of Post-graduation and Research in Engineering at Universidade Federal do Rio de Janeiro - Rio de Janeiro, RJ - Brazil, In charge of the Underwater Acoustic Systems Group at Instituto de Pesquisas da Marinha - Rio de Janeiro, RJ - Brazil. E-mail: barreira@ipqm.mar.mil.br

## 1. INTRODUCTION

The Brazilian Passive Sonar (SONAP) is a project from the Underwater Acoustic Systems Group (GSAS), from the *Instituto de Pesquisas da Marinha* (IPqM), and consists of the development of a sonar system. Throughout the years, IPqM has been training researchers and engineers in order to solidify knowledge on acoustic systems, being the demonstrator of the developed technology with the reunion of these fields of knowledge.

An advance in sonar research has taken place with the development of the Detection, Tracking and Classification System (SDAC), which, by being installed in the submarines of the Brazilian Navy (MB), enabled the collection of signals from the hydrophones, already installed in the submarine. However, when installed in the submarine, this system received signals after beamformer. Beamforming, which will be described later, is a stage of sensitive processing, that is, the technology of this process can compromise the final result.

Basically, it is possible to divide the passive sonar system into two areas (L1, 2012): the development of hydroacoustic elements (hydrophones, transducers and staves), referred to here as the wet part of the sonar; and the development of signal processing (beamforming, data treatment presentation and analyses), called the dry part.

Therefore, with the commercial materials available, the technology demonstrator aims at advancing toward the wet part, building an array, acquiring the signals, leading to beamforming, and integration with SDAC.

## 2. RESEARCH METHODOLOGY

It is possible to consider that the entire chain of processes involved in the passive sonar system begins, when an underwater acoustic wave collides with a piezoelectric element (hydrophone), making it excited, thus generating electric signal in its terminals (SHERMAN e BUTLER, 2007). From the electrical signals generated in the hydrophone terminals, the process of acquiring these signals begins. This stage consists of conditioning the signal and acquiring it in a computer, digitally.

The array of hydrophones is considered to be an antenna, and, at first, the interest is to direct that antenna

to emphasize signals coming from a given direction. This is named beamforming.

There are several beamforming techniques. The simplest one is known as delay-and-sum (VAN TREES, 2004). Owing to its simplicity and agility, this technique was chosen for this study.

The stages of analysis begin after the beams are formed, when processing takes place to characterize the signals. Among the analyses contained in a sonar system, this paper will approach the following: low frequency analysis and recording (LOFAR) and detection of envelope modulation on noise (DEMON). These analyses lead the signal to the frequency domain, bringing spectral information that help to classify the signal (TORRES; SEIXAS; SOARES FILHO, 2004; MOURA, 2013).

The research methodology shows how each one of the stages of the system was treated and implemented. A diagram of the system helps to visualize the structure of the processes, followed later with a detailed description.

### 2.1. SYSTEM DIAGRAM

Figure 1 presents the general diagram of the sonar system developed in IPqM. It is possible to notice the processes involved, that were described previously: array of sensors, amplification, digitalization, initial treatment of the signals acquired by the acquisition software, amplification control, sending data using the network through a switch, and, finally, presenting the data in SDAC.

### 2.2. CYLINDRICAL ARRAY

A sonar system may contain a single hydrophone. But, in practice, it is known that, in general, these elements are omnidirectional, that is, they “listen” in all directions. When the intention is to obtain the direction of a sound source, hydrophone arrays are used (WAITE, 2002). This study utilizes the cylindrical hydrophone array, or CHA.

The CHA is composed of an array of staves grouped in a circular shape. The staff is a structure that clusters the elements (hydrophones) and encapsulates them in a specific material, making sure they do not lose their features. Encapsulation also prevents the hydrophones from having direct contact with salt water. Finally, they are designed to muffle one of the sides, in order to direct the beam.

The construction of a sensor array in a reduced scale, compared to the arrays of the submarines in MB, aims at facilitating array tests in the hydroacoustic tank of IPqM, besides facilitating the logistics of transportation, placement, and boarding of the array.

With this array, it is possible to collect raw data, that is, signals coming directly from each element without any processing. The array is composed of 32 staves, has 1 meter in diameter, and each one of them has three hydrophones serially connected. The output of each staff is the sum of the signals of each hydrophone. Figure 2 presents the array of hydrophones.

### 2.3. SIGNAL ACQUISITION SYSTEM

The initial conditioning of the signals received by the staves comprehends amplification and, later, the digitalization of the signal. Conditioning and digitalization, when carried out properly, lead to results that are more accurate and minimize errors characteristic of quantization and saturation (DINIZ, DA SILVA and NETTO, 2014). Amplification is necessary to obtain signals at levels compatible with digitalization, since the intensity of the

electric voltage in the output of hydrophones is low, possibly to the order of  $\mu\text{V}$ .

Digitalization is made to allow data processing in a computer. In the case of a sonar system, digitalization has to be conducted in a synchronous manner, which is a requirement for the beamforming.

In this study, an acquisition system was put together using commercial hardware. However, the reading, recording and

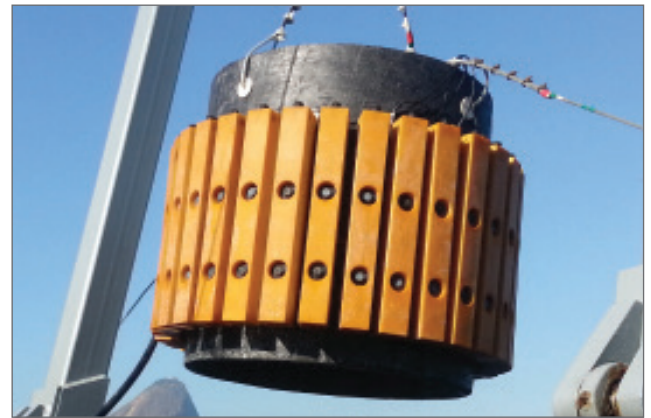


Figure 2. 32 staff sensor array.

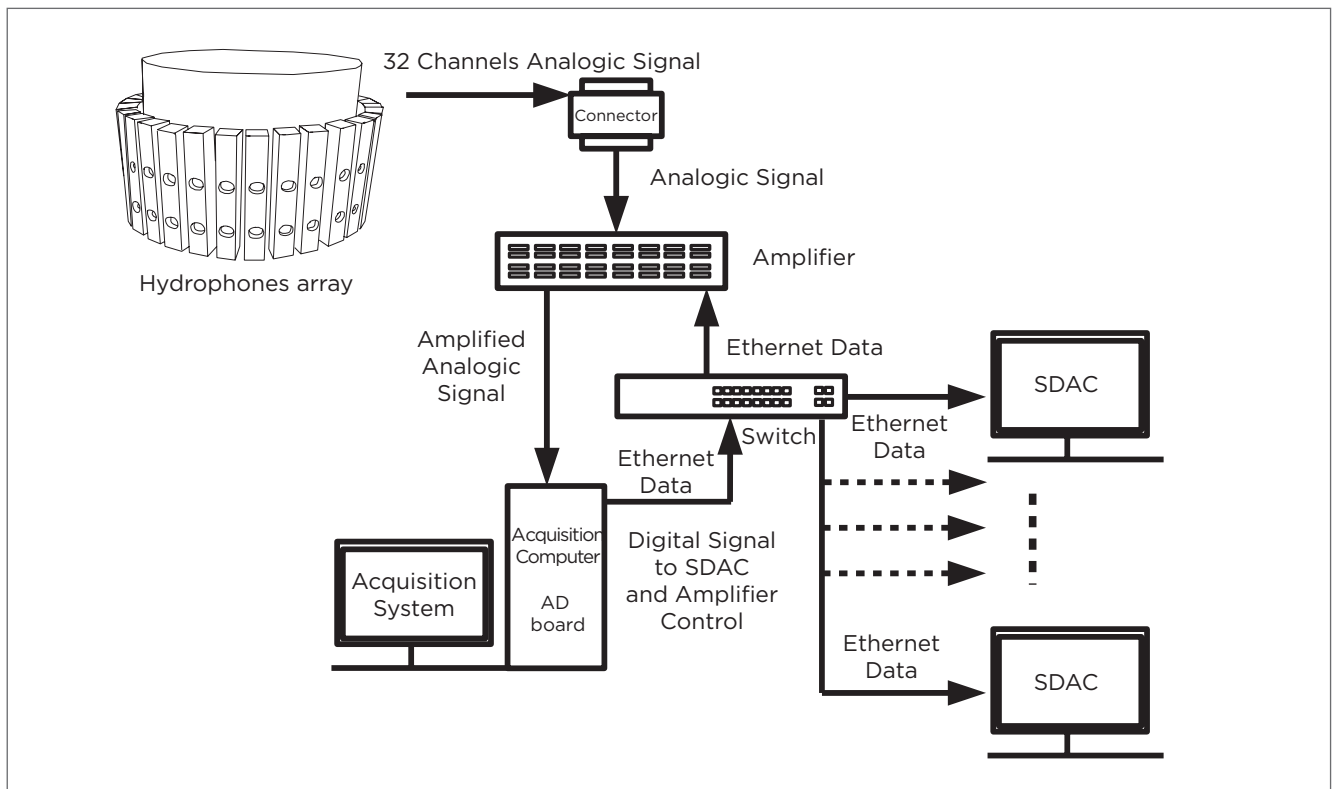


Figure 1. General diagram of the sonar system.

pre-processing of the acquired signals were conducted with a software developed in IPqM. Therefore, it was possible to have better control over the acquisition, guaranteeing the integrity of the data.

## 2.4. SIGNAL PROCESSING: BEAMFORMING

Among several array geometry configurations, the uniform linear array (ULA) is the one with more extensive bibliography among the existing configurations, being preferably adopted for the beginning of array studies. In the case of ULA, its model and analytical expressions for power and pattern are problems that have already been studied and analyzed (RODRIGUES, 2006). A diagram of the delay-and-sum beamforming for a uniform linear array is presented in Figure 3.

This array is composed of N elements, with a spacing, d, between them. If the signal  $s(z, p)$  incides over each sensor, where  $p$  refers to the position in space, and  $w$  is a weight vector, therefore, according to Van Trees (2004), (Equation 1):

$$D(\theta) = \frac{1 \sin \left( \frac{N\pi d}{\lambda} \cos(\theta) \right)}{N \sin \left( \frac{\pi d}{\lambda} \cos(\theta) \right)}, 0 \leq \theta \leq \pi \quad (1)$$

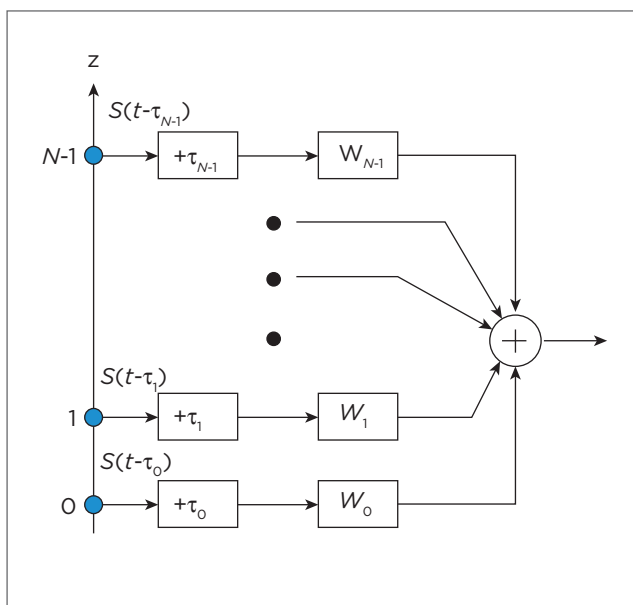


Figure 3. Delay-and-sum beamforming for a linear array.

where  $D(\theta)$  represents the beam pattern. The beam pattern of a sensor, or of an array, represents the frequency/number of wave response of the array *versus* direction. Its information represents the irradiation of the sensor/array for a specific direction, and this is what determines its performance.

The implementation of the delay-and-sum beamforming in the circular array was widely approached by (RODRIGUES, 2006; FELZKY, 2007; BOZZI, 2016) and is explained in detail in Figure 4, where the circular geometry of the array is presented, as well as a wave front coming from a specific direction. A sector of the array containing a specific number of elements to form the direction beam referring to the wave front, is used (in this case, elements 1 to 5 and 28 to 32 were used). After this section was chosen, delays are applied to the elements in order to compensate for the different wave front paths.

The delay procedure is a way to “synchronize” the signals, making the circular array to be considered as an unequally spaced linear array. This fact can also be interpreted as a projection of the signals in a chord of a circle. After applying the respective delays, the signals of this sector are added up, resulting in a beam referring to the direction called broadside, perpendicular to the array in an equivalent line.

Figure 4 shows the representation of the irradiation it can receive by using an individual signal of a sensor and the diagram of irradiation after the beamforming, where a directional gain is observed. This procedure is repeated with the use of adjacent elements. Therefore, there are N beams formed, in which N is the number of sensors (ATLAS ELEKTRONIK KRUPP, 1988).

The delay-and-sum outputs are the formed beams. However, it is common to calculate the energy of these beams to visualize the sound sources around the array. The result of this operation is usually presented in a graphic comparing energy x time x azimuth, known as the waterfall energy graphic. When there is a signal in one of the directions, it will have more intensity (energy), and that can be observed in the waterfall. The waterfall energy graphic is used to visualize the scenario, that is, to present the sound sources around the array throughout time. Therefore, it is possible to track this source. This type of graphic will be presented with the results of the experiments.

## 2.5. SIGNAL PROCESSING: ANALYSES

Based on the identification of contacts in the scenario, through the waterfall energy graphic, the directional beam of a contact is selected to conduct the LOFAR and DEMON analyses.

LOFAR is narrowband frequency analysis that allows visualizing the spectrum of the signal and its characteristic tones. This spectrum carries all information of the noise irradiated by the contact. If the contact is in another boat, it is possible to extract the characteristics of the machines and their propulsion.

DEMON is a narrowband analysis aiming at extracting information coming from the cavitation on a boat. This analysis shows the shaft rotation, the number of shafts and the number of blades. Studies, implementations and use of these analyses to classify submarine contacts were approached by Torres, Seixas and Soares Filho (2004) and Moura (2013).

## 2.6. SYSTEM OF DETECTION, TRACKING AND CLASSIFICATION OF CONTACTS

SDAC is a software – developed in IPqM, installed in the MB submarines – widely accepted for its graphic tools. It innovated the old sonar system installed in the submarines

(CSU-83 – Atlas). The technology demonstrator aims at integrating this system to the part of acquisition and beamforming developed.

The SDAC installed in the submarines receives the signals after beamforming, digitally. It was necessary to adapt SDAC to receive the network data for this new array configuration. Besides this change, the SDAC installed in the submarines receives signals from 96 staves, whereas the array built has 32 staves. Therefore, the interpolation of 32 channels to 96 channels is conducted by using the concepts by Diniz, da Silva and Netto (2014) and Mitra (2011).

## 3. RESULTS AND DISCUSSION

Two commissions were organized for the technology demonstrator of the passive sonar. These commissions aimed at collecting data, monitoring the sea environment and assessing the system.

### 3.1. FIRST COMMISSION

The first commission was carried out in the Fuel Storage of the Navy, in Rio de Janeiro (DepComb), between May 5

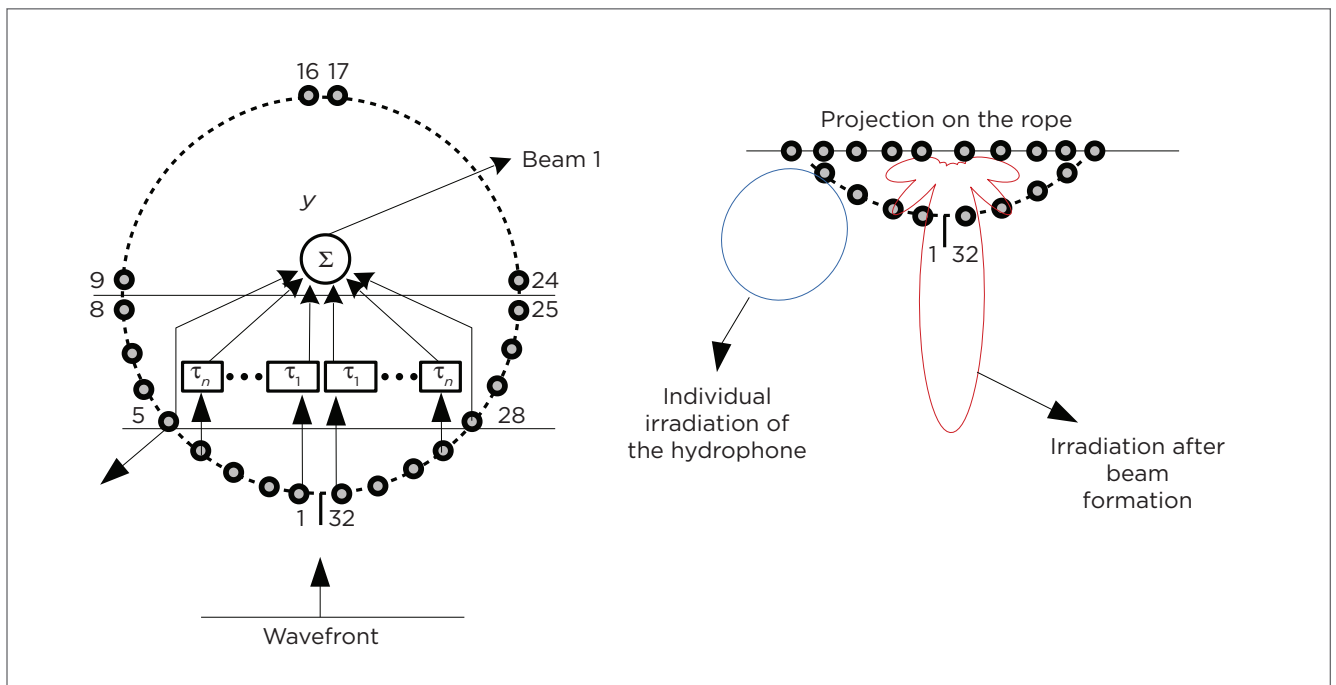


Figure 4. Beamforming.

and 29, 2015. This commission especially aimed at collecting data for an off-line processing and at evaluating the acquisition system.

Boats from the DepComb were used to make rounds around specific areas around the array, in a controlled way. In these runs, the position of the boat was monitored by a GPS. Eighteen runs were made to monitor the position. Some will be reported next.

- Run 1 – A boat was used so that, from a point away from the pier, it would be possible to get close in a straight line. The speed was kept constant and high. The duration of the round was of about 2.5 minutes. Figure 5 shows the route taken by the boat (obtained via GPS) and its representation in the waterfall energy graphic. It is important to observe that there are reflections on the lateral walls of the pier where the array was placed, and that is demonstrated in the energy graphic. The strongest energy intensity is represented by red, and the weakest energy, by blue.
- Run 2 – A fishing boat was seen in the surroundings of the array, and the boat, which was placed away from the array, was triggered to reach it. Figure 6 shows the recording was initiated when only the fishing boat was around, and about 100 seconds later, the boat was activated (when the azimuth was  $-50^\circ$ ).
- Run 3 – The boat was used so that, from a point away from the pier, it would get closer in a zig-zag path. The

duration of the round was of seven minutes approximately. Figure 7 shows the boat path leaving from the “a” position, moving through “b”, “c”, until it reaches “d”. There was a short break between “b” and “c”, when the recording was interrupted. The energy graphic shows the path of the boat.

- Run 4 – The boat and the motorboat were used for simultaneous run, in a path circular to the array, but in different directions. Since the circumference of the boat run was smaller, it took two laps whereas the motorboat only took one. There was no speed control. The duration of the round was of about three minutes. Figure 8 presents round 4. The energy graphic shows that the boat energy is more intense, because it was closer to the array.

### 3.2. SECOND COMMISSION

The second commission was conducted in the Research Ship “Aspirante Moura” (“AspMoura”), between August 12 and 21, 2015. This commission aimed at demonstrating the technology of a passive sonar to some sectors of MB. The ship was based close to the Navy Academy, where marine traffic was monitored in the region, being that a path for ships and boats sailing between Rio, Niterói and other regions nearby. Figure 9 shows the placement of the array on board, its placement in the anchorage point and the place where SDAC was exposed.

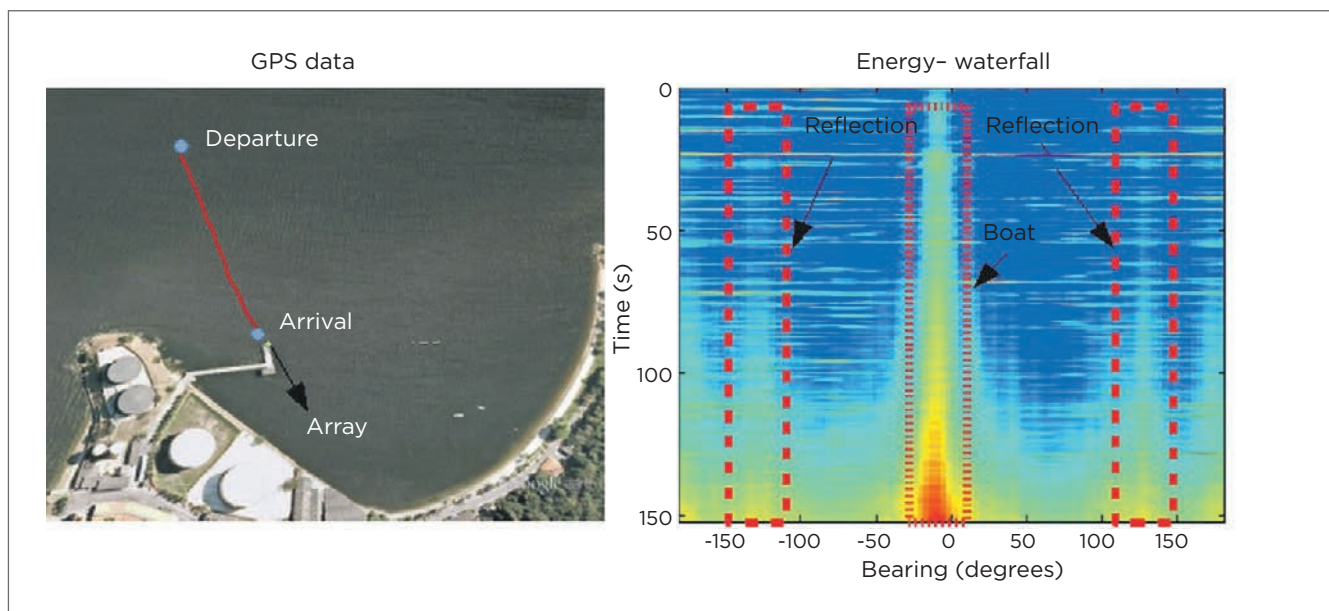


Figure 5. Run 1.

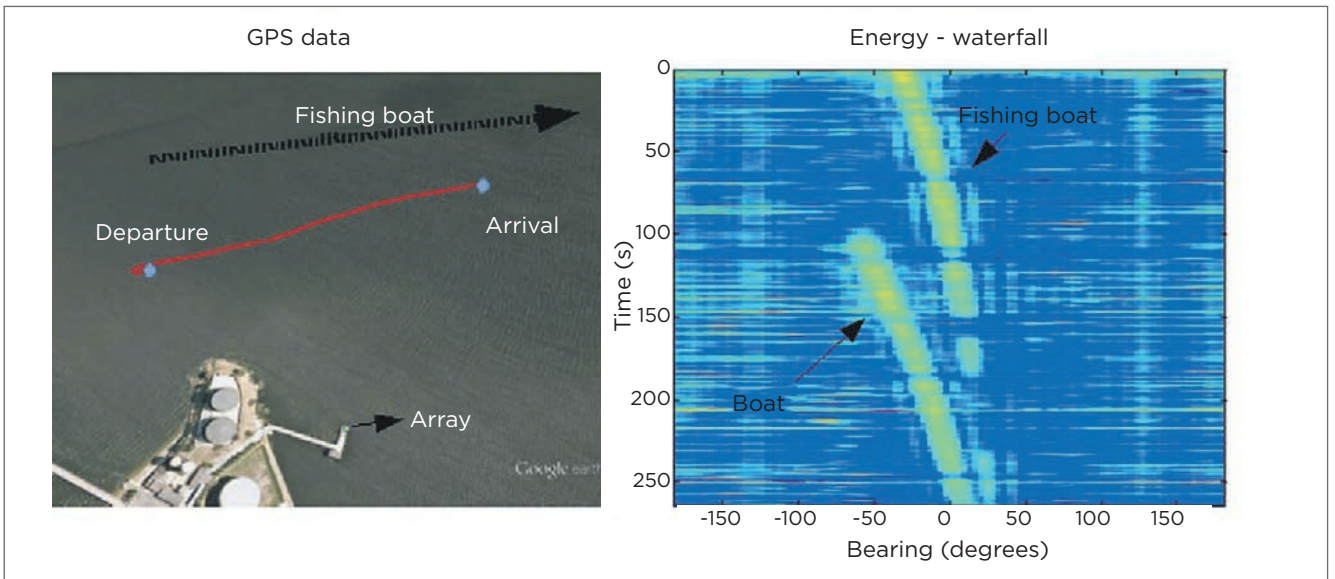


Figure 6. Run 2.

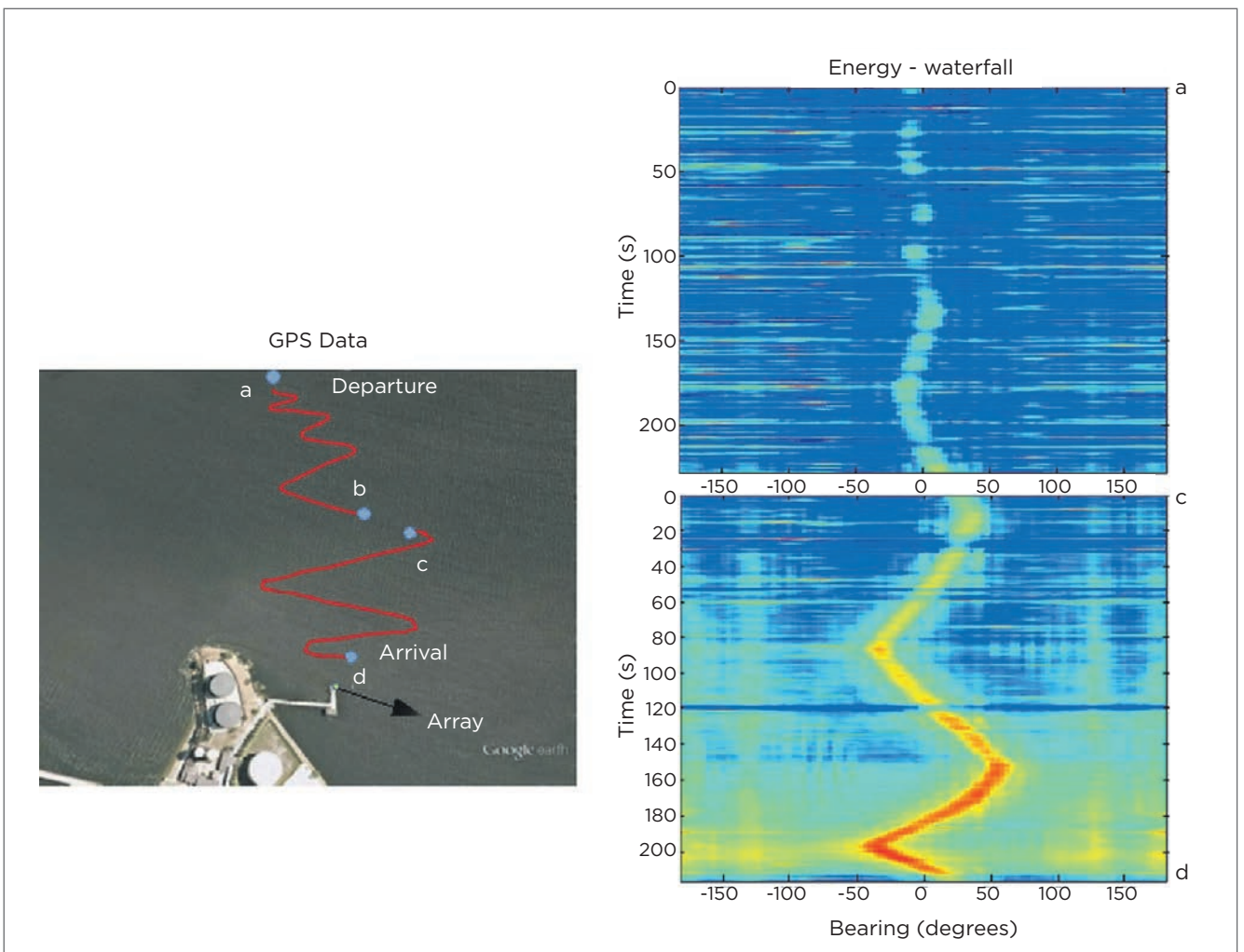


Figure 7. Run 3.

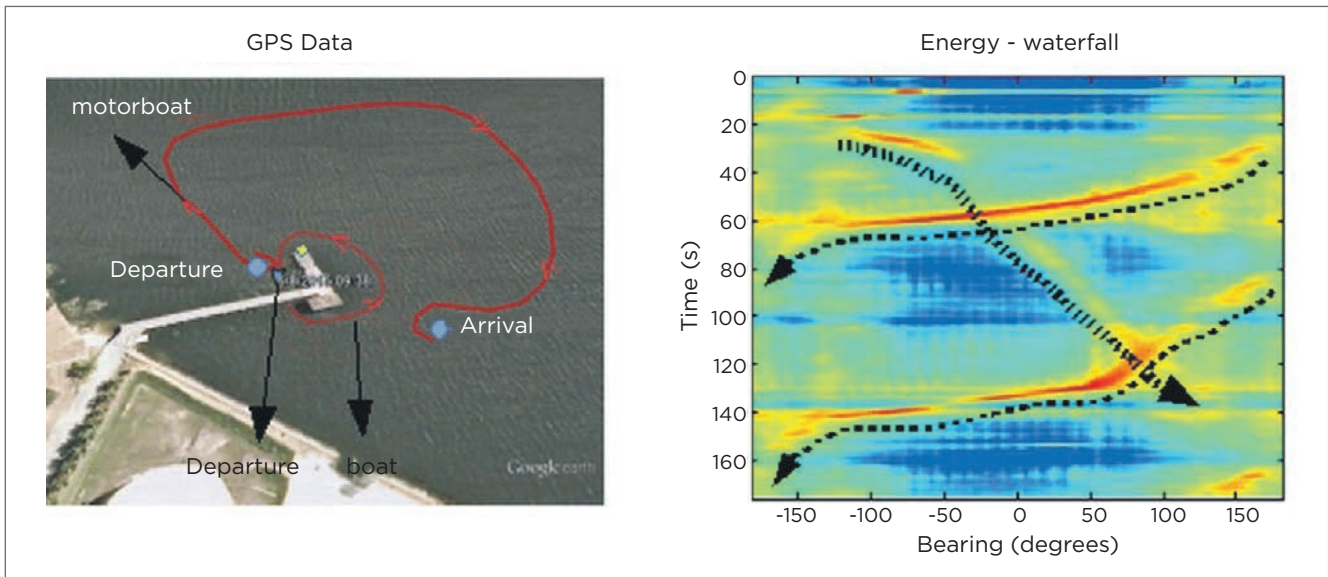


Figure 8. Run 4.

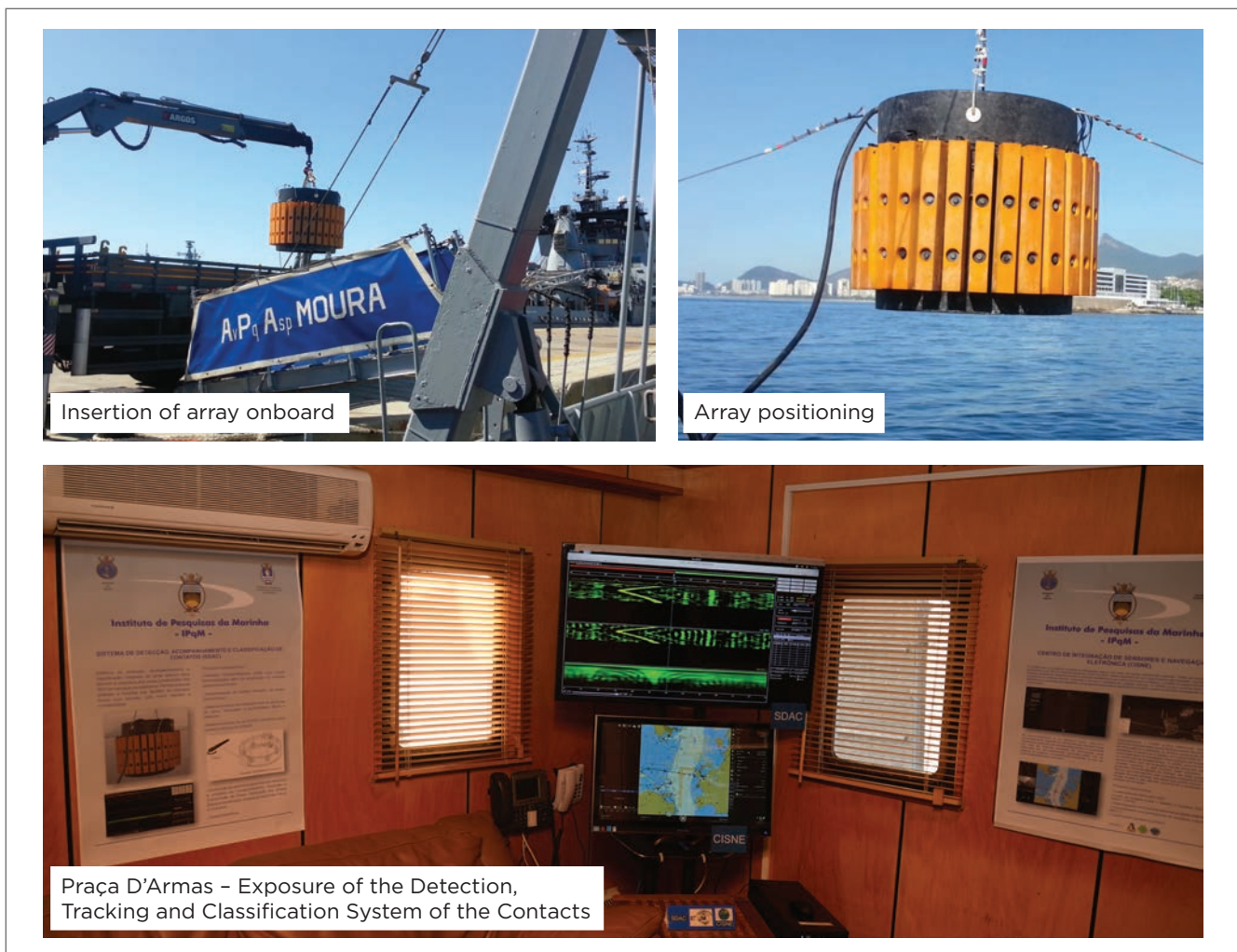


Figure 9. "Aspirante Moura" commission.

During the commission, marine traffic in the region was monitored with photos and notes, and the data acquired about the array were recorded for further



**Figure 10.** Merchant ship leaving Baía de Guanabara.

research. Figure 10 presents a Merchant ship leaving from Baía de Guanabara.

The detection and the analyses of this ship are presented in Figure 11. This figure has the waterfall energy graphic (A), which detected the contact in the azimuth of 90°, moving to 120°. LOFAR (B), indicates a characteristic tone of the singing propeller in 1,238 Hz. DEMON (C) clearly shows 4 simple consecutive harmonics, indicating 1 shaft and 4 blades shaft, at 95 rpm. This characterization could not be confirmed for the referred ship; however, based on experts' experience, it is known that ships of this size generate results similar to the ones we presented here.

Due to the large flow of boats navigating in Baía de Guanabara, another frequent scenario was the passing of several boats simultaneously. This fact is shown in Figure 12.

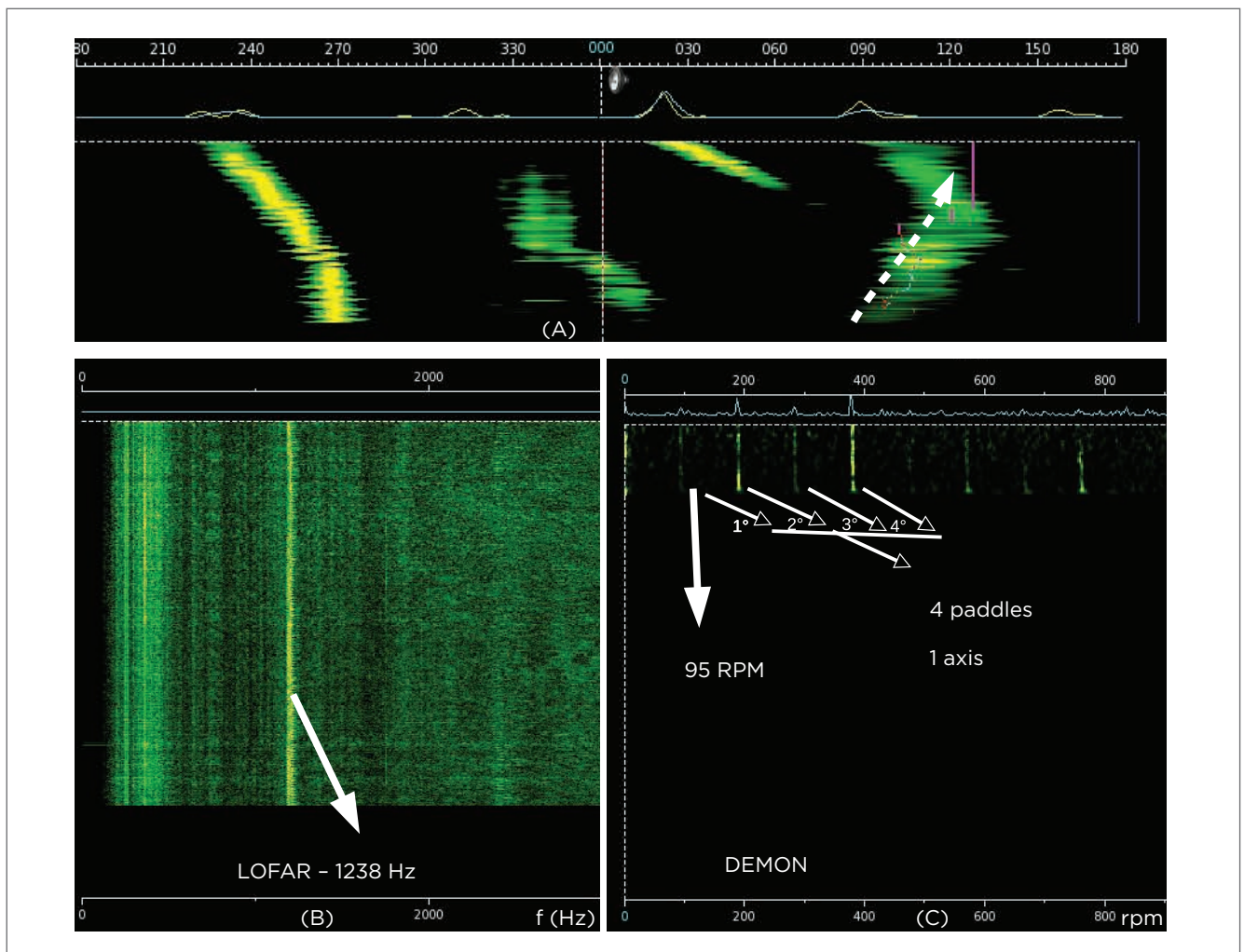


**Figure 11.** Merchant ship analyses - screen of the Detection, Tracking and Classification System (SDAC).

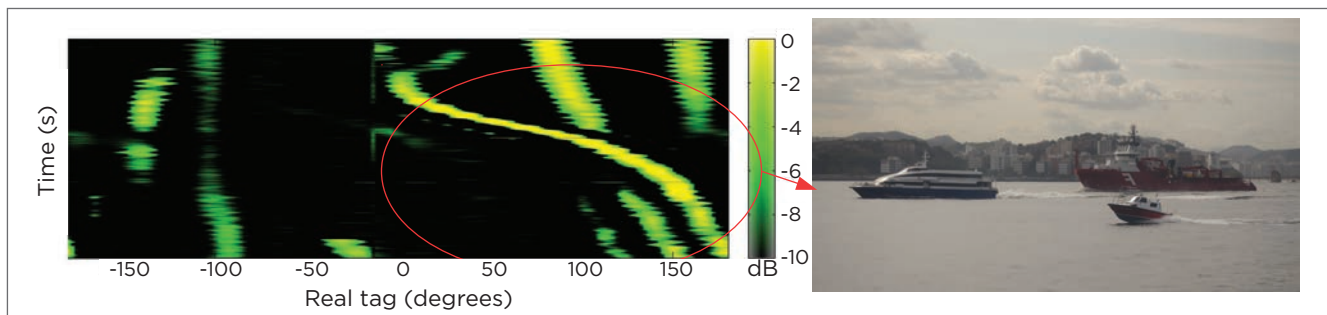


Figure 12. Crossing of vessels.

## 4. CONCLUSIONS

The technology demonstrator of a passive sonar aimed at dominating all stages of development present in a sonar. The results presented here indicate that, currently, the GSAS, from IPqM, is able to reproduce, within a research point of view, all processes of a sonar system.

It is possible to consider great advances in the fields of signal acquisition and processing. Commercial hardware was used, and it was controlled by IPqM.

Therefore, the acquisition system, which is the link between the sensors and SDAC, was widely explored in this study. So, with the commissions conducted, data were recorded directly from the sensors, which allow many areas of research to be developed. SDAC, which is present in MB submarines, was updated and integrated with this configuration of sensors.

It is believed that the new challenges will have a specialist character, that is, to improve what has been done so far. This will happen by replacing industrial hardware with national ones, also developed in IPqM. Besides, improvements in the types of signal processing, in the fields of beamforming and detection, can also lead to benefits for the next chain of analyses.

The advantage of the domain of the stages of acquisition and processing is the access to all parameters and variables, for instance, filtering.

Generally, the results of the commissions show that it was possible to detect, track, and conduct analyses, which are the necessary functions for a sonar.

## 5. ACKNOWLEDGMENTS

The GSAS team appreciates the collaboration, the commitment, and the enthusiasm of the public employee Márcio Pereira Baptista, who was present in all stages of this project and played an essential role in its development. Also, the public employee Jacqueline Chiara Moura Karraz and everyone who collaborated for the success of this project.

To the Fuel Storage from Rio de Janeiro's Navy, for granting the location, support and the boats for the experiment.

To the Research Ship "Aspirante Moura", which worked hard for the commission to take place in a planned and organized way, providing a peaceful environment for the research.

To the Group of Digital Systems of IPqM, who provided material and personnel resources to fulfill all of the stages in the project. This group also installed CISNE on board, in order to help sonar presentation.

## REFERENCES

ATLAS ELEKTRONIK KRUPP - TED WESTERN GERMANY PRESS. Atlas Sonar Equipment CSU 83-1/014 - Operating and Repair Instructions, Março 1988.

BOZZI, A.F. Conformação de Feixe em Sonar Passivo para um Arranjo Cilíndrico de Hidrofonos", Dissertação de Mestrado. COPPE, Universidade Federal do Rio de Janeiro, Rio de Janeiro, RJ, 2016.

DINIZ, P.; DA SILVA, E.; NETTO, S. Processamento Digital de Sinais - 2.ed.: Projeto e Análise de Sistemas. Bookman Editora, 2014.

FELZKY, A.M. Uma contribuição às técnicas de localização de fontes sonoras através de um sistema sonar passivo utilizando filtros fracionários. Dissertação de Mestrado. COPPE, Universidade Federal do Rio de Janeiro, Rio de Janeiro, RJ, 2007.

LI, Q. *Digital Sonar Design in underwater acoustics: principles and applications*. Springer Science & Business Media, 2012.

MITRA, S. *Digital Signal Processing: a Computer-based Approach*. McGraw-Hill series in electrical and computer engineering. McGraw-Hill, 2011.

MOURA, N.N. *Detecção e Classificação de Sinais de Sonar Passivo Usando Métodos de Separação Cega de Fontes*. Tese de Doutorado. PEE/COPPE, Universidade Federal do Rio de Janeiro, Rio de Janeiro, RJ, 2013.

RODRIGUES, P.S.M. *Estudo e análise de métodos empregados em array cilíndrico passivo para determinação da direção de fontes sonoras*. Dissertação de Mestrado. COPPE, Universidade Federal do Rio de Janeiro, Rio de Janeiro, RJ, 2006.

SHERMAN, C.; BUTLER, J. *Transducers and arrays for underwater sound*. The Underwater Acoustics Series. Springer New York, 2007.

SOARES FILHO, W. *Classificação do Ruído Irrradiado por Navios usando Redes Neurais*. Tese de Doutorado. Ph.D. Thesis, PEE/COPPE, Universidade Federal do Rio de Janeiro, Rio de Janeiro, RJ, 2001.

TORRES, R.C.; SEIXAS, J.M.; SOARES FILHO, W.S. *Classificação de sinais de sonar passivo com base em componentes principais não-lineares*. *Learning and Nonlinear Models - Revista da Sociedade Brasileira de Redes Neurais*, v. 2, n. 2, p. 60-72, 2004.

VAN TREES, H.L. *Detection, estimation, and modulation theory, optimum array processing*. John Wiley & Sons, 2004.

WAITE, A.D. *Sonar for practising engineers*. John Wiley & Sons Incorporated, 2002.

# AN ARCHITECTURE TO MANAGE SOFTWARE ENGINEERING PROJECTS AIMED AT INTEGRATION WITHIN THE BRAZILIAN ARMED FORCES

Uma arquitetura para a gestão dos projetos de engenharia de *software* visando à integração nas Forças Armadas

Geraldo da Silva Souza<sup>1</sup>, Rodrigo Abrunhosa Collazo<sup>2</sup>,  
Jones de Oliveira Avelino<sup>3</sup>, Carlos Eduardo Barbosa<sup>4</sup>

**Abstract:** Despite some federal government initiatives aimed at implementing best practices in project management, it is still not possible to detect the employment of standardized tools or techniques in the Ministry of Defense for guiding, monitoring, and controlling project development. The aim of this study was to propose a systemic approach for the performance evaluation of software engineering projects under two aspects: project management and information architecture. The methodology employed produces a model using elements of the United States Department of Defense Architecture Framework (DoDAF), coupled to the concepts of Capabilities Based Planning (CBP) and Portfolio Management (PfM). The suggested model was validated through data queries for Earned Value Management (EVM) and evaluated in a real case, in the performance analysis of a real project. The proposed approach can be applied to any project, allowing its continuous diagnosis.

**Keywords:** Project management. Software engineering. Department of Defense Architecture Framework. Earned Value Management.

**Resumo:** Apesar de algumas iniciativas do governo federal no uso de boas práticas em gestão de projetos, ainda não é possível identificar o emprego de ferramentas nem de técnicas padronizadas no Ministério da Defesa para orientar, monitorar e controlar a condução de projetos. Este estudo teve por objetivo propor uma abordagem sistêmica para a avaliação de desempenho de projetos de engenharia de *software* de interesse da Defesa sob dois aspectos: gestão de projetos e arquitetura da informação. A metodologia utilizada produz um modelo com elementos do Department of Defense Architecture Framework (DoDAF), associado aos conceitos de *Capabilities Based Planning* (CBP) e de *Portfolio Management* (PfM). O modelo sugerido foi validado por meio de consultas de dados provenientes da técnica *Earned Value Management* (EVM) e avaliado em um caso real, na análise do desempenho de um projeto real. A abordagem proposta pode ser aplicada a qualquer projeto, permitindo o seu diagnóstico contínuo.

**Palavras-chave:** Gestão de projetos. Engenharia de *software*. Department of Defense Architecture Framework. Earned Value Management.

1. Technologist, Master in Applied Computing. Center for Naval Systems Analysis, Project Planning and Control Division – Rio de Janeiro, RJ – Brazil. E-mail: geraldo@casnav.mar.mil.br

2. Commander, PhD in Statistics, Center for Naval Systems Analysis, Department of Systems Engineering – Rio de Janeiro, RJ – Brazil. Email: rodrigocollazo@uol.com.br

3. Technologist, Systems Analysis, Management and Design expert. Center for Naval Systems Analysis, Administrative Systems Division – Rio de Janeiro, RJ – Brazil. E-mail: jones@casnav.mar.mil.br

4. Technologist, Master in Systems Engineering and Computing. Center for Naval Systems Analysis, Administrative Systems Division – Rio de Janeiro, RJ – Brazil. E-mail: eduardo@casnav.mar.mil.br

## 1. INTRODUCTION

Among the goals defined by the Ministry of Defense (MD) strategic planning are the modernization of the Armed Forces (AF), the development of joint-operation capabilities, and the promotion of integrated logistics (BRASIL, 2010a; 2011a). To achieve these goals, it is necessary to improve the operational capabilities of all three AF by increasing the coordination of human elements – doctrines, operational procedures, and interpersonal relationships – and by decreasing the distance between the technological and operational aspects.

In line with the National Defense Strategy (BRASIL, 2010a), the MD and the AF have attempted to substantiate this greater systemic integration through investment in projects related to software engineering. Some of these projects also require cooperative and integrated management, as there are several military organizations (MO) with software requirements in common. Therefore, the MD should create programs under its supervision to gather similar projects in order to obtain synergistic benefits among the gathered projects that would not be feasible if these projects were to be managed separately.

This scenario requires the use of best practices in information technology (IT) project management (BRASIL, 2011b), such as the ISO/IEC/IEEE 42010:2011 standards and the Reference Model for Open Distributed Processing (RM-ODP). However, despite some initiatives on the part of the federal government, the institutional employment of instruments based on a holistic vision is not yet adopted. In other words, it is not yet possible to observe the use of tools that allow for effective integrated control of deadline, cost, and scope within the MD.

The last survey of IT governance applied in the Federal Public Administration level, carried out by the Federal Court of Auditors (“Tribunal de Contas da União” - TCU), confirms the situation described above: over half of the organizations has not yet adopted a project management process based on internal or market standards. When looking at the survey’s results, one point draws attention: 17% of organizations do not make use of any project management process, even in the face of the complexity inherent in developing IT services and products (BRASIL, 2010b).

The search for instruments that allow for the coordination of political and military interests and for integrated control

and monitoring is justified by the high rates of failure still associated with IT projects (STANDISH GROUP, 2012), as well as by a concern in ensuring a proper use of the governmental financial.

IT projects involve risks so well known that in many cases they come to be expected, such as the increase of costs beyond what was initially forecast and the delay of key milestones (BRASIL, 2010b). Research shows that in 2009, 44% of projects achieved partial success – that is, they do not fully respect their estimated cost, time, or scope– and 24% failed – that is, they were canceled or were not used–, compromising organizational actions (STANDISH GROUP, 2012). It then becomes increasingly important to implement information systems capable of supporting project management, addressing the complexity and risks involved, and allowing for the coordination of the political and military interests at stake.

In this paper our objective is to propose an approach for systemic management of the MD software engineering projects that allows for continuous evaluation of project performance, matches the initiatives adopted by the Federal Government and respects the goals of the General Strategy for Information Technology (*“Estratégia Geral de Tecnologia da Informação”* – EGTI 2013-2015), as recommended by its prospect no. 4 – “To achieve effectiveness in IT management.”

## 2. MINISTRY OF DEFENSE PROJECT MANAGEMENT

As a discipline, project management arose from different fields. Many of the numerous tools and techniques currently considered as best practices by the industry have appeared in the military environment. As examples, we may cite the Work Breakdown Structure (WBS) and the Gantt chart. These tools were both created to meet the demands for vessel construction at the US Navy. Analyzing the current reality in the Brazilian Ministry of Defense and the progress seen in the field of software management, it is necessary to adopt the opposite direction of this past history; i.e. thus bringing knowledge widely circulated in the market to the MD.

In this sense, if the MD aims to continue showing advances in project management, it is crucial that it makes

investments for creating a Project Management Office (PMO) (COTIN-MD, 2012) The PMO should focus on planning, prioritizing, and coordinating programs and projects linked to the general objectives of MD. For these purposes, the PMO needs to find instruments to support its tasks and to ensure a standardized management among different military organizations (KERZNER, 2006).

The importance of these instruments is confirmed by Kerzner (2006), who defines four information systems within the PMO: aggregate value system, risk management system, performance failure system, and the learned lesson system. An adaptation of this model for the MD context is shown in Figure 1.

In order for the Ministry to achieve maturity and excellence in project management (KERZNER, 2006, SUN, 2013), we opted for the aggregate value system, aimed at the evaluation of project performance using the Earned Value Management (EVM) technique. It should be indicated that the aggregate value system is the only system able to simultaneously deal with the three essential variables for controlling a project: time, cost, and scope (KERZNER, 2006), all of which are crucial in developing quality and high-level management for projects and programs. Driven by a more pragmatic and well-defined goal, the solution proposed will prioritize two aspects: project management and information architecture.

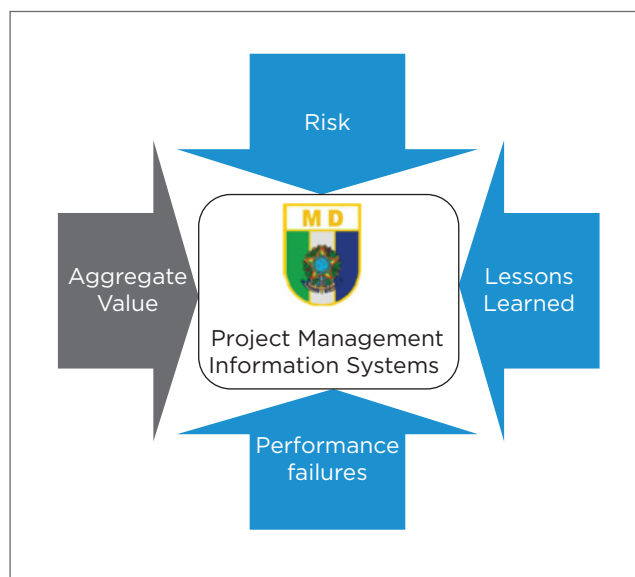


**Figure 1.** Project management information systems in the Ministry of Defense.

Regarding project management, the MD does not have, as of yet, any normative criterion to control or monitor the performance of software projects, although there exist principles and procedures applicable to IT projects (BRASIL, 2003). Tools and techniques relating to best practices in project management such as the EVM are a viable solution already in use in other organizations, notably at the US Department of Defense (DoD) (USA-DOD, 2006).

With respect to information architecture, the MD does not have a strategy for developing its information architecture that establishes policies, guidelines, and technical specifications (BRASIL 2003). In this case, a reference architecture would contribute to the construction and strengthening of systemic interoperability, as well as to promote financial resources savings in the medium and long terms (THE OPEN GROUP, 2011).

### 3. EARNED VALUE MANAGEMENT AND SOFTWARE ENGINEERING

The EVM is a technique that combines deadline, cost, and scope control in a single integrated system (SUN, 2013). In doing this it significantly contributes to monitoring project evolution clearly and objectively. Another important feature is the possibility of following performance trends by means of a graphical representation called the *S Curve*, which enable managers to compare planned, accomplished, and aggregated values over time.

EVM has become the norm for the DoD's largest purchases and has turned into an effective instrument for understanding performance, because it quickly and efficiently detects deviations, minimizes systemic losses, and maximizes return on invested resources.

Although traditionally used in civil engineering, adapting EVM for software engineering is not simple because of the intangible nature of software (SOUZA, 2013). It then requires a technique that makes such product tangible so it can be properly valued.

This difficulty had already been detected by Court of Auditors and was the focus of their Normative Instruction no. 4, dated November 12, 2010 (IN SLTI 04/2010). To minimize this drawback it was established that Function Point

Analysis (FPA) was adopted as the standard technique for assessing the value of software components that the federal government buys (BRASIL, 2012).

## 4. ENTERPRISE ARCHITECTURE

IT usually focuses on solving specific short-term problems, resulting in higher costs in the medium and long terms. For instance, a poorly planned information system may be too rigid and inflexible to withstand rapid changes in business, demanding constant maintenance or even the replacement of the system in the medium term. To minimize this problem, it is recommended to define an enterprise architecture (EA) that serves as a reference for systems development within the organization.

According to the Open Group, an AE is defined as a set of principles, methods, and models used to describe the organization's IT and business processes, supporting the decision of what should be created, restructured, discontinued, integrated, or standardized upon implementing its strategy.

For the MD, defining an AE would help guide IT investments. In practice, implementing these activities involves the use of a conceptual framework for creating a *roadmap* (THE OPEN GROUP, 2011) that orients changes needed for moving from a current state (*As is*) of IT resources (the organization's IT assets) to a future, desired state (*To be*), as shown in Figure 2, as to obtain a set of previously identified operational capabilities.

Currently, though Zachman, Gartner and the Open Group Architecture Framework (TOGAF) are examples of frameworks used in corporate IT environments. Note that many of their practices derive from frameworks applied in the military environment. The DoDAF (Department of Defense Architecture Framework) is an example of the TOGAF, being the norm in US Defense agencies.

## 5. THE DODAF FRAMEWORK

The DoDAF is a framework designed to guide the development of the DoD information architecture through a conceptual model. It focuses on the architecture of the data

required by decision makers (*Data-centric*), instead of isolated information systems (*Product-centric*), an approach that allows such data to be adequate for management purposes (*Fit-for-purpose*) (USA-DOD, 2015). Its use results in an architecture designed to facilitate data reuse and sharing through services (*Net-centric*), and presents two potential benefits: avoiding data copying in multiple systems without prescribing software products' final compositions; and allowing each AF to seek individualized solutions according to their operational specificities (SOUZA, 2013).

The DoDAF *Meta Model* (DM2) is a key component of this framework, as it defines elements of integration by establishing a semantic base and ensuring data consistency. DM2 describes a roadmap for the reuse of data in an environment with geographically distributed databases, aiding the architecture's management and orderly progression, and providing specific levels of abstraction for understanding its elements, allowing for the understanding of what has been done by other managers, optimizing software development efforts. The DM2 also prescribes that modeling should be performed at three levels: conceptual (CDL - *Conceptual Data Model*), logical (LDM - *Logical Data Model*), and physical (PES - *Physical Exchange Specification*). Another important concept in the framework is called "viewpoint." It is defined as a set of templates organized to facilitate the visualization of information that must appear in individual "views" (or "information systems"). These views can be used to express and analyze information, assisting decision-making under a particular aspect.

For this work, we focused on the Viewpoint related to project management, or *Project Viewpoint*.

## 6. PROJECT VIEWPOINT

Early DoDAF versions were based on traditional architecture models, in which describing programs and projects was considered out of scope (USA-DOD, 2015). As to take such concepts into account, the DoDAF version 2.0 created the *Project Viewpoint*, comprised three models: PV-1, which describes the interdependence of programs and projects; PV-2, which defines time frames; and PV-3, which assists in mapping operational capabilities.

The use of these models expands the usability of the architecture framework in processes related to Portfolio Management (PfM) and Capabilities Based Planning (CBP), which allows to capture different levels of cost data (USA-DOD, 2015).

## 7. PROPOSED APPROACH

The proposed approach consists in the definition of a data model that can be shared by the AF. This data model enables the control and monitoring of projects through a reference architecture to support the MD's PMO's attributions.

Regarding information architecture, the DoDAF leverage the creation of a reference architecture for the MD that is able to promote interoperability, guiding the adoption of IT standards through a common data model and a service-oriented architecture (SOA) approach – a service bus, as shown in Figure 3.

On the other hand, implementing EVM would significantly contribute to best practices in project monitoring, standardizing project managing procedures in the Defense sphere.

The implementation of this approach falls under one of the four information systems described by the literature as a PMO tool: the aggregate value system (KERZNER, 2006). Such an approach also allows for the measurement

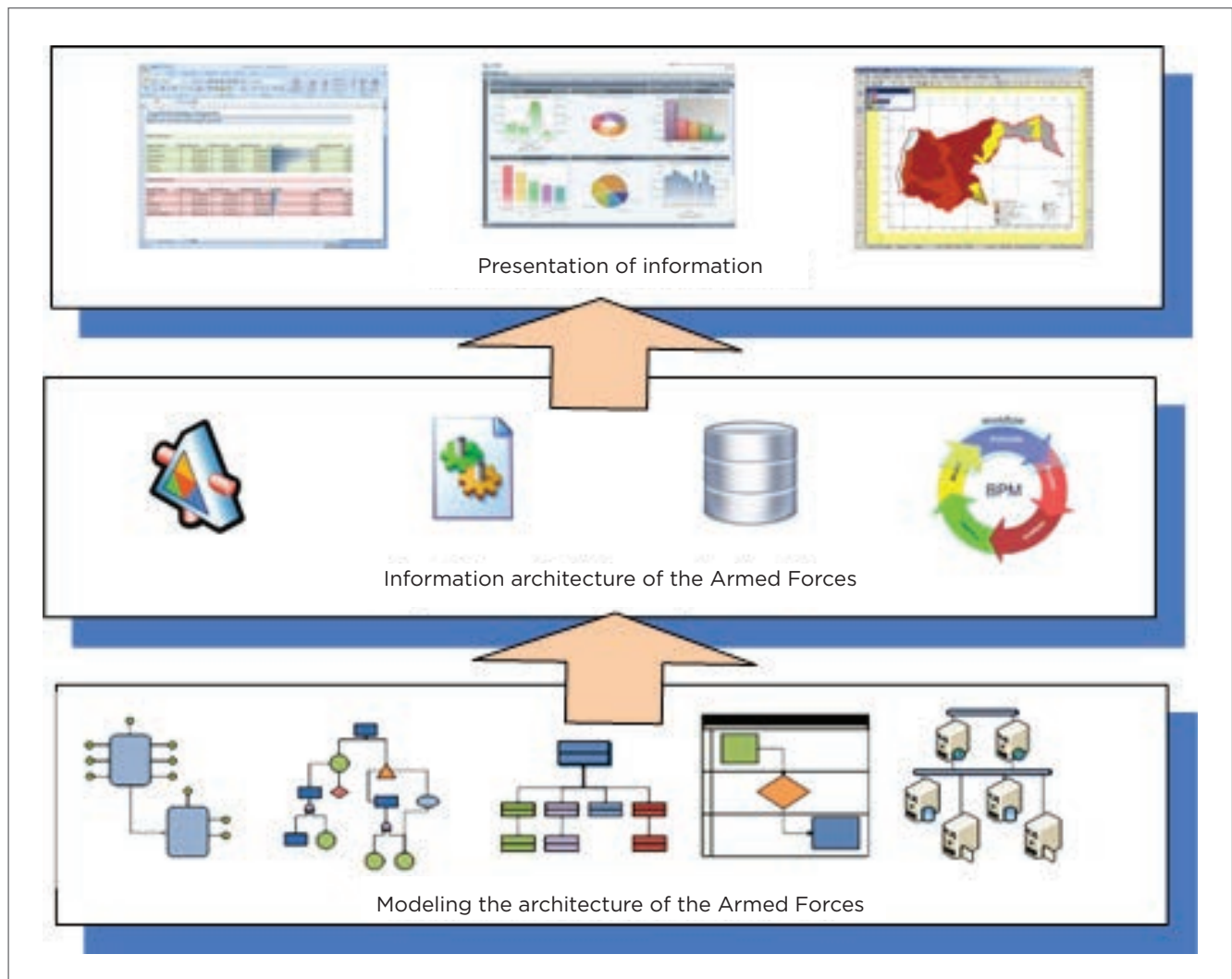


Figure 2. Modeling example of the current status of IT resources.

and analysis of project implementation, a key aspect of the decision-making process at the strategic, tactical, and operational levels of the command chain.

Furthermore, it would meet the demand for standardization of performance analysis at the Science, Technology and Innovation System of Interest to National Defense (*“Sistema de Ciência, Tecnologia e Inovação da Defesa Nacional”* – SisCTID), for instance within the system that defines the preparation and follow-up of research and development (R&D) projects at the MD (COTIN-MD, 2012).

To this end, the model implementation should be performed in three stages: identification and selection of elements of interest for the DoDAF; creation of models at the conceptual, logical, and physical levels for each element; and the assembly of queries that show the necessary values for the use of EVM.

In fact, the first step consists of the selection of models and elements that are relevant to the MD needs and linked to the focus of the work, in accordance the Project Viewpoint. In this phase, the main source of data for analysis is the Data Dictionary and Mapping, and the product generated consists in a matrix relating models and elements provided by the DoDAF, as can be partially seen in Figure 4.

The matrix shown in Figure 4 labels each of the element-model pairs as necessary (n) or optional (o) in an implementation. Thus, it also serves as an instrument for identifying selected elements in order to solving the problem of project performance analysis, as highlighted in the same figure, adapted to the MD management needs.

The first of the models listed as required is related to project management: the PV-1 (Project Portfolio Theory). Hierarchically, its elements describe the possible relations between projects, their interdependencies, and how they influence the delivery of a capability that contributes to a planned state.

Thus, to the extent that new capabilities are introduced in the portfolio, stages between the current state and the desired state need to be controlled. This management configuration is possible by implementing CV-3 (Capability Phasing), a model that is not addressed in this work.

The PV-2 (Project Timelines) provides a time-based vision, allowing for greater detail of lower levels of workflows and their dependencies. The information provided by this model can be used to determine impacts, planning changes, and identifying opportunities based on an integrated vision between projects. The suggested format for presenting the PV-2 is a Gantt chart, showing milestones, time relationships,

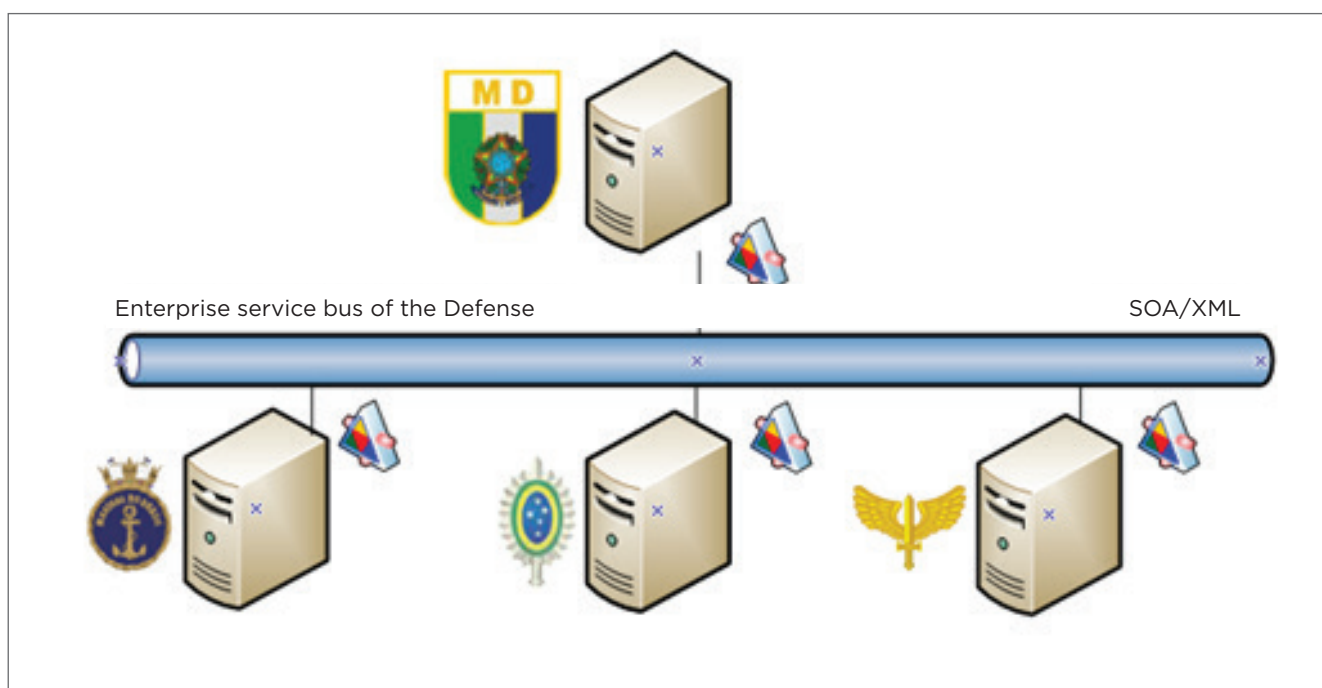


**Figure 3.** Ministry of Defense Service-Oriented Architecture (SOA)

interdependencies, and life cycles of each project. This model supports integrated management practices and the incremental capabilities acquisition strategy to achieve future states.

The PV-3 (*Project to Capability Mapping*) model describes, at a high level, the mapping between capabilities,

programs, projects, and portfolios and the requirements of a desired capability stage. The suggested visualization for this model's data is a traceability matrix, which may additionally include dates and phases pertaining to its elements.

Technical Term	Composite Definition	AV-1	AV-2	OV-1	OV-2	OV-3	OV-4	OV-5a	OV-5b	OV-6a	OV-6b	OV-6c	SV-1	SV-2	SV-3	SV-4	SV-5a	SV-5b	SV-6	SV-7	SV-8	SV-9	SV-10a	SV-10b	SV-10c	StdV-2	PV-1	PV-2	PV-3	CV-1	CV-2	CV-3
activityChangesResourceTypeInstanceOfMeasure	activityChangesResource is a member of Measure	0								0	0	0											0	0	0				n	n	n	n
activityPartOfCapability	A disposition to manifest an Activity. An Activity to be performed to achieve a desired effect under specified [performance] standards and conditions through combinations of ways and means																0												n	n	n	n
activityPartOfCapabilityTypeInstanceOfMeasure	activityPartofCapability is a member of Measure																0												n	n	n	n
activityPartOfProjectType	A wholePart relationship between a Project and an Activity (Task) that is part of the Project																									0	0				n	
activityPerformableUnderCondition	Represents that an activity was/is/can be/ must be conducted under certain conditions with a spatiotemporal overlap of the activity with the condition	0		0	0			0	0	0	0					0	0	0	0	0	0	0	0	0	0	0	n	n	n	n	n	n
activityPerformableUnderConditionTypeInstanceOfMeasure	activityPerformableUnderCondition is a member of Measure							0	0	0	0				0	0						0	0	0				n	n	n	n	n
activityPerformedByPerformer	An overlap between a performer and an Activity that is non-specific as to whether: 1. the Activity is solely performed by the Performer 2. the Activity is performed by several Performers 3. the Performer performs only this Activity 4. the Performer performs other Activities	0		0	0			0	0	0	0					0	0	0	0	0	0	0	0	0	0	n	n	0	0		0	
activityPerformedByPerformerTypeInstanceOfMeasure	activityPerformerOverlap is a member of Measure	0		0				0	0	0	0				0	0			0	0	0	0	0	0	0		0	0	0		0	
activityPerformedByPerformerTypeInstanceOfRule	activityPerformerOverlap is a member of Rule							0	0	0	0			0		0						0	0	0	n							

**Figure 4.** Matrix of elements and templates from the Data Dictionary and Mapping of the Department of Defense Architecture Framework.

The second step comprises modeling the selected elements of each model in a single conceptual model (CDM), describing the relationships between such elements in an abstract manner. The CDM combined with technical persistence details leads to the logical model (LDM). For these two levels, the modeling language used was the Unified Modeling Language (UML), as it is widely used in software design and throughout the DoDAF documentation. The result is the model partially illustrated in Figure 5.

The third step is the implementation of a set of queries that groups data, providing the necessary parameters for applying EVM in real projects. For querying these data, it is recommended to use the Structured Query Language (SQL). The final result of the logic modeling is represented in Figure 6 (SOUZA, 2013).

The described model is designed to be applied to any project, though it is more useful in projects whose implementation deviate from their planning, as it allows managers to continuously diagnose the project. Finally, the model provides ways to verify whether the corrective actions taken by managers are effective.

Within the MD, tools guided by a common architecture would aim to reuse and share data between the AF and the MD, as shown in Figure 7. Projects with similar characteristics could be grouped and analyzed, aiming at the estimation of deadlines, costs, scopes, and risks for new projects. It would also be possible to analyze the viability of new hires and to monitor the implementation of outsourcing projects.

Over time, the consolidation of these data would comprise a knowledge base, allowing the analysis, transfer, and application of such knowledge in order to improve the performance of projects. In addition, this repository would also be compatible with planning practices such as the PfM and the CBP.

In order to achieve the implementation of the knowledge base at the MD, to create a PMO that allows for two actions is crucial:

1. The use of the DoDAF, in order to create a reference architecture for the MD, to promote systemic interoperability and to guide the IT standards;
2. the adoption of the EVM, with the purpose of developing an information system for project management within the MD (SOUZA, 2013).

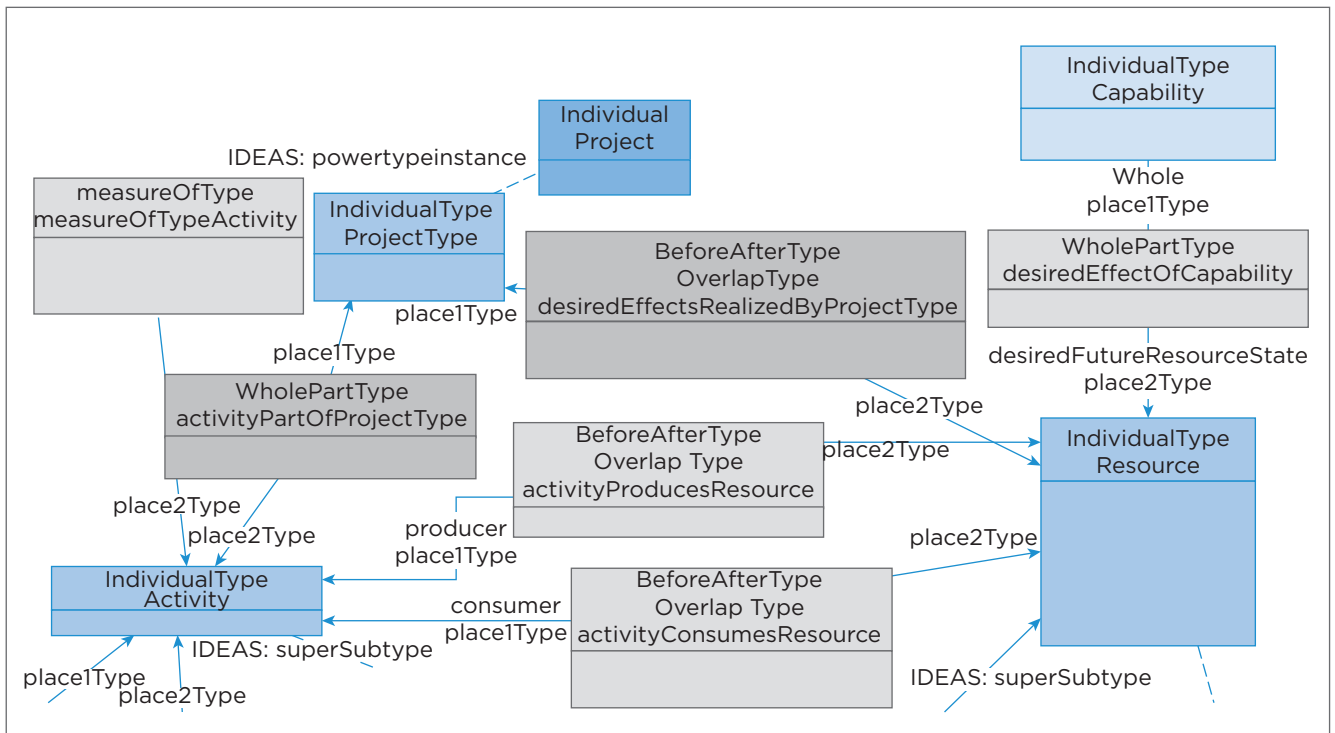


**Figure 5.** Partial View of the resulting model of Department of Defense Architecture Framework elements adapted to the needs of the Ministry of Defense project management.

## 8. CASE STUDY

Aiming at evaluating the data model proposed, as shown in Figure 5, we carried out a case study using historical control data of a project carried out between August 2006 and April 2009, with a team ranging between 2 and 12 members and with 6 planned partial deliveries (iterations). Though not a recent project, the choice was based on the quality and completeness of the records, requiring adjustments to match them with the model's existing matrix structure.

Among the records used, the following are especially important, periodically collected during the time frame above: the size of the software as function points; the effort as man-hour; and the costs, in Brazilian Real (R\$).

The size of the software was measured in three moments through Function Point Analysis (FPA): an indicative count, representing the EVM planned value (PV),

performed at the beginning of the project over its high-level requirements; the estimate count, which represents the aggregate value (AV), performed at the beginning of each iteration according to each project's specification; and the detailed count, which represents the actual cost (AC), performed at the end of each iteration over its completed software product.

After loading data through SQL, a preliminary graphical analysis was performed by plotting the S curve (Figure 8), allowing us to observe the performance trends of the project's execution.

The S curve represents the distribution of three variables – planned, aggregate, and real – of resources delivered (function points - FP) cumulatively, linked to the time elapsed during the project's execution. The chart shows that although the project's actual value was greater than what was planned, the aggregate value enables you to identify whether more FP were delivered than originally planned

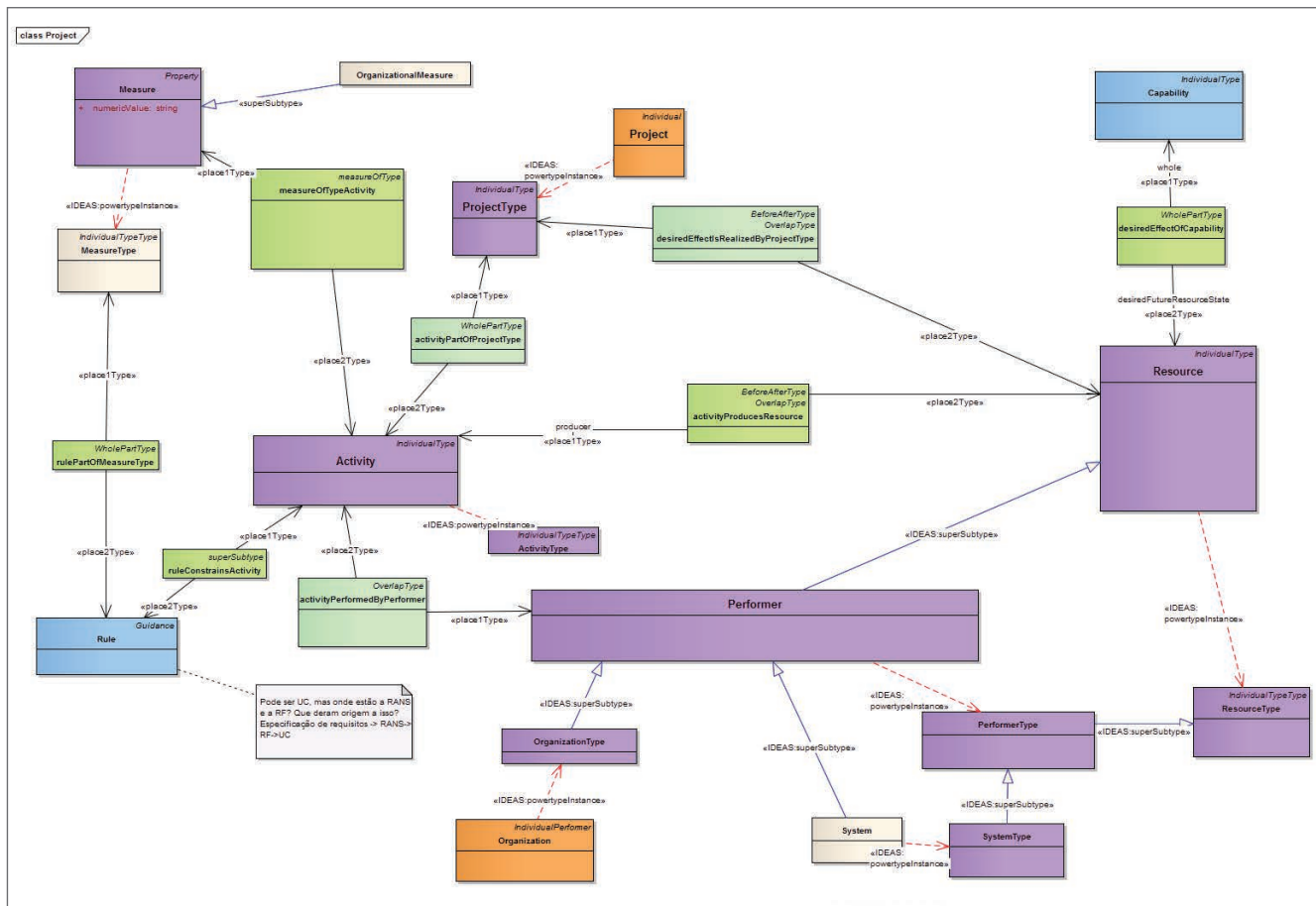


Figure 6. Resulting logic model created from elements of the Department of Defense Architecture Framework Meta Model.

as a consequence of an increased scope ratified by management records.

The use of the S curve facilitates the creation of a visualization for monitoring and controlling of projects based on indicators that represent actual performance trends (SUN, 2013). This approach allows decision-makers to monitor a project's implementation and to provide corrective actions to realign its expected performance (SOUZA, 2013).

The proposed approach is useful to managers even during the early stages of a project: with about 10 or 15% of the work completed, it is possible to have a holistic view of its implementation (USA-DOD, 2006). At the end of the project, historical data can be used to generate a knowledge base for later use in the organization, minimizing future risks in projects with similar characteristics.

## 9. FINAL CONSIDERATIONS

In this study, we analyzed two common problems that occur in IT projects within the federal government: the lack of a standard for managing such projects and high rates of failure presented by them. These issues are relevant, as they increase projects' costs and decrease the already limited throughput of government investments.

The proposed approach provides a model for exchanging data among the strategic, operational and tactical levels within the MD. As a benefit, decision-makers would be able to monitor the implementation of a project and, if necessary, to perform corrective actions to bring the project back to its expected performance.

Furthermore, the proposed approach is also in conformance with the strategic objectives recommended by the General Strategy of Information Technology

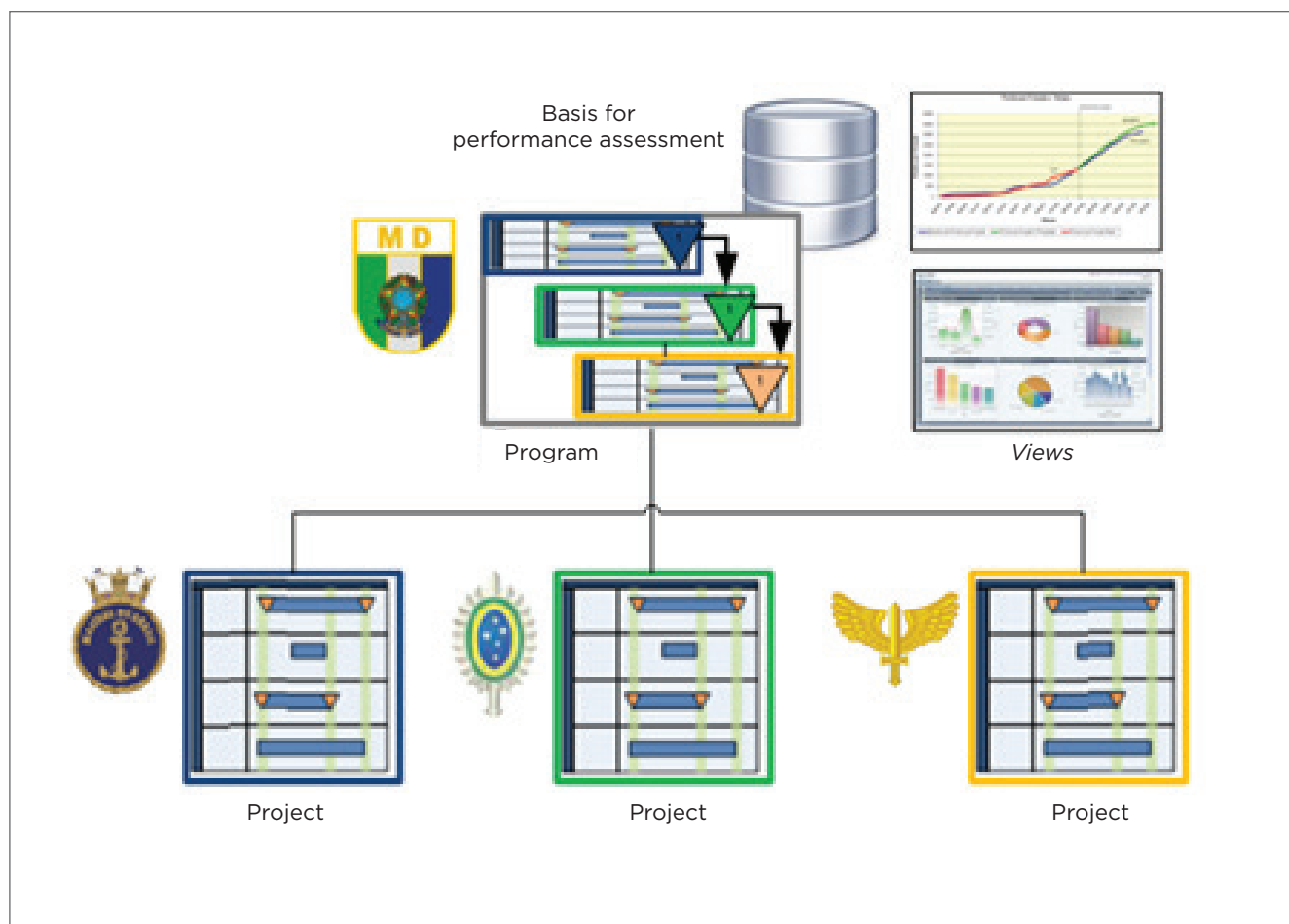


**Figure 7.** Proposal lay-out: establishment of a repository for managing Defense-related projects.

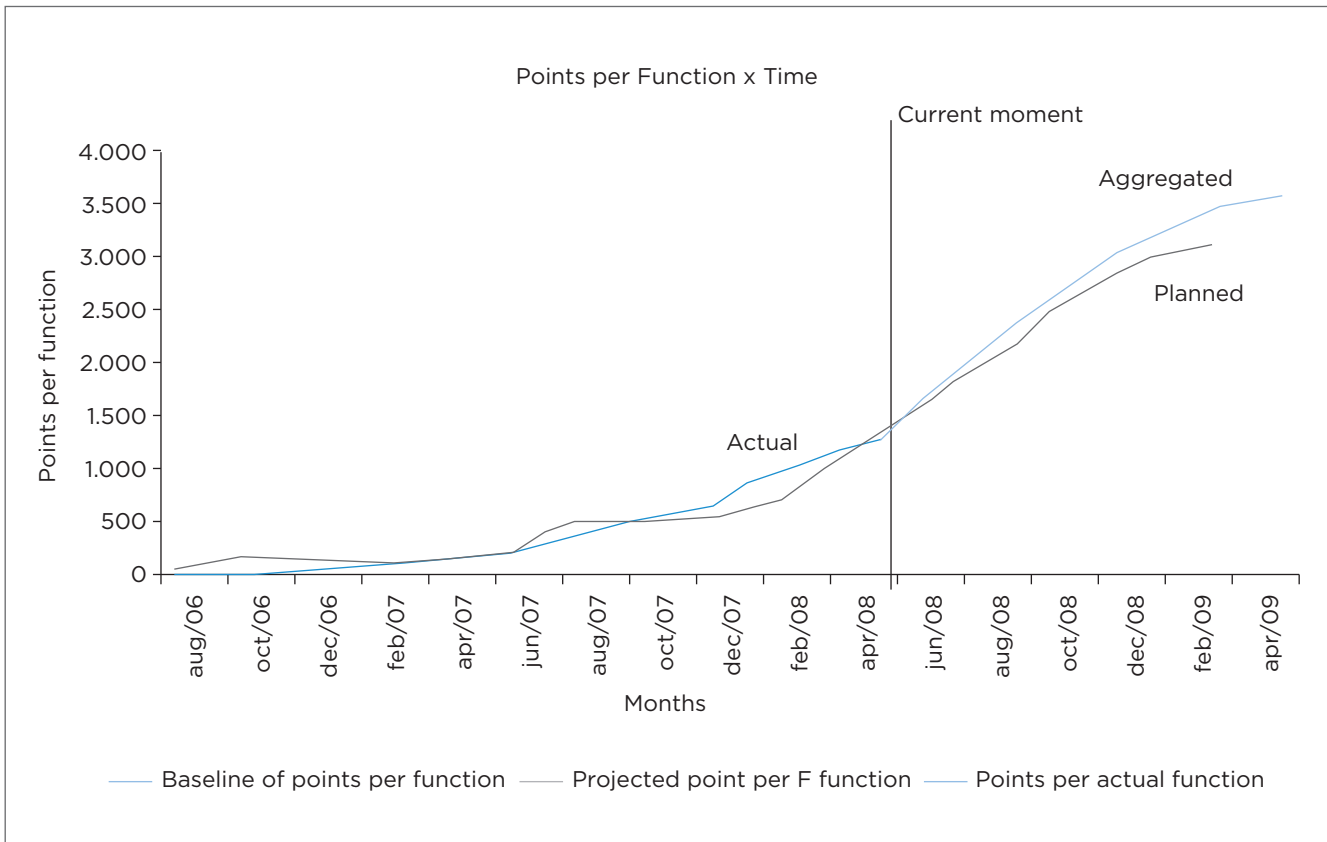


**Figure 8.** Determining the Term Performance Index, S Curve, for software engineering.

(“Estratégia Geral de Tecnologia da Informação” - EGTI) by meeting the following goals: Goal 8 - adoption of a formal process for project management based on the best practices in the market; Goal 9 - Adoption of a service hiring process in accordance with Normative Instruction SLTI 04/2010 and IT Services Hiring Manual (“Manual de Contratações de Soluções de TI”); and, partially, Goal

10 - definition and formalization of a software development process (BRASIL, 2012).

As a limitation of our approach, we can highlight the lack of data on further projects, as well as projects in different situations, which would allow for a more comprehensive analysis of the model. As a future work, we intend to develop a tool that uses this methodology to be actually implemented within the Brazilian Navy.

## REFERENCES

BRASIL. Ministério da Defesa. A Política Nacional de Defesa (PND) e Estratégia Nacional de Defesa. 2010a.

BRASIL. Ministério da Defesa. Caderno Setorial do Ministério da Defesa. Plano Plurianual, 2011a.

BRASIL. Ministério da Defesa. Secretaria de Logística e Mobilização. Gerenciando projetos no Sistema de Ciência, Tecnologia e Inovação de interesse da Defesa Nacional Ministério da Defesa, Divisão de Apoio à Pesquisa e Desenvolvimento, 2003.

BRASIL. Ministério do Planejamento, Orçamento e Gestão. Secretaria de Logística e Tecnologia da Informação. Levantamento de governança de TI 2012. Tribunal de Contas da União, Secretaria de Fiscalização de Tecnologia da Informação, 2010b.

BRASIL. Ministério do Planejamento, Orçamento e Gestão. Secretaria de Logística e Tecnologia da Informação. SISP. Metodologia de gerenciamento de projetos do SISP, 2011b.

BRASIL. Ministério do Planejamento, Orçamento e Gestão. Secretaria de Logística e Tecnologia da Informação. Estratégia Geral de Tecnologia da Informação do SISP 2013-2015, 2012. Disponível em: <<http://www.planejamento.gov.br/>>. Acesso em: 24 mar. 2012.

COTIN-MD. Plano Diretor de Tecnologia da Informação e Comunicação (PDTIC). [s.l.] Brasília, 2012.

KERZNER, H. *Gestão de projetos*. [s.l.]: Bookman, 2006.

SOUZA, G.S. *Proposta de uma abordagem sistêmica para a gestão dos projetos de engenharia de software no âmbito do Ministério da Defesa*. Dissertação de mestrado. Universidade Estadual do Ceará. Fortaleza, CE, 2013.

STANDISH GROUP. *The CHAOS report*. 2012. Disponível em: <<http://www.standishgroup.com>>. Acesso em: jan. 2017.

SUN, L. *A guide to the project management body of knowledge*. [s.l.]: Project Management Institute, Incorporated, 2013.

THE OPEN GROUP. TOGAF Versão 9.1. [s.l.]: Van Haren, 2011.

USA. Department of Defense - DOD. Department of Defense Earned Value Management System Interpretation Guide. Department of Defense USA, 2006.

USA. Department of Defense - DOD. DoDAF Architecture Framework Version 2.02. Department of Defense USA, 2015.



